NOVEL METHODOLOGIES AND MEASUREMENT SOFTWARE FOR TRANSISTOR AMPLIFIER SYNTHESIS IN PLANAR COUPLED-TRANSMISSION LINES

BY

JOSHUA GEORGE NICKEL

B.S., Pennsylvania State University, 1997
M.S., The University of Illinois at Urbana-Champaign, 1999

THESIS

Submitted in partial fulfillment of the requirements
for the degree of Doctor of Philosophy in Electrical Engineering
in the Graduate College of the
University of Illinois at Urbana-Champaign, 2001

Urbana, Illinois

NOVEL METHODOLOGIES AND MEASUREMENT SOFTWARE FOR TRANSISTOR AMPLIFIER SYNTHESIS IN PLANAR COUPLED-TRANSMISSION LINES

Joshua George Nickel, Ph.D.
Department of Electrical and Computer Engineering
University of Illinois at Urbana-Champaign, 2001
José E. Schutt-Ainé, Adviser

This thesis conerns the synthesis of active devices in coupled-microstrip and coupled-coplanar technology. We first discuss several aspects of multiconductor transmission line (MTL) theory, including longitudinal dependenices of immittance functions. We next describe a frequency domain normal mode parameter extraction method for a symmetric, uniform, MTL section. This is applied to coupled microstrip and coplanar lines for distributed circuit parameter extraction from S-parameter simulation. Measurement techniques for characterization of MTL structures with multiple ports and multiple propagating modes are then discussed and applied. Finally, these analyses and tools form a basis for the synthesis of several matching networks strategies (stubs, reactances, transformers) to maximize power to a load for the unilateral and bilateral cases. Measurement of synthesized structures verifies the reflection reduction and power savings. Using these matching networks, a preliminary MTL transistor amplifier is presented, and a methodology for an advanced design technique with maximum accuracy is developed.

For my mother, father, and brother.

ACKNOWLEDGMENTS

First, I am profoundly grateful to my adviser, Professor Jose Schutt-Aine, for initiating this project and providing numerous suggestions, ideas, and guidance. He has supported all the various endeavors and directions of my research, and his technical discussions increased my awareness and understanding of electromagnetic computation and simulation. Furthermore, his collaboration in computer projects, maintenance, and administration has been greatly helpful.

I also wish to acknowledge each of my committee members. Professor Paul Klock has been keenly interest in all stages of this work from the start. Furthermore, his discussions in the lab and measurement tips have been invaluable. His assistance with the automation software allowed quick and ordered gathering and processing of the measurements, which saved much time in gathering what would have been a series of very tedious measurements. Professor Andreas Cangellaris provided theoretical assistance and guidance through several very patient and helpful discussions. All his questions and comments have been welcomed, and I have enjoyed his company at conferences and on miscellaneous occasions. Professor Milton Feng has collaborated with our project goals, offered direction concerning fabrication issues, and initiated helpful interactions with his students and colleagues.

Many colleagues and students in and around the lab also deserve acknowledgment. Professor Chew, Professor Jin, and Professor Michielssen all expressed interest and addressed questions I had regarding my project and miscellaneous topics in electromagnetics. They are all also extraordinary teachers. Professor Jennifer Bernhard and her students (particularly Randy Clark) allowed me access to their circuit board equipment without which much of the significant measurements presented here would not have been possible. Karen Coperich always offered much advice and encouragement. Marc Kowalski shared invaluable software and formatting tips. Sanjaynath Velamparambil, with whom I shared literally hundreds of enlightening intellectual and philosophical discussions, assisted in fixing and debugging several annoying programming errors. Lijun Jiang and Chris Pan offered suggestions and shared their experience with C++. Vladimir Okhmatovsky shared many technical and intellectual discussions; his friendship is invaluable. I also wish to acknowledge Vikas Kawadia, Dan Lambalot, Fernando Teixeira, Patrick Wilson, Bin Hu, and others from CCEM.

During my final semester, we were able to design a coplanar version of a coupled-line amplifier with matching networks, and in this endeavor I must acknowledge David Caruth for his helpful support, suggestions, recommendation, and motivation. Furthermore, I was very grateful for the assistance of two undergraduate students, Mark Hampson and Ho Chung, who not only assisted in the layout of this amplifier but also performed numerous matching network measurements which resulted in much of the data generation and algorithm validation in Chapters 5 and 6.

Finally, I wish to acknowledge my family, to whom this thesis is dedicated, for their constant support and encouragment through my entire graduate studies program.

TABLE OF CONTENTS

CHAPTER **PAGE**

LIST OF TABLES

Table **Page**

LIST OF FIGURES

Figure **Page**

Please note that a significant portion of the material covered Chapter 3 resulted from research which will be published in *IEEE Trans. Microwave Theory Tech.* in 2001. Some was also submitted to *J. Franklin Inst.* A portion of the material in Chapter 4 will be published in *IEEE Trans. Electromagn. Compat.* in 2001, while the remainder is unpublished. Some of Chapters 5 and 6 has been submitted to *IEEE Trans. Microwave Theory Tech.* and *IEEE Trans. Compon. Packag. Manuf. Technol. Pt. B*, and has been presented in *the Proceedings of Electr. Perform. Electr. Packaging.*

CHAPTER 1

INTRODUCTION

Much literature has addressed the numerical analysis and engineering concerns of quasi-TEM propagation in multiconductor transmission line (MTL) systems [1]–[14] Faster signal speeds, smaller trace sizes, and increasingly compact package structuring are increasing the importance of this analysis.

Full-wave electromagnetic modelling of coupled transmission line systems is currently a heavy research topic, especially for high-frequency microwave applications where discontinuities and radiation become significant. In many instances, however, rigorous modelling is often unnecessary for two reasons: quasi-static circuit methods are much less computationally expensive and are often implemented easily. In addition, in many cases, board and package level interconnects are simply not used when they radiate or behave very electromagnetically.

Currently, designers and signal integrity engineers apply much effort in crosstalk suppression for on-chip interconnects as well as low-loss off-chip interconnects and buses. Use of proper current-mode drivers on the lines and layout flexibility are two methods, but together they may not be satisfactory. Consideration of the terminations is therefore of paramount importance. However, little has been presented regarding general matching strategies for coupled microstrip given mismatched MTL terminations. Ponchak and Katehi [15] applied tuning stub matching to coplanar waveguide systems on silicon. Kuo and Tzuang [5] reduced reflections below -30 dB using matched termination networks on six-line closely coupled microstrip circuits. Amari and Bornemann [6] minimized reflected power numerically by determining an optimum resistive termination based on random and deterministic source excitations. Sun [16] presented a multiconductor quarter-wave transformer.

Measurement of coupled transmission line systems includes both frequency and time-domain characterization. In the frequency domain, two-port scattering parameter (S-parameter) measurements can be extended to uniform symmetric lossy coupled-line systems on chip to determine propagation constants [17] or estimate crosstalk

[7]. Impedance measurements of short- and open-circuited MTL structures yield the circuit parameters [18] and characteristic matrices [19]. Multiport time-domain reflectometry (TDR) measurements were conducted by Tripathi and Tripathi [20], [21], and Schutt-Aine and Mittra [8], [9]. Despite all this pioneering work, much remains. For example, MTL characterization is generally difficult or outright infeasible due to not only measurement and probe engineering concerns, but also software processing.

The central thrust of this present work is to develop a methodology for synthesizing microwave transistor amplifiers in coupled-line systems. This involves new longitudinal analysis in MTL systems, new transformation and extraction methods from both measurement and simulation, the synthesis of new matching networks and biasing schemes in coupled-line topologies, and new stability and gain derivations in such topologies. These are all embodied in this work.

Thus, this thesis is organized into seven chapters. In Chapter 2, MTL theory is overviewed. The electrical parameters of the system, resistance, inductance, conductance, and capacitance, are expressed as matrices, and their physical interpretations are explained. Wave propagation is described by the telegraphist's equations, using the electrical parameter matrices. These equations are decoupled and solved via the equivalent eigenvalue problem yielding the modal domain variables. Complete descriptions and relations between the modal and state variables for the quasi-TEM approximation are given, concentrating on symmetric, uniform, coupled-line microstrip structures. Reflections on the coupled lines due to source and termination mismatches are also analyzed.

Chapter 3 focuses on inhomogeneous MTL structures such as coupled microstrip, where propagation is characterized by multiple quasi-TEM modes with distinct propagation constants. These "mode delays" cause the MTL functions to exhibit longitudinal behavior which superficially appears problematic in the context of passive, lossless, reciprocal systems. This chapter presents a thorough investigation of the longitudinal MTL functions. Using MTL formulation and computer simulation, we explain the mathematics and physics of mode delays so that their effects are not misinterpreted or attributed to error in the numerical analysis of MTLs.

In Chapter 4, a normal mode parameter extraction method is presented to obtain normal mode parameters (NMP) or per-unit-length resistance, inductance, conductance, and capacitance ($RLGC$) parameters from S-parameters of a coupled-line sys-

tem operating in the quasi-TEM regime. The major application of this method is to extract NMP/$RLGC$ data for coupled microstrip or coupled coplanar line full-wave S-parameter simulations.

An overview of measurement techniques for MTL structures is presented in Chapter 5. We concentrate on a renormalization method which allows for full, 50 Ω S-parameter measurements for a device with an arbitrary number of ports using only a two-port vector network analyzer (VNA) and known loads not necessarily equal to 50 Ω. This alogirithm is often essential to a multimode thru-reflect line (TRL) algorithm recently developed for multimode characterization of MTL lines.

Chapter 5 extends traditional matching networks for transmission lines to the coupled-line problem. Tuning stubs, tuning reactances, and transformers are all synthesized in coupled-line systems and applied to the coupled-line mismatches assuming arbitrary boundary conditions. For the unilateral case, simple resistive mismatches are considered, though the relations derived account for terminations with complex impedance networks. The matching methods will be applied to a three-coupled line system to exemplify matching for general n-line applications. These may include transistor amplifier circuits substituting microstrip for coplanar technology, optoelectronics packaging, chip- and package-level interconnections, and parallel data buses. We then present some numerical results and simulations of the synthesized matching networks and validated the sythesis with frequency-domain scattering parameter measurements. Reasonable engineering approximations are utilized in simulation and measurement where necessary.

In Chapter 6, we present a generalized methodology for synthesizing narrowband amplifiers in coupled microstrip systems and detail a novel narrowband amplifier in a three-coupled microstrip topology utilizing chip capacitors for matching networks. The purpose of such a configuration is to validate the synthesis of microwave amplifiers in coupled microstrip technology (the ground plane being common to many fabrication technologies) where the planarity inherent to coplanar designs alleviates the need for vias, thereby reducing fabrication cost.

Finally, Chapter 7, provides conclusions and directions for future work.

CHAPTER 2

COUPLED-LINE THEORY

In this chapter multiconductor transmission line (MTL) theory is overviewed. Circuit parameter matrices that characterize MTL structures are formulated and physically interpreted. Fundamental relations for MTL systems are then derived, which differ from single-line systems in that each quantity may be expressed as a state variable (describing the conductor relations) and modal variable (describing the modal relations). Reflection and transmission of voltage and current signals travelling on the line and their power relations are derived. Finally, the basic longitudinal matrices and power relations of an MTL structure are introduced.

2.1 Circuit Parameters for Coupled-Line Systems

A system of N total conductors or $n(= N - 1)$ coupled lines (one conductor ground/reference) where $N > 2$ is characterized by $(n \times n)$ complex matrices of Maxwellian per-unit-length resistance, conductance, inductance, and capacitance matrices, $\boldsymbol{R}$, $\boldsymbol{G}$, $\boldsymbol{L}$, $\boldsymbol{C}$, respectively (all matrices in this thesis will be denoted by italicized boldfaced capitals). All four parameters depend upon the geometry and materials in the multiconductor structure. Although many common geometries such as coaxial line, twisted pair, and parallel plate waveguides have closed-form expressions for these parameters, they are generally determined using numerical techniques. Several of these will be overviewed in the next chapter.

In systems where $N = 2$, the circuit parameter matrices that characterize the transmission line represent the scalar line-to-ground inductance L and capacitance C, respectively. But for $N > 2$, the state voltages and currents are described by vectors. The subsequent physics will demonstrate a general interdependence among each state voltage and current, represented by generally full circuit matrices. Inductance and capacitance between each conductor and ground shall be referred to here as *self*-inductance and *self*-capacitance when $N > 2$. Line-to-line inductance

and capacitance shall be referred to as *mutual* capacitances and inductances. Their relations to matrix elements in $\boldsymbol{L}$ and $\boldsymbol{C}$ will be detailed shortly.

First, however, a capacitance matrix should be derived. The mutual capacitance between conductor lines is due to the charge-potential effect of each system conductor upon the others. In general multiconductor systems, a system of N conductors will result in N equations relating each charge to each potential [22]:

$$\begin{aligned} Q_1 &= c_{11}V_1 + c_{12}V_2 + \cdots + c_{1N}V_N, \\ Q_2 &= c_{21}V_1 + c_{22}V_2 + \cdots + c_{2N}V_N, \\ &\vdots \\ Q_N &= c_{N1}V_1 + c_{N2}V_2 + \cdots + c_{NN}V_N. \end{aligned} \tag{2.1}$$

In the above system, the coefficients c_{ii} are called the coefficients of capacitance, and the coefficients c_{ij} $(i \neq j)$ are known as the coefficients of induction. Q_i denotes the charge per-unit-length on the ith conductor in the longitudinal direction $\hat{\boldsymbol{z}}$, and V_i is the potential of the ith conductor. These may be compactly expressed as vectors (where all vectors in this thesis will be denoted by italicized boldfaced lowercase) $\boldsymbol{q}$ and $\boldsymbol{v}$, respectively. Thus,

$$\boldsymbol{q} = \boldsymbol{C}\boldsymbol{v}. \tag{2.2}$$

To solve for these coefficients, consider a physical capacitance C_{ij} connecting conductors i and j. From reciprocity, $C_{ij} = C_{ji}$ and each of the N conductors can be interconnected to each other using $N(N-1)/2$ or $n(n+1)/2$ capacitors. From this network, the scalar version of (2.2) leads to n equations

$$\begin{aligned} Q_1 &= C_{1,N}V_1 + C_{1,2}(V_1 - V_2) + \cdots + C_{1,N-1}(V_1 - V_{N-1}), \\ Q_2 &= C_{1,2}(V_2 - V_1) + C_{2,N}V_2 + \cdots + C_{2,N-1}(V_2 - V_{N-1}), \\ &\vdots \\ Q_{N-1} &= C_{1,N-1}(V_{N-1} - V_1) + C_{2,N-1}(V_{N-1} - V_2) + \cdots + C_{N-1,N}(V_{N-1}). \end{aligned} \tag{2.3}$$

With common voltage terms these are regrouped as

$$\begin{aligned} Q_1 &= (C_{1,N} + C_{1,2} + \cdots + C_{1,N-1})V_1 - C_{1,2}V_2 - \cdots - C_{1,N-1}V_{N-1}, \\ Q_2 &= -C_{1,2}V_1 + (C_{2,1} + C_{2,N} + \cdots + C_{2,N-1})V_2 - \cdots - C_{2,N-1}V_{N-1}, \\ &\vdots \\ Q_{N-1} &= -C_{1,N-1}V_1 - C_{2,N-1}V_2 - \cdots + (C_{N-1,N} + C_{1,N-1} + \cdots + C_{N-1,N})V_{N-1}. \end{aligned} \tag{2.4}$$

For a general N-conductor system these relations can be more easily obtained from [2]

$$[\boldsymbol{C}]_{ii} = C_{iN} + \sum_{j=1, j\neq i}^{n} C_{ij} \qquad \text{and} \qquad [\boldsymbol{C}]_{ij} = -C_{ij}, \quad j \neq i; \tag{2.5}$$

repeated here for convenience.

This capacitance interpretation is practically demonstrated using the three-coupled microstrip line system to be analyzed and measured in this thesis (see Fig. 2.1; all figures and tables appear at the end of each chapter). Conductor 4 (the microstrip ground plane) is designated the reference conductor. The lines are symmetric about the $x = 0$ plane, thus $C_{1,2} = C_{3,2}$ and $C_{1,4} = C_{3,4}$.

Comparing (2.4) with (2.1), the capacitance matrix is assembled as

$$\begin{bmatrix} c_{11} & c_{12} & c_{13} \\ c_{21} & c_{22} & c_{23} \\ c_{31} & c_{32} & c_{33} \end{bmatrix} = \begin{bmatrix} C_{14} + C_{12} + C_{13} & -C_{12} & -C_{13} \\ -C_{21} & C_{24} + C_{12} + C_{23} & -C_{23} \\ -C_{31} & -C_{32} & C_{34} + C_{13} + C_{23} \end{bmatrix}. \tag{2.6}$$

$C_{i,4}$ represents the capacitance of conductor 1 to ground, commonly referred to as *self-capacitance*. Note that this capacitance may differ with i due to the different charge distributions on different conductors (this is significant for microstrip lines). Thus, it may be denoted $C_{\text{self}-i}$ (though the i will be omitted when $i = 1, 3$). Off-diagonal terms $c_{i,j}$, $i \neq j$, correspond to negative mutual capacitance $C_{i,j}$ between the two lines i and j. In three-line systems, a more specific definition will denote mutual capacitance between nearest neighbors ($|i - j| = 1$) C_{mut}, and mutual capacitance between nonadjacent neighbors ($|i - j| = 2$) C_{non}. By reciprocity, $c_{ij} = c_{ji}$. The capacitance matrix terms for three-line systems are thus:

$$\begin{aligned} c_{11} = c_{33} &= C_{\text{self}} + C_{\text{mut}} + C_{\text{non}}, \\ c_{22} &= C_{\text{self}-2} + 2\,C_{\text{mut}}, \\ c_{12} = c_{21} = c_{23} = c_{32} &= -C_{\text{self}}, \\ c_{13} = c_{31} &= -C_{\text{non}}. \end{aligned} \tag{2.7}$$

The self-partial capacitances are positive, and the self-mutual capacitances are negative, a physically intuitive result given that a positive potential applied to the ith conductor results in positive charge on the ith conductor and negative charges on the remaining conductors excluding ground.

For planar noncyclic structures like microstrip, the mutual capacitances between adjacent lines are typically much larger than the capacitances between nonadjacent lines (including second-neighbors and beyond). Large matrices in real systems are often sparse or banded because the capacitive coupling between distant nonadjacent conductors is negligible compared to the self and near-neighbor mutual capacitance.

Next, the inductance matrix $\boldsymbol{L}$ relates the currents on the signal conductors to the magnetic flux between each signal conductor and the reference conductor:

$$\psi = \boldsymbol{L}\boldsymbol{i}. \tag{2.8}$$

Inductances are generally obtained by solving a magnetostatic problem involving the calculation of a magnetic vector potential. There exists an isomorphism between magnetostatic and electrostatic problems, however, which allows the longitudinal magnetic vector potential to be solved via an equivalent electrostatic problem. Given that typical microstrip problems will involve no magnetic media, this procedure is commonly employed to characterize lines in the quasi-TEM regime.

The conductance matrix $\boldsymbol{G}$ accounts for loss due to an imperfect dielectric. It is computed for arbitrary geometries by solving Laplace's equation (see Chapter 3) while accounting for the complex permittivity of lossy dielectric media. A result similar to the capacitance matrix follows for the conductance matrix; (2.2) becomes

$$\boldsymbol{i} = \boldsymbol{G}\boldsymbol{v}, \tag{2.9}$$

with all mutual conductance elements negative. This property, like that governing the capacitance terms, follows from network analysis of the circuit conductances.

The resistance matrix $\boldsymbol{R}$ relates the longitudinal conductor voltages to the currents. It is typically used to characterize the power loss on conductors. It contains positive or negative off-diagonal terms which account for the excitation dependence which arises as a consequence of the resistance of the conductors depends on the the conductor current distributions. Thus, the nondiagonal resistance matrix which relates voltages and currents cannot be computed unless the excitation is known.

However, in [23], it is shown that $\boldsymbol{R}$ may be defined as diagonal (as it is for dc), because the diagonal elements of the nondiagonal $\boldsymbol{R}$ are realtively insensitive to excitation, as opposed to the off-diagonal elements. The elements of the diagonal matrix are obtained by assuming different excitations and solving a linear system of equations describing the power loss of the entire multiconductor system, as opposed to the power loss in each conductor.

In the general case of n lossy lines, $(n \times n)$ impedance and admittance matrices describe the distributed circuits. For passive systems, these matrices are symmetric and consist of $n(n+1)/2$ independent elements. For microstrip lines symmetric about the $x = 0$ plane, the matrices contain $\frac{1}{4}(n^2+2n+\mathrm{mod}(n/2))$. Or, for a set of n general lossless, a total of $n(n+1)$ independent L and C parameters characterize the system; physical symmetry assumed reduces that number by $2(n-1)$ [24].

The per-unit-length impedance and admittance $\boldsymbol{Z}$ and $\boldsymbol{Y}$ are given by

$$\boldsymbol{Z} = \boldsymbol{R} + j\omega\boldsymbol{L} \tag{2.10a}$$

$$\boldsymbol{Y} = \boldsymbol{G} + j\omega\boldsymbol{C}. \tag{2.10b}$$

The admittance matrix elements will be identically labelled with the subscripts employed for capacitance,

$$\boldsymbol{Y}_{11} = \boldsymbol{Y}_{33} = Y_{\mathrm{self}} + Y_{\mathrm{mut}} + Y_{\mathrm{non}}, \tag{2.11a}$$

$$\boldsymbol{Y}_{22} = Y_{\mathrm{self}} + 2\,Y_{\mathrm{mut}}, \tag{2.11b}$$

$$\boldsymbol{Y}_{12} = \boldsymbol{Y}_{21} = \boldsymbol{Y}_{23} = \boldsymbol{Y}_{32} = -Y_{\mathrm{self}}, \tag{2.11c}$$

$$\boldsymbol{Y}_{13} = \boldsymbol{Y}_{31} = -Y_{\mathrm{non}}, \tag{2.11d}$$

and can be realized physically as a network of impedances through the similar well-known relations

$$\boldsymbol{Z}_{ii} = \left(\sum_{k=1}^{N} \boldsymbol{Y}_{ik} \right)^{-1}, \qquad i = 1, 2, \ldots, N \tag{2.12}$$

and

$$\boldsymbol{Z}_{ij} = (-\boldsymbol{Y}_{ij})^{-1}, \qquad 1 \le i < j \le N \tag{2.13}$$

where Z_{ii} is the impedance connecting node i to ground, and Z_{ij} is the impedance connecting node i to node j. These impedances may be grouped into an impedance termination matrix, which shall be defined $\boldsymbol{\mathcal{Z}}_{\mathrm{S,L}}$, for the source or load termination.

Because most practical multiconductor transmission line systems can be characterized as low-loss [19], computation of $\boldsymbol{R}$ and $\boldsymbol{G}$ are omitted in this thesis. However, the MTL formulations detailed in this chapter and the matching results presented in later chapters will assume general lossy lines and include $\boldsymbol{R}$ and $\boldsymbol{G}$, except where specific lossless assumptions are stated.

2.2 MTL Fundamentals

The MTL equations in frequency domain matrix form (sinusoidal, steady-state conditions) for an n-line system are

$$\frac{d}{dz}\boldsymbol{v}(z) = -\boldsymbol{Z}\boldsymbol{i}(z) \tag{2.14a}$$

$$\frac{d}{dz}\boldsymbol{i}(z) = -\boldsymbol{Y}\boldsymbol{v}(z), \tag{2.14b}$$

where $\boldsymbol{v}(z)$ and $\boldsymbol{i}(z)$ are the $(n \times 1)$ phasor line voltages and current vectors, respectively, with z the longitudinal coordinate and $e^{j\omega t}$ suppressed.

It should be stressed that this theory does not apply in a strict sense to microstrip lines, which are inhomogeneous and therefore cannot support TEM modes. However, at sufficiently low frequencies, the lines support quasi-TEM modes which approximately satisfy the MTL equations [7]. In quasi-TEM analysis of n coupled lines, n modes propagate. These are obtained through the uncoupling of the telegrapher's equations [1]–[4], usually via numerical eigenanalysis, though other methods for computing the propagation constants exist [11].

Given quasi-TEM propagation, the propagating modes are interpreted as physical system voltages and currents [1]. It will be shown next that the pair of adjoint matrices $\boldsymbol{ZY}$ and $\boldsymbol{YZ}$ resulting from the decoupling of (2.14) allows generalization of the inhomogeneous dielectric case [1] for all microstrip structures. This change of variables (between line and mode) is the most frequently used method to obtain modal solutions to coupled-line systems [3].

The transformation to modal quantities is accomplished through the relations [9]

$$\boldsymbol{v}_{\mathrm{m}}(z) = \boldsymbol{E}\boldsymbol{i}(z) \tag{2.15a}$$

$$\boldsymbol{i}_{\mathrm{m}}(z) = \boldsymbol{H}\boldsymbol{i}(z) \tag{2.15b}$$

where $\boldsymbol{E}$ and $\boldsymbol{H}$ are $(n \times n)$ matrices whose ith rows are the voltage and current transformation vectors associated with the ith mode. The n column vectors $\boldsymbol{v}_{\mathrm{m}}$ and $\boldsymbol{i}_{\mathrm{m}}$ are the modal voltage and current vectors which relate to the electric and magnetic field configurations for the n modes.

Second-order MTL equations result from differentiating (with respect to z) and combining (2.14),

$$\frac{d^2}{dz^2}\boldsymbol{v}(z) = \boldsymbol{ZY}\,\boldsymbol{v}(z) \tag{2.16a}$$

$$\frac{d^2}{dz^2}\boldsymbol{i}(z) = \boldsymbol{YZ}\,\boldsymbol{i}(z), \tag{2.16b}$$

to which the transformations in (2.15) are applied; rearrangement yields

$$\frac{d^2}{dz^2}\boldsymbol{v}_{\mathrm{m}}(z) = \boldsymbol{EZYE}^{-1}\,\boldsymbol{v}_{\mathrm{m}}(z) \tag{2.17a}$$

$$\frac{d^2}{dz^2}\boldsymbol{i}_{\mathrm{m}}(z) = \boldsymbol{HYZH}^{-1}\,\boldsymbol{i}_{\mathrm{m}}(z). \tag{2.17b}$$

These equations are decoupled by finding an $\boldsymbol{E}$ and $\boldsymbol{H}$ which diagonalize $\boldsymbol{ZY}$ and $\boldsymbol{YZ}$ and convert (2.17) into wave equations with propagation constants

$$\frac{d^2}{dz^2}\boldsymbol{v}_{\mathrm{m}}(z) = \boldsymbol{\Lambda}_{\mathrm{m}}^2\,\boldsymbol{v}_{\mathrm{m}}(z) \tag{2.18a}$$

$$\frac{d^2}{dz^2}\boldsymbol{i}_{\mathrm{m}}(z) = \boldsymbol{\Lambda}_{\mathrm{m}}^2\,\boldsymbol{i}_{\mathrm{m}}(z). \tag{2.18b}$$

The diagonal modal propagation constant matrix $\boldsymbol{\Lambda}_{\mathrm{m}}$ contains the ordered complex propagation constants $\gamma_{i=1,2,\ldots,n}$ for modes $i = 1, 2, \ldots, n$.

Transformation matrices $\boldsymbol{E}$ and $\boldsymbol{H}$ must consist of linearly independent eigenvectors; this orthogonal diagonalization is only accomplished if $\boldsymbol{ZY}$ and $\boldsymbol{YZ}$ are symmetric [25]. Recalling symmetry of all structures studied in this thesis, $\boldsymbol{Z} = \boldsymbol{Z}^T$ and $\boldsymbol{Y} = \boldsymbol{Y}^T$, so that

$$(\boldsymbol{ZY})^T = \boldsymbol{Y}^T\boldsymbol{Z}^T = \boldsymbol{YZ}, \tag{2.19}$$

a critical result which states that only $\boldsymbol{E}$ or $\boldsymbol{H}$ is required to decouple the equations. Hence,

$$\boldsymbol{EZYE}^{-1} = \boldsymbol{HYZH}^{-1} = \boldsymbol{\Lambda}_{\mathrm{m}}^2, \tag{2.20}$$

and $\boldsymbol{\Lambda}_{\mathrm{m}}^2$ is the eigenvalue matrix for $\boldsymbol{ZY}$ and $\boldsymbol{YZ}$. Because microstrip is inhomogeneous, there will in general be n distinct eigenvalues [1].

The transformation matrices $\boldsymbol{E}$ and $\boldsymbol{H}$ are inverses of the left-hand eigenvector matrices for the general eigenvalue problem $\boldsymbol{Ax} = \lambda\boldsymbol{x}$. As previously mentioned, they are easily determined using numerical eigenvalue routines. Eigenanalysis does have drawbacks; its nonuniqueness for multiple eigenvalue occurence in the general case where symmetry is not assumed can present problems. Reiss and Palusinski [11] work around these with an algorithm capable of computing the square root of the matrix $\boldsymbol{LC}$, a definition from the same eigenvalue problem discussed in this paper. For this thesis, eigenanalysis will be applied given symmetry in all cases.

Solving (2.20) yields the eigenvector matrices. For three lines, $\boldsymbol{E}$ assumes the form

$$\begin{bmatrix} 1 & \alpha & 1 \\ 1 & 0 & -1 \\ 1 & -\xi & 1 \end{bmatrix}$$

where each row represents the normalized field configuration of the alpha, beta, and xi modes (α, β, ξ), respectively. Matrix $\boldsymbol{H}$ will equal $\boldsymbol{E}$ for symmetric microstrip lines. The normalization factors for distinct eigenvalues are arranged in a diagonal normalization matrix and do not introduce ambiguity in the definitions of modal impedance or admittance as described in [12] because the eigenvector matrices are orthogonal. Constants α and ξ depend on coupling magnitude, though orthogonality requires that $|\alpha\xi| = 2$.

2.3 Voltage, Admittance, Impedance, and Reflection

Typically, coupled lines are terminatated at the source and load, resulting in reflection and transmission of the signals in the system. In this thesis, termination networks consisting of passive, linear components are analyzed. Before considering the terminations, however, wave reflection expressions are formulated. The modal vectors $\boldsymbol{v}_{\mathrm{m}}(z)$ and $\boldsymbol{i}_{\mathrm{m}}(z)$ in (2.17) may also be expressed as the superposition of forward and backward going waves

$$\boldsymbol{v}_{\mathrm{m}}(z) = \boldsymbol{Q}(-z)\boldsymbol{v}_{\mathrm{m}}^{+} + \boldsymbol{Q}(z)\boldsymbol{v}_{\mathrm{m}}^{-} = \boldsymbol{Y}_{\mathrm{ch}}^{\mathrm{m}\,-1}\left[\boldsymbol{Q}(-z)\boldsymbol{i}_{\mathrm{m}}^{+} + \boldsymbol{Q}(z)\boldsymbol{i}_{\mathrm{m}}^{-}\right] \tag{2.21a}$$

$$\boldsymbol{i}_{\mathrm{m}}(z) = \boldsymbol{Q}(-z)\boldsymbol{i}_{\mathrm{m}}^{+} - \boldsymbol{Q}(z)\boldsymbol{i}_{\mathrm{m}}^{-} = \boldsymbol{Z}_{\mathrm{ch}}^{\mathrm{m}\,-1}\left[\boldsymbol{Q}(-z)\boldsymbol{v}_{\mathrm{m}}^{+} - \boldsymbol{Q}(z)\boldsymbol{v}_{\mathrm{m}}^{-}\right] \tag{2.21b}$$

where $\boldsymbol{v}_{\mathrm{m}}^{\pm}$ and $\boldsymbol{i}_{\mathrm{m}}^{\pm}$ are the modal coefficient vectors determined by boundary conditions at the load, and $\boldsymbol{Q}(z)$ is a diagonal propagator matrix of ordered modal phasors $e^{\gamma_1 z}$, $e^{\gamma_2 z}$, ... , $e^{\gamma_n z}$. The characteristic modal impedance matrix $\boldsymbol{Z}_{\mathrm{ch}}^{\mathrm{m}}$ is the inverse of the characteristic modal admittance matrix $\boldsymbol{Y}_{\mathrm{ch}}^{\mathrm{m}}$.

Substitution of (2.21) into (2.14) yields

$$\boldsymbol{E}^{-1}\frac{d}{dz}\left[\boldsymbol{Q}(-z)\boldsymbol{v}_{\mathrm{m}}^{+} + \boldsymbol{Q}(z)\boldsymbol{v}_{\mathrm{m}}^{-}\right] = -\boldsymbol{Z}\boldsymbol{H}^{-1}\left[\boldsymbol{Q}(-z)\boldsymbol{i}_{\mathrm{m}}^{+} - \boldsymbol{Q}(z)\boldsymbol{i}_{\mathrm{m}}^{-}\right] \tag{2.22a}$$

$$\boldsymbol{H}^{-1}\frac{d}{dz}\left[\boldsymbol{Q}(-z)\boldsymbol{i}_{\mathrm{m}}^{+} - \boldsymbol{Q}(z)\boldsymbol{i}_{\mathrm{m}}^{-}\right] = -\boldsymbol{Y}\boldsymbol{E}^{-1}\left[\boldsymbol{Q}(-z)\boldsymbol{v}_{\mathrm{m}}^{+} + \boldsymbol{Q}(z)\boldsymbol{v}_{\mathrm{m}}^{-}\right]. \tag{2.22b}$$

Differentiating with respect to z, cancelling negative signs, and rearranging leads to

$$\boldsymbol{\Lambda}_{\mathrm{m}}\left[\boldsymbol{Q}(-z)\boldsymbol{v}_{\mathrm{m}}^{+} - \boldsymbol{Q}(z)\boldsymbol{v}_{\mathrm{m}}^{-}\right] = \boldsymbol{E}\boldsymbol{Z}\boldsymbol{H}^{-1}\left[\boldsymbol{Q}(-z)\boldsymbol{i}_{\mathrm{m}}^{+} - \boldsymbol{Q}(z)\boldsymbol{i}_{\mathrm{m}}^{-}\right] \tag{2.23a}$$

$$\boldsymbol{\Lambda}_{\mathrm{m}}\left[\boldsymbol{Q}(-z)\boldsymbol{i}_{\mathrm{m}}^{+} + \boldsymbol{Q}(z)\boldsymbol{i}_{\mathrm{m}}^{-}\right] = \boldsymbol{H}\boldsymbol{Y}\boldsymbol{E}^{-1}\left[\boldsymbol{Q}(-z)\boldsymbol{v}_{\mathrm{m}}^{+} + \boldsymbol{Q}(z)\boldsymbol{v}_{\mathrm{m}}^{-}\right]. \tag{2.23b}$$

Combining (2.21) with (2.23), the characeteristic modal impedance and admittance

matrices are expressed as

$$\boldsymbol{Z}_{\mathrm{ch}}^{\mathrm{m}} = \boldsymbol{\Lambda}_{\mathrm{m}}^{-1}\boldsymbol{E}\boldsymbol{Z}\boldsymbol{H}^{-1} \tag{2.24}$$

$$\boldsymbol{Y}_{\mathrm{ch}}^{\mathrm{m}} = \boldsymbol{\Lambda}_{\mathrm{m}}^{-1}\boldsymbol{H}\boldsymbol{Y}\boldsymbol{E}^{-1}. \tag{2.25}$$

Transformation matrices $\boldsymbol{E}$ and $\boldsymbol{H}$ must simultaneously diagonalize both $\boldsymbol{Z}$ and $\boldsymbol{Y}$ [3] to uncouple the MTL equations, and obviously must be nonsingular [3], [10] to enable transformation between both modal and state variables. Matrices $\boldsymbol{Z}_{\mathrm{ch}}^{\mathrm{m}}$ and $\boldsymbol{Y}_{\mathrm{ch}}^{\mathrm{m}}$ are therefore diagonal where the ith entry denotes the characteristic impedance or admittance of the ith mode. Transformation matrix $\boldsymbol{H}$ may be redefined with a normalization matrix $\boldsymbol{D}$ [3] as $\boldsymbol{H}' = (\boldsymbol{D}^T)^{-1}$ so that

$$\boldsymbol{E}^T\boldsymbol{H}' = \mathbf{1}_n. \tag{2.26}$$

Similarly, characteristic impedance and admittance matrices $\boldsymbol{Z}_{\mathrm{ch}}$ and $\boldsymbol{Y}_{\mathrm{ch}}$ for the system can be derived by defining $\boldsymbol{v}(z) = \boldsymbol{Z}_{\mathrm{ch}}\boldsymbol{i}(z)$ for forward and backward waves separately [8]. From (2.15) and (2.21) we can write

$$\boldsymbol{Q}(\mp z)\boldsymbol{H}\boldsymbol{i}^{\pm} = [\boldsymbol{Z}_{\mathrm{ch}}^{\mathrm{m}}]^{-1}\boldsymbol{Q}(\mp z)\boldsymbol{E}\boldsymbol{v}^{\pm}, \tag{2.27}$$

but $\boldsymbol{Z}_{\mathrm{ch}}^{\mathrm{m}}$ and $\boldsymbol{Y}_{\mathrm{ch}}^{\mathrm{m}}$ are diagonal so $\boldsymbol{Q}(\mp z)$ cancels leaving

$$\boldsymbol{v}^{\pm} = \left(\boldsymbol{E}^{-1}\boldsymbol{Z}_{\mathrm{ch}}^{\mathrm{m}}\boldsymbol{H}\right)\boldsymbol{i}^{\pm}. \tag{2.28}$$

Therefore, by definition of characteristic impedance,

$$\boldsymbol{Z}_{\mathrm{ch}}^{\mathrm{c}} = \boldsymbol{E}^{-1}\boldsymbol{Z}_{\mathrm{ch}}^{\mathrm{m}}\boldsymbol{H} = \boldsymbol{E}^{-1}\boldsymbol{\Lambda}_{\mathrm{m}}^{-1}\boldsymbol{E}\boldsymbol{Z}, \tag{2.29}$$

and

$$\boldsymbol{Y}_{\mathrm{ch}}^{\mathrm{c}} = \boldsymbol{Z}_{\mathrm{ch}}^{\mathrm{c}\ -1} = \left(\boldsymbol{E}^{-1}\boldsymbol{\Lambda}_{\mathrm{m}}^{-1}\boldsymbol{E}\boldsymbol{Z}\right)^{-1} = \boldsymbol{Z}^{-1}\boldsymbol{E}^{-1}\boldsymbol{\Lambda}_{\mathrm{m}}\boldsymbol{E}. \tag{2.30}$$

This definition agrees with [8], [10], [11] when $\boldsymbol{Z}$ is replaced with $\boldsymbol{L}$ for the lossless case.

Now consider a terminated microstrip structure as shown in Fig. 2.2. Each of the N nodes are interconnected with impedances. The resulting network is expressed as an $(n \times n)$ matrix $\boldsymbol{\mathcal{Z}}_{\mathrm{L}}$, where the ij term denotes the impedance connecting line i to line j at the load plane $z = 0$ if $i \neq j$, or the impedance terminating line i to ground if $i = j$.

In MTL analysis, terminations of an n-line system at the source or load are represented as $(n \times n)$ open-circuit impedance matrices $\boldsymbol{Z}_{\mathrm{S}}^{\mathrm{c}}$, $\boldsymbol{Z}_{\mathrm{L}}^{\mathrm{c}}$, respectively, or $(n \times n)$ short-circuit admittance matrices $\boldsymbol{Y}_{\mathrm{S}}^{\mathrm{c}}$, $\boldsymbol{Y}_{\mathrm{L}}^{\mathrm{c}}$, respectively.

From Ohm's law, the line voltage and current vectors are related at the load by the load admittance matrix $\boldsymbol{Y}_{\mathrm{L}}^{\mathrm{c}} = \boldsymbol{Y}_{\mathrm{L}}^{\mathrm{c}}(z=0)$ as

$$\boldsymbol{Y}_{\mathrm{L}}^{\mathrm{c}} \cdot \boldsymbol{v}(z=0) = \boldsymbol{i}(z=0). \tag{2.31}$$

Conversion to modal quantities using (2.21) with $z=0$ produces

$$\boldsymbol{Y}_{\mathrm{L}}^{\mathrm{c}} \boldsymbol{E}^{-1} \left[\boldsymbol{v}_{\mathrm{m}}^{+} + \boldsymbol{v}_{\mathrm{m}}^{-}\right] = \boldsymbol{H}^{-1} \boldsymbol{Z}_{\mathrm{ch}}^{\mathrm{m}\,-1} \left[\boldsymbol{v}_{\mathrm{m}}^{+} - \boldsymbol{v}_{\mathrm{m}}^{-}\right], \tag{2.32}$$

and solving for the forward going modal voltage vector in terms of the reverse going modal voltage vector leads to

$$\boldsymbol{v}_{\mathrm{m}}^{-} = -\left[\mathbf{1}_n + \boldsymbol{E}\boldsymbol{Y}_{\mathrm{L}}^{\mathrm{c}\,-1} \boldsymbol{H}^{-1} \boldsymbol{Z}_{\mathrm{ch}}^{\mathrm{m}\,-1}\right]^{-1} \left[\mathbf{1}_n - \boldsymbol{E}\boldsymbol{Y}_{\mathrm{L}}^{\mathrm{c}\,-1} \boldsymbol{H}^{-1} \boldsymbol{Z}_{\mathrm{ch}}^{\mathrm{m}\,-1}\right] \boldsymbol{v}_{\mathrm{m}}^{+}. \tag{2.33}$$

Defining a modal reflection coefficient matrix at the load $\boldsymbol{\Gamma}_{\mathrm{L}}^{\mathrm{m}}$ as

$$\boldsymbol{v}_{\mathrm{m}}^{-} = \boldsymbol{\Gamma}_{\mathrm{L}}^{\mathrm{m}}(z=0)\boldsymbol{v}_{\mathrm{m}}^{+}, \tag{2.34}$$

and substituting (2.24) and pulling in the negative sign results in

$$\boldsymbol{\Gamma}_{\mathrm{L}}^{\mathrm{m}}(z=0) = \left[\mathbf{1}_n + \boldsymbol{\Lambda}_{\mathrm{m}}^{-1} \boldsymbol{E}\boldsymbol{Z}\boldsymbol{Y}_{\mathrm{L}}^{\mathrm{c}} \boldsymbol{E}^{-1}\right]^{-1} \left[\mathbf{1}_n - \boldsymbol{\Lambda}_{\mathrm{m}}^{-1} \boldsymbol{E}\boldsymbol{Z}\boldsymbol{Y}_{\mathrm{L}}^{\mathrm{c}} \boldsymbol{E}^{-1}\right]; \tag{2.35}$$

similarly for the source,

$$\boldsymbol{\Gamma}_{\mathrm{S}}^{\mathrm{m}}(z=0) = \left[\mathbf{1}_n + \boldsymbol{\Lambda}_{\mathrm{m}}^{-1} \boldsymbol{E}\boldsymbol{Z}\boldsymbol{Y}_{\mathrm{S}}^{\mathrm{c}} \boldsymbol{E}^{-1}\right]^{-1} \left[\mathbf{1}_n - \boldsymbol{\Lambda}_{\mathrm{m}}^{-1} \boldsymbol{E}\boldsymbol{Z}\boldsymbol{Y}_{\mathrm{S}}^{\mathrm{c}} \boldsymbol{E}^{-1}\right]; \tag{2.36}$$

these are more compactly expressed in terms of (2.24) as

$$\boldsymbol{\Gamma}_{\mathrm{S}}^{\mathrm{m}}(z=-D) = \left[\boldsymbol{Z}_{\mathrm{S}}^{\mathrm{m}} + \boldsymbol{Z}_{\mathrm{ch}}^{\mathrm{m}}\right]^{-1} \left[\boldsymbol{Z}_{\mathrm{S}}^{\mathrm{m}} - \boldsymbol{Z}_{\mathrm{ch}}^{\mathrm{m}}\right] \tag{2.37}$$

$$\boldsymbol{\Gamma}_{\mathrm{L}}^{\mathrm{m}}(z=0) = \left[\boldsymbol{Z}_{\mathrm{L}}^{\mathrm{m}} + \boldsymbol{Z}_{\mathrm{ch}}^{\mathrm{m}}\right]^{-1} \left[\boldsymbol{Z}_{\mathrm{L}}^{\mathrm{m}} - \boldsymbol{Z}_{\mathrm{ch}}^{\mathrm{m}}\right] \tag{2.38}$$

or in terms of (2.25) as

$$\boldsymbol{\Gamma}_{\mathrm{S}}^{\mathrm{m}}(z=-D) = \left[\boldsymbol{Y}_{\mathrm{ch}}^{\mathrm{m}} + \boldsymbol{Y}_{\mathrm{S}}^{\mathrm{m}}\right]^{-1} \left[\boldsymbol{Y}_{\mathrm{ch}}^{\mathrm{m}} - \boldsymbol{Y}_{\mathrm{S}}^{\mathrm{m}}\right] \tag{2.39}$$

$$\boldsymbol{\Gamma}_{\mathrm{L}}^{\mathrm{m}}(z=0) = \left[\boldsymbol{Y}_{\mathrm{ch}}^{\mathrm{m}} + \boldsymbol{Y}_{\mathrm{L}}^{\mathrm{m}}\right]^{-1} \left[\boldsymbol{Y}_{\mathrm{ch}}^{\mathrm{m}} - \boldsymbol{Y}_{\mathrm{L}}^{\mathrm{m}}\right], \tag{2.40}$$

where $\boldsymbol{Z}_{\mathrm{L}}^{\mathrm{m}}$ and $\boldsymbol{Y}_{\mathrm{ch}}^{\mathrm{m}}$ are the modal load impedance and admittance, respectively. It is apparent from (2.33) that these quantities are derived directly from the line load impedance and admittance matrices:

$$\boldsymbol{Z}_{\mathrm{L}}^{\mathrm{m}} = \boldsymbol{E}\boldsymbol{Z}_{\mathrm{L}}^{\mathrm{c}} \boldsymbol{H}^{-1} \tag{2.41}$$

$$\boldsymbol{Y}_{\mathrm{L}}^{\mathrm{m}} = \boldsymbol{H}\boldsymbol{Y}_{\mathrm{L}}^{\mathrm{c}} \boldsymbol{E}^{-1}. \tag{2.42}$$

The $(n \times n)$ reflection coefficient matrices (2.37)-(2.40) have several notable properties. First, $\boldsymbol{\Gamma}_{\mathrm{S,L}}^{\mathrm{m}}$ relate modal voltages, not line voltages. For example, the ith diagonal entry represents the *self*-reflection coefficient of mode i, or the ratio between the reverse- and forward-travelling mode i voltage waves. Off-diagonal entries ij correspond to *intermode* partial reflection from mode j to mode i. Thus, $\boldsymbol{\Gamma}_{\mathrm{S,L}}^{\mathrm{m}}$ will

generally be asymmetric. Secondly, if terminated symmetrically, $\boldsymbol{\Gamma}^{\mathrm{m}}_{\mathrm{S,L}}$ will typically contain $[n/2]$ (where brackets denote integral part) zero-valued elements due to the lack of partial reflection between *even* and *odd* modes, to be defined by symmetry about the center line. For the three-line case, the α and ξ modes are the even modes, while β is the single odd mode. Since the odd and even modes are arranged in alternating rows of $\boldsymbol{E}$, matrix $\boldsymbol{\Gamma}^{\mathrm{m}}_{\mathrm{S,L}}$ will be "checkered" with $[n/2]$ zeros (i.e., $[\boldsymbol{\Gamma}^{\mathrm{m}}_{\mathrm{S,L}}]_{ij} = 0$ unless i,j are both odd or both even). Third, self-reflection of a particular mode i will be zero if all lines are terminated by $[\boldsymbol{Z}^{\mathrm{m}}_{\mathrm{ch}}]_{ii}$. Finally, it is generally very difficult to gauge the signs of the elements in $\boldsymbol{\Gamma}^{\mathrm{m}}_{\mathrm{L}}$ given $\boldsymbol{Z}^{\mathrm{m}}_{\mathrm{ch}}$, due to the nonlinear dependence on the load admittance matrix, $\boldsymbol{Y}^{\mathrm{c}}_{\mathrm{L}}$.

Correspondingly, the line reflection coefficient matrix which relates forward and backward going line voltages $\boldsymbol{v}^{+}$ and $\boldsymbol{v}^{-}$ is derived by premultiplying both voltages in (2.34) by $\boldsymbol{E}^{-1}$ and applying (2.15); its definition then yields

$$\boldsymbol{E}^{-1}\boldsymbol{\Gamma}^{\mathrm{m}}_{\mathrm{L}}\boldsymbol{E}\boldsymbol{v}^{+} = \boldsymbol{v}^{-}, \tag{2.43}$$

a result from which a line reflection coefficient is defined to relate forward and reverse travelling line voltages as

$$\boldsymbol{\Gamma}^{\mathrm{c}}_{\mathrm{L}} = \boldsymbol{E}^{-1}\boldsymbol{\Gamma}^{\mathrm{m}}_{\mathrm{L}}\boldsymbol{E}. \tag{2.44}$$

From (2.35) and (2.36) one obtains

$$\boldsymbol{\Gamma}^{\mathrm{c}}_{\mathrm{L}} = \left[\mathbf{1}_n + \boldsymbol{E}^{-1}\boldsymbol{\Lambda}^{-1}_{\mathrm{m}}\boldsymbol{E}\boldsymbol{Z}\boldsymbol{Y}_{\mathrm{L}}\right]^{-1}\left[\mathbf{1}_n - \boldsymbol{E}^{-1}\boldsymbol{\Lambda}^{-1}_{\mathrm{m}}\boldsymbol{E}\boldsymbol{Z}\boldsymbol{Y}_{\mathrm{L}}\right] \tag{2.45}$$

$$\boldsymbol{\Gamma}^{\mathrm{c}}_{\mathrm{S}} = \left[\mathbf{1}_n + \boldsymbol{E}^{-1}\boldsymbol{\Lambda}^{-1}_{\mathrm{m}}\boldsymbol{E}\boldsymbol{Z}\boldsymbol{Y}_{\mathrm{S}}\right]^{-1}\left[\mathbf{1}_n - \boldsymbol{E}^{-1}\boldsymbol{\Lambda}^{-1}_{\mathrm{m}}\boldsymbol{E}\boldsymbol{Z}\boldsymbol{Y}_{\mathrm{S}}\right], \tag{2.46}$$

which are more compactly expressed by multiplying through by $\boldsymbol{Z}^{\mathrm{c}}_{\mathrm{ch}}$ as

$$\boldsymbol{\Gamma}^{\mathrm{c}}_{\mathrm{L}} = \left[\boldsymbol{Z}^{\mathrm{c}}_{\mathrm{L}} + \boldsymbol{Z}^{\mathrm{c}}_{\mathrm{ch}}\right]^{-1}\left[\boldsymbol{Z}^{\mathrm{c}}_{\mathrm{L}} - \boldsymbol{Z}^{\mathrm{c}}_{\mathrm{ch}}\right] \tag{2.47}$$

$$\boldsymbol{\Gamma}^{\mathrm{c}}_{\mathrm{S}} = \left[\boldsymbol{Z}^{\mathrm{c}}_{\mathrm{S}} + \boldsymbol{Z}^{\mathrm{c}}_{\mathrm{ch}}\right]^{-1}\left[\boldsymbol{Z}^{\mathrm{c}}_{\mathrm{S}} - \boldsymbol{Z}^{\mathrm{c}}_{\mathrm{ch}}\right] \tag{2.48}$$

or by multiplying through by $\boldsymbol{Y}_{\mathrm{ch}}$ as

$$\boldsymbol{\Gamma}^{\mathrm{c}}_{\mathrm{L}} = \left[\boldsymbol{Y}^{\mathrm{c}}_{\mathrm{ch}} + \boldsymbol{Y}^{\mathrm{c}}_{\mathrm{L}}\right]^{-1}\left[\boldsymbol{Y}^{\mathrm{c}}_{\mathrm{ch}} - \boldsymbol{Y}^{\mathrm{c}}_{\mathrm{L}}\right] \tag{2.49}$$

$$\boldsymbol{\Gamma}^{\mathrm{c}}_{\mathrm{S}} = \left[\boldsymbol{Y}^{\mathrm{c}}_{\mathrm{ch}} + \boldsymbol{Y}^{\mathrm{c}}_{\mathrm{S}}\right]^{-1}\left[\boldsymbol{Y}^{\mathrm{c}}_{\mathrm{ch}} - \boldsymbol{Y}^{\mathrm{c}}_{\mathrm{S}}\right], \tag{2.50}$$

which agrees with the reflection matrices derived in [5], [6]. The ith diagonal entries correspond to the ratio of reverse-to-forward line voltages on the ith line; off-diagonal elements refer to ratios of the reverse voltage on line i to the forward voltage on line j [5].

2.3.1 Longitudinal dependencies

Line and modal reflection coefficient, impedance, and admittance matrices are functions of the longitudinal coordinate z. These functions are required to calculate signals along the coupled line system and optimize the matching networks that will be introduced in Chapter 4. For a uniform two-conductor transmission line the familiar scalar result $\Gamma(z) = \Gamma(0)\, e^{2\gamma z} = \Gamma_{\mathrm{L}} e^{2\gamma z}$ applies, from which impedance and admittance transformations are derived. In a general n-line system, the modal reflection coefficient at position z resulting from the given termination is determined using the propagator matrix $\boldsymbol{Q}(\mathrm{z})$. Modal signals along the coupled lines are superpositions of forward and backward travelling waves (2.21) and when applied to (2.34) for some position z,

$$\boldsymbol{Q}(z)\boldsymbol{v}_{\mathrm{m}}^{-} = \boldsymbol{Q}(z)\boldsymbol{\Gamma}_{\mathrm{L}}^{\mathrm{m}}\boldsymbol{Q}(z)\boldsymbol{Q}(-z)\boldsymbol{v}_{\mathrm{m}}^{+}, \tag{2.51}$$

obtaining

$$\begin{aligned}\boldsymbol{v}_{\mathrm{m}}(z) &= \boldsymbol{Q}(-z)\boldsymbol{v}_{\mathrm{m}}^{+} + \boldsymbol{Q}(z)\boldsymbol{\Gamma}_{\mathrm{L}}^{\mathrm{m}}\boldsymbol{Q}(z)\boldsymbol{Q}(-z)\boldsymbol{v}_{\mathrm{m}}^{+} \\ &= \left[\mathbf{1}_n + \boldsymbol{Q}(z)\boldsymbol{\Gamma}_{\mathrm{L}}^{\mathrm{m}}\boldsymbol{Q}(z)\right]\boldsymbol{Q}(-x)\boldsymbol{v}_{\mathrm{m}}^{+} \\ &= \left[\mathbf{1}_n + \boldsymbol{\Gamma}^{\mathrm{m}}(z)\right]\boldsymbol{Q}(-z)\boldsymbol{v}_{\mathrm{m}}^{+}. \end{aligned} \tag{2.52}$$

Thus, the modal reflection coefficient matrix of the three-line system at a position z is the phase-shifted $\boldsymbol{\Gamma}_{\mathrm{L}}^{\mathrm{m}}$,

$$\boldsymbol{\Gamma}_{\mathrm{L}}^{\mathrm{m}}(z) = \boldsymbol{Q}(z)\boldsymbol{\Gamma}_{\mathrm{L}}^{\mathrm{m}}(0)\boldsymbol{Q}(z), \tag{2.53}$$

and from (2.44) the line reflection coefficient matrix as a function of length is obtained,

$$\boldsymbol{\Gamma}_{\mathrm{L}}^{\mathrm{c}}(z) = \boldsymbol{E}^{-1}\boldsymbol{Q}(z)\boldsymbol{\Gamma}_{\mathrm{L}}^{\mathrm{m}}\boldsymbol{Q}(z)\boldsymbol{E}. \tag{2.54}$$

Expanded into n^2 equations, (2.54) reveals the presence of every mode in each $\boldsymbol{\Gamma}_{\mathrm{L}}^{\mathrm{c}}(z)$ term. Matrix $\boldsymbol{Q}(z)$ contains propagation constants $e^{\gamma_i z}$ scaled by constants composing $\boldsymbol{E}$, $\boldsymbol{E}^{-1}$, and $\boldsymbol{\Gamma}_{\mathrm{L}}^{\mathrm{m}}$. Every term is consequently expressed as a sum of n^2 distinct z-varying phasors, each containing some combination of γ_i: $\gamma_1+\gamma_1$, $\gamma_1+\gamma_2$, $\gamma_1+\gamma_3$, ... For lossless lines with symmetric $\boldsymbol{Y}_{\mathrm{L}}$, $\boldsymbol{\Gamma}_{\mathrm{L}}^{\mathrm{m}}$ is "checkered" with zeros; in this case each term in $\boldsymbol{\Gamma}_{\mathrm{L}}^{\mathrm{c}}(z)$ contains the sum of $\frac{1}{4}\left[n^2 + 2n + 2(\mathrm{mod}\ n)\right]$ distinct constant magnitude phasors containing separate even-mode and odd-mode additive combinations of γ_i: $\gamma_1 + \gamma_1$, $\gamma_1 + \gamma_3$, $\gamma_1 + \gamma_5$, ... $\gamma_2 + \gamma_2$, $\gamma_2 + \gamma_4$, ...

The result is that unlike lossless, dispersionless, single transmission lines where the reflection coefficient phase varies linearly and its magnitude remains constant with respect to z (or ω), the terms of $\boldsymbol{\Gamma}_{\mathrm{L}}^{\mathrm{c}}(z)$ for lossless, dispersionless coupled lines exhibit

nonlinear phase and magnitude dependence with z. For practical applications, close proximity ($z < \lambda/2$) between the matching networks and the load is often desired. In this region of small coupling length, $\boldsymbol{\Gamma}_{\mathrm{L}}^{\mathrm{c}}(z)$ terms maintain approximately constant magnitude.

Equations (2.37), (2.38), (2.47), and (2.48) may be generalized as

$$\boldsymbol{\Gamma}_{\mathrm{S,L}}^{\mathrm{m,c}}(z) = \left[\boldsymbol{Z}_{\mathrm{S,L}}^{\mathrm{m,c}}(z) + \boldsymbol{Z}_{\mathrm{ch}}^{\mathrm{m,c}}\right]^{-1}\left[\boldsymbol{Z}_{\mathrm{S,L}}^{\mathrm{m,c}}(z) - \boldsymbol{Z}_{\mathrm{ch}}^{\mathrm{m,c}}\right] \tag{2.55}$$

Modal and line admittance and impedance matrices for the coupled-line system are derived directly from this result and exist in multiple forms. Matching procedures detailed in Chapter 4 will mainly deal with load matching, so the most direct forms for modal load admittance and impedance are

$$\boldsymbol{Z}_{\mathrm{L}}^{\mathrm{m}}(z) = \boldsymbol{Z}_{\mathrm{ch}}^{\mathrm{m}}\left[\mathbf{1}_n + \boldsymbol{\Gamma}_{\mathrm{L}}^{\mathrm{m}}(z)\right]\left[\mathbf{1}_n - \boldsymbol{\Gamma}_{\mathrm{L}}^{\mathrm{m}}(z)\right]^{-1} \tag{2.56}$$

$$\boldsymbol{Y}_{\mathrm{L}}^{\mathrm{m}}(z) = \left[\mathbf{1}_n - \boldsymbol{\Gamma}_{\mathrm{L}}^{\mathrm{m}}(z)\right]\left[\mathbf{1}_n + \boldsymbol{\Gamma}_{\mathrm{L}}^{\mathrm{m}}(z)\right]^{-1}\boldsymbol{Y}_{\mathrm{ch}}^{\mathrm{m}}, \tag{2.57}$$

while several expressions for the line impedance matrix

$$\boldsymbol{Z}_{\mathrm{L}}^{\mathrm{c}}(z) = \boldsymbol{Z}_{\mathrm{ch}}^{\mathrm{c}}\left[\mathbf{1}_n + \boldsymbol{\Gamma}_{\mathrm{L}}^{\mathrm{c}}(z)\right]\left[\mathbf{1}_n - \boldsymbol{\Gamma}_{\mathrm{L}}^{\mathrm{c}}(z)\right]^{-1} \tag{2.58a}$$

$$= \boldsymbol{Z}_{\mathrm{ch}}^{\mathrm{c}}\boldsymbol{H}^{-1}\left[\mathbf{1}_n + \boldsymbol{\Gamma}_{\mathrm{L}}^{\mathrm{m}}(z)\right]\left[\mathbf{1}_n - \boldsymbol{\Gamma}_{\mathrm{L}}^{\mathrm{m}}(z)\right]^{-1}\boldsymbol{H} \tag{2.58b}$$

$$= \boldsymbol{E}^{-1}\left[\mathbf{1}_n + \boldsymbol{\Gamma}_{\mathrm{L}}^{\mathrm{m}}(z)\right]\left[\mathbf{1}_n - \boldsymbol{\Gamma}_{\mathrm{L}}^{\mathrm{m}}(z)\right]^{-1}\boldsymbol{\Lambda}_{\mathrm{m}}^{-1}\boldsymbol{E}\boldsymbol{Z}, \tag{2.58c}$$

and the line admittance matrix

$$\boldsymbol{Y}_{\mathrm{L}}^{\mathrm{c}}(z) = \boldsymbol{Z}^{-1}\boldsymbol{E}^{-1}\boldsymbol{\Lambda}_{\mathrm{L}}^{\mathrm{m}}\left[\mathbf{1}_n - \boldsymbol{\Gamma}_{\mathrm{m}}(z)\right]\left[\mathbf{1}_n + \boldsymbol{\Gamma}_{\mathrm{L}}^{\mathrm{m}}(z)\right]^{-1}\boldsymbol{E}, \tag{2.59a}$$

$$= \boldsymbol{H}^{-1}\left[\mathbf{1}_n - \boldsymbol{\Gamma}_{\mathrm{L}}^{\mathrm{m}}(z)\right]\left[\mathbf{1}_n + \boldsymbol{\Gamma}_{\mathrm{L}}^{\mathrm{m}}(z)\right]^{-1}\boldsymbol{H}\boldsymbol{Y}_{\mathrm{ch}}^{\mathrm{c}}, \tag{2.59b}$$

are valid.

If the short-circuit line admittance matrix is diagonally dominant and real at z, it may be realized as an impedance network consisting of, in general, $2n$ nodes [26]. Furthermore, if all of the off-diagonal terms of the admittance matrix are nonpositive, then a conductance network of $n+1$ nodes (with a common ground for all n ports) may be synthesized [26, Theorem 8-4] according to the real parts (2.12) and (2.13). This theorem may be extended to complex admittance matrices if the impedances interconnecting the $n+1$ nodes are realized as parallel RL or RC circuits, where

$$R_{ij} = \Re\mathrm{e}\{[\boldsymbol{Y}_{\mathrm{L}}^{\mathrm{c}}]_{ij}\}. \tag{2.60}$$

Longitudinal modal and line voltage distributions exhibit standing wave patterns and ratios similar to single transmission lines. Modal decoupling results in constant

modal voltage standing wave ratios (SWRs) along the line. Mode voltage i from (2.52) is given by

$$\boldsymbol{v}_{\mathrm{m}}]_i = [\boldsymbol{Q}(-z)]_{ii}\, \boldsymbol{v}_{\mathrm{m}}^{+}]_i \left(1 + \frac{\boldsymbol{Q}(-z)^2 \boldsymbol{\Gamma}_{\mathrm{L}}^{\mathrm{m}} \boldsymbol{v}_{\mathrm{m}}^{+}]_i}{\boldsymbol{v}_{\mathrm{m}}^{+}]_i}\right). \tag{2.61}$$

SWR for the ith mode is the ratio of the maximum and minimum modal voltage evaluated from (2.61),

$$\mathrm{SWR}_{\mathrm{m}}]_i = \frac{1 + \frac{\boldsymbol{\Gamma}_{\mathrm{L}}^{\mathrm{m}} \boldsymbol{v}_{\mathrm{m}}^{+}]_i}{\boldsymbol{v}_{\mathrm{m}}^{+}]_i}}{1 - \frac{\boldsymbol{\Gamma}_{\mathrm{L}}^{\mathrm{m}} \boldsymbol{v}_{\mathrm{m}}^{+}]_i}{\boldsymbol{v}_{\mathrm{m}}^{+}]_i}}. \tag{2.62}$$

It will be evident from simulated data plots in Chapter 4 that SWRs of the longitudinal line voltages are not uniform. From (2.15), each line voltage is a linear combination of all modal voltages, each with distinct modal phase constants. Through direct observation of particular modal voltage standing wave at $z = 0$, the sign of the mode's self reflection coefficent may be ascertained. If the termination is purely resistive, a standing wave minimum or maximum will occur exactly at $z = 0$, indicating a negative or postive real reflection coeffient, respectively. As described earlier in this chapter, the modal reflection coefficent matrix self elements $[\boldsymbol{\Gamma}_{\mathrm{L}}^{\mathrm{m}}]_{ii}$ can be cancelled out if each line is terminated by the impedance of the ith mode.

2.4 Power Relations

To quantify power savings with a matching network included we must first obtain voltage or current values as functions along z. The source excitations are given in Thevenin form with line voltage source vector $\boldsymbol{v}_{\mathrm{S}}$ and source admittance matrix $\boldsymbol{Y}_{\mathrm{S}}$.

The modal and line transmission coefficients are obtained from the voltage divider at $z = -D$:

$$\boldsymbol{T}_{\mathrm{S}}^{\mathrm{m}} = \left[\mathbf{1} + \boldsymbol{E}\boldsymbol{Z}_{\mathrm{S}}\boldsymbol{Z}_{\mathrm{ch}}^{-1}\boldsymbol{E}^{-1}\right]^{-1}, \tag{2.63}$$

$$\boldsymbol{T}_{\mathrm{S}}^{\mathrm{c}} = \boldsymbol{Z}_{\mathrm{ch}}^{\mathrm{c}}\left[\boldsymbol{Z}_{\mathrm{ch}}^{\mathrm{c}} + \boldsymbol{Z}_{\mathrm{S}}^{\mathrm{c}}\right]^{-1} \tag{2.64}$$

which can be rewritten in terms of admittance matrices to facilitate computation. Use of the characteristic admittances applies to time domain computations, as in [9]. But under steady-state single-frequency conditions, the admittance looking into the coupled lines toward the load depends on the load reflection coefficient, or an equivalent impedance transformation along the line.

Maximum power is delivered to the load if the nonzero input impedance to the system is equal to the complex conjugate of the source impedance (which in practice is usually 50 Ω). The voltage incident upon the line is

$$\boldsymbol{v}(z = -D) = \boldsymbol{T}_{\mathrm{S}}^{\mathrm{c}} \boldsymbol{v}_{\mathrm{S}} \tag{2.65}$$

from either modal or line voltage and current vectors, incident power upon the coupled line system can be determined from Paul [3, Eqs. (53), (55)]. The orthogonality properties of microstrip lines allow either definition; for simplicity the first (using line quantites $\boldsymbol{v}(z = -D)$, $\boldsymbol{i}(z = -D)$) will be employed here:

$$\mathrm{P}_{\mathrm{inc}} = \frac{1}{2} \Re\mathrm{e}\{\boldsymbol{v}^{\mathrm{T}} \boldsymbol{i}^{*}\}. \tag{2.66}$$

The results are similar to the relations derived by Amari and Bornemann [6], though their terminations and characteristic admittance are considered strictly real, thus the line reflection coefficients are real. In this analysis, we must consider complex reflection coefficient matrices for arbitrary z. Forward travelling power on the system depends on the forward travelling voltage at the load, $\boldsymbol{v}_{\mathrm{m}}^{+}$, found from (2.52). Forward travelling current is determined from Ohm's law using $\boldsymbol{Y}_{\mathrm{m}}$.

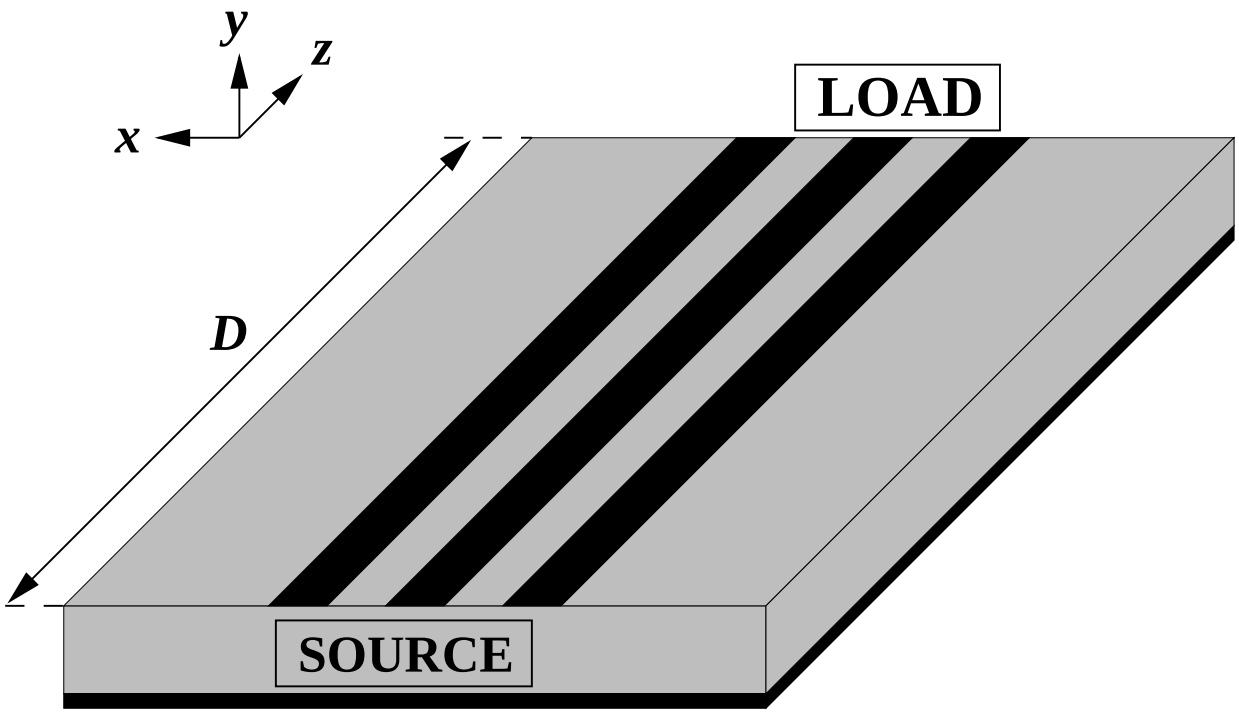

Figure 2.1 Three-coupled line system with source and load planes.

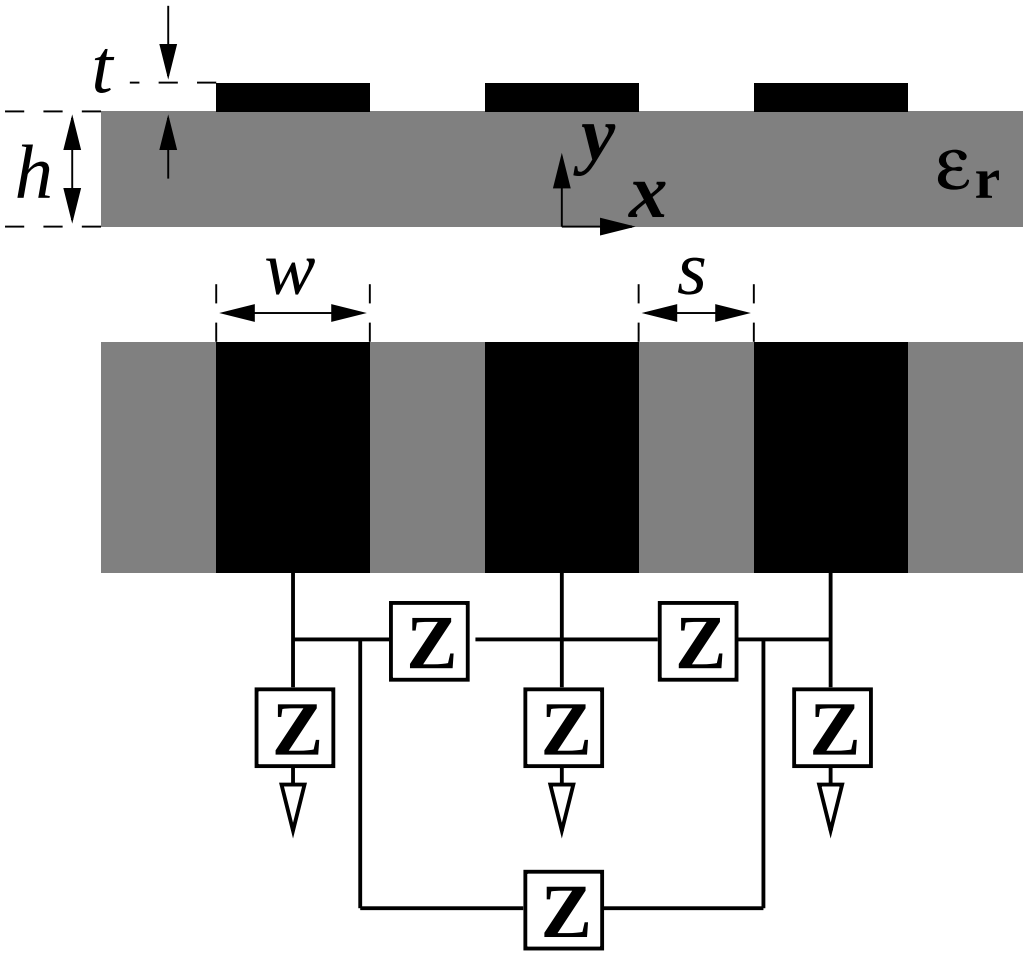

Figure 2.2 Cross-sectional and top view of microstrip structure showing dimensions and geometries. An arbitrary complex load is assumed with the Z network.

CHAPTER 3

GENERAL MTL ANALYSIS AND MODE DELAYS

In inhomogeneous multiconductor transmission line (MTL) systems, the distinct propagation constants result in "mode delays" along the longitudinal direction. The general well-known MTL conductor- and mode-domain formulations that consider mode delays [1], [2], [3], [14], [27], [28], are widely applicable to many microwave problems with moderate to high coupling (e.g., crosstalk prediction). But to our knowledge, no comprehensive study of these MTL quantities as functions of longitudinal distance from a termination or discontinuity has been undertaken. One present motivation for such analysis is MTL matching network synthesis and transistor amplifier design [29].

In this chapter, we will present an investigation that focuses on the longitudinal behavior of the MTL functions, including the signals and longitudinal immittance matrix functions (LIMFs). Past work on MTL immittance matrices has concerned their derivation for fixed length structures [13], [30], [31]. *Immittance* in this chapter implies the impedance, admittance, reflection coefficient, or scattering matrix *looking into a terminated line of some specified length.* In particular, we will address several seemingly problematic effects of the mode delays on these longitudinal MTL functions. For example, consider that lossless, reciprocal, two-conductor transmission lines exhibit several intuitive longitudinal properties: positive resistive and conductive components of input impedances and admittances, and constant reflection coefficient magnitude. However, these properties *do not* generally apply to the matrix and vector elements of the longitudinal MTL functions in steady-state conditions. We will show how the longitudinal conductor admittance matrices (in a passive system) do not necessarily have negative off-diagonal real parts. Similar works have considered the signs of characteristic matrix terms in asymmetric lines [32].

Our principal goal here is to investigate, explain, and validate these effects, so they are not attributed to numerical errors or nonphysical behavior. First, the MTL equations are overviewed briefly. Next, the longitudinal properties of immittance

matrices and signals in symmetric, lossless, reciprocal MTL systems are detailed (we limit this analysis to inhomogeneous, symmetric systems and terminations) for arbitrary, passive, linear termination. The effects of mode delays on all MTL functions is detailed and relevant physical interpretations are drawn. Numerical results from simulation illustrate these effects.

3.1 Multiconductor Transmission Line Equations

Consider the coupled microstrip structure in Fig. 3.1 with an arbitrary number of lines n and $N = n + 1$ conductors where the ground plane is reference. Unless otherwise stated, we assume symmetry about the $x = 0$ plane, and while we focus on the three-line ($n = 3$) case, results are generalized to n lines (excluding the ground plane) where possible. The MTL equations are equivalent to the telegrapher's equations in frequency domain matrix form (sinusoidal, steady-state conditions) for an n-line system, and include the $(n \times n)$ symmetric complex matrices of per-unit-length impedance and admittance $\boldsymbol{Z}$ and $\boldsymbol{Y}$, composed of the Maxwellian per-unit-length resistance, conductance, inductance, and capacitance matrices, $\boldsymbol{R}$, $\boldsymbol{G}$, $\boldsymbol{L}$, and $\boldsymbol{C}$, respectively.

In n-line quasi-TEM analysis, the n propagating modes are interpreted as physical system voltages and currents [1]. The decoupled telegrapher's wave equations are solved with a linear transformation for the state (conductor) and modal variables,

$$\boldsymbol{v}_{\mathrm{m}}(z) = \boldsymbol{E} \cdot \boldsymbol{v}(z) \tag{3.1a}$$

$$\boldsymbol{i}_{\mathrm{m}}(z) = \boldsymbol{H} \cdot \boldsymbol{i}(z) \tag{3.1b}$$

where $\boldsymbol{E}$ and $\boldsymbol{H}$ are $(n \times n)$ transformation matrices which simultaneously diagonalize both $\boldsymbol{Z}$ and $\boldsymbol{Y}$ to uncouple the MTL equations. The n-column vectors $\boldsymbol{v}_{\mathrm{m}}(z)$ and $\boldsymbol{i}_{\mathrm{m}}(z)$ are the modal wave voltage and current vectors along the line. Vectors $\boldsymbol{v}(z)$ and $\boldsymbol{i}(z)$ are the $(n \times 1)$ conductor wave voltage and current vectors, respectively, with z the longitudinal coordinate and $e^{j\omega t}$ suppressed. For microstrip there are generally n distinct eigenvalues, which are complex modal propagation constants $\gamma_{i=1,2,\ldots,n}$ arranged in matrix $\boldsymbol{\Lambda}_{\mathrm{m}}$.

The total modal wave voltage and current vectors in the n-line system are ex-

pressed as the superposition of forward and backward going waves,

$$\boldsymbol{v}_{\mathrm{m}}(z) = \boldsymbol{Q}(-z)\boldsymbol{v}_{\mathrm{m}}^{+} + \boldsymbol{Q}(z)\cdot\boldsymbol{v}_{\mathrm{m}}^{-} \tag{3.2a}$$

$$\boldsymbol{i}_{\mathrm{m}}(z) = \boldsymbol{Q}(-z)\boldsymbol{i}_{\mathrm{m}}^{+} - \boldsymbol{Q}(z)\cdot\boldsymbol{i}_{\mathrm{m}}^{-}, \tag{3.2b}$$

where $\boldsymbol{v}_{\mathrm{m}}^{\pm}$ and $\boldsymbol{i}_{\mathrm{m}}^{\pm}$ are the modal wave coefficient vectors at the load ($z = 0$), and $\boldsymbol{Q}(z)$ is a diagonal matrix whose entries are $e^{\gamma_i z}$, with γ_i denoting the complex propagation constant of the ith mode.

Diagonal modal impedance and admittance matrices are [8], [9]

$$\boldsymbol{Z}_{\mathrm{ch}}^{\mathrm{m}} = \boldsymbol{\Lambda}_{\mathrm{m}}^{-1}\cdot\boldsymbol{E}\cdot\boldsymbol{Z}\cdot\boldsymbol{H}^{-1} = \boldsymbol{E}\cdot\boldsymbol{Y}^{-1}\cdot\boldsymbol{H}^{-1}\cdot\boldsymbol{\Lambda}_{\mathrm{m}} \tag{3.3a}$$

$$\boldsymbol{Y}_{\mathrm{ch}}^{\mathrm{m}} = \boldsymbol{\Lambda}_{\mathrm{m}}^{-1}\cdot\boldsymbol{H}\cdot\boldsymbol{Y}\cdot\boldsymbol{E}^{-1} = \boldsymbol{H}\cdot\boldsymbol{Z}^{-1}\cdot\boldsymbol{E}^{-1}\cdot\boldsymbol{\Lambda}_{\mathrm{m}}, \tag{3.3b}$$

where the ith entry denotes the characteristic impedance or admittance of the ith mode. The characteristic impedance and admittance matrices that relate the conductor voltage and current vectors via Ohm's law are

$$\boldsymbol{Z}_{\mathrm{ch}}^{\mathrm{c}} = \boldsymbol{E}^{-1}\cdot\boldsymbol{\Lambda}_{\mathrm{m}}^{-1}\cdot\boldsymbol{E}\cdot\boldsymbol{Z} = \boldsymbol{Y}^{-1}\cdot\boldsymbol{H}^{-1}\cdot\boldsymbol{\Lambda}_{\mathrm{m}}\cdot\boldsymbol{H} \tag{3.4a}$$

$$\boldsymbol{Y}_{\mathrm{ch}}^{\mathrm{c}} = \boldsymbol{H}^{-1}\cdot\boldsymbol{\Lambda}_{\mathrm{m}}^{-1}\cdot\boldsymbol{H}\cdot\boldsymbol{Y} = \boldsymbol{Z}^{-1}\cdot\boldsymbol{E}^{-1}\cdot\boldsymbol{\Lambda}_{\mathrm{m}}\cdot\boldsymbol{E}, \tag{3.4b}$$

where the superscript c denotes *conductor*.

3.1.1 The terminated MTL structure

Now suppose an extent of coupled lines is terminated with a passive, linear circuit network comprised of unique impedances interconnecting each of the N conductors in a common-ground topology at the termination plane $z = 0$ as illustrated in Fig. 3.2. This entire termination network may be conveniently grouped in an $(n\times n)$ impedance network matrix $[\boldsymbol{\mathcal{Z}}_{\mathrm{L}}]$. The diagonal term $[\boldsymbol{\mathcal{Z}}_{\mathrm{L}}]_{ii}$ represents the impedance connecting line i to ground; the off-diagonal term $[\boldsymbol{\mathcal{Z}}_{\mathrm{L}}]_{ij}$ represents the impedance connecting lines i and j, as illustrated in Fig. 3.2. A dual admittance network matrix $\boldsymbol{\mathcal{Y}}_{\mathrm{L}}$ may also be defined as the term-by-term reciprocal of the impedance network matrix,

$$[\boldsymbol{\mathcal{Y}}_{\mathrm{L}}]_{ij} = \left([\boldsymbol{\mathcal{Z}}_{\mathrm{L}}]_{ij}\right)^{-1}. \tag{3.5}$$

Note that these network matrices have little mathematical meaning ($[\boldsymbol{\mathcal{Y}}_{\mathrm{L}}] \neq [\boldsymbol{\mathcal{Z}}_{\mathrm{L}}]^{-1}$); they are merely compact physical representations of circuit networks, hence the calligraphic denotation.

To analyze reflections on a general coupled line system like Fig. 3.3 (a specific three-line system which will be considered in the numerical results) the termination networks must be expressed as $(n \times n)$ open-circuit impedance or short-circuit admittance matrices. We denote these as $\boldsymbol{Z}_{\mathrm{L}}^{\mathrm{c}}$ and $\boldsymbol{Y}_{\mathrm{L}}^{\mathrm{c}}$ ($[\boldsymbol{Z}_{\mathrm{L}}^{\mathrm{c}}] = [\boldsymbol{Y}_{\mathrm{L}}^{\mathrm{c}}]^{-1}$). Values for

the termination matrices are easily calculated by first determining the conductor admittance matrix from the interconnecting circuit impedances using the well-known admittance matrix relations:

$$[\boldsymbol{Y}_{\mathrm{L}}^{\mathrm{c}}]_{ii} = \sum_{k=1}^{n} \left([\boldsymbol{\mathcal{Z}}_{\mathrm{L}}]_{ik}\right)^{-1}, \qquad i = 1, 2, \ldots, n \tag{3.6a}$$

$$[\boldsymbol{Y}_{\mathrm{L}}^{\mathrm{c}}]_{ij} = \left(-[\boldsymbol{\mathcal{Z}}_{\mathrm{L}}]_{ij}\right)^{-1}, \qquad i \neq j. \tag{3.6b}$$

$$\tag{3.6c}$$

The conductor reflection coefficient at the load that relates the conductor voltage vectors $\boldsymbol{v}^+$ to $\boldsymbol{v}^-$ by

$$\boldsymbol{v}^- = \boldsymbol{\Gamma}_{\mathrm{L}}^{\mathrm{c}} \cdot \boldsymbol{v}^+ \tag{3.7}$$

is expressed in several forms, and is usually derived from boundary conditions [3], [29], [33], as

$$\boldsymbol{\Gamma}_{\mathrm{L}}^{\mathrm{c}} = \boldsymbol{Z}_{\mathrm{ch}}^{\mathrm{c}} \cdot [\boldsymbol{Z}_{\mathrm{L}}^{\mathrm{c}} + \boldsymbol{Z}_{\mathrm{ch}}^{\mathrm{c}}]^{-1} \cdot [\boldsymbol{Z}_{\mathrm{L}}^{\mathrm{c}} - \boldsymbol{Z}_{\mathrm{ch}}^{\mathrm{c}}] \cdot \boldsymbol{Y}_{\mathrm{ch}}^{\mathrm{c}} \tag{3.8a}$$

$$= [\boldsymbol{Z}_{\mathrm{L}}^{\mathrm{c}} - \boldsymbol{Z}_{\mathrm{ch}}^{\mathrm{c}}] \cdot [\boldsymbol{Z}_{\mathrm{L}}^{\mathrm{c}} + \boldsymbol{Z}_{\mathrm{ch}}^{\mathrm{c}}]^{-1} \tag{3.8b}$$

$$= [\boldsymbol{Y}_{\mathrm{ch}}^{\mathrm{c}} + \boldsymbol{Y}_{\mathrm{L}}^{\mathrm{c}}]^{-1} \cdot [\boldsymbol{Y}_{\mathrm{ch}}^{\mathrm{c}} - \boldsymbol{Y}_{\mathrm{L}}^{\mathrm{c}}], \tag{3.8c}$$

Term $[\boldsymbol{\Gamma}_{\mathrm{L}}^{\mathrm{c}}]_{ij}$ is the ratio of the backward-traveling voltage on conductor i to the forward-traveling voltage on conductor j. The modal reflection coefficient at the load which relates modal voltage vectors $\boldsymbol{v}_{\mathrm{m}}^+$ to $\boldsymbol{v}_{\mathrm{m}}^-$ is easily found using (3.1) and (3.2) evaluated at $z = 0$:

$$\boldsymbol{\Gamma}_{\mathrm{L}}^{\mathrm{m}} = \boldsymbol{Z}_{\mathrm{ch}}^{\mathrm{m}} \cdot [\boldsymbol{Z}_{\mathrm{L}}^{\mathrm{m}} + \boldsymbol{Z}_{\mathrm{ch}}^{\mathrm{m}}]^{-1} \cdot [\boldsymbol{Z}_{\mathrm{L}}^{\mathrm{m}} - \boldsymbol{Z}_{\mathrm{ch}}^{\mathrm{m}}] \cdot \boldsymbol{Y}_{\mathrm{ch}}^{\mathrm{m}} \tag{3.9a}$$

$$= [\boldsymbol{Z}_{\mathrm{L}}^{\mathrm{m}} - \boldsymbol{Z}_{\mathrm{ch}}^{\mathrm{m}}] \cdot [\boldsymbol{Z}_{\mathrm{L}}^{\mathrm{m}} + \boldsymbol{Z}_{\mathrm{ch}}^{\mathrm{m}}]^{-1} \tag{3.9b}$$

$$= [\boldsymbol{Y}_{\mathrm{ch}}^{\mathrm{m}} + \boldsymbol{Y}_{\mathrm{L}}^{\mathrm{m}}]^{-1} \cdot [\boldsymbol{Y}_{\mathrm{ch}}^{\mathrm{m}} - \boldsymbol{Y}_{\mathrm{L}}^{\mathrm{m}}], \tag{3.9c}$$

where $\boldsymbol{Y}_{\mathrm{L}}^{\mathrm{m}}$ is the modal admittance matrix at the load,

$$\boldsymbol{Y}_{\mathrm{L}}^{\mathrm{m}} = \boldsymbol{H} \cdot \boldsymbol{Y}_{\mathrm{L}}^{\mathrm{c}} \cdot \boldsymbol{E}^{-1}. \tag{3.10}$$

Similarly, the term $[\boldsymbol{\Gamma}_{\mathrm{L}}^{\mathrm{m}}]_{ij}$ is the ratio of the backward-traveling mode voltage i to the forward-traveling mode voltage j. Since the remainder of this paper focuses on admittance matrices, the admittance forms (3.8c) and (3.9c) will be utilized in admittance matrix passivity and realizability discussions, while the impedance forms are useful in deriving S-parameters.

Both reflection coefficient matrices are asymmetric in general, even for symmetric lines and terminations. However, this structural symmetry leads to several simplifications. Matrix $\boldsymbol{\Gamma}_{\mathrm{L}}^{\mathrm{m}}$ contains $[n/2]$ zeros (where brackets denote integer part) for

terms whose indices are related by

$$(i-j) \bmod 2 = 1, \tag{3.11}$$

for symmetric terminations [29]. This is a consequence of the line-termination symmetry, which prevents incident even modes from exciting reflected odd modes, and vice versa. Matrix $\mathbf{\Gamma}_{\mathrm{L}}^{\mathrm{c}}$ does possess some symmetry (if symmetric terminations are assumed), namely,

$$[\mathbf{\Gamma}_{\mathrm{L}}^{\mathrm{c}}]_{i,j} = [\mathbf{\Gamma}_{\mathrm{L}}^{\mathrm{c}}]_{n-i+1,n-j+1}. \tag{3.12}$$

This property follows from the assumption that the n lines are symmetric about the $x = 0$ plane. The asymmetry about the diagonal of the conductor reflection coefficient does not violate reciprocity of the system, as will be shown shortly.

A conductor current reflection coefficient matrix $[\mathbf{\Gamma}_{\mathrm{L}}^{\mathrm{c}}]^{cur}$ may be defined to relate the conductor current vectors $\boldsymbol{i}^{+}$ to $\boldsymbol{i}^{-}$. This matrix may be derived directly from boundary conditions (as was $[\mathbf{\Gamma}_{\mathrm{L}}^{\mathrm{c}}]^{vol}$), or directly from $[\mathbf{\Gamma}_{\mathrm{L}}^{\mathrm{c}}]^{vol}$,

$$[\mathbf{\Gamma}_{\mathrm{L}}^{\mathrm{c}}]^{cur} = \boldsymbol{Y}_{\mathrm{ch}}^{\mathrm{c}} \cdot [\mathbf{\Gamma}_{\mathrm{L}}^{\mathrm{c}}]^{vol} \cdot \boldsymbol{Z}_{\mathrm{ch}}^{\mathrm{c}} \tag{3.13a}$$

$$= [\boldsymbol{Z}_{\mathrm{L}}^{\mathrm{c}} + \boldsymbol{Z}_{\mathrm{ch}}^{\mathrm{c}}]^{-1} \cdot [\boldsymbol{Z}_{\mathrm{L}}^{\mathrm{c}} - \boldsymbol{Z}_{\mathrm{ch}}^{\mathrm{c}}] \tag{3.13b}$$

$$= [\boldsymbol{Y}_{\mathrm{L}}^{\mathrm{c}} + \boldsymbol{Y}_{\mathrm{ch}}^{\mathrm{c}}] \cdot [\boldsymbol{Y}_{\mathrm{ch}}^{\mathrm{c}} - \boldsymbol{Y}_{\mathrm{L}}^{\mathrm{c}}]^{-1} \tag{3.13c}$$

which is easily proven to be the transpose (superscript t; see Appendix A) of the conductor voltage reflection coefficient matrix:

$$[\mathbf{\Gamma}_{\mathrm{L}}^{\mathrm{c}}]_i = ([\mathbf{\Gamma}_{\mathrm{L}}^{\mathrm{c}}]_v)^t, \tag{3.14}$$

a fact easily shown using power relations or through direct boundary condition derivation (we highlight that this result differs in sign from [3] simply by convention). However, in consideration of only the conductor voltage reflection coefficient for the remainder of this chapter, the superscript is dropped for simplicity.

3.1.2 The longitudinal MTL functions

In the context of matching coupled transmission lines, the reflection coefficient functions of z must be calculated. This requires the n quasi-TEM propagation constants. As a function of longitudinal distance z, the modal reflection coefficient matrix looking toward the load is

$$\mathbf{\Gamma}_{\mathrm{in}}^{\mathrm{m}}(z) = \boldsymbol{Q}(z) \cdot \mathbf{\Gamma}_{\mathrm{L}}^{\mathrm{m}} \cdot \boldsymbol{Q}(z), \tag{3.15}$$

and the conductor reflection coefficient matrix is

$$\mathbf{\Gamma}_{\mathrm{in}}^{\mathrm{c}}(z) = \boldsymbol{E}^{-1} \cdot \mathbf{\Gamma}_{\mathrm{in}}^{\mathrm{m}}(z) \cdot \boldsymbol{E}. \tag{3.16}$$

At an arbitrary point $z = -a$, either matrix may be converted to an admittance matrix which, if realized and constructed, would terminate the lines at $z = -a$ with an N-node, n-port, common-ground passive circuit as in Fig. 3.4 and would provide the equivalent immittance parameters of the coupled-line section of length a between the observation point and the termination shown in Fig. 3.3.

The impedance and admittance matrices as functions of z are compactly expressed [3], [5], [6], [33], in modal form as

$$\boldsymbol{Z}^{\mathrm{m}}_{\mathrm{in}}(z) = [\mathbf{1}_n - \boldsymbol{\Gamma}^{\mathrm{m}}_{\mathrm{in}}(z)]^{-1} \cdot [\mathbf{1}_n + \boldsymbol{\Gamma}^{\mathrm{m}}_{\mathrm{in}}(z)] \cdot \boldsymbol{Z}^{\mathrm{m}}_{\mathrm{ch}} \tag{3.17}$$

$$\boldsymbol{Y}^{\mathrm{m}}_{\mathrm{in}}(z) = \boldsymbol{Y}^{\mathrm{m}}_{\mathrm{ch}} \cdot [\mathbf{1}_n + \boldsymbol{\Gamma}^{\mathrm{m}}_{\mathrm{in}}(z)]^{-1} \cdot [\mathbf{1}_n - \boldsymbol{\Gamma}^{\mathrm{m}}_{\mathrm{in}}(z)]\,, \tag{3.18}$$

and in conductor form as

$$\boldsymbol{Z}^{\mathrm{c}}_{\mathrm{in}}(z) = [\mathbf{1}_n - \boldsymbol{\Gamma}^{\mathrm{c}}_{\mathrm{in}}(z)]^{-1} \cdot [\mathbf{1}_n + \boldsymbol{\Gamma}^{\mathrm{c}}_{\mathrm{in}}(z)] \cdot \boldsymbol{Z}^{\mathrm{c}}_{\mathrm{ch}} \tag{3.19}$$

$$\boldsymbol{Y}^{\mathrm{c}}_{\mathrm{in}}(z) = \boldsymbol{Y}^{\mathrm{c}}_{\mathrm{ch}} \cdot [\mathbf{1}_n + \boldsymbol{\Gamma}^{\mathrm{c}}_{\mathrm{in}}(z)]^{-1} \cdot [\mathbf{1}_n - \boldsymbol{\Gamma}^{\mathrm{c}}_{\mathrm{in}}(z)]\,. \tag{3.20}$$

Impedance network matrices corresponding to the longitudinal input impedance and admittance functions are extensions of (3.6):

$$[\boldsymbol{\mathcal{Z}}_{\mathrm{in}}(z)]_{ii} = \left(\sum_{k=1}^{n} [\boldsymbol{Y}^{\mathrm{c}}_{\mathrm{in}}(z)]_{ik}\right)^{-1}, \quad i = 1, 2, \cdots, n$$

$$[\boldsymbol{\mathcal{Z}}_{\mathrm{in}}(z)]_{ij} = \left(-[\boldsymbol{Y}^{\mathrm{c}}_{\mathrm{in}}(z)]_{ij}\right)^{-1}, \quad i \neq j \tag{3.21a}$$

$$[\boldsymbol{\mathcal{Y}}_{\mathrm{in}}(z)]_{ij} = \left([\boldsymbol{\mathcal{Z}}_{\mathrm{in}}(z)]_{ij}\right)^{-1}, \quad \text{all } i, j. \tag{3.21b}$$

3.1.3 Asymmetry and reciprocity in MTL systems

One may easily show that $\boldsymbol{Z}^{\mathrm{c}}_{\mathrm{in}}(z)$ and $\boldsymbol{Y}^{\mathrm{c}}_{\mathrm{in}}(z)$ are symmetric in reciprocal systems. Despite the symmetry of the terms in (3.8b), these factors do not necessarily commute, resulting in general asymmetry of the reflection coefficient matrices. Physically, a voltage on line i incident upon a symmetric termination does not "see" the same circuit as an incident voltage on line j; hence, the reflected signal on line j due to the incident signal on line i does not relate in a simple manner to the reflected signal on line j due to the incident signal on line i.

However, this property has no bearing on reciprocity since it does not relate electromagnetic reactions. Instead, we must consider symmetry of the $(n \times n)$ input conductor S-parameter matrix $\boldsymbol{S}^{\mathrm{c}}_{\mathrm{in}}(z)$ (referenced to impedance $\boldsymbol{Z}^{\mathrm{c}}_{\mathrm{ch}}$), which relates the longitudinal power waves $\boldsymbol{a}^{\mathrm{c}}(z)$ and $\boldsymbol{b}^{\mathrm{c}}(z)$ by $\boldsymbol{b}^{\mathrm{c}}_{\mathrm{in}}(z) = \boldsymbol{S}^{\mathrm{c}}_{\mathrm{in}}(z) \cdot \boldsymbol{a}^{\mathrm{c}}_{\mathrm{in}}(z)$. In general, $\boldsymbol{\Gamma}^{\mathrm{c}}_{\mathrm{in}}(z)$ and $\boldsymbol{S}^{\mathrm{c}}_{\mathrm{in}}(z)$ of the n-port at z are not equivalent (the exception being for

diagonal $\boldsymbol{Z}^{\mathrm{c}}_{\mathrm{ch}}$ with all diagonal terms equal). Matrix $\boldsymbol{S}^{\mathrm{c}}_{\mathrm{in}}(z)$ is derived from (3.8) and the power wave normalizations

$$\boldsymbol{S}^{\mathrm{c}} = (\boldsymbol{Z}^{\mathrm{c}}_{\mathrm{ch}})^{1/2} \cdot [\boldsymbol{Z}^{\mathrm{c}}_{\mathrm{ch}} + \boldsymbol{Z}^{\mathrm{c}}_{\mathrm{L}}]^{-1} \cdot [\boldsymbol{Z}^{\mathrm{c}}_{\mathrm{L}} - \boldsymbol{Z}^{\mathrm{c}}_{\mathrm{ch}}] \cdot (\boldsymbol{Z}^{\mathrm{c}}_{\mathrm{ch}})^{-1/2}. \tag{3.22}$$

By reciprocity, an excitation of a_1 on port 1 is scaled by S_{21} to produce b_2 on port 2; an excitation of a_2 on port 2 is scaled by S_{12} to produce b_1 on port 1. Even for dense $\boldsymbol{Z}^{\mathrm{c}}_{\mathrm{ch}}$, $\boldsymbol{S}$ is symmetric and therefore reciprocal (see Appendix).

This result is now applicable to immittance matrices of terminated MTL systems, where the conductor voltages and currents are related by dense characteristic impedance and admittance matrices. Now, the set of n ports looking toward the load at $z = -a$ is really an infinitesimal section of coupled lines (zero phase, zero loss) with an equivalent characteristic impedance matrix as the substituted section of length a. This "port coupling" is illustrated in Fig. 3.4.

Note that the asymmetrical longitudinal transmission coefficient matrix, defined as

$$\boldsymbol{T}^{\mathrm{c}}_{\mathrm{in}}(z) = \mathbf{1}_n + \boldsymbol{\Gamma}^{\mathrm{c}}_{\mathrm{in}}(z). \tag{3.23}$$

does not account for this distribution. If $\boldsymbol{\Gamma}^{\mathrm{c}}_{\mathrm{in}}(-a) = \mathbf{0}$, then $\boldsymbol{T}^{\mathrm{c}}_{\mathrm{in}}(-a) = \mathbf{1}_n$, which effectively propagates the voltage signals already on the line an infinitesimal distance δz in the positive z direction from $z = -a$. Matrix $\boldsymbol{T}^{\mathrm{c}}_{\mathrm{in}}(z)$ cannot account for any coupling or its resultant physics (dispersion, distortion, etc.) represented in the equivalent passive circuit beyond $z = -a$.

3.2 Mode Delay Effects

At this point, we have derived the immittance matrices necessary for the discussion on modal dispersion effects. Recall several obvious properties of lossless, passive transmission line systems: power conservation, passivity (no active sources), and the ability to realize the immittance parameters of terminated lines as passive circuit networks. Mathematically, the immittance parameters are constrained by

$$V(z) = V(z - i\frac{\lambda}{2}), \quad z < 0, \quad i = 1, 2, 3, \ldots \tag{3.24a}$$

$$P(z) = P_{\mathrm{L}}, \tag{3.24b}$$

$$\frac{\partial}{\partial z}|\Gamma| = 0, \tag{3.24c}$$

$$\Re\mathrm{e}\{Z, Y\} \geq 0. \tag{3.24d}$$

However, in MTL systems, the immittance matrix behavior is considerably more complicated. This section illustrates that conditions (3.24) do not unilaterally apply to their MTL conductor matrix equivalents.

3.2.1 Signal distortion

Longitudinal modal voltage is the superposition of the forward and backward traveling modal voltages; the modal voltage in (3.2a) may be combined with (3.15) and expressed as:

$$\begin{aligned}\boldsymbol{v}_m(z) &= \boldsymbol{Q}(-z)\cdot\boldsymbol{v}_m^+ + \boldsymbol{Q}(z)\cdot\boldsymbol{\Gamma}_{\mathrm{L}}^{\mathrm{m}}\cdot\boldsymbol{Q}(z)\cdot\boldsymbol{Q}(-z)\cdot\boldsymbol{v}_{\mathrm{m}}^+ \\ &= [\mathbf{1}_n + \boldsymbol{\Gamma}_{\mathrm{in}}^{\mathrm{m}}(z)]\cdot\boldsymbol{Q}(-z)\cdot\boldsymbol{v}_{\mathrm{m}}^+, \end{aligned} \tag{3.25}$$

where modal decoupling results in constant modal voltage SWRs along the line.

Mode voltage i from (3.25) is given by

$$\boldsymbol{v}_{\mathrm{m}}(z)]_i = [\boldsymbol{Q}(-z)]_{ii}\,\boldsymbol{v}_{\mathrm{m}}^+]_i\left(1+\frac{\boldsymbol{Q}(2z)\boldsymbol{\Gamma}_{\mathrm{L}}^{\mathrm{m}}\boldsymbol{v}_{\mathrm{m}}^+]_i}{\boldsymbol{v}_{\mathrm{m}}^+]_i}\right). \tag{3.26}$$

The SWR of the ith mode is therefore [33]

$$\mathrm{SWR}_{\mathrm{m}}]_i = \frac{1+\left|\dfrac{\boldsymbol{\Gamma}_{\mathrm{L}}^{\mathrm{m}}\boldsymbol{v}_{\mathrm{m}}^+]_i}{\boldsymbol{v}_{\mathrm{m}}^+]_i}\right|}{1-\left|\dfrac{\boldsymbol{\Gamma}_{\mathrm{L}}^{\mathrm{m}}\boldsymbol{v}_{\mathrm{m}}^+]_i}{\boldsymbol{v}_{\mathrm{m}}^+]_i}\right|}. \tag{3.27}$$

Clearly, (3.27) confirms the constant longitudinal magnitudes of the modal reflection coefficient for lossless coupled lines. The terms $\boldsymbol{\Gamma}_{\mathrm{L}}^{\mathrm{m}}\boldsymbol{v}_{\mathrm{m}}^+]_i/\boldsymbol{v}_{\mathrm{m}}^+]_i$ in (3.26) and (3.27) indicate the general dependence of the ith mode on all n forward voltage coefficients at the load $\boldsymbol{v}_{\mathrm{m}}^+$ and the ith row of $\boldsymbol{\Gamma}_{\mathrm{L}}^{\mathrm{m}}$. This dependency is a physical result of mode conversion at a discontinuity. A significant consequence of this dependence is the fact that a purely real (resistive) load termination network will not necessarily result in a modal standing wave minimum or maximum at $z = 0$, unless all modes have equal propagation constants.

However, the standing wave patterns may be useful if one wishes to characterize terminations for short lines – where the modal dispersion is relatively small – as "high" or "low" impedance based on voltage maxima or minima at $z = 0$. But at present, we know of no systematic analytic evaluation available to ascertain the sign of the modal reflection coefficent terms.

As for the longitudinal conductor voltages and currents, it is evident from (3.26) that their SWRs are not uniform, since each is a linear combination (3.1) of all modal

voltages or currents, respectively. Therefore, a definition of line $\mathrm{SWR_c}$ along lossless coupled lines would only apply to successive maxima and minima.

Power along the coupled lines may be quantified in either the modal or state variable domain for microstrip [3, Eqs. (53) and (55)]. Excitations are represented in Thevenin form with a line voltage source vector $\boldsymbol{v}_\mathrm{S}$ and source impedance network matrix $\boldsymbol{\mathcal{Z}}_\mathrm{S}$. The total power traveling down a lossless line is a constant equal to the power dissipated in the arbitrary passive load,

$$P_\mathrm{L} = P(z) = \frac{1}{2}\Re\mathrm{e}\{\boldsymbol{v}^*(z)\cdot\boldsymbol{i}(z)\} \tag{3.28a}$$

$$= \frac{1}{2}\Re\mathrm{e}\{\boldsymbol{v}_\mathrm{m}^*(z)\cdot\boldsymbol{i}_\mathrm{m}(z)\}, \tag{3.28b}$$

where the superscript asterisk denotes "complex conjugate transpose."

To examine longitudinal dependence, (3.28b) is rewritten as

$$P_\mathrm{L} = P(z) = \frac{1}{2}\Re\mathrm{e}\{(\boldsymbol{v}^+)^*\cdot\boldsymbol{i}^+ - (\boldsymbol{v}^-)^*\cdot\boldsymbol{i}^-,\} \tag{3.29}$$

predicting that the individual mode powers in (3.28b) are constants in z. However, expanding (3.28a) into the sum of n terms as functions of the mode voltages, eigenvectors, and propagators reveals the conductor power fluctuations along the longitudinal direction, a result quite different from the single transmission line case (3.24b).

The total power is the sum of the powers incident on each conductor or the sum of the n modal powers. Despite the individual conductor power variations along z, the sum of n conductor powers is always P_L.

3.2.2 Power conservation of the reflection coefficient matrices

Now, we examine the features of the longitudinal reflection coefficient matrix functions. In lossless, uniform, dispersionless coupled-line systems, the magnitude of the modal reflection coefficient elements remains constant along z,

$$\frac{\partial}{\partial z}|[\boldsymbol{\Gamma}_\mathrm{in}^\mathrm{c}(z)]_{ij}| = 0, \tag{3.30}$$

and the phase is linear within each period. This fact is consistent with the power orthogonality of the quasi-TEM modes, and will be clearly demonstrated via numerical simulations in Section IV.

However, Equation (3.16) shows that each term of $\boldsymbol{\Gamma}_\mathrm{in}^\mathrm{c}(z)$ is a linear combination of n^2 distinct z-varying phasors which include *all* propagation constants γ_i. Therefore, the magnitudes of matrix terms $[\boldsymbol{\Gamma}_\mathrm{in}^\mathrm{c}(z)]_{ij}$ clearly vary with z.

For lossless lines with symmetric $\boldsymbol{Y}_\mathrm{L}^\mathrm{c}$, $\boldsymbol{\Gamma}_\mathrm{L}^\mathrm{m}$ and $\boldsymbol{\Gamma}_\mathrm{in}^\mathrm{m}(z)$ are "checkered" with zeros; in this case each term in $\boldsymbol{\Gamma}_\mathrm{in}^\mathrm{c}(z)$ contains the sum of $\frac{1}{4}\left[n^2 + 2n + (n \bmod 2)\right]$ distinct

constant magnitude phasors containing separate even-mode and odd-mode additive combinations of γ_i: $2\gamma_1$, $\gamma_1+\gamma_3$, $\gamma_1+\gamma_5$, ... $2\gamma_2$, $\gamma_2+\gamma_4$, ... A total period for the oscillations of each $\boldsymbol{\Gamma}^{\mathrm{c}}_{\mathrm{in}}(z)$ term may also be defined if each eigenvalue is quantized to $m\Delta k$, where Δk is some small propagation constant increment.

Does the longitudinal magnitude variation of $[\boldsymbol{\Gamma}^{\mathrm{c}}_{\mathrm{in}}(z)]_{ij}$ violate conservation of power? From physical intuition, lossless, passive lines should neither dissipate nor generate power; therefore, power should be conserved. It follows for such lines that the eigenvalues are purely imaginary, thus

$$|\mathrm{d}et[\boldsymbol{Q}(z)]| = 1. \tag{3.31}$$

Since a similar argument applies to the remaining matrices in (3.16), the linear algebra determinant relationship $\det(\boldsymbol{AB}\ldots\boldsymbol{C}) = \det(\boldsymbol{A})\cdot\det(\boldsymbol{B})\cdot\ldots\cdot\det(\boldsymbol{C})$, confirms that

$$\frac{\partial}{\partial z}(\det[\boldsymbol{\Gamma}^{\mathrm{c}}_{\mathrm{in}}(z)]) = 0 \tag{3.32}$$

clearly maintains a constant determinant over z assuming no active power sources are present in the coupled lines. This result is physically intuitive for lossless lines: no power is gained or lost in the longitudinal direction.

For practical applications, close proximity ($z < \lambda/2$) between the matching networks and the load is often desired. In this region of small coupling length, $\boldsymbol{\Gamma}^{\mathrm{c}}_{\mathrm{in}}(z)$ terms maintain approximately constant magnitude. However, as the length or coupling in the lossless system increases, a mixed-mode signal suffers distortion. It remains as future work to determine conditions when signal distortion due to modal dispersion dominates the dispersion encountered in a lossy dielectric system.

3.2.3 Passivity of the admittance matrix

The magnitude variations in $\boldsymbol{\Gamma}^{\mathrm{c}}_{\mathrm{in}}(z)$ for lossless lines also manifest themselves in an arguably more interesting effect. Given many passive terminations, these fluctuations in $|[\boldsymbol{\Gamma}^{\mathrm{c}}_{\mathrm{in}}(z)]|_{ij}$ result in equivalent admittance matrices with negative real admittance elements. If the admittance matrix $\boldsymbol{Y}^{\mathrm{c}}_{\mathrm{in}}(z)$ contains off-diagonal elements with positive real parts, then the equivalent impedance or admittance network matrix that realizes the mutual impedances or admittances will contain negative real parts, i.e.,

$$\Re\mathrm{e}\{[\boldsymbol{\mathcal{Z}}_{\mathrm{in}}(z)]_{ij}, [\boldsymbol{\mathcal{Y}}_{\mathrm{in}}(z)]_{ij}\} < 0, \quad i \neq j, \tag{3.33}$$

which appears to violate passivity and suggests some active power source.

Intuitively, this "active" effect seems a consequence of the reflection coefficient magnitude variations, but can be mathematically justified in a brief example. Consider a symmetric two-line ($n = 2$) system with some arbitrary symmetric termination. The condition which yields (3.33) is easily shown to be:

$$\Re\mathrm{e}\{\frac{-2[\boldsymbol{\Gamma}^{\mathrm{c}}_{\mathrm{in}}(z)]_{12}[\boldsymbol{Y}^{\mathrm{c}}_{\mathrm{ch}}]_{11}[\boldsymbol{Y}^{\mathrm{c}}_{\mathrm{ch}}]_{12}\,(1-[\boldsymbol{\Gamma}^{\mathrm{c}}_{\mathrm{in}}(z)]^2_{11}+[\boldsymbol{\Gamma}^{\mathrm{c}}_{\mathrm{in}}(z)]^2_{12})}{(1+[\boldsymbol{\Gamma}^{\mathrm{c}}_{\mathrm{in}}(z)]_{11})^2-[\boldsymbol{\Gamma}^{\mathrm{c}}_{\mathrm{in}}(z)]^2_{12}}\} > 0. \tag{3.34}$$

Given the large magnitude fluctuations (with simulation results presented in Section 3.2.4), it is clearly conceivable that this "active" effect (3.33) may occur in this situation. For $n \geq 3$, the analysis grows considerably more complicated, and numerical evaluations become necessary. However, in typical systems, this condition may be satisfied at many points along the lines, as will be demonstrated in Section 3.4.

Despite this superficially "active" result, there is no physical reason to suspect that the passivity of the admittance matrix at the points in question is violated. In fact, the passivity is easily verified considering the following derivation. The $(n \times n)$ admittance matrix at some longitudinal coordinate z represents a passive network if the total average signal power entering all the ports is greater than or equal to zero. Let the input admittance matrix $\boldsymbol{Y}^{\mathrm{c}}_{\mathrm{in}}(z)$ describe the n-dimensional driving-point short-circuit admittance matrix looking into an imaginary n-port which constitutes the load impedance at the end of a coupled-line segment of length z. The power entering these n ports is a generalization of the derivation in [34]:

$$P = \frac{1}{2}\boldsymbol{v}^* \cdot \boldsymbol{i} + \frac{1}{2}\boldsymbol{i}^* \cdot \boldsymbol{v}. \tag{3.35}$$

Using the general relations $\boldsymbol{i} = \boldsymbol{Y}\boldsymbol{v}$ and $\boldsymbol{i}^* = \boldsymbol{v}^*\boldsymbol{Y}^*$ (3.35) becomes

$$\begin{aligned} P &= \frac{1}{2}\boldsymbol{v}^* \cdot (\boldsymbol{Y} + \boldsymbol{Y}^*) \cdot \boldsymbol{v} \\ &= \boldsymbol{v}^* \cdot (\Re\mathrm{e}\{\boldsymbol{Y}\}) \cdot \boldsymbol{v} \end{aligned} \tag{3.36}$$

as a consequence of reciprocity. Therefore, the passivity of the admittance matrix $\boldsymbol{Y}^{\mathrm{c}}_{\mathrm{in}}(z)$ may be easily verified by checking the positive definiteness of the immittance function $\Re\mathrm{e}\{\boldsymbol{Y}^{\mathrm{c}}_{\mathrm{in}}(z)\}$ for all z. Simulation results for the three-line case will be shown in the next section.

3.2.4 Realizability of the admittance matrix

While we have justified the "active" result (3.33) mathematically via a simple two-line case (3.34), and subsequently provided a passivity check via (3.36), realization of the conductor admittance matrix must now be considered in the context of purely

passive systems. We therefore digress to consider the realizability conditions of an arbitrary short-circuit admittance matrix. In other words, can such an admittance matrix be realized with a passive system at a point z?

In lossless lines, the distributed admittance matrix and the propagation constants (eigenvalues) are purely imaginary. The distributed capacitance matrix $\boldsymbol{C}$ is a dominant matrix [35]; i.e.,

$$|[\boldsymbol{C}]_{kk}| \geq \sum_{m=1, m\neq k}^{n} |[\boldsymbol{C}]_{km}| \qquad k = 1, 2, \cdots, n, \tag{3.37}$$

which renders the characteristic impedance and admittance matrices real and dominant by virtue of (3.4).

In network synthesis, an $(n \times n)$ dominant real admittance matrix may be realized as a resistive/conductive network consisting of, in general, $2n$ nodes [26]. Furthermore, if all off-diagonal terms of this matrix are nonpositive, then a resistive/conductive network of N terminals (i.e., N nodes with one node designated the common ground to which all n ports are referenced) may be synthesized [26, Theorem 8-4] with the real parts of the impedance/admittance network matrices (3.21).

It follows for physical realization of a reflectionless termination or simulation of an infinite extent of uniform coupled lines that the termination matrix must be real, symmetric, and positive definite, and it must have positive diagonal elements and negative off-diagonal elements *in order to be realized as an* N*-terminal network consisting only of resistors.*

Thus, a uniform coupled-line system characterized by $\boldsymbol{Y}^{\mathrm{c}}_{\mathrm{ch}}$ may be terminated at any z by realizing $\boldsymbol{Y}^{\mathrm{c}}_{\mathrm{ch}}$ as an N-terminal resistive network (with the N-node network common ground connected to the microstrip ground plane) to yield zero reflection for all excitations.

However, when the terminations are mismatched, reflection is nonzero and the immittance matrices become longitudinal matrix functions. Furthermore, in consideration of reactive terminations, the simple realizability conditions applicable to characteristic terminations for lossless lines (i.e., when $\boldsymbol{Y}^{\mathrm{c}}_{\mathrm{ch}}$ is purely real) must be generalized to complex immittance matrices. We reiterate that the complex input impedance or admittance matrix does not physically represent loss in the conductors or dielectric. Instead, either matrix for a purely real (resistive) or purely imaginary (reactive) termination becomes complex as the observation point $z = -a$ shifts along

the lines.

To extend Theorem 8-4 [26]to the complex case, the admittance matrix is split into real and imaginary parts. The equivalent network topology of the microstrip configuration under quasi-TEM conditions (N terminals) is an N-node polygon interconnected with impedances in $\boldsymbol{\mathcal{Z}}_{\text{in}}$ (similar to Fig. 3.2). These impedances are realized as parallel RL or RC circuits where

$$R_{ij}(z) = \left(\Re\text{e}\{[\boldsymbol{\mathcal{Y}}_{\text{in}}(z)]_{ij}\}\right)^{-1}, \tag{3.38a}$$

$$L_{ij}(z) = \frac{\left(\Im\text{m}\{[\boldsymbol{\mathcal{Y}}_{\text{in}}(z)]_{ij}\}\right)^{-1}}{\omega}, \quad \Im\text{m}\{[\boldsymbol{\mathcal{Y}}_{\text{in}}]_{ij}\} < 0 \tag{3.38b}$$

$$C_{ij}(z) = \omega\left(\Im\text{m}\{[\boldsymbol{\mathcal{Y}}_{\text{in}}(z)]_{ij}\}\right)^{-1}, \quad \Im\text{m}\{[\boldsymbol{\mathcal{Y}}_{\text{in}}]_{ij}\} > 0. \tag{3.38c}$$

Since the susceptance network is realized with inductors or capacitors, the sign constraints apply only to the real parts of the admittance matrix, or the conductive network. This admittance matrix split is hence physically realized as a conductive network in parallel with a susceptive network, as shown in Fig. 3.5. Theorem 8-4 then applies strictly to the conductive network, thus the realization condition applies to general admittance matrices.

Now, if all off-diagonal terms of the dominant admittance matrix $\boldsymbol{Y}^{\text{c}}_{\text{in}}(z)$ in a microstrip system have nonpositive real parts, $\boldsymbol{Y}^{\text{c}}_{\text{in}}(z)$ is passively realized as an N-terminal RLC circuit network. This realization assumes the topology of a complete polygon with N vertices and $N(N-1)/2$ admittances, $\frac{1}{4}\left[n^2 + 2n + (n \bmod 2)\right]$ of which are independent (see Fig. 3.2). The circuit components in the parallel conductance/susceptance networks of Fig. 3.5 are given by (3.38).

However, a dominant admittance matrix $\boldsymbol{Y}^{\text{c}}_{\text{in}}(-a)$ whose off-diagonal terms have positive real components (3.33) may be realizable as an n-port RLC network that has only N nodes but no common ground for all ports (the general synthesis procedure may be found in [26]). Thus it follows for this case that the input admittance matrix at $z = -a$ is unrealizable as an N-terminal RLC circuit network. A realization consisting of $2n$ nodes and n ports exists, though it lacks a common ground. It is therefore impossible to terminate the lines at $z = -a$ with an N-terminal passive impedance network since the coupled microstrip network topology does have a common ground. Of course, this alternative $2n$-node realization exists for the case when $\boldsymbol{Y}^{\text{c}}_{\text{in}}(-a)$ has all off-diagonal real components nonpositive, since its N-terminal network realization may also take the form of $2n$-node, n-port realization with no common ground, where

both realizations are interchangeable via star-mesh conversions.

But the inherent physics of the system now seems violated: if the admittance matrix $\boldsymbol{Y}_{\text{in}}^{\text{c}}(-a)$ is not realizable as an RLC network with a common ground (i.e. an N-terminal), then the MTL section between the passive termination at $z = 0$ and $z = -a$ cannot be physically realized with an equivalent passive N-terminal impedance network at $z = -a$. How, then, can this section of lines and terminations possibly be modelled passively? This paradox is resolved by considering another passive circuit element: the ideal transformer. If ideal transformers are permitted in the equivalent RLC circuit realization of $\boldsymbol{Y}_{\text{in}}^{\text{c}}(-a)$, one node may be designated as the common ground, and the remaining ports may be isolated by these transformers and then connected to the same common ground. Therefore, at points where realized negative conductance is encountered (3.33), the application of ideal transformers to $n - 1$ ports of the $2n$-node realization without a common ground will permit the n-port, N-node realization with a common ground. This possibility arises since any synthesis procedure for realizing an n-port circuit network with ideal transformers simultaneously realizes an N-terminal network [26].

Therefore, it has been shown that the "active" elements in $\boldsymbol{Y}_{\text{in}}^{\text{c}}(z)$ for certain longitudinal points $z = -a$ do not violate passivity of the terminated system. Stable numerical analysis at $z = -a$ using the admittance matrix $\boldsymbol{Y}_{\text{in}}^{\text{c}}(-a)$ will be illustrated in the next section. However, a passive, unbalanced, N-node, n-port termination network containing resistors, capacitors, and inductors with one common ground (the microstrip ground plane) is not realizable at that distance z without transformers.

Obviously, we must expound the physical meaning of these admittance matrix properties. In regards to the ideal transformers, they dissipate no real power and store no energy. Moreover, if the turn ratios are 1:1, their only function is to isolate a port and allow for common grounding and realization of an N-terminal topology. Of course they only become necessary when condition (3.33) is encountered. Section 3.2 demonstrated several important consequences of mode delays; arguably, the most significant is the longitudinal power fluctuations along the conductors. These fluctuations, closely related to the state voltage and current magnitude variations, effectively require compensation in the immittance parameters. Condition (3.33) provides this compensation, though not in a readily discernable manner.

Finally, it should be noted that within the context of passive MTL structures,

similar physical attributes have been represented using passive circuit elements. The transformer interpretation presented in this paper is cognate to that used to synthesize SPICE models for coupled transmission lines [36], where congruence transformers with the proper turn ratios realize the eigenvectors, decouple multimode signals into their individual modes, and propagate them along a unique transmission line system for each mode.

3.3 Admittance Matrix Realizability Conditions

In MTL applications where quasi-TEM mode delay is present such as matching networks [29], filters, and amplifiers in coupled microstrip technology, the LIMFs exhibit interesting behavior in the state (conductor) domain, which was thoroughly examined in [37]. Among the most interesting manifestations of the mode delay were deviations from two common (but not necessary) properties of the input admittance matrix, namely its dominance and negative real off-diagonal terms, as were elaborated in the previous sections. As its passivity was readily demonstrated, this section concerns the topological realizability conditions on the admittance matrix in synthesizing equivalent circuits that model linear, passively terminated lengths a of coupled lines, and the interpretation of such models. We address the constraints on the realization of the admittance matrix and the physical interpretation of the realized circuits in the passive, common-ground microstrip system. Finally, we discussed the interpretations of several topologies for admittance matrices whose synthesis via *RLC* N-terminal networks was generally not possible. These admittance matrices resulted from mode delays and related the conductor voltage and current vectors at a, causing longitudinal conductor power oscillation envelope variations. The necessarily common-ground N-terminal realization used to model the length a of coupled lines and their terminations thus required ideal transformers, sometimes for the n-port realization but always for port isolation.

Physically, we considered a passive, generally lossy MTL system (n lines) terminated with linear, passive networks. The longitudinal conductor input admittance matrix $\boldsymbol{Y}^{\mathrm{c}}_{\mathrm{in}}(z = -a)$ relates the conductor voltage and current vectors on the conductors at $z = -a$. It models the length a of coupled lines between the point $z = -a$ and the prescribed termination at the output $z = 0$. This is shown in Fig. 3.3 (for a three-line case).

Coupling between the lines results in longitudinal conductor power oscillation along each conductor. The unequal z-varying amplitude envelopes of each conductor power oscillation (see [37, Fig. 11]) is perhaps the most significant consequence of the mode delays and provides the clearest physical insight to their presence. These fluctuations, directly related to the state voltage and current magnitude variations, effectively require compensation in the immittance parameters, including the admittance matrix. Though the admittance matrix accounts for these power oscillations, two of its properties superficially appear problematic: its lack of dominance,

$$|[\boldsymbol{Y}^{\mathrm{c}}_{\mathrm{in}}(z)]_{kk}| \not\geq \sum_{m=1,m\neq k}^{n} |[\boldsymbol{Y}^{\mathrm{c}}_{\mathrm{in}}(z)]_{km}| \qquad k = 1, 2, \cdots, n, \tag{3.39}$$

and the positiveness of the off-diagonal real terms for various distances $z = -a$,

$$\Re\mathrm{e}\{[\boldsymbol{Y}^{\mathrm{c}}_{\mathrm{in}}(z)]_{ij}\} > 0, \qquad i \neq j. \tag{3.40}$$

These conditions, reported in [37], provide compensation, though the general factors that govern their occurrence are not immediately apparent. However, passivity was readily shown for the matrix $\boldsymbol{Y}^{\mathrm{c}}_{\mathrm{in}}(z)$ at all points and requires only a positive definiteness test. The major issue we wish to address here is that in synthesizing a network as the model for $\boldsymbol{Y}^{\mathrm{c}}_{\mathrm{in}}(z = -a)$, realizability conditions dictate the choice in topology.

In [37], the realizability theorem [26, Theorem 8-4] was extended to general complex admittance matrices: an $(n \times n)$ dominant admittance matrix $\boldsymbol{Y}^{\mathrm{c}}_{\mathrm{in}}(z)$ may be realized as an impedance or admittance network consisting of, in general, $2n$ nodes. Furthermore, if all off-diagonal real terms of this matrix are nonpositive, then an impedance or admittance network of N terminals (i.e., $N = n + 1$ nodes, with one node designated the common ground to which all n ports are referenced) may be synthesized from the impedance or admittance network matrices.

The general $2n$-node, n-port realization of course lacks a common ground. It exists as an alternative for the case when $\boldsymbol{Y}^{\mathrm{c}}_{\mathrm{in}}(-a)$ has all off-diagonal real components nonpositive. In this case, the N-terminal realization also assumes a $2n$-node, n-port realization without a common ground, since both realizations are interchangeable via star-mesh conversions. This possibility arises since any synthesis procedure for realizing an n-port circuit network with ideal transformers simultaneously realizes an N-terminal network [26].

As shown in [37], common-ground realizations were sometimes impossible without the use of ideal transformers. Consequently, we attempted to rationalize the signif-

icance of the transformers in terms of energy and power considerations. To further elucidate the role of the transformers, we shall illustrate the realizability issues and their physical significance with two examples in an $n = 2$ system. For simplicity, we will restrict the examples to (2×2) conductance matrices (as the imaginary parts are irrelevant). The general four-node realization is shown in Fig. 3.6 for two ports. For greater numbers of ports, the sketch is obviously more difficult.

First, consider the following conductance matrix at $z = -a$ with positive off-diagonal entries,

$$\boldsymbol{Y}_{\text{in}}^{\text{c}}(-a) = \begin{bmatrix} 7 & 2 \\ 2 & 7 \end{bmatrix}. \tag{3.41}$$

A cursory glance reveals the dominance of this matrix, and simple eigenanalysis verifies its positive definiteness. Clearly, the assumption of a two-port, three-terminal realization of (3.41) (referred to as a "pi" network in the two-port case), as illustrated in Fig. 3.7(a) is not passive, as this realization requires the active conductance element $y = -2$ connecting the nodes labeled with a plus sign (+). Since we wish to construct the equivalent passive microstrip system with only passive elements, we resort to the general synthesis procedure.

In this case, a passive four-node realization as shown in Fig. 3.7(b) based on Fig. 3.6 is possible. Unfortunately, this realization lacks a common ground, and thus appears to contradict the physics of a lossless microstrip system. We reconcile this by recalling that an nth-order symmetric admittance matrix is realized as an n-port with not only RLC elements, but also mutual inductances, and ideal transformers if and only if it is positive definite [26, Theorem 7-2].

Therefore, at points where (3.40) holds in the generalized n-line case, ideal transformers may be included in the $2n$-node RLC circuit realization. One node is designated as the common ground, and to the remaining $n - 1$ ports we apply ideal transformers (with turn ratios 1:1) which permit port isolation and allows for their common grounding, thus realizing an N-terminal topology. Thus a third realization for (3.41) using isolation transformers to establish a common ground is shown in Fig. 3.8.

Now, consider the following positive real conductance matrix with positive off-

diagonal entries and which lacks diagnal dominance:

$$\boldsymbol{Y}_{\text{in}}^{\text{c}}(-a) = \begin{bmatrix} 10 & 3 \\ 3 & 2 \end{bmatrix}. \tag{3.42}$$

Again, the assumption of common-ground precludes a passive realization; Fig. 3.9(a) requires an active circuit element. Fig. 3.9(b) is an ad hoc realization for (3.42). We are unaware of a systematic realization procedure for positive definite, but nondominant, admittance matrices, though we repeat that a realization using ideal transformers or mutual inductance or both is always possible for this case [26, Theorem 7-2]. Nevertheless, realization Fig. 3.9(b) also requires isolation transformers for a common-ground realization, as shown in Fig. 3.10.

3.4 Interpreting the Ideal Transformers

Having resolved the initially troublesome positive real off-diagonal elements and the nondominance of the input admittance matrix by considering network synthesis realizability conditions, we now seek an interpretation of the ideal transformers.

We first stress that certain nondominant matrices require no ideal transformers in their general n-port realizations. The conditions and interpretation of this synthesis is beyond the scope of this dissertation, though such examples are given in [26]. However, their topologies are not N-terminal, and therefore, a common ground could only be achieved with isolation transformers.

Intuitively, an ordinary N-terminal RLC termination on n coupled lines must have a dominant admittance matrix with negative real off-diagonal terms [1]. As the longitudinal distance from the load increases, the mode delays change the voltage-current relationships (as reflected in the longitudinal power envelope variations), and consequently, the input admittance matrix. For short distances, low frequencies, or small mode delays, the impact on $\boldsymbol{Y}_{\text{in}}^{\text{c}}(z)$ is negligible. Nevertheless, any significance of the mode delays must somehow be accounted for in $\boldsymbol{Y}_{\text{in}}^{\text{c}}(z)$, and therefore, in its ultimate realization, which we have shown may include transformers, as the N-terminal RLC networks used to model the section in Fig. 3.3 are generally not capable of accounting for the relative power levels between the n lines at $z = -a$ if this system has mode delays.

All three circuit models (using both active and passive elements) for each case ((3.41) and (3.42)) are acceptable theoretical realizations. Passivity of these models,

though physically obvious, still applies in Figs. 3.7(a) and 3.9(a); circuit analysis verifies that the positive resistors dissipate more power than is generated by the negative resistors. Furthermore, the transformers dissipate no real power and store no energy. While they have been theoretically shown to be permissible in the realizations, their exact physical role, other than power transfer devices between the ports of the realization, is not readily discernible.

3.5 Numerical Results

Numerical results presented in this section have previously appeared in the literature [29], though more longitudinal details are presented. A three-coupled line microstrip structure with characteristic impedance matrix

$$\boldsymbol{Z}_{\mathrm{ch}}^{\mathrm{c}} = \begin{bmatrix} 50.1615 & 8.52729 & 2.29226 \\ 8.52729 & 49.4542 & 8.52729 \\ 2.29226 & 8.52729 & 50.1615 \end{bmatrix} \Omega \tag{3.43}$$

and circuit parameters $\boldsymbol{R} = \boldsymbol{0}$, $\boldsymbol{G} = \boldsymbol{0}$, and

$$\boldsymbol{L} = \begin{bmatrix} 310.887 & 67.4845 & 22.2536 \\ 67.4845 & 305.963 & 67.4845 \\ 22.2536 & 67.4845 & 310.887 \end{bmatrix} \mathrm{nH} \tag{3.44}$$

$$\boldsymbol{C} = \begin{bmatrix} 125.143 & -15.4225 & -0.81741 \\ -15.4225 & 128.346 & -15.4225 \\ -0.81741 & -15.4225 & 125.143 \end{bmatrix} \mathrm{pF} \tag{3.45}$$

was simulated, analyzed, and synthesized on board for a three-coupled line matching network. Moderate coupling ensured distinct quasi-TEM propagation constants for an operating frequency of 2.0 GHz and therefore quasi-TEM modal dispersion. A low impedance reflection termination at the load with impedance network matrix

$$\boldsymbol{\mathcal{Z}}_{\mathrm{L}} = \begin{bmatrix} 20 & 287.152 & 2883.71 \\ 287.152 & 69.1719 & 287.152 \\ 2883.71 & 287.152 & 20 \end{bmatrix} \Omega \tag{3.46}$$

resulted in multimode reflections simulated via an MTL digital computer program.

As predicted by (3.30), the elements of $\boldsymbol{\Gamma}_{\mathrm{in}}^{\mathrm{m}}(z)$ maintain constant longitudinal magnitudes. Simulation with the low impedance termination (3.46) verifies this result, with all five nonzero elements plotted in Fig. 3.11. The three distinct modal propagation constants, as well as the intermode propagation constants (in this case

the arithmetic mean of modes 1 and 3), are readily apparent in the phase plot. Also evident is the phase shift at the load (180°) due to the low impedance termination.

Clearly, $\mathbf{\Gamma}^{\mathrm{c}}_{\mathrm{in}}(z)$ for lossless, dispersionless coupled lines exhibits nonlinear phase and magnitude dependence with z. Matrix $\mathbf{\Gamma}^{\mathrm{c}}_{\mathrm{in}}(z)$ terms are shown in Fig. 3.12. Within practical working distance from the terminations ($z > -10$ cm), the magnitude of the all voltage reflection terms increase with the coupling length, except for the self reflection terms $[\mathbf{\Gamma}^{\mathrm{c}}_{\mathrm{in}}(z)]_{11,33}$, which steadily decrease. For moderate to low coupling or short distances from the terminations, the impact from these effects is obviously minimum.

Observing the reflection coefficient at very large distances from the load, however, (Fig. 3.13) reveals the oscillatory nature of the elements due to modal dispersion. In tightly coupled systems with negligible loss, these values would prove problematic in a multimode measurement. The actual period of each $\mathbf{\Gamma}^{\mathrm{c}}_{\mathrm{in}}(z)$ term has, in this simulation, been found to be too large for practical use.

To illustrate the contrast in the standing wave pattern for a high impedance termination, the 20 Ω resistors in (3.46) were replaced with 430 Ω resistors and the simulation was repeated. Mode and conductor voltage standing wave patterns are shown in Fig. 3.14. The "open" case corresponds to the high impedance termination, where the standing wave maximum falls almost exactly on the load (mode and conductor voltages); the "short" case corresponds to the low impedance termination, where the standing wave minimum falls almost exactly on the load. Clearly, as predicted analytically, the mode SWRs remain constant, and have periods of $z = \frac{\beta_i}{2}$. Conductor voltage standing wave patterns have neither a fixed maximum-minimum ratio nor simply quantifiable periods.

To better exemplify the longitudinal mode and line voltages magnitude properties of lossless lines, a large length $D = 50$ cm was simulated. The standing wave patterns are shown in Fig. 3.15. As predicted, each mode voltage standing wave pattern is characterized by a minima offset from the load and a distinct, constant SWR. At large distances from the load, a phase offset between the standing wave patterns becomes apparent. The resulting dispersion in the line voltage signals is shown in the lower half of Fig. 3.15.

Obviously more complicated terminations are encountered in practical systems and require more detailed numerical or analytic attention, since the mode standing

wave patterns differ greatly from their conductor counterparts as different combinations of modes are incident and reflected from a termination. Our goal was simply to verify the longitudinal voltage features (analytically detailed in Section 3.2.1) resulting from mode delays.

Power behaves similarly; constant longitudinal mode powers are observed in the top plot of Fig. 3.16, while the line power fluctuations due to the modal dispersion are shown in the lower plot of Fig. 3.16. Careful graphical analysis reveals that the sum of the three conductor powers at any z is constant.

Finally, the longitudinal input admittance matrix function is plotted to illustrate "active" effect (3.33). Matrix $\boldsymbol{Y}^{\mathrm{c}}_{\mathrm{in}}(z)$ is symmetrically normalized via

$$\boldsymbol{y} = [\boldsymbol{Z}^{\mathrm{c}}_{\mathrm{ch}}]^{\frac{1}{2}} \cdot \boldsymbol{Y}^{\mathrm{c}}_{\mathrm{in}}(z) \cdot [\boldsymbol{Z}^{\mathrm{c}}_{\mathrm{ch}}]^{\frac{1}{2}} \,, \tag{3.47}$$

though the following element-based normalization is helpful in examining the specific locations were (3.33) holds:

$$Y_{\mathrm{self}}(z) = \frac{\sum_{k=1}^{n} [\boldsymbol{Y}^{\mathrm{c}}_{\mathrm{in}}(z)]_{1k}}{[\boldsymbol{Y}^{\mathrm{c}}_{\mathrm{ch}}]_{11} + [\boldsymbol{Y}^{\mathrm{c}}_{\mathrm{ch}}]_{12} + [\boldsymbol{Y}^{\mathrm{c}}_{\mathrm{ch}}]_{13}} \tag{3.48a}$$

$$Y_{\mathrm{self}-2}(z) = \frac{[\boldsymbol{Y}^{\mathrm{c}}_{\mathrm{in}}(z)]_{22} + 2[\boldsymbol{Y}^{\mathrm{c}}_{\mathrm{in}}(z)]_{23}}{[\boldsymbol{Y}^{\mathrm{c}}_{\mathrm{ch}}]_{22} + 2[\boldsymbol{Y}^{\mathrm{c}}_{\mathrm{ch}}]_{21}} \tag{3.48b}$$

$$Y_{\mathrm{mut}}(z) = \frac{[\boldsymbol{Y}^{\mathrm{c}}_{\mathrm{in}}(z)]_{12}}{[\boldsymbol{Y}^{\mathrm{c}}_{\mathrm{ch}}]_{12}} \tag{3.48c}$$

$$Y_{\mathrm{non}}(z) = \frac{[\boldsymbol{Y}^{\mathrm{c}}_{\mathrm{in}}(z)]_{13}}{[\boldsymbol{Y}^{\mathrm{c}}_{\mathrm{ch}}]_{13}} \tag{3.48d}$$

where the admittance Y_{self} connects lines 1 and 3 to ground, $Y_{\mathrm{self}-2}$ connects line 2 to ground, Y_{mut} is the mutual admittance between nearest neighbors, and Y_{non} is the admittance between nonadjacent neighbors, as shown in Fig. 3.17.

Fig. 3.18 shows locations for which

$$\Re\mathrm{e}[\boldsymbol{Y}^{\mathrm{c}}_{\mathrm{in}}(z)]_{ij} > 0 \quad i \neq j. \tag{3.49}$$

Clearly, the periodicity of the effect is evident. An evaluation of how the passive termination choice affects the longitudinal location and occurrence frequency of (3.49) is a highly nonlinear problem beyond the scope of this paper.

If the numerical analysis is extended to a length of 1 m, we observe locations where normalized admittances Y_{self} and $Y_{\mathrm{self}-2}$ have negative real parts, as illustrated in Fig. 3.18. It therefore has been shown *a posteriori* that $\boldsymbol{Y}^{\mathrm{c}}_{\mathrm{in}}(z)$ is no longer dominant for certain longitudinal distances. However, none of the diagonal terms

of $[\boldsymbol{Y}^{\mathrm{c}}_{\mathrm{in}}(z)]_{ii}$ contain negative real parts in these instances. In fact, the passivity check involved computing all eigenvalues in verifying postitive definiteness, and the admittance matrix satisfied passivity at all points along the system, demonstrating numerical stability and correct MTL immittance matrix functions for passive network description. In regards to the realizability of $\boldsymbol{Y}^{\mathrm{c}}_{\mathrm{in}}(z)$, the condition of dominance is sufficient, but not necessary for realization; the condition required for realization of a nondominant matrix $\boldsymbol{Y}^{\mathrm{c}}_{\mathrm{in}}(-a)$ at $z = -a$ with ideal transformers is that $\boldsymbol{Y}^{\mathrm{c}}_{\mathrm{in}}(-a)$ is positive real [26]. Indeed, the function $\boldsymbol{Y}^{\mathrm{c}}_{\mathrm{in}}(z)$ was found to be positive real for all longitudinal points in simulation, resulting in three-port, common-ground realizability including transformers for all distances z.

3.6 Conclusions

The objective of this chapter was to detail the effects of mode delays on longitudinal immittance matrix functions and justify the results mathematically and clarify their physical meanings where possible. In conclusion, the study showed how quasi-TEM modal dispersion in lossless, symmetric lines was responsible for the following:

- Longitudinal conductor power variations
- Varying conductor voltage SWRs
- Multimode signal distortion
- Conductor reflection coefficient magnitude variations
- Impedance networks with directly realized negative real elements

Passivity, reciprocity, and lossless properties of the immittance matrices were demonstrated numerically for the cases encountered, and passive circuits of proper topology in the microstrip structure (N-terminal) could be synthesized if ideal transformers were included. Furthermore, this passive circuit network topology was shown to be possible for all longitudinal admittance matrices of the terminated lossless coupled lines; no active elements were required for the admittance matrix realization.

For the lossy case, such analysis becomes considerably more complicated, since mode orthogonality breaks down and frequency dependence of the circuit parameters

becomes significant. But this analysis should be useful for many circuits of practical interest modeled using lossless assumptions. These longitudinal immittance matrix properties are already encountered in the design and simulation of coupled-line matching networks, and will become increasingly significant as application speeds and coupling increase. Modal dispersion must clearly be accounted for in lossy, high-coupling MTL simulation to ensure that large longitudinal reflection coefficient magnitude fluctuations, conductor power variations, and signal distortion are not attributed solely to power loss or other mechanisms.

Detailed analysis regarding the effects of modal dispersion on loss calculation, as well as experimental validation on low-loss structures, remains as a topic of future work. Thus far we know of no systematic analytical passivity check, though given the emphasis on numerical techniques, such a check may be unnecessary. Also, an extension of realizability conditions with transformers for nondominant admittance matrices should be examined in depth.

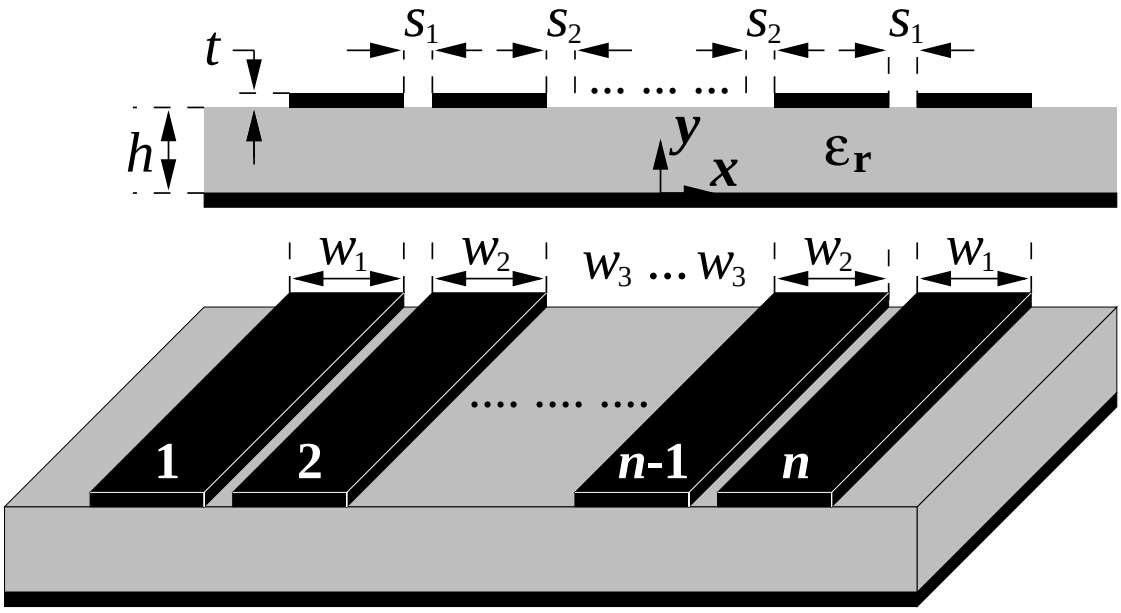

Figure 3.1 Relative dimensions for n coupled microstrip lines. Line numbers shown in white. Note that width and spacing of lines may change from line to line, but the overall structure is symmetric about the $x = 0$ plane.

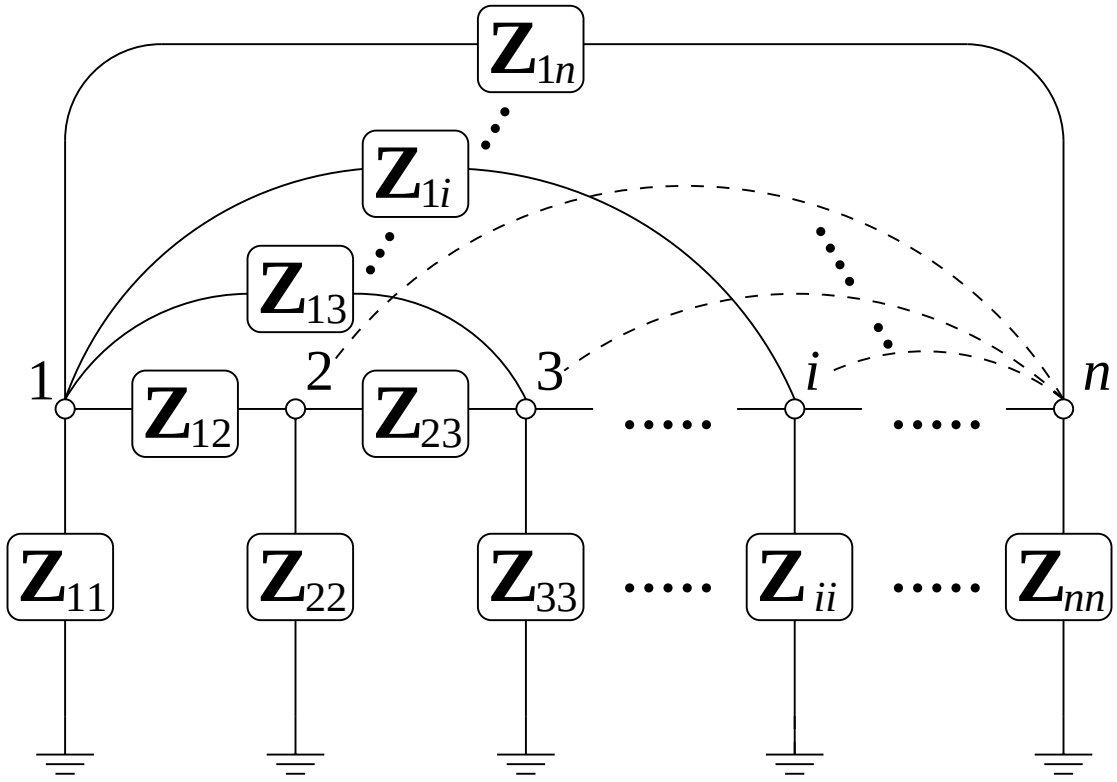

Figure 3.2 The n-port, N-node common-ground impedance network matrix physical circuit realization for an $(n \times n)$ admittance matrix. Note: $\mathbf{Z}_{ij} = [\boldsymbol{\mathcal{Z}}_{\mathrm{L}}]_{ij}$.

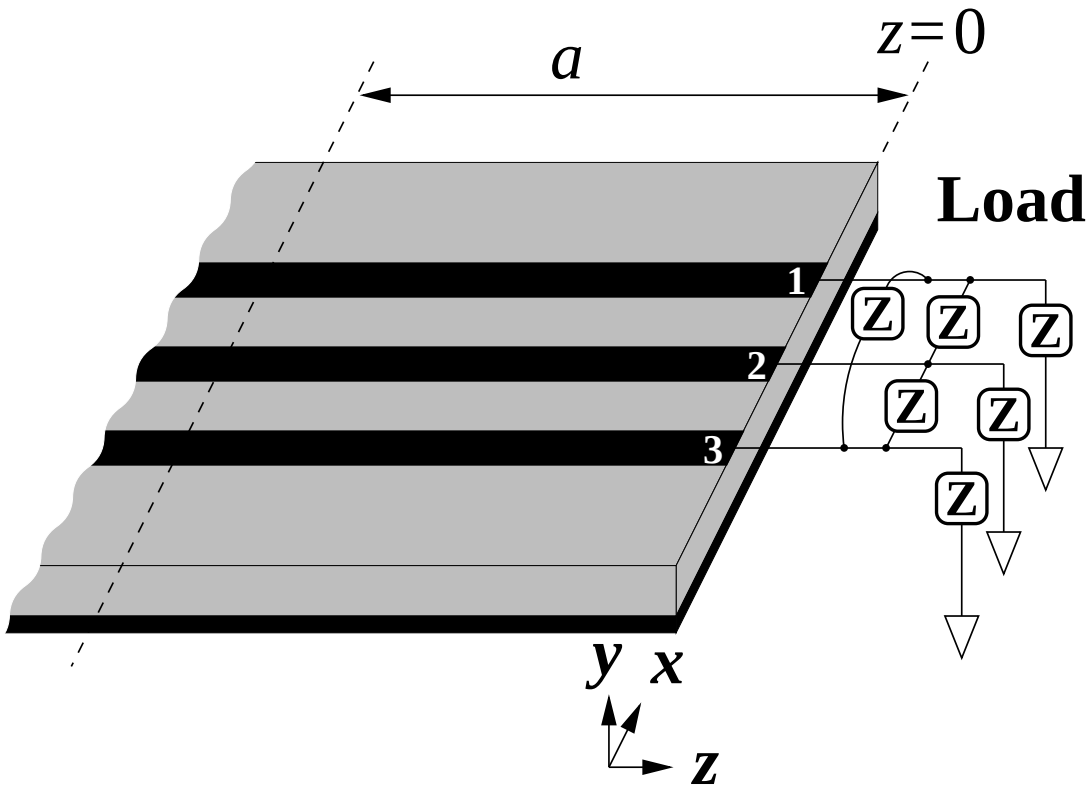

Figure 3.3 Coupled transmission line section with load terminations and immittance matrices at $z = -a$.

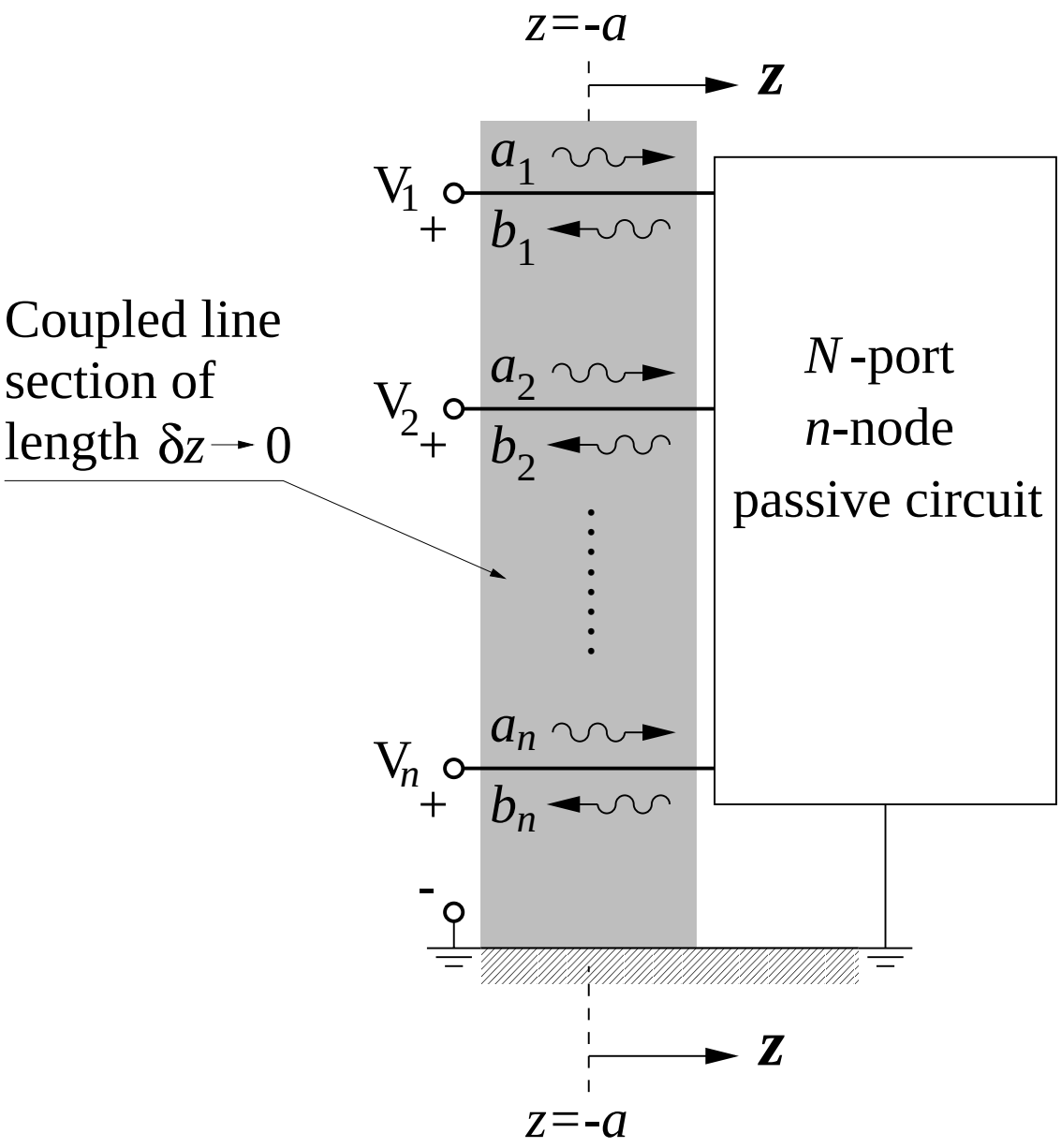

Figure 3.4 The n-port, N-node common-ground circuit network which realizes immittance matrices $\boldsymbol{\Gamma}^{\rm c}_{\rm in}(z=-a)$, $\boldsymbol{Z}^{\rm c}_{\rm in}(z=-a)$, $\boldsymbol{Y}^{\rm c}_{\rm in}(z=-a)$, $\boldsymbol{T}^{\rm c}_{\rm in}(z=-a)$, and $\boldsymbol{S}_{\rm in}(z=-a)$.

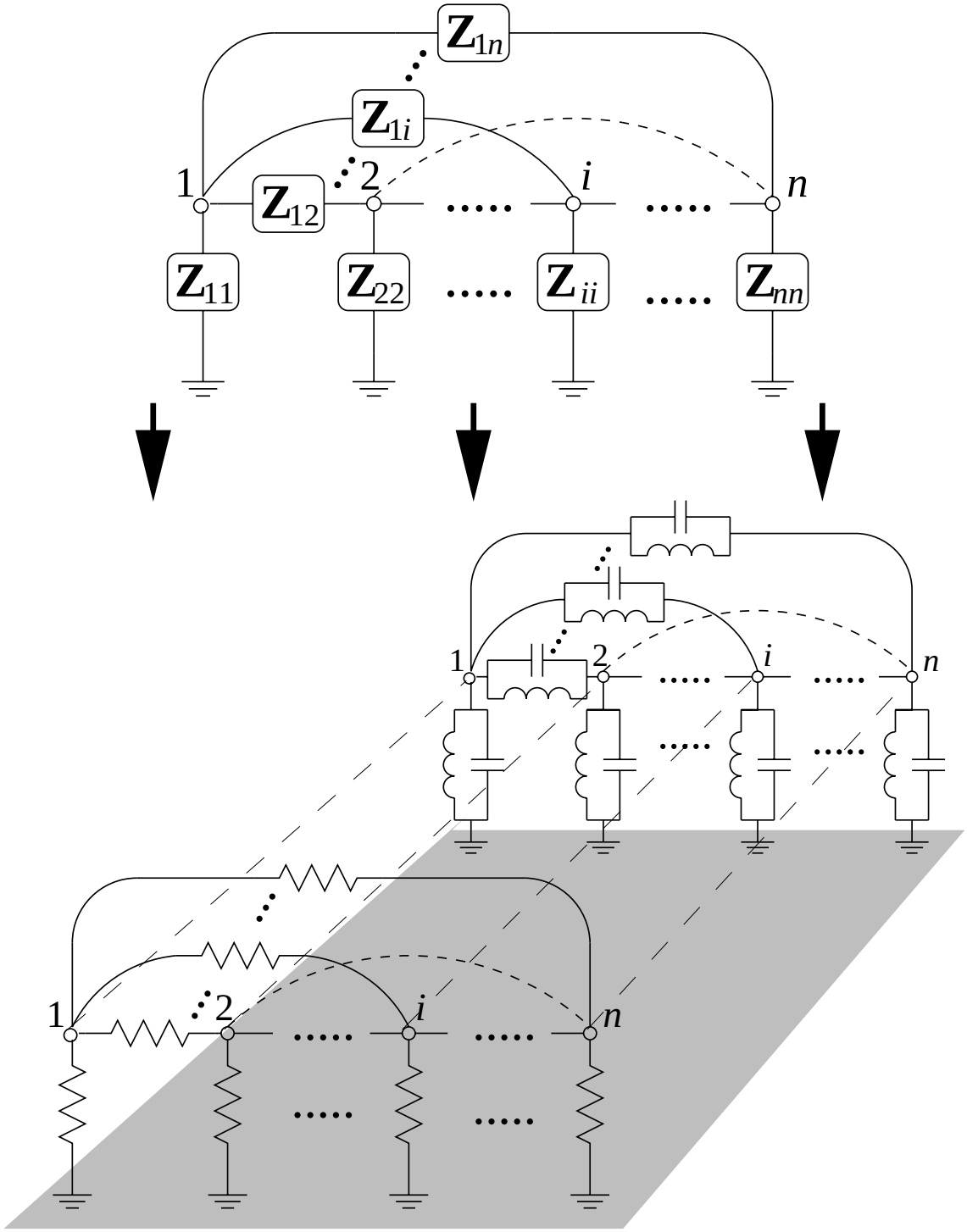

Figure 3.5 Parallel conductance and susceptance circuits composing an N-node, n-terminal impedance network with a common ground.

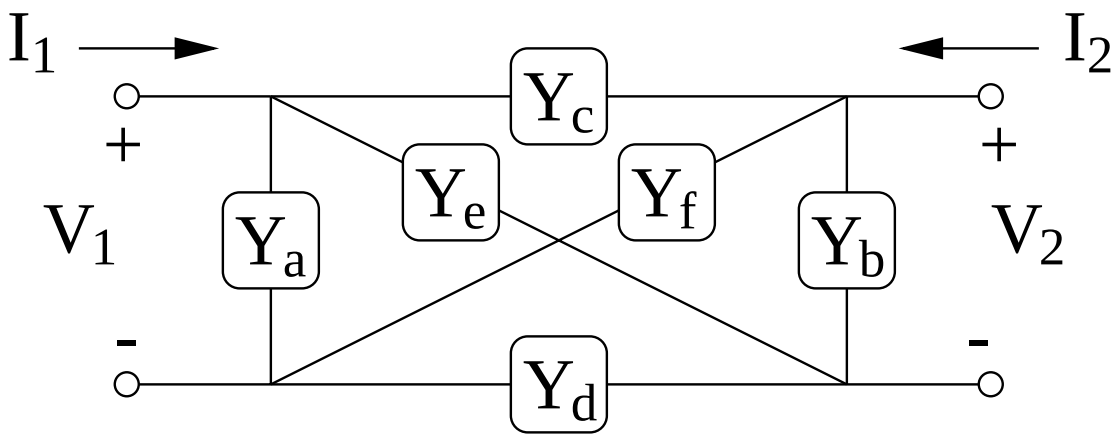

Figure 3.6 The general two-port admittance nodal structure.

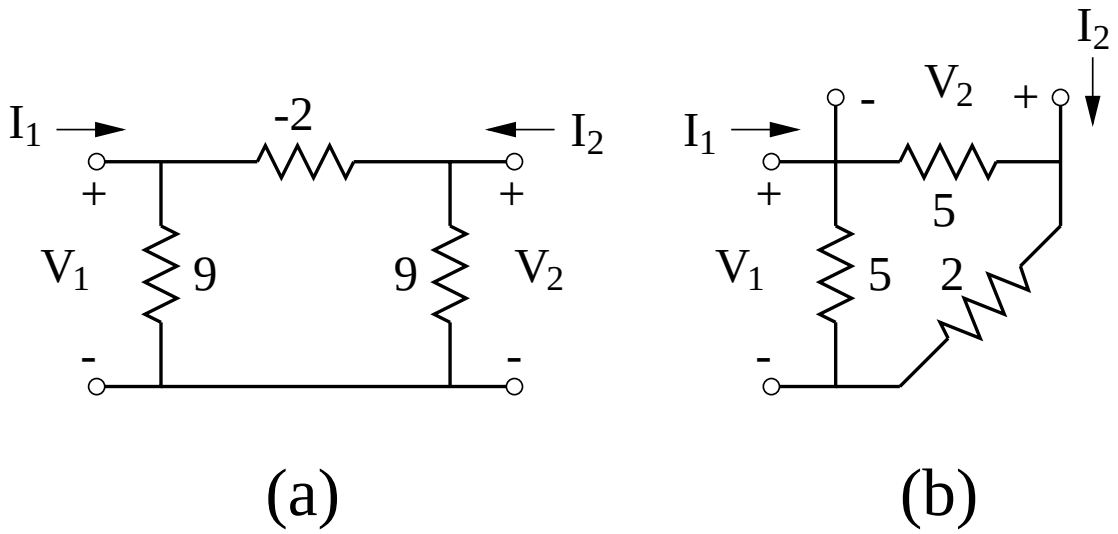

Figure 3.7 Possible realizations for the admittance matrix given in (3.41). (a) Non-passive realization assuming a pi topology. (b) Passive realization based on $2n$-node synthesis procedure.

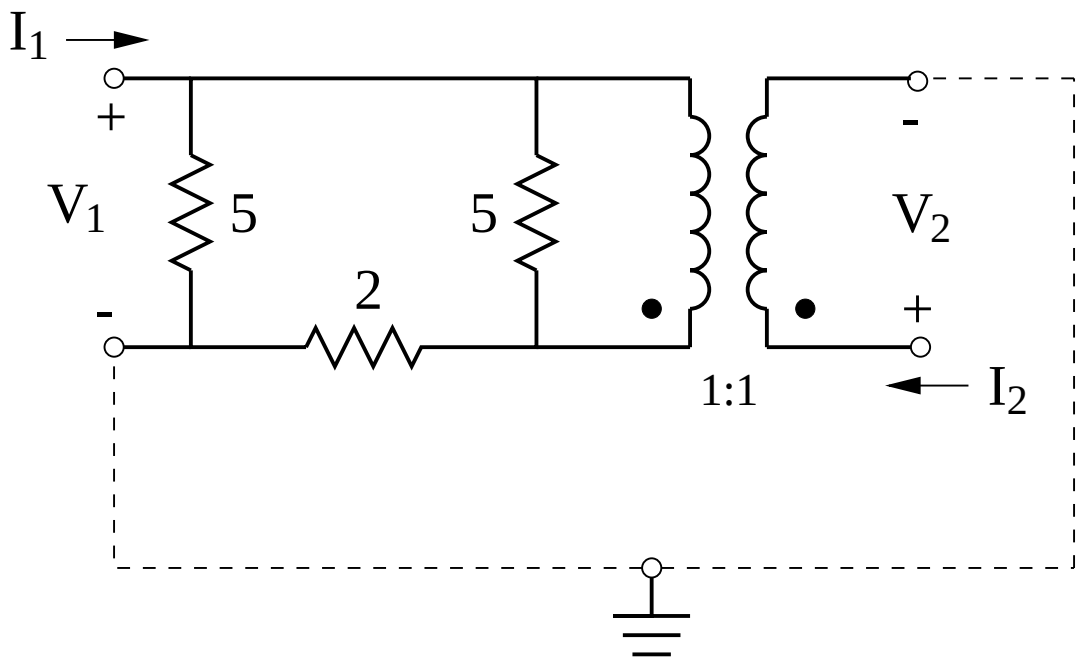

Figure 3.8 Realization of Fig. 3.7(b) using port isolation transformers for common grounding.

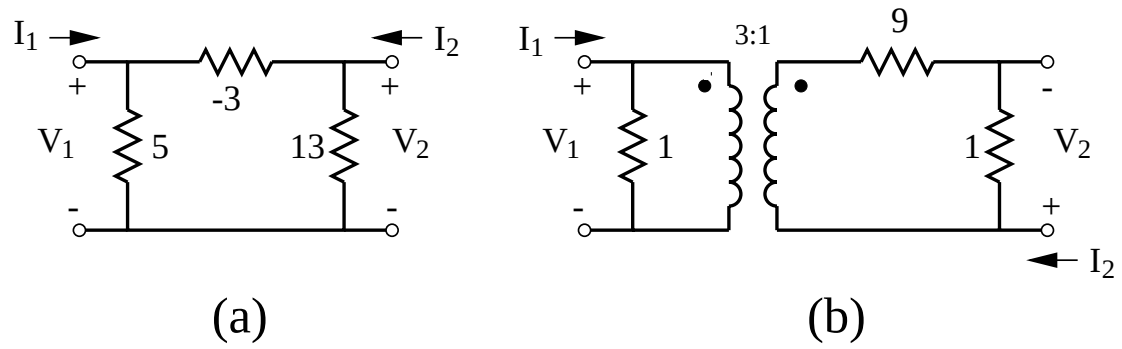

Figure 3.9 Possible realizations for the admittance matrix given in (3.42). (a) Non-passive realization assuming a pi topology. (b) Passive realization using an ideal transformer.

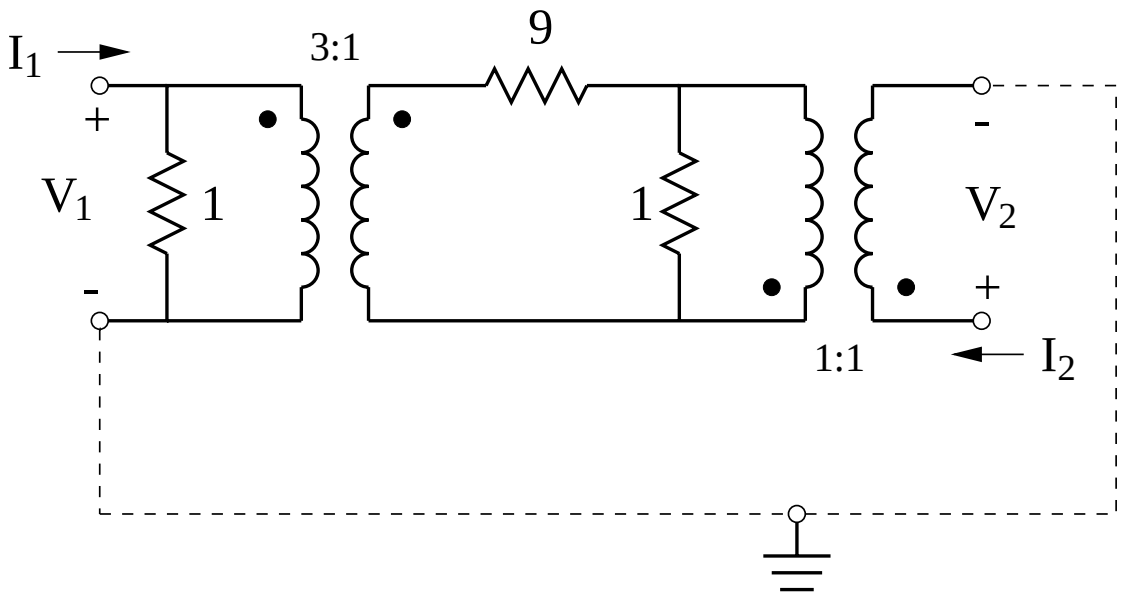

Figure 3.10 Realization of Fig. 3.9(b) using port isolation transformers for common grounding.

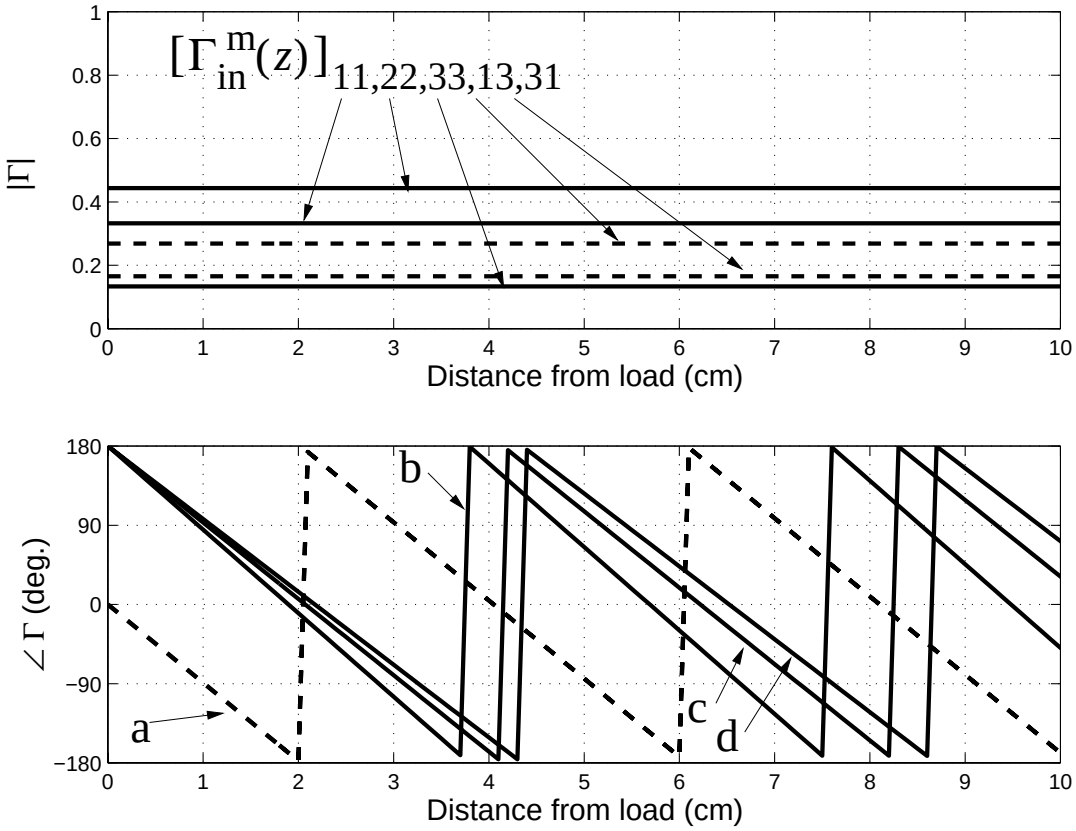

Figure 3.11 Longitudinal variations of the input modal reflection coefficient matrix terms. Note: $a = [\mathbf{\Gamma}^{\mathrm{m}}_{\mathrm{in}}(z)]_{13,31}$, $b = [\mathbf{\Gamma}^{\mathrm{m}}_{\mathrm{in}}(z)]_{11}$, $c = [\mathbf{\Gamma}^{\mathrm{m}}_{\mathrm{in}}(z)]_{22}$, and $d = [\mathbf{\Gamma}^{\mathrm{m}}_{\mathrm{in}}(z)]_{33}$.

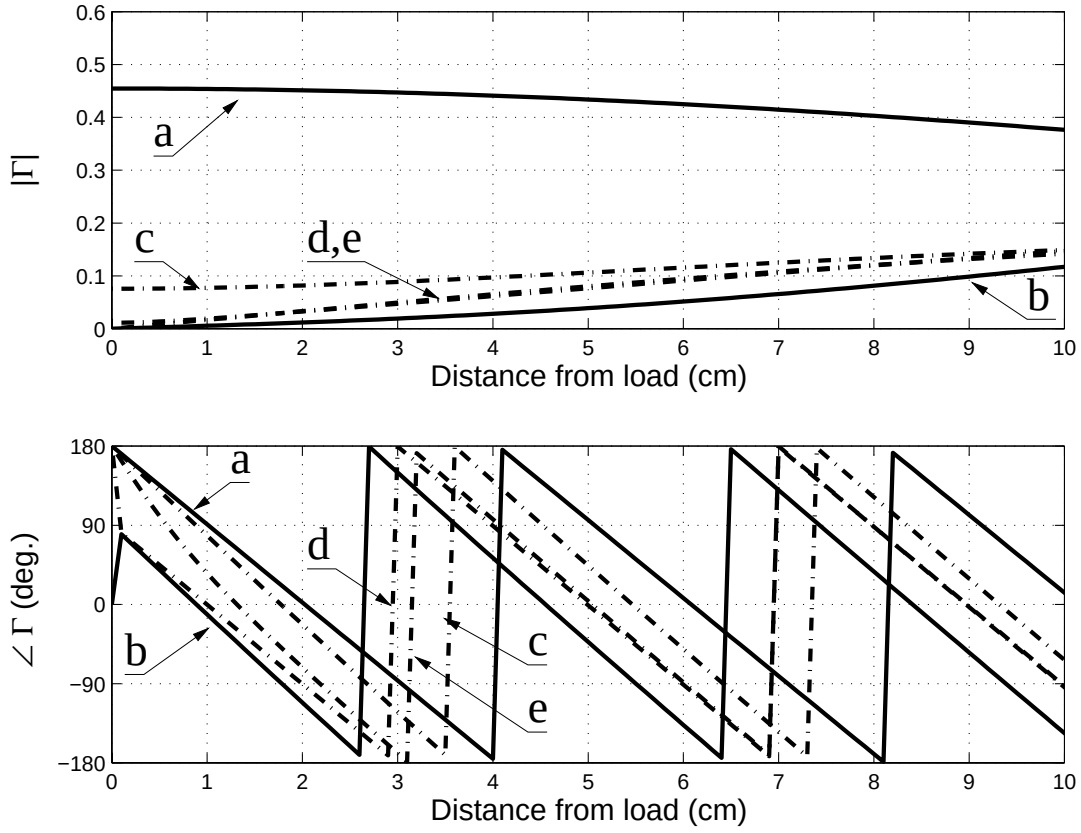

Figure 3.12 Longitudinal variations of the input conductor reflection coefficient matrix $\mathbf{\Gamma}^{\mathrm{c}}_{\mathrm{in}}(z)$ terms. Note: $a = [\mathbf{\Gamma}^{\mathrm{c}}_{\mathrm{in}}(z)]_{11,33}$, $b = [\mathbf{\Gamma}^{\mathrm{c}}_{\mathrm{in}}(z)]_{22}$ $c = [\mathbf{\Gamma}^{\mathrm{c}}_{\mathrm{in}}(z)]_{21,23}$, $d = [\mathbf{\Gamma}^{\mathrm{c}}_{\mathrm{in}}(z)]_{12,32}$, $e = [\mathbf{\Gamma}^{\mathrm{c}}_{\mathrm{in}}(z)]_{13,31}$.

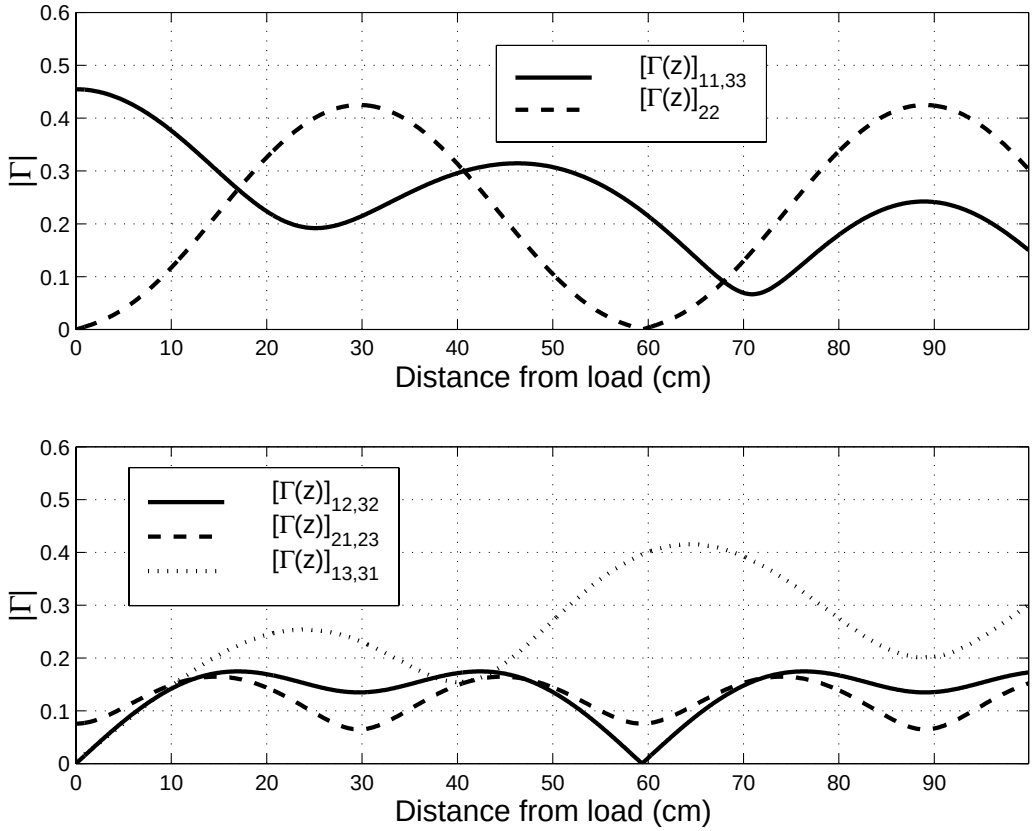

Figure 3.13 Long distance longitudinal variations of input conductor reflection coefficient matrix $\mathbf{\Gamma}_{\text{in}}^{\text{m}}(z)$ terms. Note: $a = [\mathbf{\Gamma}_{\text{in}}^{\text{m}}(z)]_{13,31}$, $b = [\mathbf{\Gamma}_{\text{in}}^{\text{m}}(z)]_{11}$, $c = [\mathbf{\Gamma}_{\text{in}}^{\text{m}}(z)]_{22}$, $d = [\mathbf{\Gamma}_{\text{in}}^{\text{m}}(z)]_{33}$.

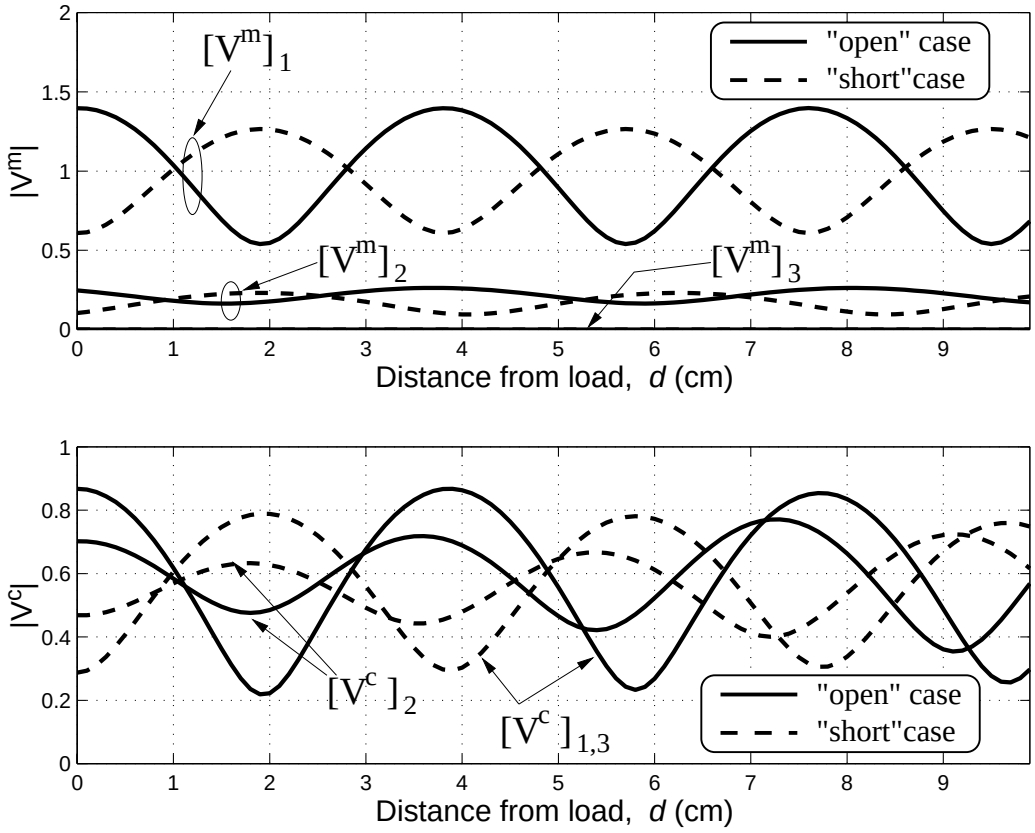

Figure 3.14 Simulated longitudinal variation of modal and conductor voltage magnitudes with the "open" and "short" terminations at 2.0 GHz.

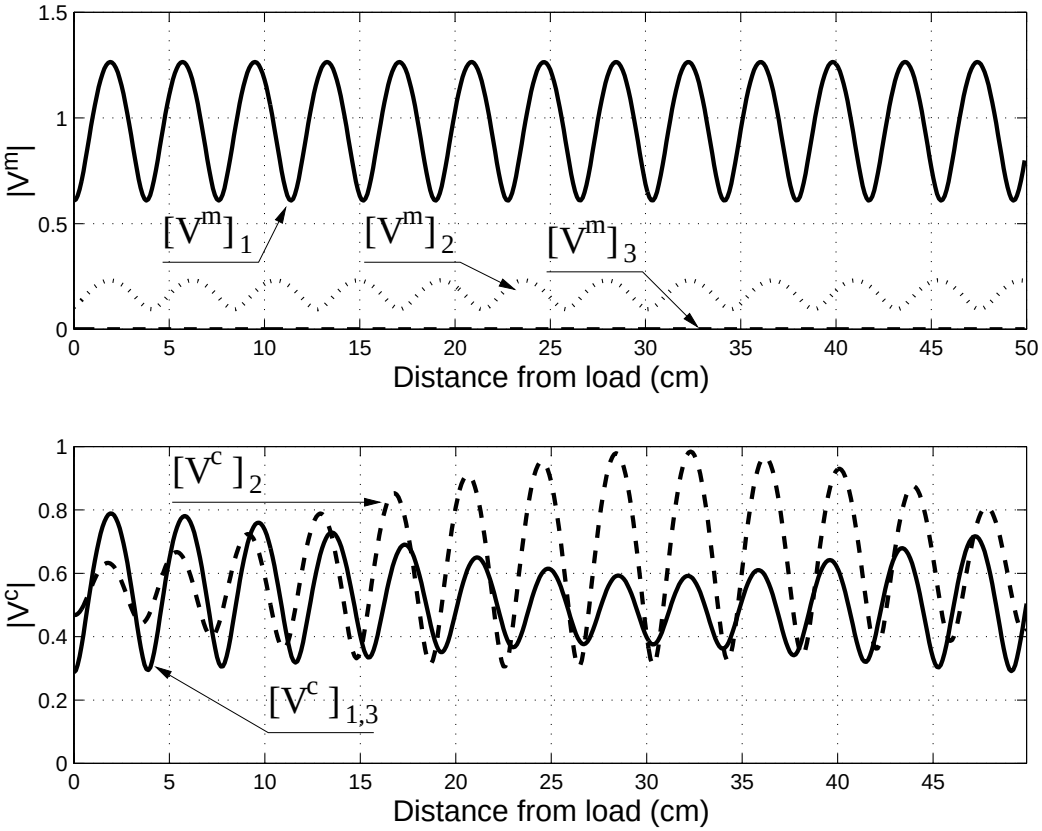

Figure 3.15 Simulated longitudinal variation (from load to $z = -50$ cm) of modal and conductor voltage magnitudes for "short" termination at 2.0 GHz, showing the magnitude properties for lossless lines.

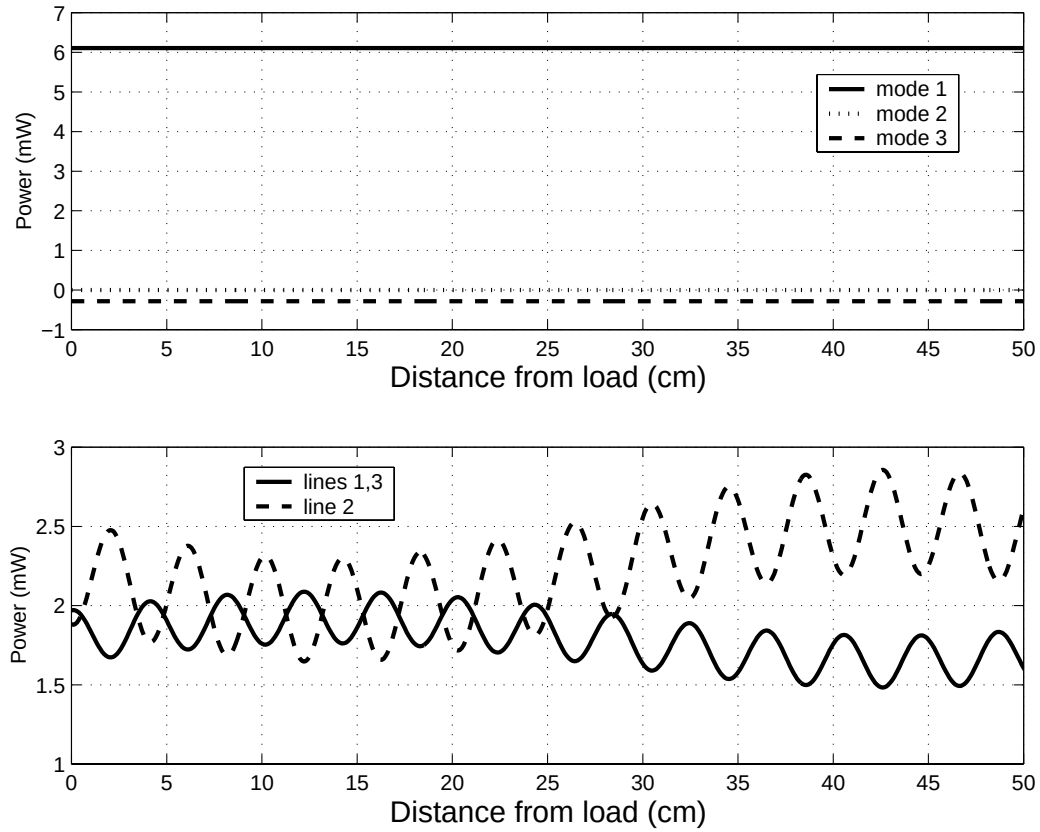

Figure 3.16 Longitudinal distribution of the conductor and modal powers (from load to $z = -50$ cm).

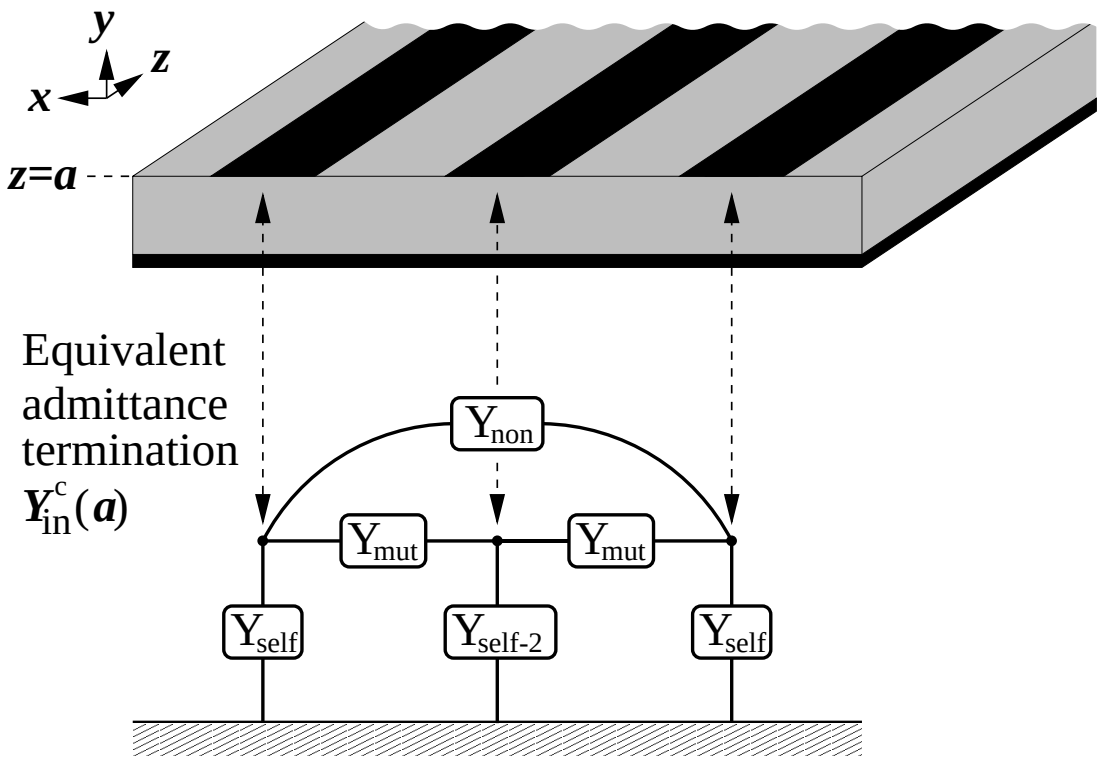

Figure 3.17 Elements of a realized (3×3) input admittance matrix at $z = a$.

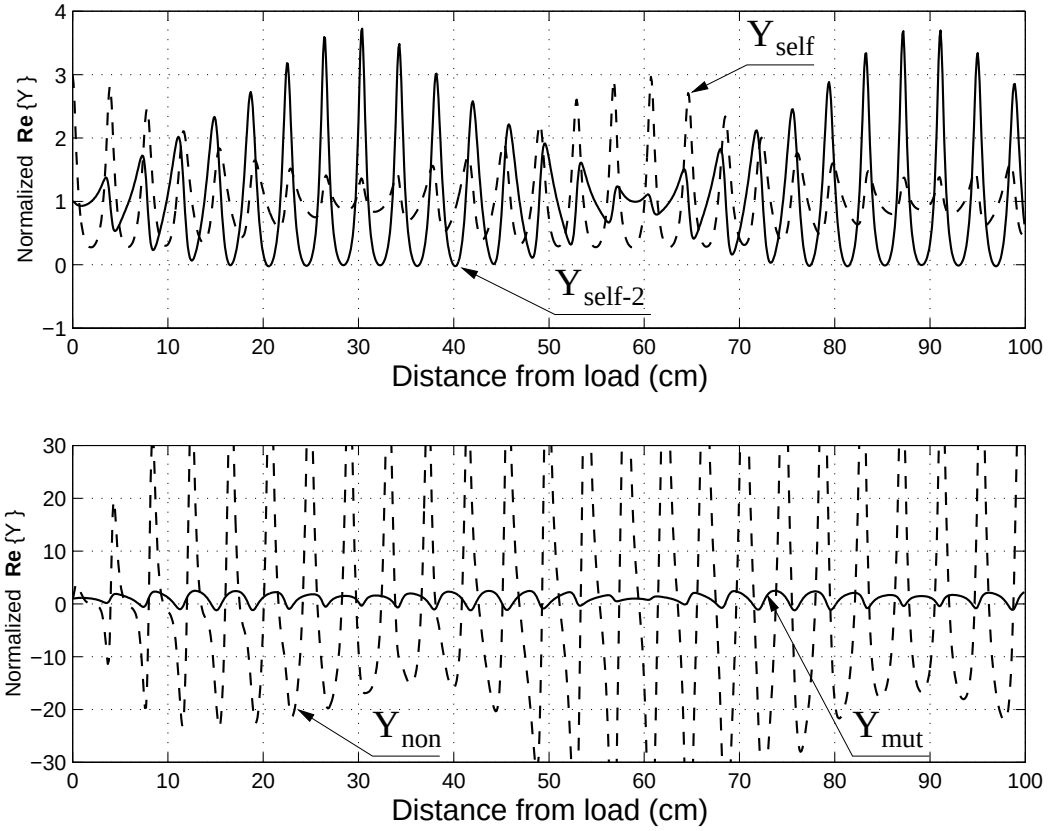

Figure 3.18 Simulated longitudinal variation (from load to $z = -100$ cm) of $\Re\mathrm{e}\{\boldsymbol{Y}_{\mathrm{in}}^{\mathrm{c}}(z)\}$ for "short" termination at 2.0 GHz, showing the negative real components of the element-normalized admittance matrix.

CHAPTER 4

NORMAL MODE AND DISTRIBUTED PARAMETER EXTRACTION

Frequency domain methods have become very popular with the availability of accurate, powerful microwave measurement and data processing systems. Automatic vector network analyzers (VNAs) provide S-parameter measurements over very broad frequency ranges. For devices with an arbitrary number of ports, complete S-parameter characterization is possible using such methods as [38] or [39].

In regards to parameter extraction, Agrawal et al. [18] presented a method to extract distributed circuit parameters from experimental data in the frequency domain and applied it to a three-line system. The method, however, requires short- and open-circuited impedance measurements using voltage and current probes.

Similarly, Williams [40] characterized a lossy, two-coupled line system by extracting the distributed circuit parameters, characteristic impedances, and propagation constants. However, extraction required measurement on multiple length sections of the coupled line system and employed a nonlinear orthogonal distance regression algorithm.

Winkel et al. [17] developed a method to determine the propagation constant of symmetric, coupled lossy lines based on high-frequency S-parameter measurements. The method is only applied to an even-odd mode system, however, as the transformation matrices (eigenvectors) for such a system are known *a priori*, which holds true only for two-conductor, two-mode symmetric systems.

Wang and Ling [41] extracted broadband multimode parameters of coupled microstrip lines using finite-difference time-domain (FDTD) simulation and then employed signal-processing techniques. Wang and Ling carefully address the physical meaning of the modal impedance and use a definition ideal for the full-wave behavior, namely the unique modal current and power flow.

Finally, Merwe et al. [19] conducted measurements on a low-loss three-coupled microstrip line strip and extracted the distributed inductance and capacitance ma-

trices. Again, this method also requires fabrication and measurement of short- and open-circuit MTL structures.

In this chapter, we present a method to extract the "normal mode parameters," which include the characteristic impedance matrices, eigenvectors (modes), and eigenvalues (propagation constants) [42]. Coupled-port S-parameter theory is first explained in the framework of MTL analysis. Then, the characteristic matrices are extracted. From these we renormalize the 50-Ω S-parameters to the characteristic impedance of the uniform coupled-line section. Finally, we employ simple MTL and S-parameter theory to extract the eigenvalues and eigenvectors numerically. We validate this method using simulated S-parameters from analytic formulas and standard commercial software packages.

The problem and the extraction method are formulated in both the state (conductor) domain and the modal domain. S-parameter data in practice is usually obtained in the state domain, or using the terminology of [43], the mixed-mode domain. Via modal decoupling, the eigenvectors allow a diagonalization of most of the conductor matrices. A comprehensive examination of the properties of the conductor and mode MTL matrices is given in [37].

4.1 Generalized Scattering Parameters in Reference Systems with Coupled Ports

Consider the n-coupled line system depicted in Fig. 4.1 with specified physical length l. This section is uniform in the longitudinal direction and symmetric in the transverse plane; the line widths w_i are such that $w_1 = w_n$, $w_2 = w_{n-1}, \ldots$. The $(n \times n)$ mode and conductor characteristic impedance matrices describing this section are denoted $\boldsymbol{Z}^{\mathrm{m}}_{\mathrm{ch}}$ and $\boldsymbol{Z}^{\mathrm{c}}_{\mathrm{ch}}$, respectively. Let the port numbers be defined such that ports 1 to n constitute the n-dimensional *input* port and ports $n+1$ to $2n$ constitute the n-dimensional *output* port. In longitudinal MTL analysis (such as [29], [37], [44]), there are input and output $(n \times n)$ immittance matrix functions looking into, respectively, the input or output side of the coupled-line system, while the opposite side is terminated with some prescribed boundary condition, normally an impedance or admittance network. Any of the $(2n \times 2n)$ frequency domain immittance matrices provide a convenient representation of this $2n$-port. In this paper, however, we focus on the $(2n \times 2n)$ S-parameter matrix from which we will extract the normal mode

parameters. In practice these S-parameters could be obtained using new methods such as the multimode TRL algorithm [45], though this paper will not concern those details.

4.1.1 Coupled ports

Measured S-parameters are usually referenced (or "normalized") to 50-Ω terminations; the characteristic or "reference" impedance for such a $2n$-port system (such as the coupled-line section in Fig. 4.1 is therefore respresented by a diagonal $(2n \times 2n)$ matrix

$$\boldsymbol{Z}_0 = 50 \cdot \mathbf{1}_{2n}, \tag{4.1}$$

where $\mathbf{1}_{2n}$ is the $(2n \times 2n)$ identity matrix. If all n characteristic impedances are equal, as in the above case, then the $(2n \times 2n)$ mode and conductor reflection coefficient matrices $\boldsymbol{\Gamma}^{\mathrm{m,c}}$ and S-parameter matrices $\boldsymbol{S}^{\mathrm{m,c}}$ of the n-port are equivalent,

$$\boldsymbol{v}^{-}_{\mathrm{m,c}} = [\boldsymbol{S}^{\mathrm{m,c}}] \cdot \boldsymbol{v}^{+}_{\mathrm{m,c}}. \tag{4.2}$$

More generally, the characteristic impedances of the ports which constitute this reference system may not all be equal, as in some devices such as pre-amplifiers. Let us also consider a $2n$-port section of n coupled lines whose $2n$ ports referenced to $2n$ different impedances. In this case,

$$\boldsymbol{Z}^{\mathrm{c}}_{\mathrm{CH}} = [\mathrm{diag}\,(Z_{01},\ Z_{02},\ Z_{03},\ \ldots,\ Z_{02n})] \tag{4.3}$$

denotes the $(2n \times 2n)$ diagonal conductor characteristic impedance matrix (the capital notation in the subscript will henceforth distinguish $2n$-dimensional matrices and vectors from their n-dimensional counterparts in n-coupled line systems).

We denote the $(2n \times 1)$-dimensional entering and exiting power waves $\boldsymbol{a}^{\mathrm{m,c}}$ and $\boldsymbol{b}^{\mathrm{m,c}}$. They are given by

$$\boldsymbol{a}^{\mathrm{m,c}} = \begin{bmatrix} \boldsymbol{a}^{\mathrm{m,c}}_{\mathrm{in}}]_1 \\ \boldsymbol{a}^{\mathrm{m,c}}_{\mathrm{in}}]_2 \\ \vdots \\ \boldsymbol{a}^{\mathrm{m,c}}_{\mathrm{in}}]_n \\ \boldsymbol{a}^{\mathrm{m,c}}_{\mathrm{out}}]_1 \\ \boldsymbol{a}^{\mathrm{m,c}}_{\mathrm{out}}]_2 \\ \vdots \\ \boldsymbol{a}^{\mathrm{m,c}}_{\mathrm{out}}]_n \end{bmatrix}, \qquad \boldsymbol{b}^{\mathrm{m,c}} = \begin{bmatrix} \boldsymbol{b}^{\mathrm{m,c}}_{\mathrm{in}}]_1 \\ \boldsymbol{b}^{\mathrm{m,c}}_{\mathrm{in}}]_2 \\ \vdots \\ \boldsymbol{b}^{\mathrm{m,c}}_{\mathrm{in}}]_n \\ \boldsymbol{b}^{\mathrm{m,c}}_{\mathrm{out}}]_1 \\ \boldsymbol{b}^{\mathrm{m,c}}_{\mathrm{out}}]_2 \\ \vdots \\ \boldsymbol{b}^{\mathrm{m,c}}_{\mathrm{out}}]_n \end{bmatrix}, \tag{4.4}$$

where $\boldsymbol{a}_{\text{in}}^{\text{m,c}}$ is the $(n \times 1)$ mode and conductor power wave vector entering the input port and $\boldsymbol{b}_{\text{in}}^{\text{m,c}}$ is the $(n \times 1)$ mode and conductor power wave vector exiting the input port. Similarly, at the ouput port, we have the entering power waves $\boldsymbol{a}_{\text{out}}^{\text{m,c}}$ and exiting power waves $\boldsymbol{b}_{\text{out}}^{\text{m,c}}$. Note that the wave $\boldsymbol{a}_{\text{out}}^{\text{m,c}}]_n$ denotes the mode or conductor power wave entering the nth output port (port number $2n$ in Fig. 4.1).

The mode and conductor power waves are now defined and normalized as

$$\boldsymbol{a}^{\text{m,c}} = [\boldsymbol{Z}_{\text{CH}}^{\text{m,c}}]^{-1/2} \cdot \boldsymbol{v}_{\text{m,c}}^{+}, \tag{4.5a}$$

$$\boldsymbol{b}^{\text{m,c}} = [\boldsymbol{Z}_{\text{CH}}^{\text{m,c}}]^{-1/2} \cdot \boldsymbol{v}_{\text{m,c}}^{-}. \tag{4.5b}$$

Thus, the generalized mode or conductor $(2n \times 2n)$ S-parameter matrix, denoted $\boldsymbol{S}^{\text{m,c}}$, relates these mode or conductor power waves by

$$\boldsymbol{b}^{\text{m,c}} = \boldsymbol{S}^{\text{m,c}} \cdot \boldsymbol{a}^{\text{m,c}}, \tag{4.6}$$

where $\boldsymbol{S}^{\text{m,c}}$ consists of the four $(n \times n)$ submatrices $\boldsymbol{S}_{\text{in,in}}^{\text{m,c}}$, $\boldsymbol{S}_{\text{in,out}}^{\text{m,c}}$, $\boldsymbol{S}_{\text{out,in}}^{\text{m,c}}$, and $\boldsymbol{S}_{\text{out,out}}^{\text{m,c}}$,

$$\boldsymbol{S}^{\text{m,c}} = \begin{bmatrix} \boldsymbol{S}_{\text{in,in}}^{\text{m,c}} & \boldsymbol{S}_{\text{in,out}}^{\text{m,c}} \\ \boldsymbol{S}_{\text{out,in}}^{\text{m,c}} & \boldsymbol{S}_{\text{out,out}}^{\text{m,c}} \end{bmatrix}, \tag{4.7}$$

relating the $(n \times 1)$ mode or conductor power wave vectors at the n-dimensional input and output ports.

Consider a device with an arbitrary number of ports p, referenced to some diagonal $(p \times p)$ characteristic impedance matrix as in (4.3). In this case, the inward-traveling conductor power waves $\boldsymbol{a}^{\text{c}}]_i$ on each port are independent. We will refer to this reference system as *uncoupled*; in other words, an excitation at port i produces only the inward-traveling wave $\boldsymbol{a}^{\text{c}}]_i$ if all ports are matched. It follows in uncoupled reference systems (whose characteristic impedance matrices are always diagonal) that the independent excitation $\boldsymbol{a}^{\text{c}}]_i$ only depends on $\boldsymbol{v}_{\text{S}}^{\text{c}}]_i$ and $\boldsymbol{b}^{\text{c}}]_i$.

For the general case, we consider reference systems with two or more ports coupled to one another. We term these reference systems with port coupling *coupled* reference systems. In other words, their reference systems have characteristic impedance matrices $\boldsymbol{Z}_{\text{CH}}^{\text{c}}$ with nonzero off-diagonal terms. In scattering analysis, this matrix property has an obvious physical interpretation: it leads to interdependent power wave coupling, by virtue of (4.5). In other words, if port i is coupled to port j ($[\boldsymbol{Z}_{\text{ch}}^{\text{c}}]_{ij} = [\boldsymbol{Z}_{\text{ch}}^{\text{c}}]_{ji} \neq 0$), the inward-traveling wave $\boldsymbol{a}^{\text{c}}]_i$ depends on $\boldsymbol{v}_{\text{S}}^{\text{c}}]_j$.

Where would such a reference system be encountered in practice? It would obviously be encountered in MTL systems such as Fig. 4.1, manifested in the section of coupled lines on the right or left which feed the section of coupled lines of length l,

the device under test (DUT) considered in this paper. The $(n \times 1)$ conductor voltages and currents in this MTL section are generally related by dense $(n \times n)$ characteristic impedance and admittance matrices $\boldsymbol{Z}^{\mathrm{c}}_{\mathrm{ch}}$ and $\boldsymbol{Y}^{\mathrm{c}}_{\mathrm{ch}}$. The feedline connection is clearly uniform across the reference plane, thus the $2n$-port symmetric, coupled reference system $\boldsymbol{Z}^{\mathrm{c}}_{\mathrm{CH}}$ is described by the $2n \times 2n$ matrix

$$\boldsymbol{Z}^{\mathrm{c}}_{\mathrm{CH}} = \begin{bmatrix} \boldsymbol{Z}^{\mathrm{c}}_{\mathrm{ch}} & \mathbf{0} \\ \mathbf{0} & \boldsymbol{Z}^{\mathrm{c}}_{\mathrm{ch}} \end{bmatrix}. \tag{4.8}$$

Although $\boldsymbol{Z}^{\mathrm{c}}_{\mathrm{ch}}$ may be dense, the zero matrices indicate no coupling between ports on the input and output, an assumption which applies to the analysis in this paper.

Now, the set of n ports looking into the input (or output) of the DUT is really an infinitesimal section of coupled lines (zero phase, zero loss) with an equivalent characteristic impedance matrix as the substituted section of length l. This "port coupling" is illustrated in Fig. 4.2.

4.1.2 Decoupled-to-coupled S-parameter re-referencing

Once again, microwave device and system S-parameters are normally referenced with uncoupled, 50-Ω characteristic impedance ports. However, to extract modal information from the conductor S-parameter matrix $\boldsymbol{S}^{\mathrm{c}}$, the reference system should be identical to the characteristic impedance matrix of the coupled-line section, given by (4.8).

Therefore, we must re-reference the $(2n \times 2n)$ S-parameter matrix of the DUT (of length l) from $\boldsymbol{Z}_0$ to $\boldsymbol{Z}^{\mathrm{c}}_{\mathrm{CH}}$. (Note that for an uncoupled system, $\boldsymbol{Z}^{\mathrm{c}}_0 = \boldsymbol{Z}^{\mathrm{m}}_0$; therefore, we omit the superscript.) To accomplish this, we convert the S-parameter matrix to a $(2n \times 2n)$ open-circuit impedance matrix for the $2n$-port.

The S-parameter matrix for a system (in this case, a $2n$-port system of n-coupled lines) in terms of its open-circuit impedance matrix referenced to a general coupled or uncoupled characteristic impedance matrix $\boldsymbol{Z}^{\mathrm{c}}_{\mathrm{CH}}$ was derived in [37], [44], [46] and is repeated here for convenience using the uncoupled 50-Ω reference characteristic impedance matrix $\boldsymbol{Z}_0$:

$$\boldsymbol{S}^{\mathrm{c}} = (\boldsymbol{Z}_0)^{1/2} \cdot [\boldsymbol{Z}^{\mathrm{c}} + \boldsymbol{Z}_0]^{-1} \cdot [\boldsymbol{Z}^{\mathrm{c}} - \boldsymbol{Z}_0] \cdot (\boldsymbol{Z}_0)^{-1/2}. \tag{4.9}$$

Rearranging this equation for an S-parameter set referenced to $\boldsymbol{Z}_0$ and solving for the impedance matrix yields

$$\boldsymbol{Z} = \boldsymbol{Z}_0 \cdot \left([\boldsymbol{Z}_0]^{-1/2} \cdot \boldsymbol{S}^{\mathrm{c}} \cdot [\boldsymbol{Z}_0]^{1/2} + \mathbf{1}_{2n}\right) \cdot \left(\mathbf{1}_{2n} - [\boldsymbol{Z}_0]^{-1/2} \cdot \boldsymbol{S}^{\mathrm{c}} \cdot [\boldsymbol{Z}_0]^{1/2}\right)^{-1}. \tag{4.10}$$

Finally, we re-reference $\boldsymbol{S}^{\mathrm{c}}$ to $\boldsymbol{Z}^{\mathrm{c}}_{\mathrm{CH}}$ by solving (4.10) and combining $\boldsymbol{Z}^{\mathrm{c}}$ with the coupled reference system $\boldsymbol{Z}^{\mathrm{c}}_{\mathrm{CH}}$ in place of $\boldsymbol{Z}_0$ in (4.9).

4.1.3 Solution for power waves

Given an S-parameter matrix referenced to some prescribed characteristic impedance matrix $\boldsymbol{Z}^{\mathrm{c}}_{\mathrm{CH}}$, and given both port and interport boundary conditions (in the form of termination matrices), the conductor power wave vectors are solved quite easily; the mode power vectors are not required by this extraction method but are nonetheless derived with the analogous mode quantities.

Consider a general n-coupled-port system with given $(2n \times 2n)$ conductor S-parameter matrix $\boldsymbol{S}^{\mathrm{c}}$, referenced to the characteristic impedance matrix $\boldsymbol{Z}^{\mathrm{c}}_{\mathrm{CH}}$. Suppose all $2n$ ports are terminated with $(2n \times 2n)$ impedance matrix $\boldsymbol{Z}^{\mathrm{c}}_{\mathrm{T}}$ and excited with a $(2n \times 1)$ Thevenin voltage source $\boldsymbol{v}^{\mathrm{c}}_{\mathrm{S}}$. We may easily determine the forward and backward power waves given these boundary conditions and the scattering parameters $\boldsymbol{S}^{\mathrm{c}}$ by first expressing the independent power wave $\boldsymbol{a}^{\mathrm{c}}$ as the contribution from the voltage divider at the $2n$ ports and the reflection from the port termination impedances:

$$\boldsymbol{a}^{\mathrm{c}} = [\boldsymbol{Z}^{\mathrm{c}}_{\mathrm{CH}}]^{-1/2} \cdot \boldsymbol{T}^{\mathrm{c}}_{\mathrm{S}} \cdot \boldsymbol{v}^{\mathrm{c}}_{\mathrm{S}} + \boldsymbol{\Gamma}^{\mathrm{c}}_{\mathrm{S}} \cdot \boldsymbol{b}^{\mathrm{c}}, \tag{4.11}$$

where $\boldsymbol{\Gamma}^{\mathrm{c}}_{\mathrm{S}}$ is the port reflection coefficient matrix, looking from the DUT towards its terminations, given by

$$\boldsymbol{\Gamma}^{\mathrm{c}}_{\mathrm{S}} = [\boldsymbol{Z}^{\mathrm{c}}_{\mathrm{T}} + \boldsymbol{Z}^{\mathrm{c}}_{\mathrm{CH}}]^{-1} \cdot [\boldsymbol{Z}^{\mathrm{c}}_{\mathrm{T}} - \boldsymbol{Z}^{\mathrm{c}}_{\mathrm{CH}}], \tag{4.12}$$

and $\boldsymbol{T}^{\mathrm{c}}_{\mathrm{S}}$ is the source voltage transmission coefficient matrix given by

$$\boldsymbol{T}^{\mathrm{c}}_{\mathrm{S}} = \boldsymbol{Z}^{\mathrm{c}} \cdot [\boldsymbol{Z}^{\mathrm{c}}_{\mathrm{S}} + \boldsymbol{Z}^{\mathrm{c}}]^{-1}, \tag{4.13}$$

where $\boldsymbol{Z}^{\mathrm{c}}$ is given by

$$\boldsymbol{Z}^{\mathrm{c}} = (\boldsymbol{Z}^{\mathrm{c}}_{\mathrm{CH}})^{1/2} \cdot [\mathbf{1}_{2n} - \boldsymbol{S}^{\mathrm{c}}]^{-1} \cdot [\mathbf{1}_{2n} + \boldsymbol{S}^{\mathrm{c}}] \cdot (\boldsymbol{Z}^{\mathrm{c}}_{\mathrm{CH}})^{1/2}. \tag{4.14}$$

The second relation between the independent and dependent power waves is of course the S-parameter matrix. Combining (4.11) and (4.6), we arrive at

$$\boldsymbol{a}^{\mathrm{c}} = \mathcal{L}^{\mathrm{c}}_{a} \boldsymbol{v}^{\mathrm{c}}_{\mathrm{S}} \tag{4.15}$$

where the operator $\mathcal{L}^{\mathrm{c}}_{a}$ is

$$\mathcal{L}^{\mathrm{c}}_{a} = \left[[\mathbf{1}_{2n} - \boldsymbol{\Gamma}^{\mathrm{c}}_{\mathrm{S}} \cdot \boldsymbol{S}^{\mathrm{c}}]^{-1} \cdot [\boldsymbol{Z}^{\mathrm{c}}_{\mathrm{CH}}]^{-1/2} \cdot \boldsymbol{T}^{\mathrm{c}}_{\mathrm{S}} \cdot \right]; \tag{4.16}$$

similarly, the relationship for $\boldsymbol{b}$ is easily shown to be

$$\boldsymbol{b}^{\mathrm{c}} = \mathcal{L}^{\mathrm{c}}_{b} \boldsymbol{v}^{\mathrm{c}}_{\mathrm{S}}. \tag{4.17}$$

with

$$\mathcal{L}_b^{\mathrm{c}} = \left[[\mathbf{1}_{2n} - \boldsymbol{S}^{\mathrm{c}} \cdot \boldsymbol{\Gamma}_{\mathrm{S}}^{\mathrm{c}}]^{-1} \cdot \boldsymbol{S}^{\mathrm{c}} \cdot [\boldsymbol{Z}_{\mathrm{ch}}^{\mathrm{c}}]^{-1/2} \cdot \boldsymbol{T}_{\mathrm{S}}^{\mathrm{c}} \cdot \right] . \tag{4.18}$$

Therefore, as expected by the definition of power waves, $\boldsymbol{a}^{\mathrm{c}}$ results from the input voltage at the ports with voltage sources in addition to the contribution from the reflection of outward waves at "unmatched" ports.

4.2 Frequency Domain Mode Extraction

To illustrate the normal mode parameter extraction numerically, we consider the analytic form of conductor and mode S-parameters as functions of the normal mode parameters. This will provide an analytical test to which we can apply the characteristic impedance and mode extraction procedures.

The central assumption regarding the success of this optimization is that good initial guesses for the normal mode parameters exist. Numerous EM field and circuit extraction tools may be employed to approximate the eigenvectors; these will usually provide satisfactory initial guesses.

4.2.1 Multimode analytic S-parameter expressions

The relationship between the conductor and mode S-parameters has been derived for a two-mode system [43], but in the general n-line case where the voltage and current eigenvectors are not equal, this relationship is not so simple. Here, we derive a general relationship applicable to n-line systems with arbitrary characteristic impedance matrices. While multiple formulations exist, the most direct utilizes multimode signal flow graph theory, analogous to the common scalar derivation of the S-parameters of a known length of line of some specified characteristic impedance (e.g., [47]).

First, we consider a section of n coupled lines of length l. In this $2n$-port device, with port numbers defined at the reference planes as per Fig. 4.1, we have four $(n \times n)$ mode or conductor S-parameter submatrices as in (4.7). Symmetry leads to $\boldsymbol{S}_{\mathrm{in,in}}^{\mathrm{m,c}} = \boldsymbol{S}_{\mathrm{out,out}}^{\mathrm{m,c}}$; reciprocity leads to $\boldsymbol{S}_{\mathrm{out,in}}^{\mathrm{m,c}} = \boldsymbol{S}_{\mathrm{in,out}}^{\mathrm{m,c}}$. Now we extend scalar signal flow graph analysis such that the nodes correspond to vector power waves and the branches correspond to matrices. Figure 4.3 shows the signal flow graph for a length l of coupled lines with characteristic impedance matrix $\boldsymbol{Z}_{\mathrm{ch}}^{\mathrm{m,c}}$ referenced to some system $\boldsymbol{Z}_0^{\mathrm{m,c}}$.

Power wave scattering in the coupled line section results not only from the coupled length l but also from the junctions between the test and reference system at the input and output, since, in general, the reference and coupled line characteristic impedance matrices are not equal. Therefore, the signal flow representation for the total section of coupled lines in some reference system is the cascade of three $2n$-port systems: the input junction, the lines, and the output junction, as shown in Fig. 4.3.

Next, we simultaneously derive the conductor and mode S-parameters of the reference-to-test junction. For both these domains, the antisymmetry and reciprocity yield $\boldsymbol{S}_{11}^{\text{jun}} = -\boldsymbol{S}_{22}^{\text{jun}}$ and $\boldsymbol{S}_{12}^{\text{jun}} = \boldsymbol{S}_{21}^{\text{jun}}$ (where $\boldsymbol{S}_{11}^{\text{jun}}$ looks into the input junction from the reference side and $\boldsymbol{S}_{22}^{\text{jun}}$ looks into the output junction from the DUT side). For simplicity, we denote $\boldsymbol{\Gamma} = \boldsymbol{S}_{11}^{\text{jun}}$ and $\boldsymbol{T} = \boldsymbol{S}_{12}^{\text{jun}}$, applicable as either a conductor or mode variable. S-parameter analysis on the junction yields

$$\boldsymbol{\Gamma}^{\text{m,c}} = (\boldsymbol{Z}_{\text{ch}}^{\text{m,c}} - \boldsymbol{Z}_0) \cdot (\boldsymbol{Z}_{\text{ch}}^{\text{m,c}} + \boldsymbol{Z}_0)^{-1}, \tag{4.19}$$

$$\boldsymbol{T}^{\text{m,c}} = 2[\boldsymbol{Z}_{\text{ch}}^{\text{m,c}}]^{-1/2} \cdot \left(\boldsymbol{1}_n + \boldsymbol{Z}_0 \cdot [\boldsymbol{Z}_{\text{ch}}^{\text{m,c}}]^{-1}\right)^{-1} \cdot [\boldsymbol{Z}_0]^{-1/2}. \tag{4.20}$$

We now consider propagation on the coupled section (between the dashed lines in Fig. 4.3), quantified by the mode or conductor power wave propagator matrix $\boldsymbol{\Psi}^{\text{m,c}}(-l)$, as shown in Fig. 4.3.

The mode or conductor MTL propagator matrix $\boldsymbol{Q}^{\text{m,c}}(-l)$ relates the conductor (or mode) inward-traveling voltage on the input side of the coupled-line section to the conductor (or mode) outward-traveling voltages on the output side as

$$\bar{\boldsymbol{b}}_{\text{out}}^{\text{m,c}} = [\boldsymbol{Z}_{\text{ch}}^{\text{m,c}}]^{1/2} \cdot \boldsymbol{Q}^{\text{m,c}}(-l) \cdot [\boldsymbol{Z}_{\text{ch}}^{\text{m,c}}]^{-1/2} \cdot \bar{\boldsymbol{a}}_{\text{in}}^{\text{m,c}}, \tag{4.21}$$

where we have used an overbar to identify the vector as one entering or exiting the coupled-line section between the center dashed lines in Fig. 4.3.

Since the mode voltages and currents are propagated by the MTL propagator matrix

$$\boldsymbol{Q}^{\text{m}}(-l) = \text{diag}\left(e^{-\gamma_1 l}, e^{-\gamma_2 l}, \ldots, e^{-\gamma_n l}\right), \tag{4.22}$$

an expression for the conductor propagator matrix follows if we relate conductor and mode power waves from (4.5). Using (4.5b) and the eigenvector definition we can write

$$\begin{aligned} \bar{\boldsymbol{b}}_{\text{out}}^{\text{m}} &= [\boldsymbol{Z}_{\text{ch}}^{\text{m}}]^{-1/2} \cdot \boldsymbol{E} \cdot \bar{\boldsymbol{v}}_{\text{c-out}}^{-} \\ &= [\boldsymbol{Z}_{\text{ch}}^{\text{m}}]^{-1/2} \cdot \boldsymbol{E} \cdot [\boldsymbol{Z}_{\text{ch}}^{\text{c}}]^{1/2} \cdot \bar{\boldsymbol{b}}_{\text{out}}^{\text{c}}. \end{aligned} \tag{4.23}$$

Similarly,

$$\bar{\boldsymbol{a}}_{\text{in}}^{\text{m}} = [\boldsymbol{Z}_{\text{ch}}^{\text{m}}]^{-1/2} \cdot \boldsymbol{E} \cdot [\boldsymbol{Z}_{\text{ch}}^{\text{c}}]^{1/2} \cdot \bar{\boldsymbol{a}}_{\text{in}}^{\text{c}}, \tag{4.24}$$

and the relationship between the conductor and mode propagator matrices is thus

$$\boldsymbol{Q}^{\mathrm{c}}(z) = [\boldsymbol{Z}^{\mathrm{c}}_{\mathrm{ch}}]^{-1/2} \cdot \boldsymbol{E}^{-1} \cdot \boldsymbol{Q}^{\mathrm{m}}(z) \cdot \boldsymbol{E} \cdot [\boldsymbol{Z}^{\mathrm{c}}_{\mathrm{ch}}]^{1/2}. \tag{4.25}$$

Therefore, the mode or conductor power wave propagator matrix is

$$\boldsymbol{\Psi}^{\mathrm{m,c}}(-l) = [\boldsymbol{Z}^{\mathrm{m,c}}_{\mathrm{ch}}]^{1/2} \cdot \boldsymbol{Q}^{\mathrm{m,c}}(-l) \cdot [\boldsymbol{Z}^{\mathrm{m,c}}_{\mathrm{ch}}]^{-1/2}, \tag{4.26}$$

and the $(n \times n)$ submatrices

$$\boldsymbol{S}_{\mathrm{in,in}} = \boldsymbol{\Gamma} - \boldsymbol{T} \cdot \boldsymbol{\Psi}(-l) \cdot \boldsymbol{\Gamma} \cdot \boldsymbol{Q}(-l) \cdot [\mathbf{1}_n - \boldsymbol{\Gamma} \cdot \boldsymbol{\Psi}(-l) \cdot \boldsymbol{\Gamma} \cdot \boldsymbol{\Psi}(-l)]^{-1} \cdot \boldsymbol{T} \tag{4.27a}$$

$$\boldsymbol{S}_{\mathrm{in,out}} = \boldsymbol{T} \cdot [\mathbf{1}_n - \boldsymbol{\Gamma} \cdot \boldsymbol{\Psi}(-l) \cdot \boldsymbol{\Gamma} \cdot \boldsymbol{\Psi}(-l)]^{-1} \cdot \boldsymbol{\Psi}(-l)\boldsymbol{T} \tag{4.27b}$$

are easily derived from the signal flow graph (note that we have omitted the mode and conductor superscript labels for simplicity). The final $(2n \times 2n)$ S-parameter matrix of the coupled lines is assembled from (4.7).

4.2.2 Characteristic matrix extraction

Extraction of modal coefficients and propagation constants for the n-line DUT becomes trivial if we can reference the S-parameter matrix to the $(n \times n)$ characterisitc impedance matrix $\boldsymbol{Z}^{\mathrm{c}}_{\mathrm{ch}}$ of the DUT. This implies that we must first directly extract $\boldsymbol{Z}^{\mathrm{c}}_{\mathrm{ch}}$, which is not initially known, from the S-parameters referenced to $\boldsymbol{Z}_0$.

A single, uniform, lossless transmission line terminated with an impedance Z_0 equal to its characteristic impedance is matched; its longitudinal immittance functions are constant, and the input impedance is everywhere equal to Z_0. Optimization of Z_0 given only one line-length S-parameter set requires only a relatively good intial guess. Uniform, lossless MTL characteristic impedance matrix extraction simply extends this property to its matrix form. The input impedance matrix $\boldsymbol{Z}^{\mathrm{c}}_{\mathrm{in}}(z)$ will only remain constant and equal $\boldsymbol{Z}^{\mathrm{c}}_{\mathrm{ch}}$ if the output is terminated with $\boldsymbol{Z}^{\mathrm{c}}_{\mathrm{ch}}$.

We denote the $(n \times n)$ initial guess $\tilde{\boldsymbol{Z}}^{\mathrm{c}}_{\mathrm{ch}}$. The $(n \times n)$ reflection coefficient matrix looking into the output from a $\boldsymbol{Z}_0$ system terminated by $\tilde{\boldsymbol{Z}}^{\mathrm{c}}_{\mathrm{ch}}$ is

$$\boldsymbol{\Gamma}^{\mathrm{c}}_{\mathrm{t}} = \left(\tilde{\boldsymbol{Z}}^{\mathrm{c}}_{\mathrm{ch}} - \boldsymbol{Z}_0\right) \cdot \left(\tilde{\boldsymbol{Z}}^{\mathrm{c}}_{\mathrm{ch}} + \boldsymbol{Z}_0\right)^{-1}, \tag{4.28}$$

and the $(n \times n)$ reflection coefficient at the input with this termination is thus

$$\boldsymbol{\Gamma}^{\mathrm{c}}_{\mathrm{in}} = [\boldsymbol{S}^{\mathrm{c}}]_{\mathrm{in,in}} + [\boldsymbol{S}^{\mathrm{c}}]_{\mathrm{in,out}} \cdot \left([\boldsymbol{\Gamma}^{\mathrm{c}}_{\mathrm{t}}]^{-1} - [\boldsymbol{S}^{\mathrm{c}}]_{\mathrm{out,out}}\right)^{-1} \cdot [\boldsymbol{S}^{\mathrm{c}}]_{\mathrm{out,in}} \tag{4.29}$$

where we have indexed the four $(n \times n)$ submatrices of $\boldsymbol{S}^{\mathrm{c}}$, from (4.7). Now, we terminate the output side with the initial guess $\tilde{\boldsymbol{Z}}^{\mathrm{c}}_{\mathrm{ch}}$. If $\tilde{\boldsymbol{Z}}^{\mathrm{c}}_{\mathrm{ch}}$ matches the actual

characteristic impedance of the unknown section of coupled lines under test, then

$$\tilde{\boldsymbol{Z}}^{\mathrm{c}}_{\mathrm{ch}} = \boldsymbol{Z}^{\mathrm{c}}_{\mathrm{in}}(-l) \tag{4.30a}$$

$$= (\mathbf{1}_n - \boldsymbol{\Gamma}^{\mathrm{c}}_{\mathrm{in}}(-l))^{-1} \cdot (\mathbf{1}_n + \boldsymbol{\Gamma}^{\mathrm{c}}_{\mathrm{in}}(-l)) \cdot \boldsymbol{Z}_0 \tag{4.30b}$$

$$= \boldsymbol{Z}^{\mathrm{c}}_{\mathrm{ch}}. \tag{4.30c}$$

Obviously with a decent initial guess we may optimize the solution $\tilde{\boldsymbol{Z}}^{\mathrm{c}}_{\mathrm{ch}}$ by minimizing the Frobenius matrix norm

$$|||[\tilde{\boldsymbol{Z}}^{\mathrm{c}}_{\mathrm{ch}}] - [\boldsymbol{Z}^{\mathrm{c}}_{\mathrm{in}}(-l)]|||. \tag{4.31}$$

We then re-reference the $2n$-port S-parameters of the DUT to their characteristic impedance $\tilde{\boldsymbol{Z}}^{\mathrm{c}}_{\mathrm{ch}}$, and denote the result $\tilde{\boldsymbol{S}}^{\mathrm{c}}$. The accuracy of the solution $\tilde{\boldsymbol{Z}}^{\mathrm{c}}_{\mathrm{ch}}$ may now be estimated by examining the submatrix $\tilde{\boldsymbol{S}}^{\mathrm{c}}_{\mathrm{in,in}}$. Since the junctions at the input and output is uniform when the reference system characteristic impedance equals the characteristic impedance of the DUT (coupled-line section), all elements of $\tilde{\boldsymbol{S}}^{\mathrm{c}}_{\mathrm{in,in}}$ (or $\tilde{\boldsymbol{S}}^{\mathrm{c}}_{\mathrm{out,out}}$, since $\tilde{\boldsymbol{S}}^{\mathrm{c}}_{\mathrm{in,in}} = \tilde{\boldsymbol{S}}^{\mathrm{c}}_{\mathrm{out,out}}$ should be zero when (4.30c) applies. Therefore, we define a figure of merit, M as

$$M = ||\tilde{\boldsymbol{S}}^{\mathrm{c}}_{\mathrm{in,in}}||. \tag{4.32}$$

However, this method is, in rare cases, susceptible to error. In single transmission line characteristic impedance extraction, the so-called half-wavelength windows, which occur when the line length is some integer multiple of $\lambda/2$, are obviously problematic. These effectively make the transmission line section transparent, repeating the output termination at the input, regardless of the magnitude of the mismatch. In MTL systems, the half-wavelength ambiguities occur when the physical length is an integer multiple of one or more mode half-wavelengths, i.e.,

$$\beta_j l = n\pi, \qquad n = 1, 2, \ldots, \tag{4.33}$$

where β_j is the imaginary part of the complex propagation constant, $\gamma_j = \alpha_j + i\beta_j$. When (4.33) occurs for the jth mode, the modal form of (4.30a) holds for all initial guesses, i.e., $[\tilde{\boldsymbol{Z}}^{\mathrm{m}}_{\mathrm{ch}}]_{jj} = [\boldsymbol{Z}^{\mathrm{m}}_{\mathrm{in}}(-l)]_{jj}$ always, and extracted values are therefore suspect. These mode half-wavelength ambiguities (MHWAs) must be carefully considered during extraction. If possible, S-parameter simulations or measurements must be avoided for physical lengths corresponding to these MHWAs. Otherwise, error could be avoided by performing a narrowband frequency sweep through the design frequency, thus simulating a slight longitudinal distance sweep through the actual design length and its MHWA.

4.2.3 Eigenvector and eigenvalue extraction

In systems where the orthogonal voltage and current eigenvectors are equal ($\boldsymbol{E} = \boldsymbol{H}$) the eigenvalues may be easily extracted by diagonalizing the $\tilde{\boldsymbol{Z}}^{\mathrm{c}}_{\mathrm{ch}}$-renormalized conductor S-parameter matrix. In general systems, however, $\boldsymbol{E} \neq \boldsymbol{H}$, and since the S-parameter matrices relate power waves and not strictly voltages and currents, it becomes necessary to determine $\boldsymbol{E}$ and $\boldsymbol{H}$ independently.

In a lossless, uniform system, orthogonal eigenvectors propagate with only a complex scaling factor k. To make the coupled lines appear uniform (or infinite in extent), the n-dimensional output port is then terminated with the optimized characteristic impedance matrix $\tilde{\boldsymbol{Z}}^{\mathrm{c}}_{\mathrm{ch}}$, and the $2n$-port termination matrix is

$$\boldsymbol{Z}^{\mathrm{c}}_{\mathrm{T}} = \begin{bmatrix} \mathbf{0} & \mathbf{0} \\ \mathbf{0} & \tilde{\boldsymbol{Z}}^{\mathrm{c}}_{\mathrm{ch}} \end{bmatrix}, \tag{4.34}$$

which absorbs all outward power waves for all modes provided that (4.30a) holds. We construct the boundary conditions (4.12) and (4.13), and the operators $\mathcal{L}_a$ and $\mathcal{L}_b$.

Then we apply a conductor voltage $\hat{\boldsymbol{v}}^{\mathrm{c}}_{\mathrm{in}}$ on the input as an initial guess for an eigenvector. The corresponding voltage source voltage vector is

$$\hat{\boldsymbol{v}}^{\mathrm{c}}_{\mathrm{S}} = \begin{bmatrix} \hat{\boldsymbol{v}}^{\mathrm{c}}_{\mathrm{in}}]_1 \\ \hat{\boldsymbol{v}}^{\mathrm{c}}_{\mathrm{in}}]_2 \\ \vdots \\ \hat{\boldsymbol{v}}^{\mathrm{c}}_{\mathrm{in}}]_n \\ 0 \\ 0 \\ \vdots \\ 0 \end{bmatrix}, \tag{4.35}$$

where the carets denote the vectors as "test" or "guess" vectors.

Power waves for these boundary conditions are calculated from (4.15) and (4.17), and from (4.5) we determine the n-dimensional input and output voltage vectors. If this input voltage vector assumes any one of the system eigenvectors, the output excitation vector will also assume the configuration of this eigenvector, scaled by a complex constant k, with unity magnitude,

$$\boldsymbol{v}^{+}_{\mathrm{c-in}} = k\boldsymbol{v}^{-}_{\mathrm{c-out}}. \tag{4.36}$$

We therefore determine an eigenvector by maximizing the coefficient of linear dependence between the input and output. Consequently, the eigenvalues for each mode are the respective values k.

Several significant drawbacks of this mode-by-mode determination include the requirement of good initial guesses for the eigenvectors, careful consideration of zero-valued elements, and the relative scalar ambiguity between any pair of eigenvectors. To eliminate the first two of these shortcomings, we should extract all eigenvectors simultaneously. When $\boldsymbol{v}^{+}_{\mathrm{c-in}}$ consists of more than one mode, (4.36) becomes a matrix equation. Vectors $\boldsymbol{v}^{+}_{\mathrm{c-in}}$ and $\boldsymbol{v}^{-}_{\mathrm{c-out}}$ are now related by

$$\boldsymbol{v}^{+}_{\mathrm{c-in}} = \boldsymbol{M} \cdot \boldsymbol{v}^{-}_{\mathrm{c-out}}, \tag{4.37}$$

where matrix $\boldsymbol{M}$ accounts for the multimode distribution. Matrix $\boldsymbol{M}$ is easily expressed in terms of the eigenvectors and eigenvalues by considering

$$\boldsymbol{E} \cdot \boldsymbol{v}^{+}_{\mathrm{c-in}} = \boldsymbol{v}^{+}_{\mathrm{m-in}}, \tag{4.38}$$

and

$$\boldsymbol{v}^{-}_{\mathrm{c-out}} = \boldsymbol{E}^{-1} \cdot \boldsymbol{v}^{-}_{\mathrm{m-out}}. \tag{4.39}$$

From MTL theory we have

$$\boldsymbol{v}^{-}_{\mathrm{m-out}} = \boldsymbol{Q}^{\mathrm{m}}(-l) \cdot \boldsymbol{v}^{+}_{\mathrm{m-in}}, \tag{4.40}$$

therefore, $\boldsymbol{M}$ must be

$$\boldsymbol{M} = \boldsymbol{E}^{-1} \cdot \boldsymbol{Q}^{\mathrm{m}}(l) \cdot \boldsymbol{E}. \tag{4.41}$$

With the boundary condition (4.34), simultaneous extraction of the n modes requires n $(2n \times 1)$ voltage "test" vectors as in (4.35), which we shall number $\hat{\boldsymbol{v}}^{\mathrm{c}}_{\mathrm{S}-1}, \hat{\boldsymbol{v}}^{\mathrm{c}}_{\mathrm{S}-2}, \ldots, \hat{\boldsymbol{v}}^{\mathrm{c}}_{\mathrm{S}-n}$. For compactness, we group the n test voltages and power waves into $(2n \times n)$ matrices,

$$\hat{\boldsymbol{V}}^{\mathrm{c}}_{\mathrm{S}} = \left[\begin{array}{cccc} \hat{\boldsymbol{v}}^{\mathrm{c}}_{\mathrm{S}-1} & \hat{\boldsymbol{v}}^{\mathrm{c}}_{\mathrm{S}-2} & \ldots & \hat{\boldsymbol{v}}^{\mathrm{c}}_{\mathrm{S}-n} \end{array} \right], \tag{4.42}$$

and

$$\hat{\boldsymbol{A}}^{\mathrm{c}} = \left[\begin{array}{cccc} \hat{\boldsymbol{a}}^{\mathrm{c}}_{1} & \hat{\boldsymbol{a}}^{\mathrm{c}}_{2} & \ldots & \hat{\boldsymbol{a}}^{\mathrm{c}}_{n} \end{array} \right], \tag{4.43}$$

which are related by

$$\hat{\boldsymbol{A}}^{\mathrm{c}} = \mathcal{L}^{\mathrm{c}}_{a} \hat{\boldsymbol{V}}^{\mathrm{c}}_{\mathrm{S}}. \tag{4.44}$$

Similarly, we have

$$\hat{\boldsymbol{B}}^{\mathrm{c}} = \mathcal{L}^{\mathrm{c}}_{b} \hat{\boldsymbol{V}}^{\mathrm{c}}_{\mathrm{S}}. \tag{4.45}$$

To solve for the components of $\boldsymbol{M}$, the power waves at the input and output must be converted to inward- and outward-travelling voltage waves using (4.5),

$$\hat{\boldsymbol{V}}^{+}_{\mathrm{c-in}} = [\tilde{\boldsymbol{Z}}^{\mathrm{c}}_{\mathrm{ch}}]^{1/2} \cdot \hat{\boldsymbol{A}}^{\mathrm{c}}_{\mathrm{in}} \tag{4.46a}$$

$$\hat{\boldsymbol{V}}^{-}_{\mathrm{c-out}} = [\tilde{\boldsymbol{Z}}^{\mathrm{c}}_{\mathrm{ch}}]^{1/2} \cdot \hat{\boldsymbol{B}}^{\mathrm{c}}_{\mathrm{out}} \tag{4.46b}$$

Now, using this result and the definition of $\boldsymbol{M}$, (4.37), we have

$$\boldsymbol{M} = \hat{\boldsymbol{V}}^{+}_{\mathrm{c-in}} \cdot [\hat{\boldsymbol{V}}^{-}_{\mathrm{c-out}}]^{-1}. \tag{4.47}$$

Now, from (4.41), we see that diagonalization of $\boldsymbol{M}$ yields the propagator matrix $\boldsymbol{Q}^{\mathrm{m}}(l)$ and its eigenvectors $\boldsymbol{E}$. However, these eigenvectors are ambiguous to an arbitrary complex constant,

$$\boldsymbol{E} = \boldsymbol{K} \cdot \boldsymbol{E}_0. \tag{4.48}$$

Consequently, only $\boldsymbol{E}_0$ is extracted. Matrix $\boldsymbol{K}$ is diagonal with $|[\boldsymbol{K}]_{ii}| = 1$. The phase bahavior of $[\boldsymbol{K}]_{ii}$, as will be shown in the next section, is nonlinear with respect to length of the coupled line section, but is minimal as length approaches zero. This is due in part to the mode delays and to their increasing significance with length or frequency.

To determine the current eigenvector matrix $\boldsymbol{H}$, an analogous derivation with current quantities could be employed, but if we chose $\boldsymbol{H}$ according to [3, Eq. 22], no such derivation is necessary.

Finally, to extract the ith propagation constant from the ith eigenvalue, we must know how many ith mode half-wavelengths occur within the physical length l, since the phase of $[\boldsymbol{Q}^{\mathrm{m}}(l)]_{ii}$ (or k for the single-mode extraction case) is only defined over the interval $[-\pi, \pi]$. For reasonably low frequencies (or short lines), good initial guesses for the propagation constants adequately provide the number of half-wavelengths, and the jth propagation constant is thus

$$\gamma_j = \frac{1}{l}\left[\ln\left([\boldsymbol{Q}^{\mathrm{m}}(l)]_{jj}\right) + 2m\pi i\right]. \qquad \begin{array}{l} j = 1, 2, \ldots, n \\ m = 0, 1, 2, \ldots \end{array} \tag{4.49}$$

4.3 Numerical Results

In order to demonstrate the method, we resort to several numerical examples based on simulations from quasi-static and full-wave electromagnetic solvers. Both lossless and low-loss three-coupled line cases over swept length are examined, as well as a swept-frequency example on a lossy three-line system. The method is shown to

be very stable, robust, and efficient. We stress that numerical optimization is only required to obtain the solution $\tilde{\boldsymbol{Z}}^{\mathrm{c}}_{\mathrm{ch}}$.

In both examples, we consider a three-line microstrip system at an operating frequency of 2.0 GHz with the following quasi-static, frequency-independent, distributed circuit parameters:

$$\boldsymbol{L} = \begin{bmatrix} 313.9 & 67.5 & 22.2 \\ 67.5 & 319.3 & 67.5 \\ 22.2 & 67.5 & 313.9 \end{bmatrix} \text{nH} \tag{4.50}$$

$$\boldsymbol{C} = \begin{bmatrix} 130.3 & -16.2 & -0.8 \\ -16.2 & 133.7 & -16.2 \\ -0.8 & -16.2 & 130.3 \end{bmatrix} \text{pF}. \tag{4.51}$$

Three distinct voltage test vectors, accounting for all three modes to keep the system well-conditioned, were employed. Our choice included $\hat{\boldsymbol{v}}^{\mathrm{c}}_{\mathrm{in}-1} = [2.0\ 1.0\ 0.0]^t$, $\hat{\boldsymbol{v}}^{\mathrm{c}}_{\mathrm{in}-2} = [1.0\ -0.8\ -1.0]^t$, $\hat{\boldsymbol{v}}^{\mathrm{c}}_{\mathrm{in}-3} = [1.0\ -0.8\ 1.0]^t$. Several trials using different test vectors failed to impact the extraction error. The Nelder-Mead simplex method was used to minimize the matrix norms (4.31) for all test cases.

4.3.1 The lossless case

The resulting normal mode parameters for this coupled line section are

$$\boldsymbol{Z}^{\mathrm{c}}_{\mathrm{ch}} = \begin{bmatrix} 49.4072 & 8.3545 & 2.2371 \\ 8.3545 & 49.5332 & 8.3545 \\ 2.2371 & 8.3545 & 49.4072 \end{bmatrix} \Omega \tag{4.52}$$

$$\boldsymbol{E} = \begin{bmatrix} -0.5198 & -0.6780 & -0.5198 \\ -0.7071 & -0.0000 & 0.7071 \\ 0.4786 & -0.7362 & 0.4786 \end{bmatrix} \tag{4.53}$$

$$\boldsymbol{H} = \begin{bmatrix} -0.5205 & -0.6768 & -0.5205 \\ -0.7071 & -0.0000 & 0.7071 \\ 0.4794 & -0.7351 & 0.4794 \end{bmatrix} \tag{4.54}$$

$$\boldsymbol{\Lambda} = [i\ \mathrm{diag}\,(13.5636,\ 12.3680,\ 11.9748)] \tag{4.55}$$

Upon extraction, error analysis is first examined for the computed characteristic impedance matrix. We consider only close initial guesses given conventional CAD tools and algorithms. The figure of merit M was extremely small, less than 2×10^{-6} normally and less than 3.5×10^{-5} around the mode half-wavelength ambiguities.

Figure 4.4 shows the only significant sources of error for $\tilde{\boldsymbol{Z}}^{\mathrm{c}}_{\mathrm{ch}}$, the MHWAs. However, the spikes are extremely narrow and require a resolution of 0.1 mm in length sample. The effect of mode delays not only includes the MHWAs but also points where $\beta_1 l = (\beta_3 l)^*$. For an overview of the effects of mode delay on the the immittance matrices, the reader is encouraged to consult [37].

The eigenvalue error is very small over a swept length from $l = 0$ m to $l = 10.0$ m, and would obviously remain so for arbitrarily large distances. With no loss in the coupled-microstrip system, the net power flux into or out of the $2n$-port system must be zero, therefore we expect convergence of $\tilde{\boldsymbol{Z}}^{\mathrm{c}}_{\mathrm{ch}}$ as in the lossless single line case, regardless of length. Eigenvalue perturbation at the MHWAs was less than $4\times10^{-6}\%$. Results for all three normal mode parameters are shown in Table 4.1. The magnitudes of the elements in the eigenvector matrices $\boldsymbol{E}_0$ and $\boldsymbol{H}_0$ were extracted with very small error, and only the phase ambiguity in $\boldsymbol{K}$, which increases with coupling length as shown in Fig. 4.5.

We reiterate that because all eigenvectors are real and all eigenvalues are imaginary in this case, solution convergence may be sensitive to the initial guess, therefore, simultaneous optimization of both eigenvector matrices was desirable to avoid numerical difficulties.

4.3.2 The lossy case

Losses in microstrip MTL are dominated by conductor imperfection (skin effect) for monolithic microwave integrated circuits (MMIC) applications and dielectric imperfection for microstrip board size structures. For a low loss case, we considered the following resistance and conductance matrices

$$\boldsymbol{R} = [\mathrm{diag}\,(\texttt{18.3453},\ \texttt{17.4558},\ \texttt{18.3453})]\,\mathrm{m}\Omega \tag{4.56}$$

$$\boldsymbol{G} = \begin{bmatrix} \texttt{251.1210} & \texttt{-22.8909} & \texttt{-0.3994} \\ \texttt{-22.8909} & \texttt{256.109} & \texttt{-22.8909} \\ \texttt{-0.3994} & \texttt{-22.8909} & \texttt{251.1210} \end{bmatrix} \mathrm{nS}, \tag{4.57}$$

together with the parameters (4.50) and (4.51). Again, extraction yielded all normal mode parameters with very little error. Fig. 4.6 shows the only significant error, the imaginary parts of $\tilde{\boldsymbol{Z}}^{\mathrm{c}}_{\mathrm{ch}}$, which are very small in magnitude for the low-loss lines. Table 4.1 details error for the eigenvectors and propagation constants.

It should be emphasized that extraction error for $\tilde{\boldsymbol{Z}}^{\mathrm{c}}_{\mathrm{ch}}$, in general, increases with

increasing coupling length. Physically, this results from the matching effect caused by a lossy line. Physically, longer lossy lines absorb greater power. As the length approaches infinity, the choice of termination becomes increasingly irrelevant since the signal reflection will be minimal by virtue of the line loss as opposed to the reflection at the load mismatch. Our example considers relatively low-loss lines, thus the large swept length has little impact on $\tilde{\boldsymbol{Z}}^{\mathrm{c}}_{\mathrm{ch}}$ extraction error. Preliminary tests showed that at least two orders of magnitude of length increase or a much higher loss were necessary to significantly impact the $\tilde{\boldsymbol{Z}}^{\mathrm{c}}_{\mathrm{ch}}$ extraction error. Thus, $\tilde{\boldsymbol{Z}}^{\mathrm{c}}_{\mathrm{ch}}$ extraction suffered minimal error, with $M < 0.01$. Again, results for all three NMPs are shown in Table 4.1. In the case of $\boldsymbol{E}_0$, we compared magnitudes (which are tabulated in the real column), not real and imaginary parts themselves.

Finally, we applied the extraction procedure to a set of simulated S-parameters from a full-wave simulation using a commercial software tool, Sonnet [48]. We considered a set of three-coupled lines 2.032 cm (800 mil) in length on a substrate of 0.762 mm (30 mil), with dimensions given in Fig. 4.7 and the following electrical parameters: $\epsilon_r = 3.43$, $\tan\delta = 0.01$, $\sigma_{\mathrm{c}} = 5.813 \times 10^7$ S/m. The simulation was performed from 1 to 10 GHz.

Ports were defined in the center of the conductor cross sections at the board edges. In several simulations, we increased the board length but used port de-embedding to move the reference planes inside the board edges, keeping the ports in the center of the conductors. This resulted in only slight overall deviations in the extracted parameters. Characteristic impedance matrix elements (Fig. 4.8) showed little deviation with frequency, except slight perturbations around 8 GHz where the board was approximately one wavelength for each mode. (The modes could not be distinguished individually since the sample interval was 0.25 GHz.) The figure of merit, M, was very small as shown in Fig. 4.9. Eigenvector elements ($\boldsymbol{E}_0$) are shown in Fig. 4.10 and exhibit little deviation with frequency. Components α and β for each mode were extracted; results are shown in Fig. 4.11. All of these NMP values agree well with those computed using a quasi-static $RLGC$ tool [49], which are also plotted as discrete points.

Per-unit-length parameters were also computed from the NMPs using known

quasi-static relations [33]:

$$\boldsymbol{Z} = \boldsymbol{E}^{-1} \cdot \boldsymbol{\Lambda}_{\mathrm{m}} \cdot \boldsymbol{E} \cdot \boldsymbol{Z}^{\mathrm{c}}_{\mathrm{ch}}, \tag{4.58a}$$

$$\boldsymbol{Y} = \boldsymbol{H}^{-1} \cdot \boldsymbol{\Lambda}_{\mathrm{m}} \cdot \boldsymbol{H} \cdot \boldsymbol{Y}^{\mathrm{c}}_{\mathrm{ch}}, \tag{4.58b}$$

where $\boldsymbol{Z} = \boldsymbol{R} + j\omega\boldsymbol{L}$ and $\boldsymbol{Y} = \boldsymbol{G} + j\omega\boldsymbol{C}$ are the distributed parameters. Matrices $\boldsymbol{L}$ and $\boldsymbol{C}$ were extracted, with results shown in Fig. 4.12, where the board resonance is also evident. Fig. 4.13 shows the non-negligible conductance values from $\boldsymbol{G}$ which were interpolated for clarity. Extracted loss was slightly greater than the calculated quasi-static loss, which is partly attributed to the greater transverse field components in a system with moderately lossy conductors and dielectrics.

Though all extracted results are sufficient for approximate modeling, they could be improved and compared with other simulation strategies and software, as well as measured data. At present we believe these inaccuracies result from the sensitivity of the S-parameters to the single-point port definitions and the inherent ambiguity of distributed circuit representations of waveguiding structures with significant cross-sections.

4.3.3 Coplanar lines

To improve upon distributed circuit models for coupled coplanar lines, our method for NMP/*RLGC* extraction was applied to a set of three lines surrounded by two ground swaths. The layout and dimensions of this structure are shown in Fig. 4.14. The gallium-arsenide (GaAs) substrate has a relative dielectric constant $\epsilon_r = 12.0$ and $\tan\delta = 0.001$. The gold conductor strips above have conductivity $\sigma = 4.1 \times 10^7$.

Each of the three center conductors have width $w = 24$ μm, thickness of 1 μm and separation between each and the ground planes is $s = 14$ μm. Overall length was $l = 2$ mm.

The first step was to simulate the 10-port shown in Fig. 4.15 to extract the 10×10 S-parameter matrix. Second, this matrix was embedded into the schematic window such that the appropriate ports could be grounded. In this case, the four ports on the outside lines (ports 7, 8, 9, and 10) at each end must be connected to the RF ground. Figure 4.16 shows the schematic of Agilent's Advanced Design System (ADS) that was used to generate and interpolate the 6×6 S-parameters from the Momentum simulation.

Results show that all of the NMPs and *RLGC* values are extracted with confi-

dence. First, the extracted characteristic impedance matrix is shown in Figs. 4.17 and 4.18. Since the imaginary values are so small, they are more suspect. The real parts, however, behave as expected and even exhibit frequency dependence. Above 25 GHz, they suffer from large error as the board length approaches $\lambda/2$. Higher impedance values result for these extracted characteristic matrices than for those in microstrip, given the higher mutual inductances and lower mutual capacitances. Low figure of merit shows good optimization (Fig. 4.19). Eigenvector elements are typical, showing field configurations for the three distinct modes in Fig. 4.20. Attenuation and phase constants are shown in Fig. 4.21. As expected, the phase constants are almost all identical, given that the field configurations of the three modes in coupled-coplanar differ only negligibly in their confinement or exclusion from the dielectric. Mode 3 loss is greatest, since the coupling between adjacent lines is strongest, confining the current to conductor edges to a greater degree than the other modes.

Inductance and capacitance matrices converted from the NMPs using (4.58) are both shown in Fig. 4.22, while the resistance and conductance elements are shown in Fig. 4.23. Notice that conductance is negligible in these coplanar lines, as the field configurations are not as heavily confined to the substrate as those in coupled microstrip. Consequently, most of the loss results from the thin metallization and is captured in the resistance matrix elements, which increase as functions of frequency due to skin effect.

4.4 Conclusions

We have introduced a novel extraction procedure applicable to an arbitrary number of uniform coupled lines. It requires only the length of the coupled line section and the S-parameters of this section referenced to an arbitrary but known impedance matrix. The method determines three normal mode parameters of interest: the characteristic impedance matrix, the eigenvector matrices, and the propagation constants. These parameters were extracted with minimal error for low-loss lines. Measurements, detailed error analysis, and extension of the method to more coupled lines are the topics of a future paper.

We suggest that such a method, in conjunction with broadbanded S-parameter measurements, could yield not only frequency-dependent normal mode parameters, but also distributed circuit parameters, notwithstanding issues of interpretation.

These would be especially useful in lossy, high-frequency systems where the quasi-TEM regime is not valid, and critical given the practical need to retain circuit models for devices with strong electromagnetic (as opposed to quasi-static) behavior.

Table 4.1 Percent error for characteristic impedance, eigenvectors, and propagation constants.

Element	Lossless	Lossy	
		real	imag
$[\tilde{\boldsymbol{Z}}^{\mathrm{c}}_{\mathrm{ch}}]_{11}$	4×10^{-4}	5×10^{-4}	4.21
$[\tilde{\boldsymbol{Z}}^{\mathrm{c}}_{\mathrm{ch}}]_{12}$	3×10^{-3}	3×10^{-3}	13.6
$[\tilde{\boldsymbol{Z}}^{\mathrm{c}}_{\mathrm{ch}}]_{13}$	1×10^{-2}	1×10^{-2}	4.68
$[\tilde{\boldsymbol{Z}}^{\mathrm{c}}_{\mathrm{ch}}]_{22}$	6×10^{-4}	6×10^{-4}	4.21
$[\tilde{\boldsymbol{E}}]_{11}$	3×10^{-4}	4×10^{-3}	-
$[\tilde{\boldsymbol{E}}]_{12}$	6×10^{-4}	5×10^{-4}	-
$[\tilde{\boldsymbol{E}}]_{21}$	2×10^{-11}	6×10^{-10}	-
$[\tilde{\boldsymbol{E}}]_{31}$	1.5×10^{-4}	3×10^{-4}	-
$[\tilde{\boldsymbol{E}}]_{32}$	4×10^{-4}	4×10^{-4}	-
$[\tilde{\boldsymbol{H}}]_{11}$	3×10^{-4}	1.5×10^{-4}	-
$[\tilde{\boldsymbol{H}}]_{12}$	3×10^{-4}	4×10^{-4}	-
$[\tilde{\boldsymbol{H}}]_{21}$	7×10^{-10}	2×10^{-10}	-
$[\tilde{\boldsymbol{H}}]_{31}$	5×10^{-4}	4×10^{-4}	-
$[\tilde{\boldsymbol{H}}]_{32}$	4×10^{-4}	3×10^{-4}	-
γ_1	1×10^{-10}	1×10^{-5}	4×10^{-6}
γ_2	5×10^{-11}	1×10^{-5}	1×10^{-5}
γ_3	4×10^{-10}	1×10^{-5}	2.5×10^{-5}

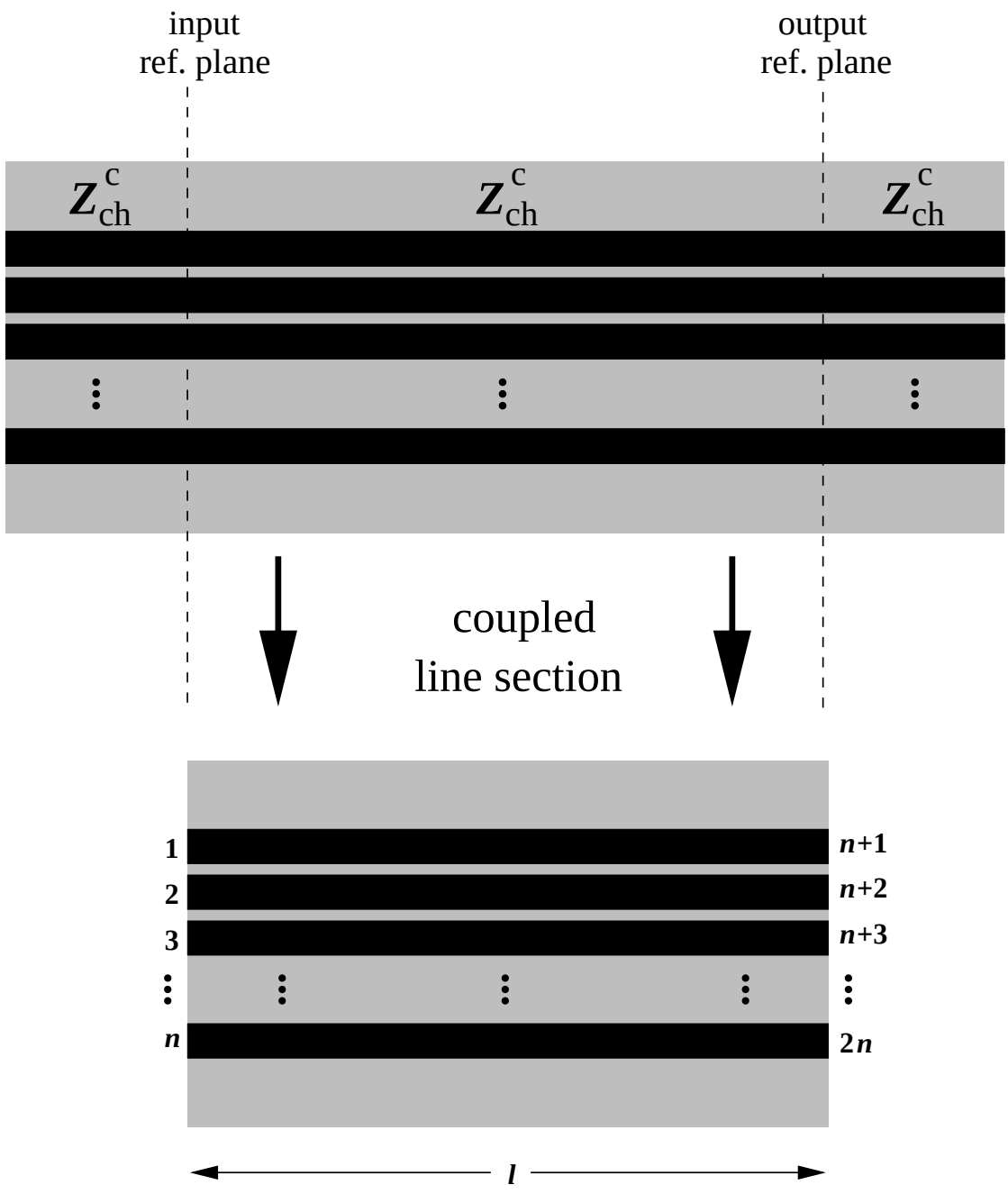

Figure 4.1 Section of symmetric coupled lines under test. The length l is the physical distance between the reference planes, defined during calibration.

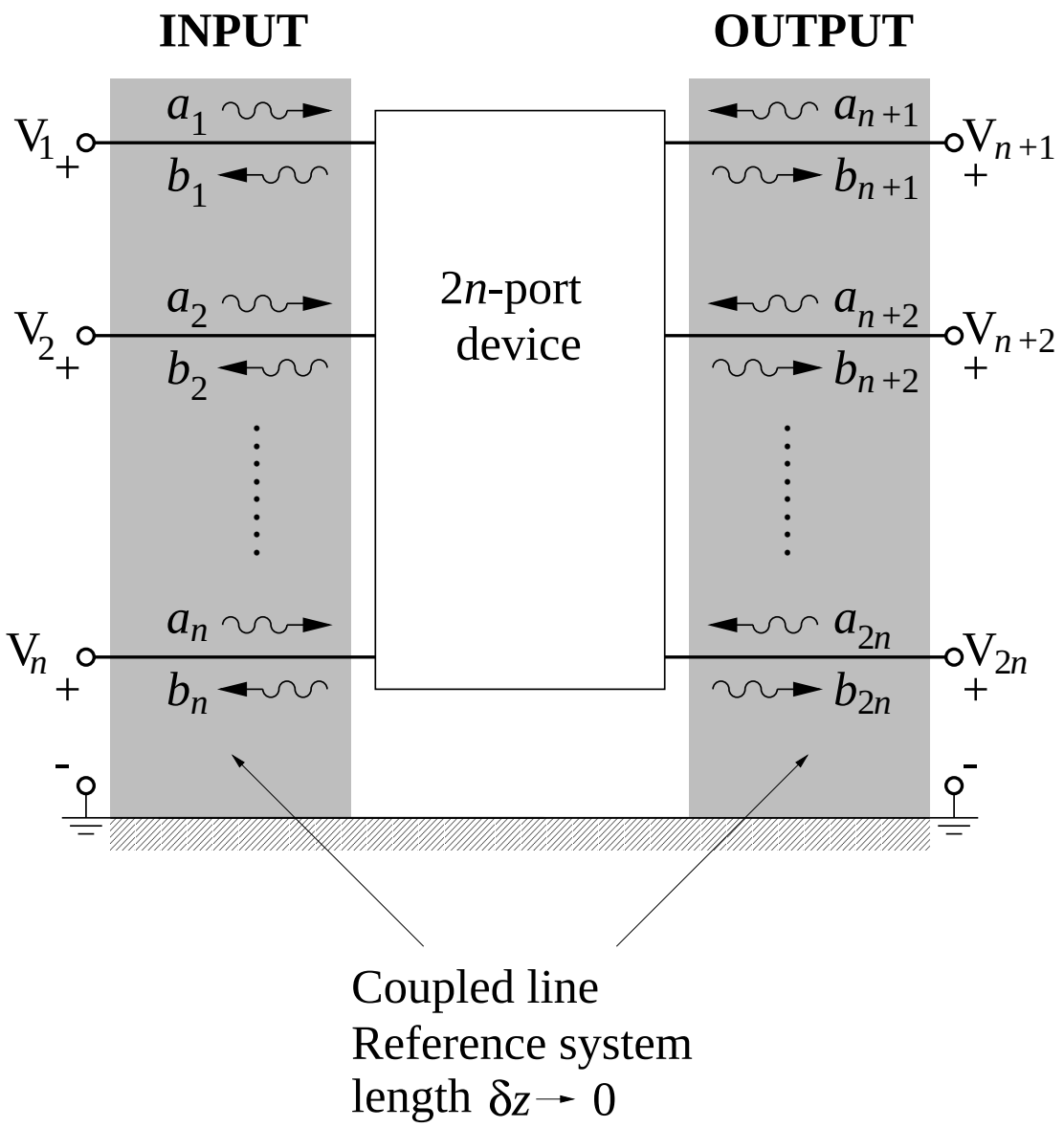

Figure 4.2 The $2n$-port representation of the coupled line under test, showing the infinitesimally short coupled-port reference system to which the S-parameters are referenced.

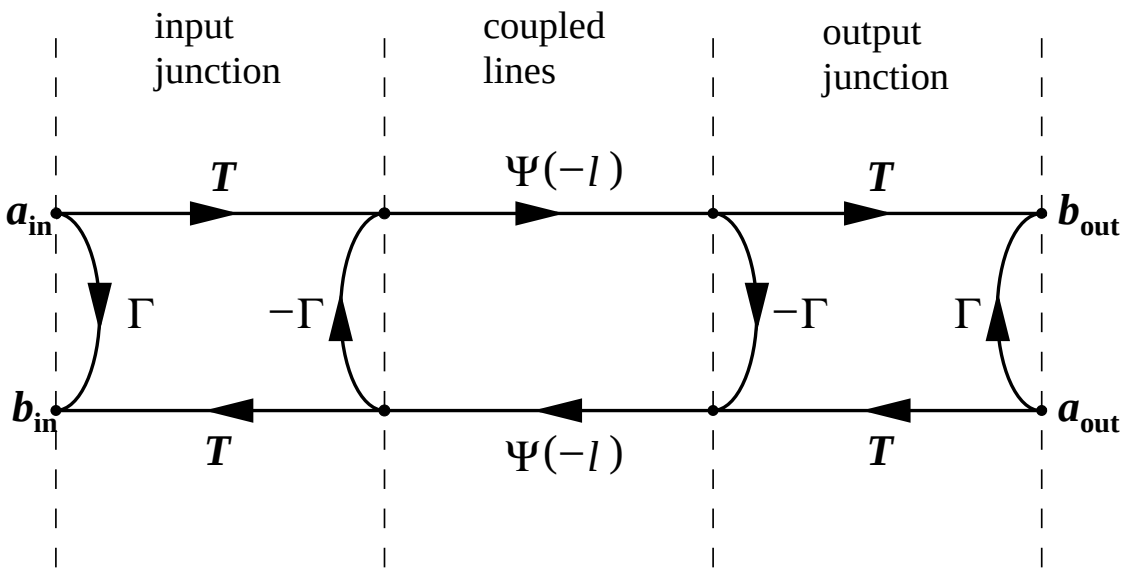

Figure 4.3 Signal flow graph representation for a section of coupled transmission lines of length l. The parameters $\boldsymbol{\Gamma}$ and $\boldsymbol{T}$ account for the scattering at the junctions between the test and reference systems.

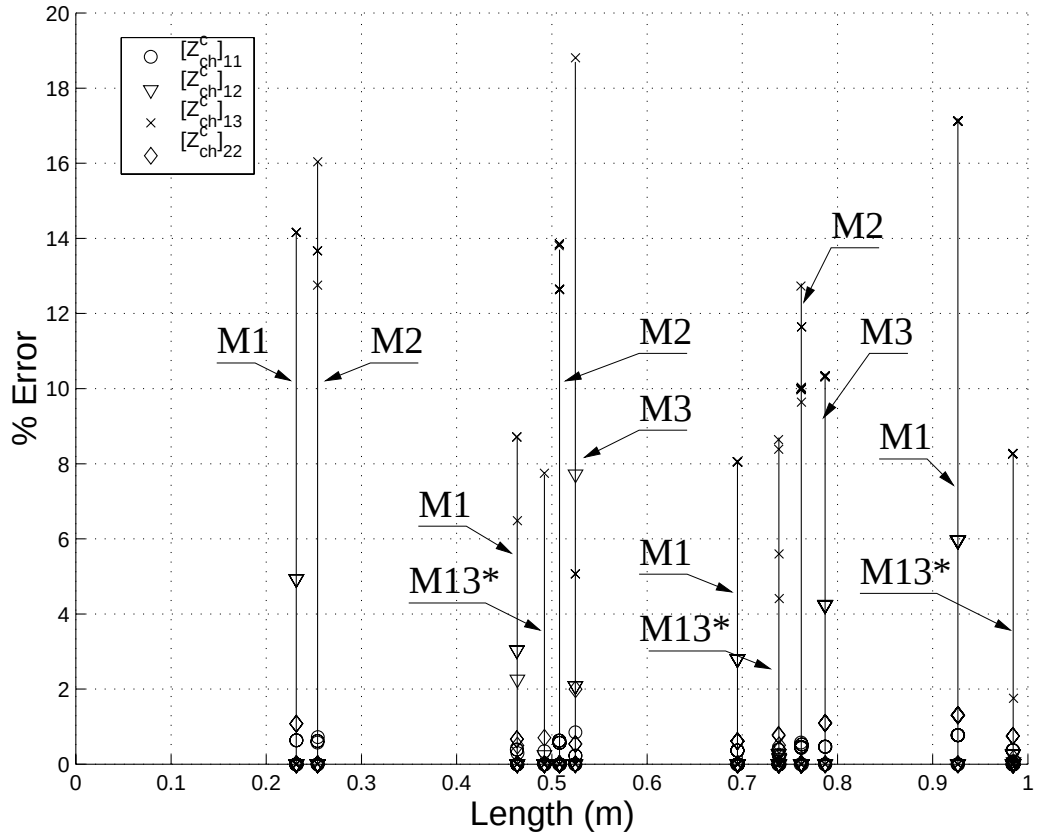

Figure 4.4 Percent error for elements of $\boldsymbol{Z}^{\mathrm{c}}_{\mathrm{ch}}$ at MHWAs along the lossless line ($f = 2$ GHz). Percent error is negligible elsewhere. The MHWAs are labelled, where "M1" indicates "mode 1 MHWA" ((4.33), $i = 1$); "M2" indicates "mode 2 MHWA"; "M3" indicates "mode 3 MHWA"; and "M13*" indicates "$\beta_1 l = (\beta_3 l)^*$ MHWA".

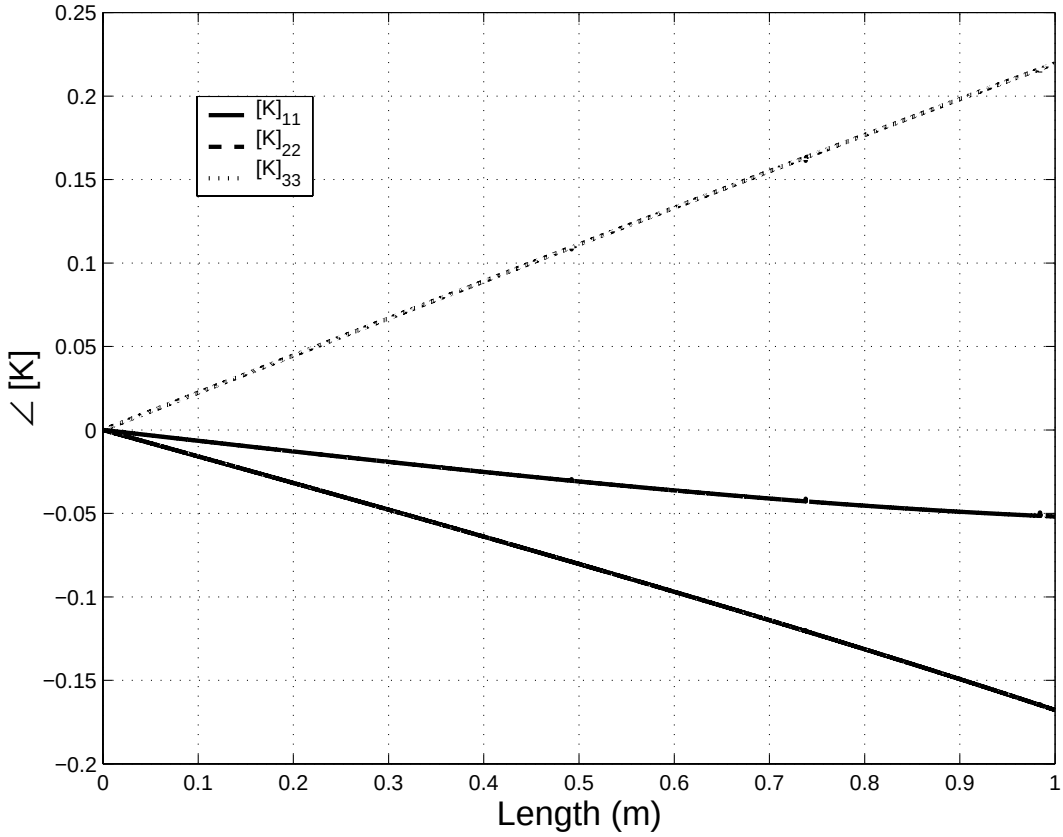

Figure 4.5 Values for the eigenvector ambiguity $\boldsymbol{K}$ as functions of the coupling length ($f = 2$ GHz).

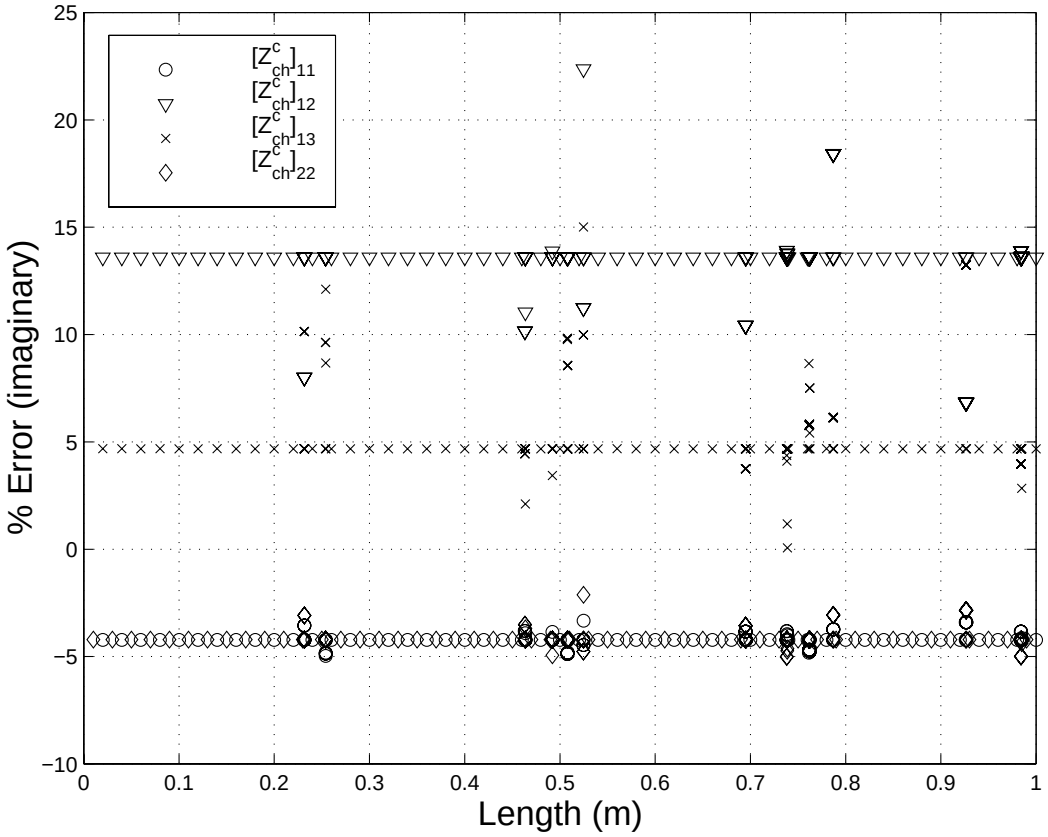

Figure 4.6 Percent error for imaginary elements of $\boldsymbol{Z}^{\mathrm{c}}_{\mathrm{ch}}$ at HWMAs along the lossy line ($f = 2$ GHz).

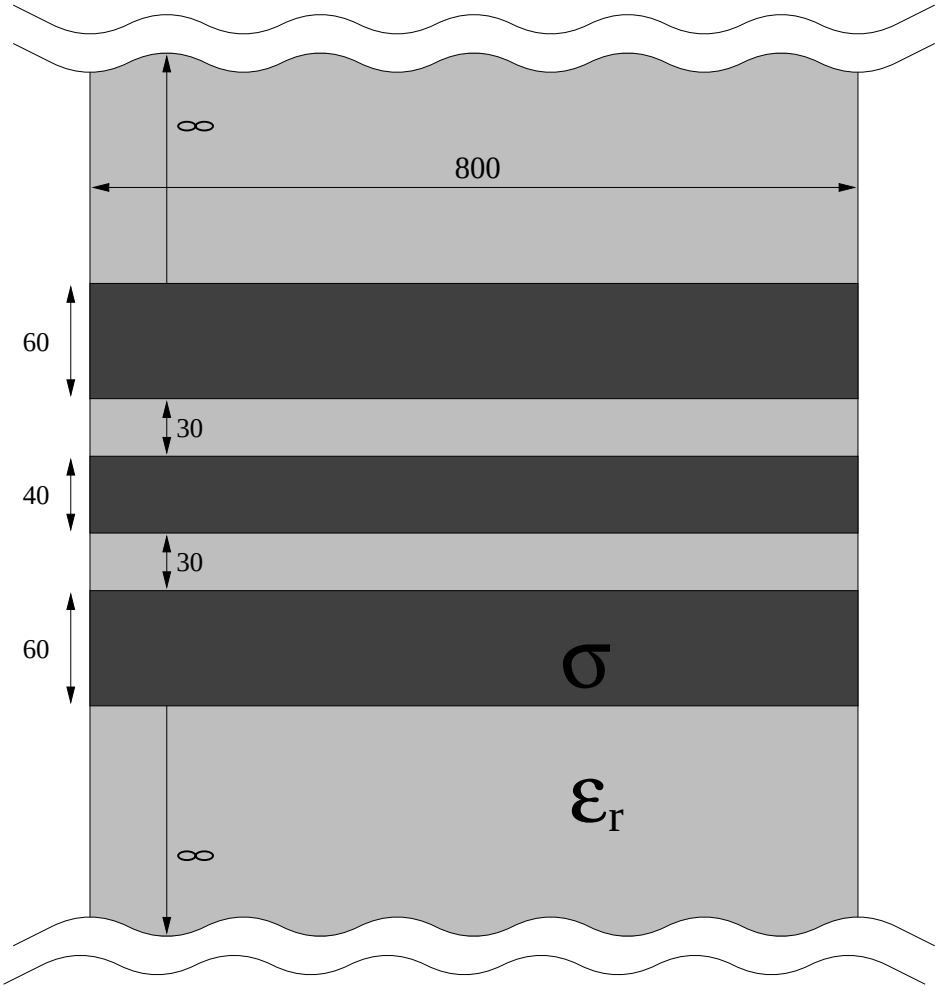

Figure 4.7 Three-coupled line board dimensions (in mil).

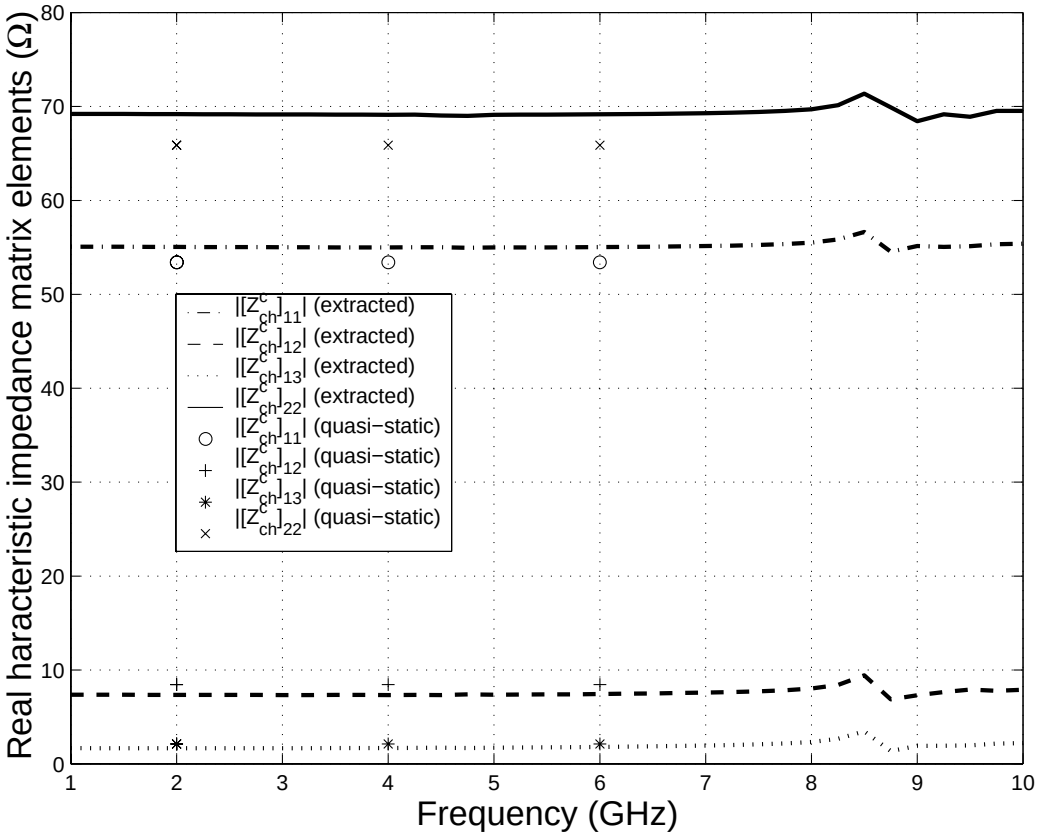

Figure 4.8 Extracted characteristic impedance matrix elements as functions of frequency for the DUT in Fig. 4.7.

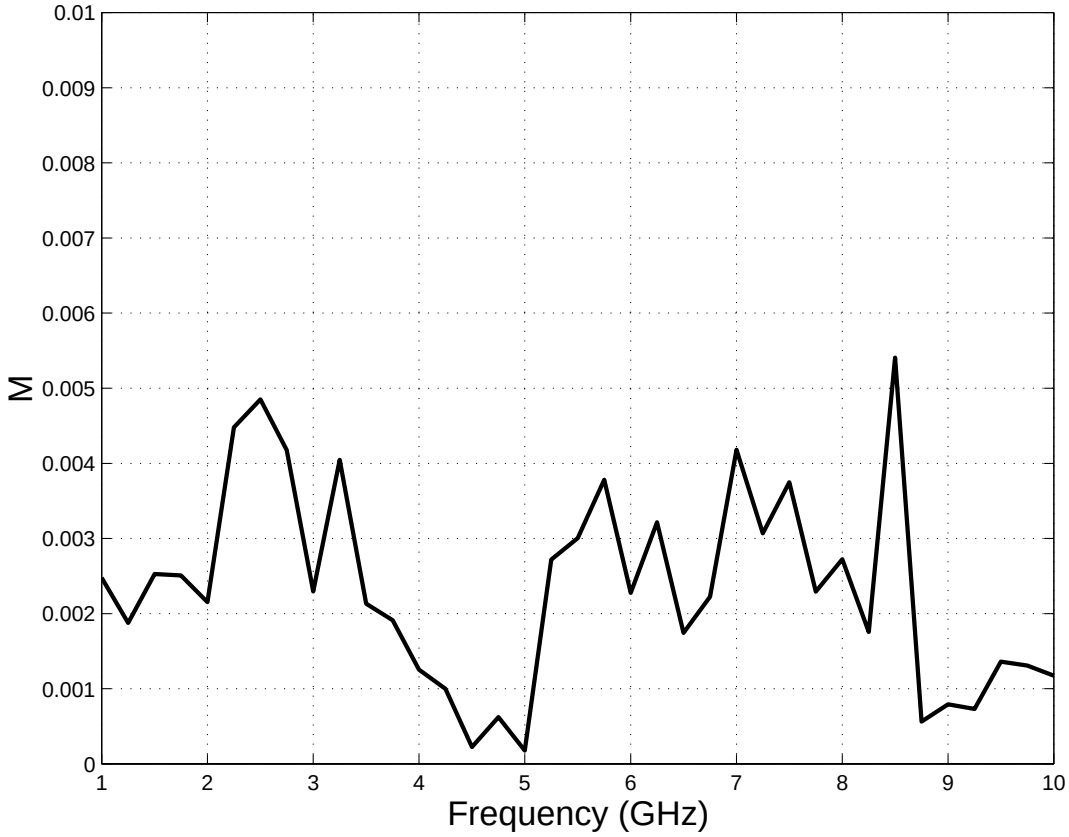

Figure 4.9 Figure of merit M for the characteristic impedance extraction, shown as a function of frequency for the DUT in Fig. 4.7.

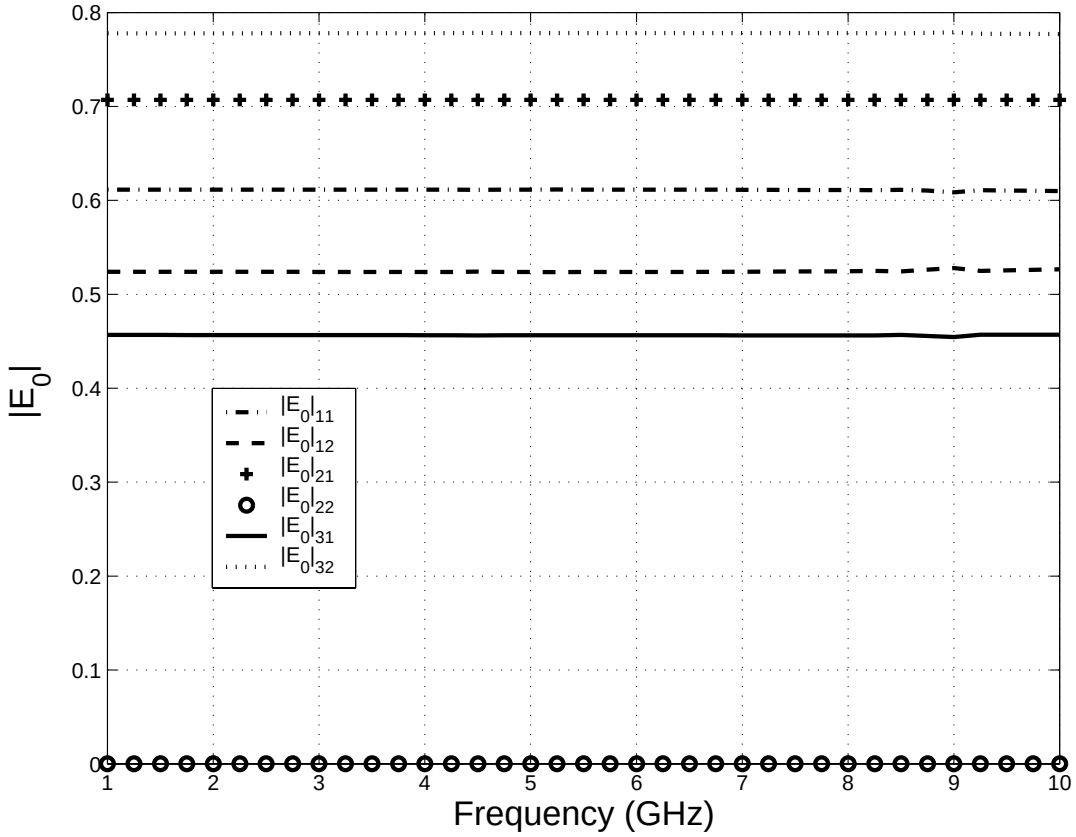

Figure 4.10 Eigenvector matrix $\boldsymbol{E}_0$ elements as functions of frequency for the DUT in Fig. 4.7.

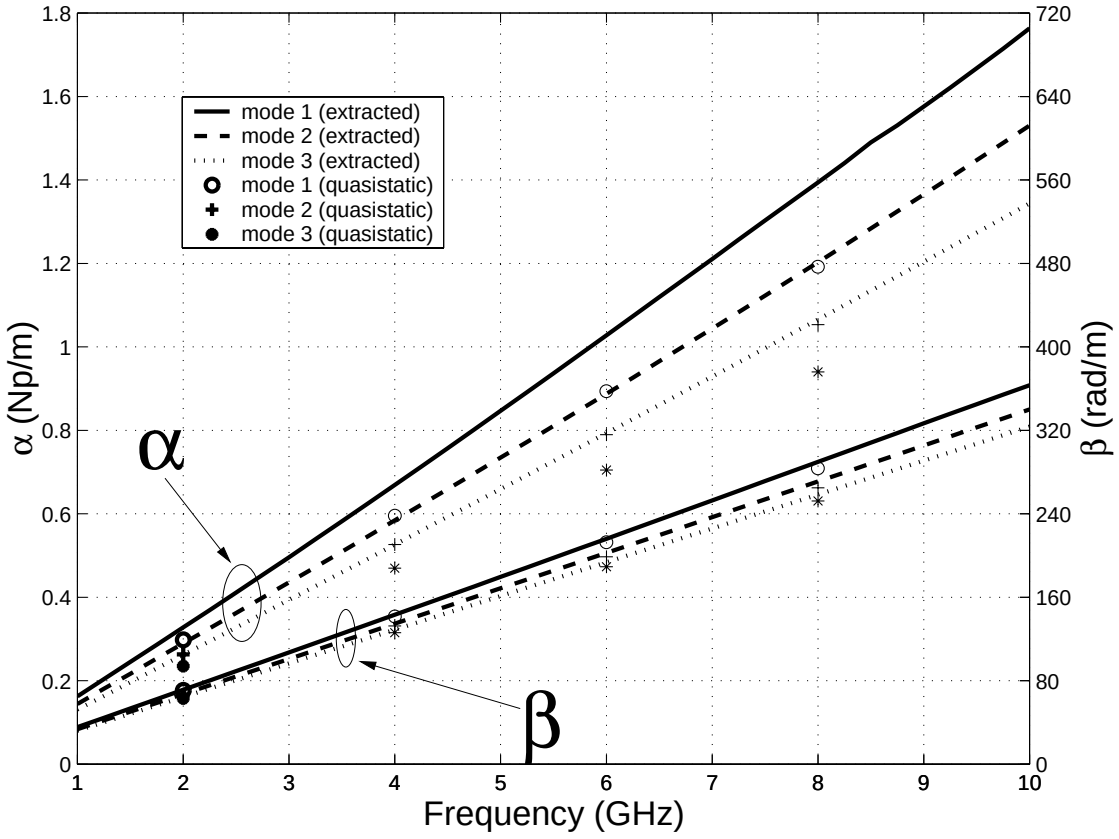

Figure 4.11 Extracted mode attenuation and phase constants as functions of frequency for the DUT in Fig. 4.7.

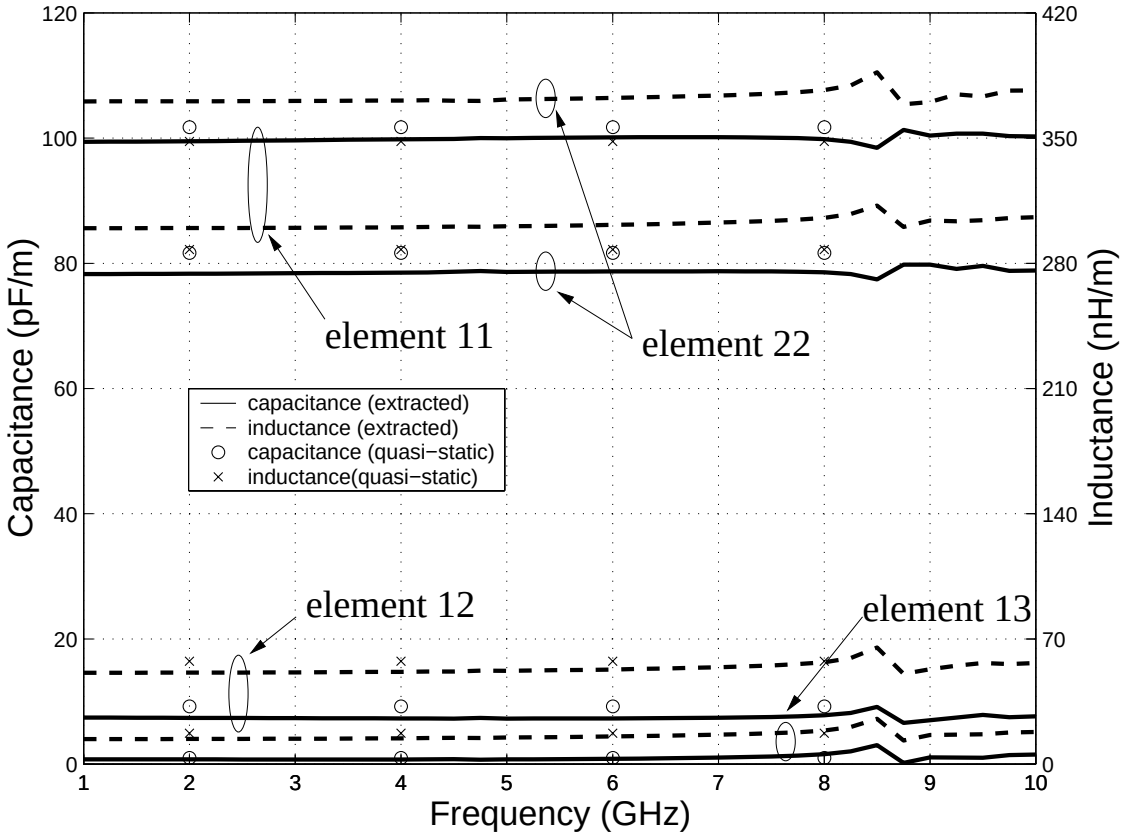

Figure 4.12 Extracted distributed inductance and capacitance matrix elements as functions of frequency for the DUT in Fig. 4.7. Note that the negative mutual capacitances have been plotted as positive for convenience.

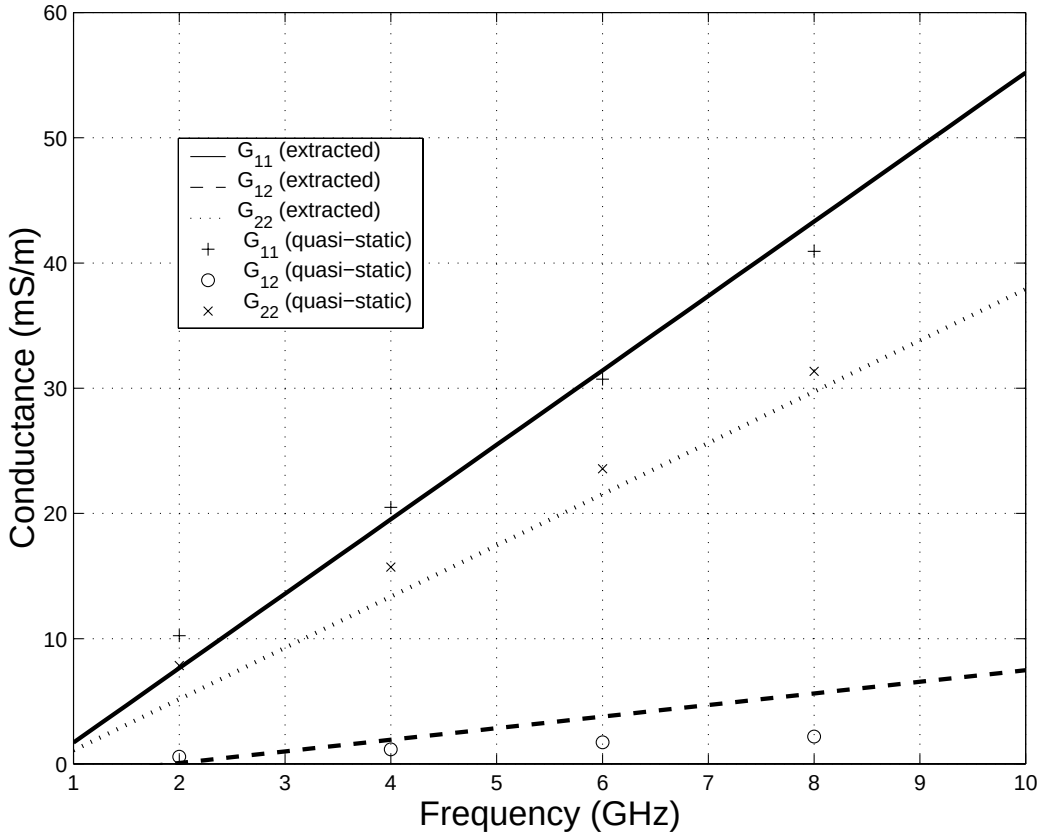

Figure 4.13 Extracted distributed conductance as a function of frequency for the DUT in Fig. 4.7. Note that the negative mutual conductances have been plotted as positive for convenience.

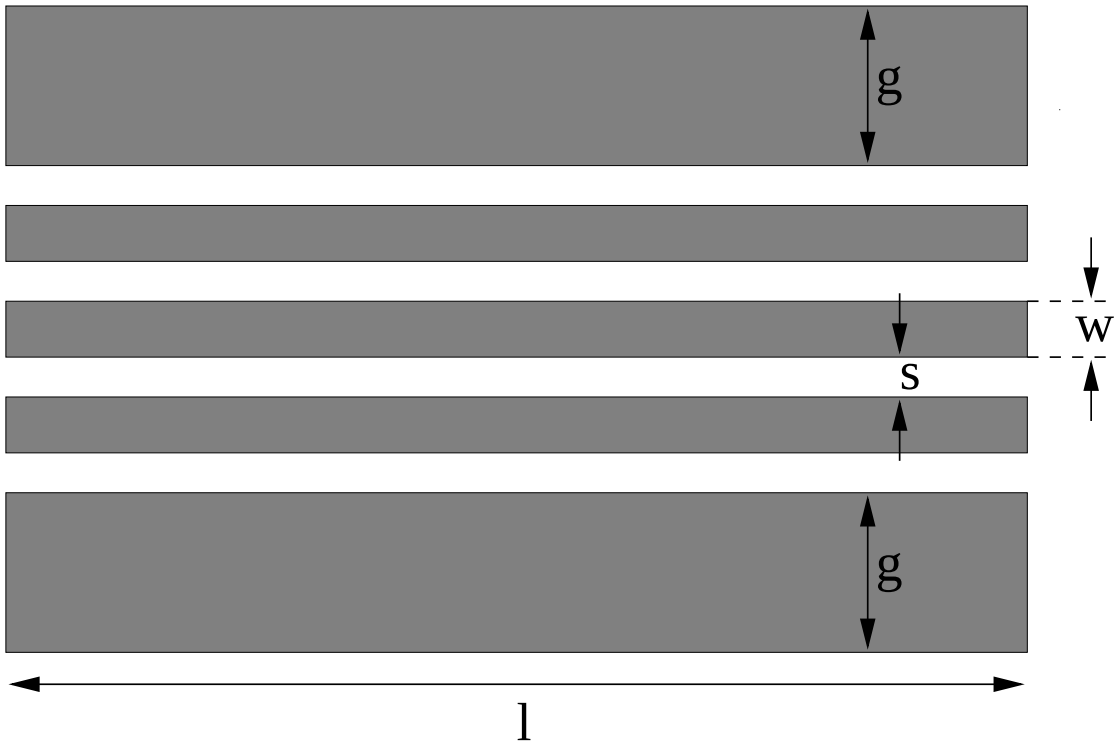

Figure 4.14 Three-coupled coplanar line dimensions. Dielectric substrate underneath (not shown).

Figure 4.15 Three-coupled coplanar layout (not to scale) with port numbers.

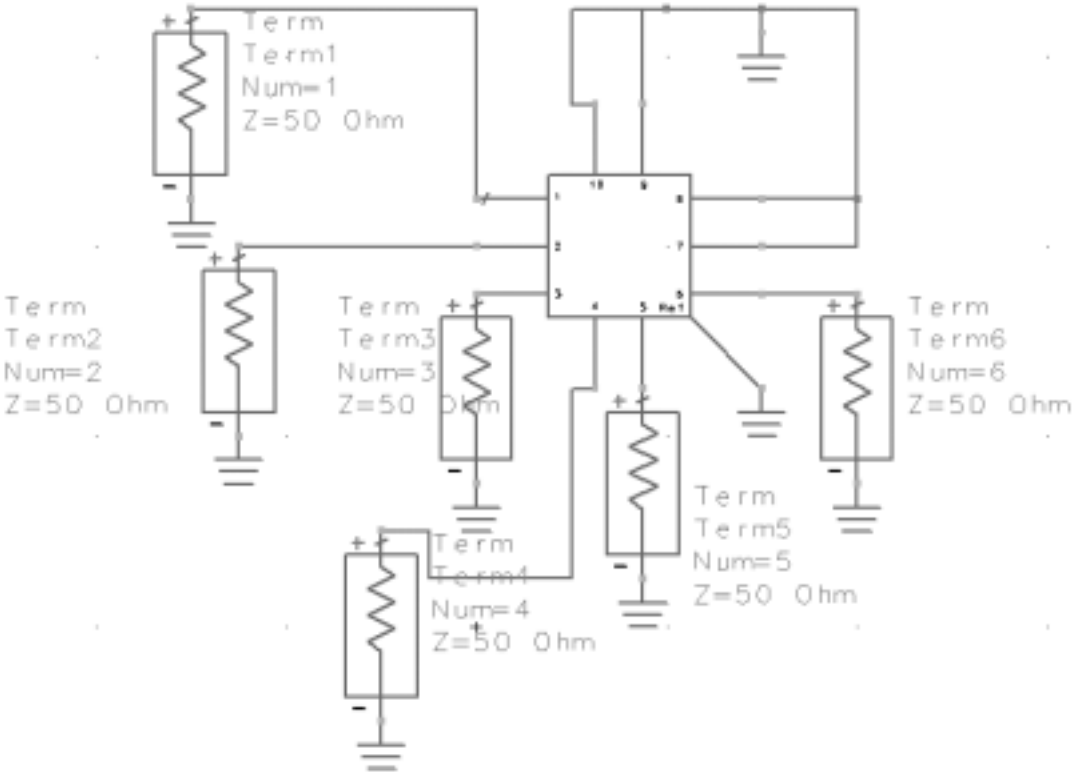

Figure 4.16 Simulation schematic and grounding for three-coupled coplanar layout S-parameter calculations.

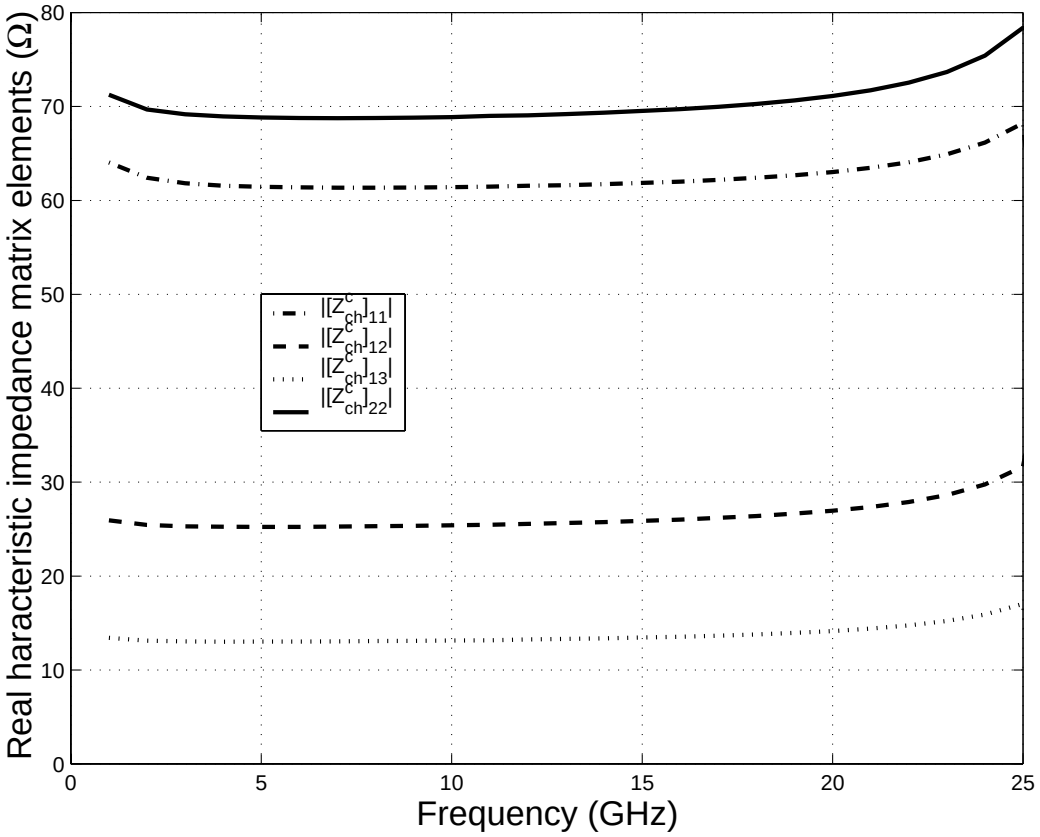

Figure 4.17 Extracted real characteristic impedance matrix elements as functions of frequency for the coplanar lines in Fig. 4.14.

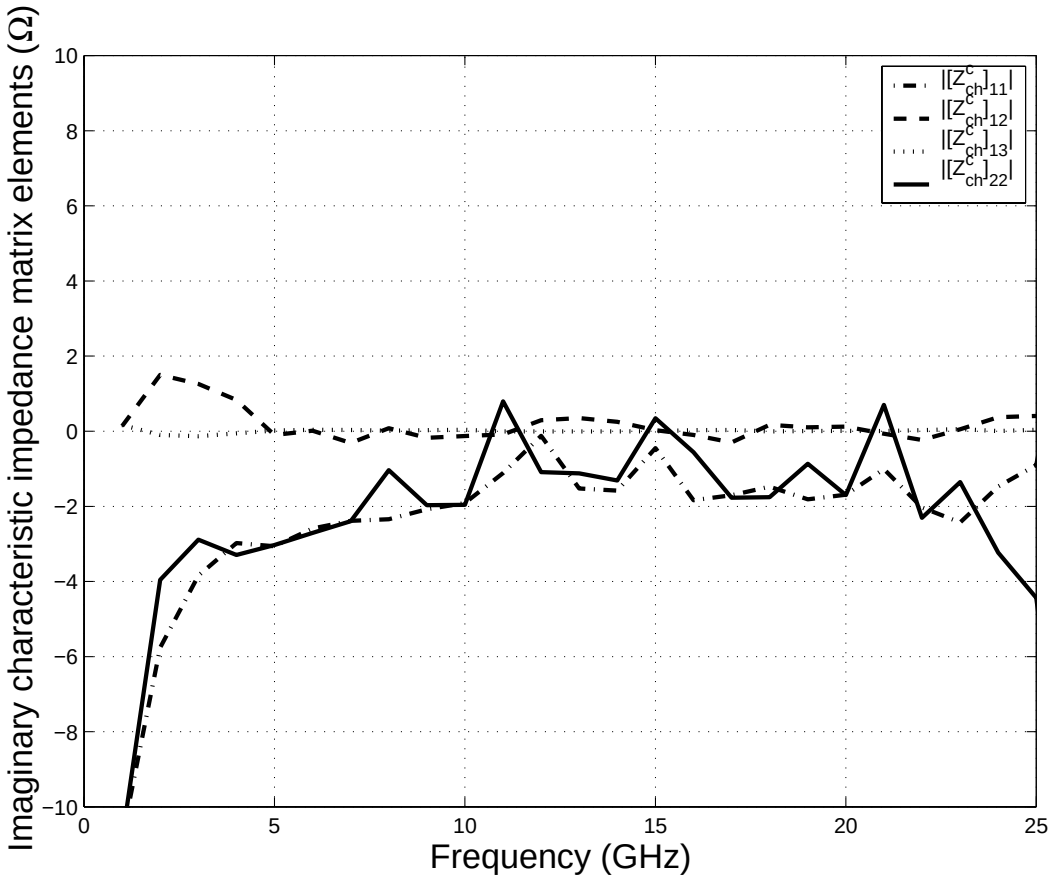

Figure 4.18 Extracted imaginary characteristic impedance matrix elements as functions of frequency for the coplanar lines in Fig. 4.14.

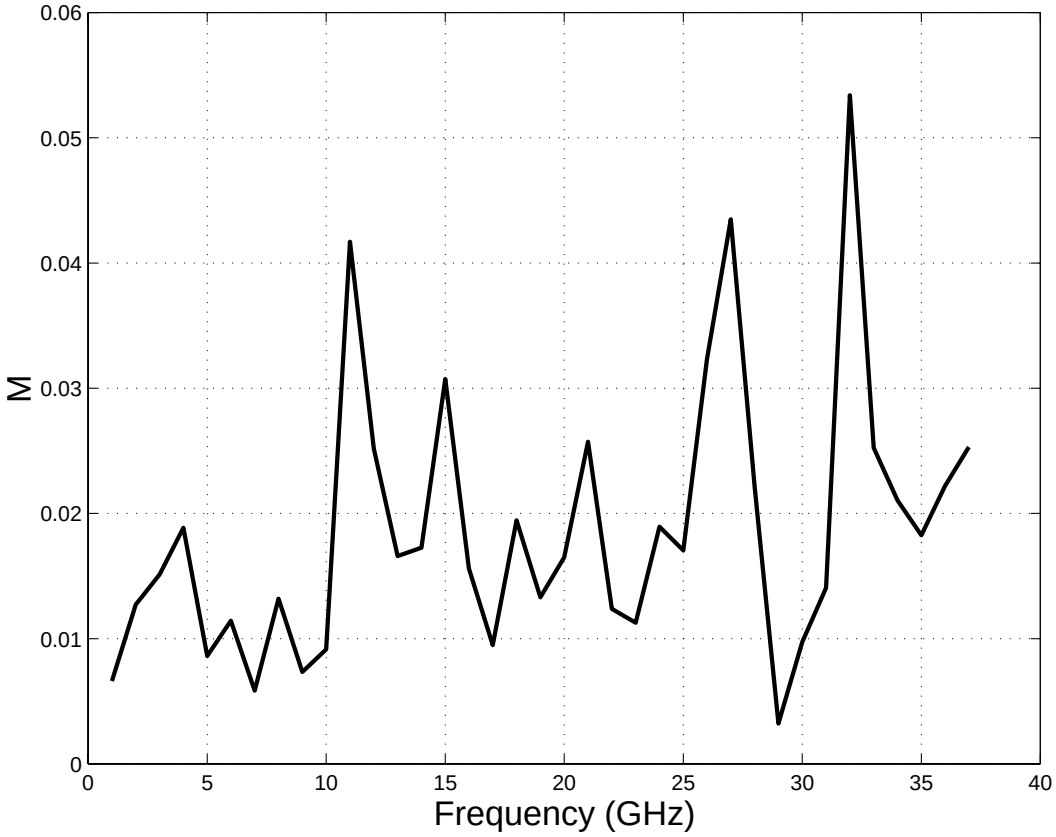

Figure 4.19 Figure of merit M as a function of frequency for the coplanar lines in Fig. 4.14.

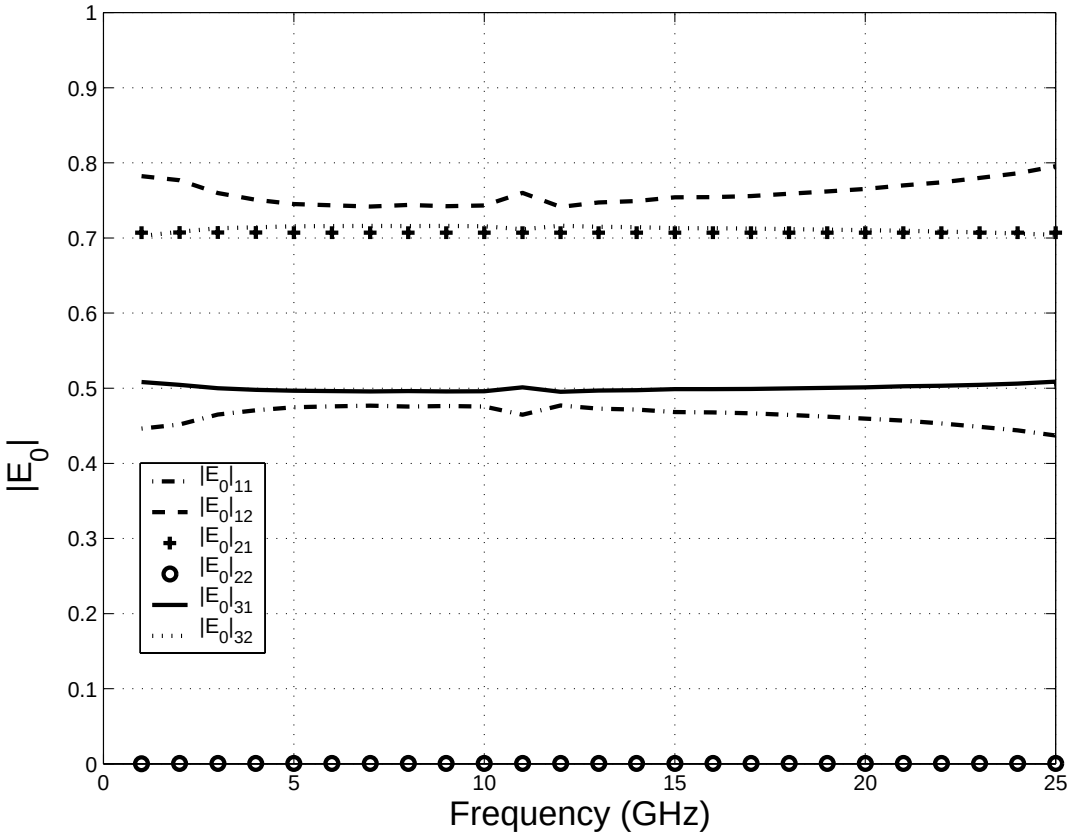

Figure 4.20 Eigenvector matrix $\boldsymbol{E}_0$ elements as functions of frequency for the coplanar lines in Fig. 4.14.

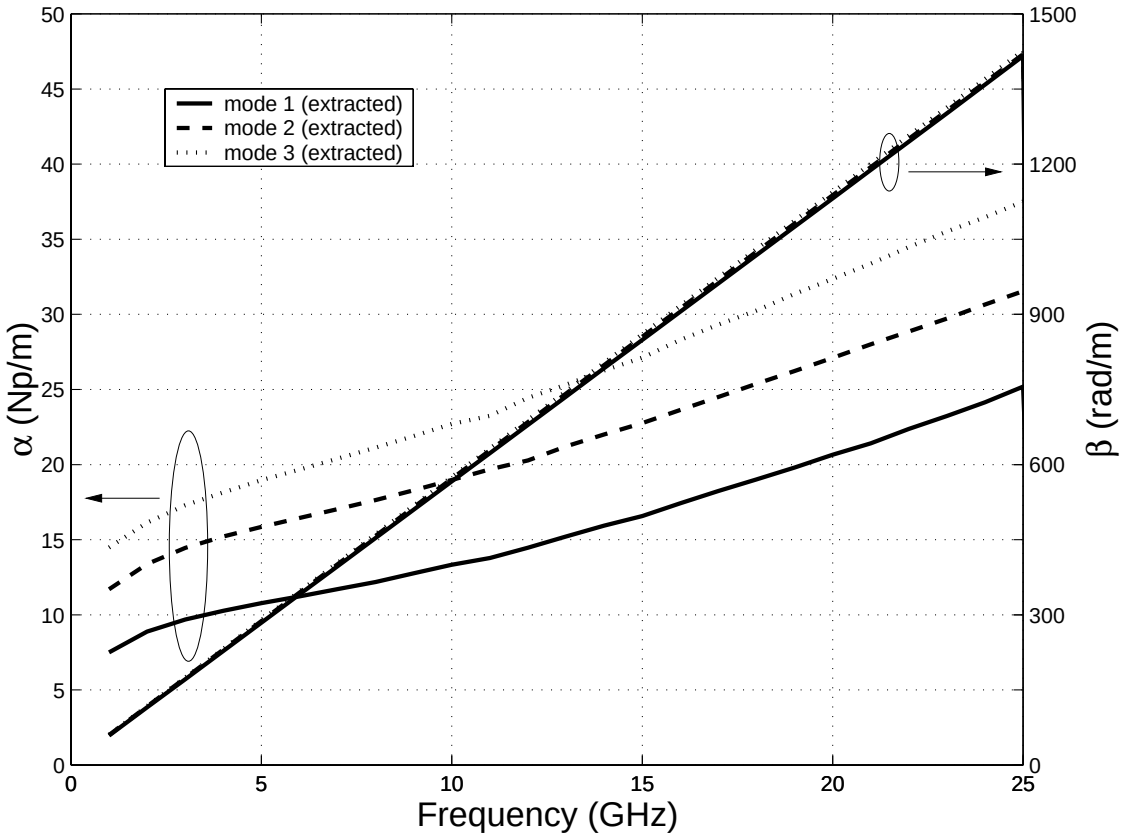

Figure 4.21 Extracted mode attenuation and phase constants as functions of frequency for the coplanar lines in Fig. 4.14.

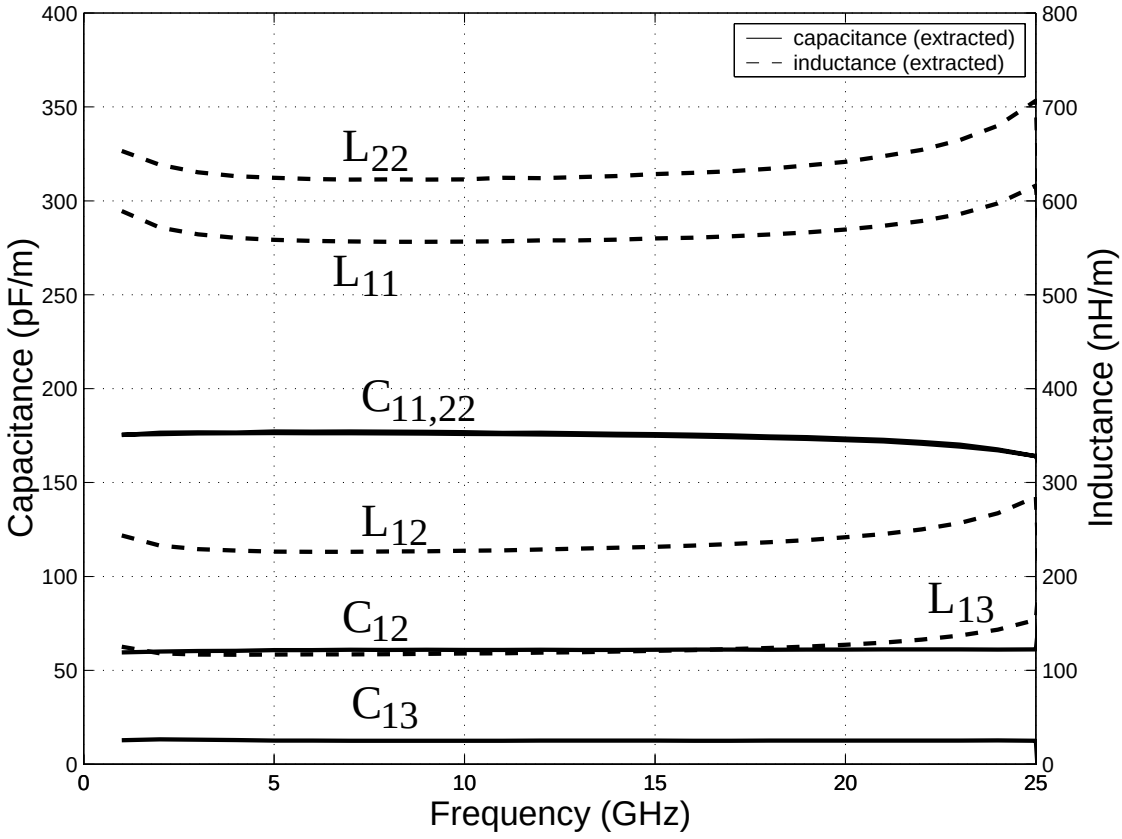

Figure 4.22 Extracted distributed inductance and capacitance matrix elements as functions of frequency for the coplanar lines in Fig. 4.14. Note that the negative mutual capacitances have been plotted as positive for convenience.

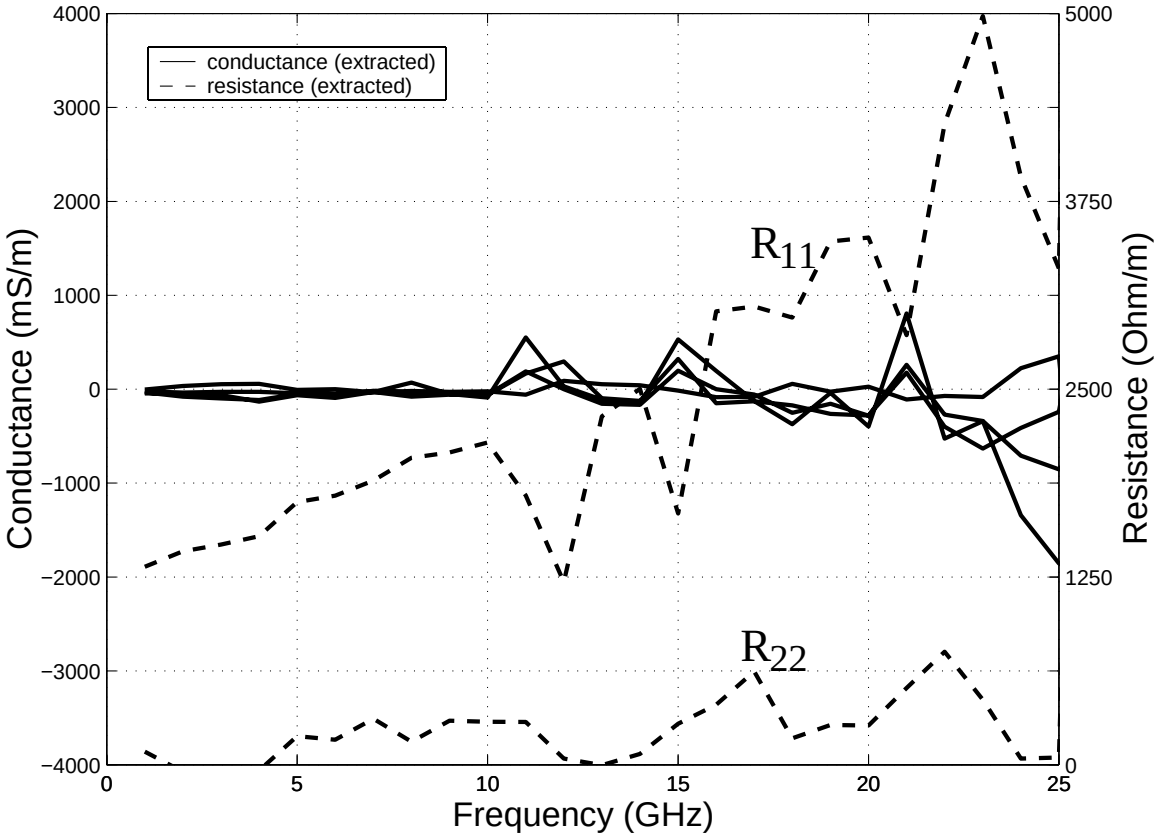

Figure 4.23 Extracted distributed resistance and conductance as a function of frequency for the DUT in Fig. 4.7. Note that the negative mutual conductances have been plotted as positive for convenience, however, they are of negligible value in this case.

CHAPTER 5

MATCHING STRATEGIES

Little work has been presented regarding general matching strategies for coupled microstrip given mismatched MTL terminations. Ponchak and Katehi [15] applied tuning stub matching to coplanar waveguide systems on silicon. Kuo and Tzuang [5] reduced reflections below -30 dB using matched termination networks on six-line closely coupled microstrip circuits. Amari and Bornemann [6] minimized reflected power numerically by determining an optimum resistive termination based on random and deterministic source excitations. Sun [16] presented a multiconductor quarter-wave transformer.

In this chapter, we synthesize several types of matching networks for symmetric mismatched terminations in symmetric, uniform, coupled-line microstrip structures in the quasi-TEM regime. Employing MTL theory, stubs, reactive elements, and transformers will be extended to coupled-line systems. Reasonable engineering approximations are utilized in simulation and measurement where necessary, and the matching methods will be applied to a three-coupled line system to exemplify matching for general n-line applications. These may include transistor amplifier circuits substituting microstrip for coplanar technology, optoelectronics packaging, chip- and package-level interconnections, and parallel data buses.

This chapter is organized as follows: in Section 5.1 we overview necessary MTL longitudinal relations. In Section 5.2 we present several matching strategies. In Section 5.3 numerical results and simulations of the synthesized matching networks are presented. Finally, the matching is validated with measurement results presented in Section 5.4.

5.1 Multiconductor Transmission Line Equations

Focusing on the microstrip structure shown in Fig. 5.1, we assume symmetry about the $x = 0$ plane and generalize the results to n lines (excluding the ground

plane) where possible.

It should be stressed that this theory does not apply in a strict sense to microstrip lines, given that they are inhomogeneous and therefore do not support TEM modes. However, at sufficiently low frequencies, the lines support quasi-TEM modes which approximately satisfy the MTL equations [7]. In quasi-TEM analysis of n coupled lines, n modes propagate. These are obtained though the uncoupling of the telegrapher's equations [1], [3], [4] usually via numerical eigenanalysis, though other methods for computing the propagation constants exist [11].

Under the quasi-TEM approximation, the propagating modes are interpreted as physical system voltages and currents [1]. The wave equations are solved with a linear transformation and change of variables (between line and mode) given by the relations [9]

$$\boldsymbol{v}_{\mathrm{m}}(z) = \boldsymbol{E}\boldsymbol{v}_{\mathrm{c}}(z) \tag{5.1a}$$

$$\boldsymbol{i}_{\mathrm{m}}(z) = \boldsymbol{H}\boldsymbol{i}_{\mathrm{c}}(z) \tag{5.1b}$$

where $\boldsymbol{E}$ and $\boldsymbol{H}$ are $(n \times n)$ matrices whose ith rows are the voltage and current transformation vectors associated with the ith mode. Transformations $\boldsymbol{E}$ and $\boldsymbol{H}$ must simultaneously diagonalize both $\boldsymbol{Z}$ and $\boldsymbol{Y}$ [3] to uncouple the MTL equations, and obviously be nonsingular [3], [10] to enable transformation between mode and state variables. The n column vectors $\boldsymbol{v}_{\mathrm{m}}$ and $\boldsymbol{I}_{\mathrm{m}}$ are the modal voltage and current vectors which relate to the electric and magnetic field configurations for the n modes.

Decoupling the MTL equations yields

$$\boldsymbol{E}\boldsymbol{Z}\boldsymbol{Y}\boldsymbol{E}^{-1} = \boldsymbol{H}\boldsymbol{Y}\boldsymbol{Z}\boldsymbol{H}^{-1} = \boldsymbol{\Lambda}_{\mathrm{m}}^{2}, \tag{5.2}$$

where $\boldsymbol{\Lambda}_{\mathrm{m}}^{2}$ is the (diagonal) eigenvalue matrix for $\boldsymbol{Z}\boldsymbol{Y}$ and $\boldsymbol{Y}\boldsymbol{Z}$. Matrix $\boldsymbol{\Lambda}_{\mathrm{m}}$ contains the ordered complex propagation constants $\gamma_{i=1,2,\ldots,n}$ for modes $i = 1, 2, \ldots, n$. Inhomogeneous media (microstrip) generally yields n distinct eigenvalues [1] resulting in *mode delays* [44]. We easily solved (5.2) using numerical eigenvalue routines.

The conductor characteristic impedance and admittance matrices $\boldsymbol{Z}_{\mathrm{ch}}^{\mathrm{c}}$ and $\boldsymbol{Y}_{\mathrm{ch}}^{\mathrm{c}}$ for the system are

$$\boldsymbol{Z}_{\mathrm{ch}}^{\mathrm{c}} = \boldsymbol{E}^{-1}\boldsymbol{\Lambda}_{\mathrm{m}}^{-1}\boldsymbol{E}\boldsymbol{Z} \Longleftrightarrow \boldsymbol{Y}_{\mathrm{ch}}^{\mathrm{c}} = \boldsymbol{Z}^{-1}\boldsymbol{E}^{-1}\boldsymbol{\Lambda}_{\mathrm{m}}\boldsymbol{E}, \tag{5.3}$$

which agree with [8], [10], [11] when $\boldsymbol{Z}$ is replaced with $\boldsymbol{L}$ for the lossless case.

The $(n \times n)$ mode reflection coefficient matrix is

$$\boldsymbol{\Gamma}_{\mathrm{L}}^{\mathrm{m}} = \left[\boldsymbol{\Lambda}_{\mathrm{m}} + \boldsymbol{E}\boldsymbol{Z}\boldsymbol{Y}_{\mathrm{L}}^{\mathrm{c}}\boldsymbol{E}^{-1}\right]^{-1}\left[\boldsymbol{\Lambda}_{\mathrm{m}} - \boldsymbol{E}\boldsymbol{Z}\boldsymbol{Y}_{\mathrm{L}}^{\mathrm{c}}\boldsymbol{E}^{-1}\right], \tag{5.4}$$

while the $(n \times n)$ conductor reflection coefficient matrix (relative to $\boldsymbol{Z}^{\mathrm{c}}_{\mathrm{ch}}$) is

$$\boldsymbol{\Gamma}^{\mathrm{c}}_{\mathrm{L}} = [\boldsymbol{Z}^{\mathrm{c}}_{\mathrm{L}} - \boldsymbol{Z}^{\mathrm{c}}_{\mathrm{ch}}] \cdot [\boldsymbol{Z}^{\mathrm{c}}_{\mathrm{L}} + \boldsymbol{Z}^{\mathrm{c}}_{\mathrm{ch}}]^{-1}. \tag{5.5}$$

Correspondingly, the conductor reflection coefficient matrix that relates forward- and backward-traveling conductor voltages $\boldsymbol{v}^{+}$ and $\boldsymbol{v}^{-}$ is easily shown by definition to be

$$\boldsymbol{\Gamma}^{\mathrm{c}}_{\mathrm{L}} = \boldsymbol{E}^{-1}\boldsymbol{\Gamma}^{\mathrm{m}}_{\mathrm{L}}\boldsymbol{E}, \tag{5.6}$$

where c denotes *conductor*.

The longitudinal input conductor reflection coefficient matrix is [29]:

$$\boldsymbol{\Gamma}^{\mathrm{c}}_{\mathrm{L}}(z) = \boldsymbol{E}^{-1}\boldsymbol{Q}(z)\boldsymbol{\Gamma}^{\mathrm{m}}_{\mathrm{L}}\boldsymbol{Q}(z)\boldsymbol{E}, \tag{5.7}$$

and is related to the longitudinal input admittance matrix

$$\boldsymbol{Y}^{\mathrm{c}}_{\mathrm{in}}(z) = \boldsymbol{Y}^{\mathrm{c}}_{\mathrm{ch}}\left[\mathbf{1}_n + \boldsymbol{\Gamma}^{\mathrm{c}}_{\mathrm{in}}(z)\right]^{-1}\left[\mathbf{1}_n - \boldsymbol{\Gamma}^{\mathrm{c}}_{\mathrm{in}}(z)\right], \tag{5.8}$$

which when approximately "matched" to $\boldsymbol{Y}^{\mathrm{c}}_{\mathrm{ch}}$ via reactive cancellation, will guide the MTL matching network synthesis.

5.2 Matching Strategies

We define *unilateral matching* as matching $\boldsymbol{Y}^{\mathrm{c}}_{\mathrm{in}}$ to the characteristic admittance matrix $\boldsymbol{Y}^{\mathrm{c}}_{\mathrm{ch}}$ of the lines, in essence disregarding the source. *Bilateral matching* accounts for the source and considers the output admittance matrix $\boldsymbol{Y}^{\mathrm{c}}_{\mathrm{out}}$ looking toward the source conjugately matched to $\boldsymbol{Y}^{\mathrm{c}}_{\mathrm{in}}$ for some point a; i.e., $[\boldsymbol{Y}^{\mathrm{c}}_{\mathrm{in}}(z=-a)] = [\boldsymbol{Y}^{\mathrm{c}}_{\mathrm{out}}(z=-a)]^{*}$. For $n > 2$, exact matching becomes impractical, especially when the termination is limited to nearest-neighbor mutual impedances. For loose coupling, the non-adjacent mutual admittance is negligible, though increasing frequencies, more compact packaging, and complex terminations will result in significant mismatches, for which we present some approximate matching strategies.

Thus we will develop approximations to roughly match certain conditions. Ideally, a "match" entails maximizing power transfer to the load. Here, voltage-wave matching will only approximate this ideal since multiple propagating modes with distinct phase velocities give rise to wavelength ambiguities. Consequently, we will start from the given excitation, as per Amari and Bornemann [6], and will determine the dominant mode to match. For moderate coupling a signal composed of multiple modes can be well matched for short lengths since the mode velocities are relatively similar. Though the unilateral, voltage-wave MTL matching to be considered here

constitutes a limited set of real-world problems, it will provide a rudimentary conceptual framework for general MTL matching synthesis.

5.2.1 Tuning stub application to simple mismatches

First, we consider applying open-circuited shunt stubs on the outside lines (1, n) when the impedance between the outside lines and ground is mismatched at the load to to the characteristic impedance. To elucidate this mismatch more clearly, we resort to the "network impedance matrix" notation of [29]. This matrix is a compact physical description of an $(n+1)$-terminal network where the ij entry represents the impedance interconnecting nodes i and j when $i \neq j$ or i to ground when $i = j$. For example, the load network is given by $\boldsymbol{\mathcal{Z}}_{\mathrm{L}}$. The conductor characteristic impedance matrix $\boldsymbol{Z}^{\mathrm{c}}_{\mathrm{ch}}$, if realized as a load for a perfect unilateral match, would be $\boldsymbol{\mathcal{Z}}_{\mathrm{ch}}$, where $[\boldsymbol{Z}^{\mathrm{c}}_{\mathrm{ch}}]_{ij} \neq [\boldsymbol{\mathcal{Z}}_{\mathrm{ch}}]_{ij}$ in general. This outside line mismatch is thus easily written as $[\boldsymbol{\mathcal{Z}}_{\mathrm{L}}]_{11,nn} \neq [\boldsymbol{\mathcal{Z}}_{\mathrm{ch}}]_{11,nn}$.

To match lines 1 and 3 using shunt stubs, we shift $\boldsymbol{Y}^{\mathrm{c}}_{\mathrm{in}}(z)$ toward the generator to a distance $z = -d$ such that

$$\Re\mathrm{e}\{[\boldsymbol{Y}^{\mathrm{c}}_{\mathrm{in}}]_{11}\} = [\boldsymbol{Y}^{\mathrm{c}}_{\mathrm{ch}}]_{11}. \tag{5.9}$$

On a Smith chart, this corresponds to the intersection of the phase-shifted reflection coefficient and the $1 + jX$ circle, provided the source impedance approximately equals the characteristic impedance (In practice, the designers may have flexibility in choosing $\boldsymbol{Y}^{\mathrm{c}}_{\mathrm{S}}$, and could choose $\boldsymbol{Y}^{\mathrm{c}}_{\mathrm{S}} = \boldsymbol{Y}^{\mathrm{c}}_{\mathrm{ch}}$ to approximate unilateral matching if possible). Figure 5.2 shows stub parameters in a three-coupled line microstrip.

We assume that the stubs do not couple to the interior lines. Their reference admittance is then the self characteristic admittance of line 1 or n to ground as if they were isolated. We define this reference admittance $Y_0 = [\boldsymbol{Y}^{\mathrm{c}}_{\mathrm{ch}}]_{11} + [\boldsymbol{Y}^{\mathrm{c}}_{\mathrm{ch}}]_{12} + [\boldsymbol{Y}^{\mathrm{c}}_{\mathrm{ch}}]_{13}$. Reactive cancellation is achieved if the normalized stub susceptance is

$$B = -j\,\frac{\Im\mathrm{m}\{[\boldsymbol{Y}^{\mathrm{c}}_{\mathrm{in}}(z)]_{11}\}}{\Re\mathrm{e}\{Y_0\}}, \tag{5.10}$$

where we have made the substitution $B = -jX$; the reflection coefficient of the stub is thus

$$\Gamma_{\mathrm{stub}} = -\frac{1-B}{1+B} = |\Gamma_{\mathrm{stub}}|e^{j\phi_{\mathrm{stub}}}. \tag{5.11}$$

Stub length should be chosen to yield a susceptance to ground of $-\Im\mathrm{m}\{[\boldsymbol{Y}^{\mathrm{c}}_{\mathrm{in}}(-d)]_{11}\}$. This calculation should utilize the propagation velocity of the dominant mode i

$$l = -\frac{\pi - \phi_{\mathrm{stub}}}{2 \cdot \Im\mathrm{m}\{[\boldsymbol{\Lambda}_{\mathrm{m}}]_{ii}\}}. \tag{5.12}$$

Now, the input admittance of lines 1 and 3 is modified to include the denormalized stub susceptance,

$$[\boldsymbol{Y}^{\mathrm{c}}_{\mathrm{in}}(-d)]'_{11,33} = [\boldsymbol{Y}^{\mathrm{c}}_{\mathrm{in}}(-d)]_{11} + B\left(Y_0\right), \tag{5.13}$$

so that the stubs reactance cancels the imaginary parts of $[\boldsymbol{Y}^{\mathrm{c}}_{\mathrm{in}}(-d)]_{11,nn}$

Again, we reiterate that this unilateral match cannot provide an exact match unless $\boldsymbol{Y}^{\mathrm{c}}_{\mathrm{S}} = \boldsymbol{Y}^{\mathrm{c}}_{\mathrm{ch}}$. Approximate matching is attained if $\boldsymbol{Y}^{\mathrm{c}}_{\mathrm{S}} \approx \boldsymbol{Y}^{\mathrm{c}}_{\mathrm{ch}}$. If $\boldsymbol{Y}^{\mathrm{c}}_{\mathrm{S}}$ has zero-valued mutual elements (independent Thevenin excitations, for example) but diagonal elements $[\boldsymbol{Z}^{\mathrm{c}}_{\mathrm{S}}]_{ii} \approx [\boldsymbol{Z}^{\mathrm{c}}_{\mathrm{ch}}]_{ii}$, a good approximate match still results in moderately coupled microstrip which physically exhibits self admittances that are usually an order of magnitude larger than the mutual admittances:

$$\Im\mathrm{m}\{Y_{\mathrm{self}}(z)\} \gg -\Im\mathrm{m}\{[\boldsymbol{Y}^{\mathrm{c}}_{\mathrm{in}}(z)]_{ij}\}, \tag{5.14}$$

where the self-admittance of line 1 and n, like the reference admittance, is defined as the sum of the first or last row or column: $Y_{\mathrm{self}}(-d) = [\boldsymbol{Y}^{\mathrm{c}}_{\mathrm{in}}(-d)]_{11} + [\boldsymbol{Y}^{\mathrm{c}}_{\mathrm{in}}(-d)]_{12} + [\boldsymbol{Y}^{\mathrm{c}}_{\mathrm{in}}(-d)]_{13} + \ldots$. For extremely tight coupling, the mutual admittances will be much more significant, and this approximation will be worse. Still, almost perfect practical stub matching results for these simple mismatches.

5.2.2 Matching mutual admittance with interline reactance

Our strategy must be expanded to account for symmetric mutual interline mismatches at the load ($[\boldsymbol{Y}^{\mathrm{c}}_{\mathrm{L}}]_{ij} \neq -[\boldsymbol{Y}^{\mathrm{c}}_{\mathrm{S}}]_{ij}$), and mismatches on $[\boldsymbol{Y}^{\mathrm{c}}_{\mathrm{in}}(z)]_{22,33,\ldots(n-1)(n-1)}$. We consider only mutual nearest-neighbor mismatches between lines. Perpendicular shunt stubs are clearly impractical for the inside lines. Parallel stubs implemented in coplanar waveguide [15] are difficult to simulate and exceed our interest in simplicity. An alternative such as a lumped reactive element, would enable similar susceptance cancellation as is accomplished with tuning stubs. Chip capacitors, microstrip gap capacitors, or variable-width trace inductance may be easily placed between mutually mismatched lines at an optimal distance $z = -d$ such that reactive cancellation occurs in one or more off-diagonal term $[Y^{\mathrm{c}}_{\mathrm{in}}(z)]_{ij}$.

Given initial guesses (in terms of fractions of wavelength) for the distance from the load, $z = -d_{\mathrm{guess}}$, several points d where condition (5.15)

$$\Re\mathrm{e}\{[\boldsymbol{Y}^{\mathrm{c}}_{\mathrm{in}}]_{ij}\} = -[\boldsymbol{Y}^{\mathrm{c}}_{\mathrm{S}}]_{ij} \tag{5.15}$$

holds may be determined numerically. The reactance at $z = -d$ may be canceled with inductance or capacitance. A positive susceptance at $z = -d$ implies inductive mismatch, which is canceled with a capacitance determined by $\Im\mathrm{m}\{Y_{\mathrm{mut}}(-d)\} = \omega C$ at

the desired frequency ω. Otherwise, inductance determined by $\Im\mathrm{m}\{Y_{\mathrm{mut}}(-d)\} = (\omega C)^{-1}$ cancels negative susceptance at $z = -d$ and matches the conductances. Matching via chip capacitance is restricted by availability of arbitrary valued capacitors and limited by three-dimensional discontinuities; matching via trace inductance is restricted by the line separation s (though the width is variable), and frequency dependent field effects.

Note again that the matching condition (5.15) depends on the source impedance. For our choice of $\boldsymbol{Y}^{\mathrm{c}}_{\mathrm{S}} \approx \boldsymbol{Y}^{\mathrm{c}}_{\mathrm{ch}}$ and assuming that the distance between the matching network is on the order of one-half wavelength or less, the output admittance is approximately the characteristic admittance, $\boldsymbol{Y}^{\mathrm{c}}_{\mathrm{out}}(z = -d) \approx \boldsymbol{Y}^{\mathrm{c}}_{\mathrm{ch}}$.

A "center tune" reactive cancellation to match $[Y^{\mathrm{c}}_{\mathrm{in}}(z)]_{22,33,\ldots(n-1)(n-1)}$ is found for some $z = -d$ where

$$\Re\mathrm{e}\{[\boldsymbol{Y}^{\mathrm{c}}_{\mathrm{in}}(z)]_{22,\ldots(n-1)(n-1)}\} = [\boldsymbol{Y}_{\mathrm{S}}]_{22,\ldots(n-1)(n-1)}. \tag{5.16}$$

For the three-line case with high impedance from line 2 to ground, we will show that this results in superior matching compared to simple interline reactive cancellation (5.15).

Finally, for next-neighbor matching where low impedance terminations "short" the high characteristic mutual admittance, inductive air bridges or wire bonds may be necessary. We will leave this synthesis problem for future work.

5.2.3 The quarter-wave transformer for coupled lines

Sun [16] examined the multiline quarter-wave transformer with two uniformly coupled lines in homogenous media and derived impedance/admittance transformations using the load reflection coefficients and propagation constant matrices. A quarter-wavelength of coupled line with admittance matrix $\boldsymbol{Y}_{\mathrm{q}}$ and terminated by $\boldsymbol{Y}_{\mathrm{L}}$ is attached to the $\boldsymbol{Y}_0$ input section. The input admittance matrix looking into the quarter-wave section toward the load is equated to $\boldsymbol{Y}_0$ and the solution obtained is

$$\boldsymbol{Y}_{\mathrm{L}} = \boldsymbol{Y}_{\mathrm{q}} \cdot \boldsymbol{Z}_0 \cdot \boldsymbol{Y}_{\mathrm{q}}. \tag{5.17}$$

Sun does not address the presence of multivalued propagation constants; again, design using the dominant mode is required.

Practical feasibility of this matching network is clearly limited by planar geometry. Furthermore, optimization will require expensive, iterated circuit parameter

extraction for the quarter-wave section of coupled lines. For certain cases, however, the trasnformer may match reasonably well and be easily fabricated. An example is presented in the next section.

5.3 Numerical Results

We now present results from numerical matching simulations performed on a tightly coupled three-line microstrip structure as in Fig. 5.1 with dimensions $t = 34.29$ μm, $h = 1.50$ mm, $s = 1.0$ mm, and $w = 2.6$ mm and permittivity $\epsilon_r = 4.7$. Electrical parameters were extracted using a quasi-static moment-method $RLGC$ tool [49]. Parameters $\boldsymbol{R}$ and $\boldsymbol{G}$ were considered negligible given the relatively short lengths of line and high coupling planned for the experiment. Matrices $\boldsymbol{L}$ and $\boldsymbol{C}$ for the microstrip were designed for 50 Ω elements in the diagonal of matrix $\boldsymbol{Z}_{\rm ch}^{\rm c}$ to approximately match the reference impedance. The MTL analysis was numerically implemented in computer code and the matching procedures used a Newton optimization scheme to determined distances $z = -d$ to satisfy the conditions (5.9), (5.15), and (5.16).

For the outer line mismatch, two simple cases are examined. The first considers lines 1 and 3 terminated at the load ($z = 0$) by an "open" (430 Ω) to ground ($[\boldsymbol{\mathcal{Z}}_{\rm L}]_{11,33} = 430$ Ω). In the second case, lines 1 and 3 are terminated by a "short" (20 Ω) to ground ($[\boldsymbol{\mathcal{Z}}_{\rm L}]_{11,33} = 20$ Ω). In both cases, line 2 is terminated with the inverse self-characteristic admittance, $[\boldsymbol{\mathcal{Z}}_{\rm L}]_{22} = \Re{\rm e}\{[\boldsymbol{\mathcal{Z}}_{\rm ch}]_{22}\} \approx 69$ Ω, and all remaining mutual terminations are matched to the characteristic admittances ($[\boldsymbol{\mathcal{Z}}_{\rm L}]_{ij} = \Re{\rm e}\{[\boldsymbol{\mathcal{Z}}_{\rm ch}]_{ij}\}$). While difficult to implement practically, these simple mismatches are easily stub-corrected and demonstrate the validity of the matching network.

Matching parameters d and l were optimized for an operating frequency of 2.0 GHz in both cases. The T-junction was modeled using three series inductors of 0.1 nH and a shunt capacitor of 0.2 pF; the open-circuited stub was modeled using an equivalent end-effect approximation for static-TEM approximations [50]. For the given geometry of these boards, an end-effect length was approximated as 0.57 mm, or a capacitance of 2.3 pF.

With the mismatch, matrix $\boldsymbol{\Gamma}_{\rm L}^{\rm c}$ had large magnitudes of self-reflections on lines 1 and 3, while reflections into line 1 from lines 2 and 3 were minimal; no forward waves

on line 2 were reflected (column 2 all zero). Given that line 2 is matched to ground and lines 1 and 3, this result is physically intuitive, and a zero column is possible since conductor reflection coefficient matrices are generally asymmetric [3], even for symmetric terminations.

Initial guesses were chosen with the aid of a Smith chart, using the wavelength of the dominant mode of the given excitation. Table 5.1 shows a listing of the first two initial guesses, optimized distances, and computed stub lengths for both mismatch cases. Only one significant digit was retained due to etching resolution of 0.005 in. (0.127 mm).

For each case, the first optimal stub attenuated self- and interline reflections. The "short" mismatch (with parameter $d = 7.3$ mm), is superior since its d is half that of the "open" case. Calculations using the simulated transformation matrix show that the matching network significantly reduces the self-mode and intermode voltage reflections. Figure 5.3 shows these simulated self-mode reflections as functions of frequency. The phase response clearly indicates the difference in modal propagation constants. Reflections are minimized for the optimization frequency, 2.0 GHz.

The mutual matching strategy was applied to a mismatched load where nearest neighbors were "shorted" with 26 Ω from their characteristic admittance-derived value of 287 Ω. Three solutions sets were found to increase the absorbed power in the three cases by an average of 28 %. Again, parameters and full power relations are shown in Table 5.1. The "center tune" match, however, increases the absorbed power by an average of 30% and almost perfectly matches this "short." Three solutions using (5.16) were obtained.

Both interline reactance match criteria, (5.15) and (5.16), were also tested on a more sophisiticated "amplifier" termination, for which $[\boldsymbol{\mathcal{Z}}_{\mathrm{L}}]_{22} \approx 20$ kΩ, $[\boldsymbol{\mathcal{Z}}_{\mathrm{L}}]_{12,21,23,32} \approx 500$ Ω, and $[\boldsymbol{\mathcal{Z}}_{\mathrm{L}}]_{13,31} \approx 10$ kΩ. Such a termination could be encountered in a transistor amplifier application. The standard interline reactance offered only one solution, which actually increased the mismatch. The "center tune" interline reactance increased absorbed power 12% - 25%, with better matching for smaller d (see Table 5.1 for complete power relations and parameters).

Finally, the quarter-wave transformer strategy was tested on a mismatch. Nonlinear equation (5.17) is generally difficult to solve when information about $\boldsymbol{Y}_q$ is not known *a priori*. However, reciprocity guarantees symmetric matrices, and symmetry

about the $x = 0$ plane reduces the independent variables to four, since the matrix is symmetric across the opposite diagonal. Thus, four nonlinear equations (quadratic with respect to each variable independently) arise from (5.17). These may be easily solved using *Mathematica* [51]. For one simulation, eight total solutions were obtained, but four were immediately discarded due to nonphysical negative terms in the impedance matrix; the remaining three violated the dominance condition on the realizable admittance matrix [26]. One solution for an "amplifier" type of termination with $[\boldsymbol{\mathcal{Z}}_{\mathrm{L}}]_{22} \approx 2$ kΩ was obtained; line 2 was narrowed in several iterations and an average increase of 19% absorbed power resulted.

In all cases, calculation of power quantities along the line verified the effectiveness of the matching networks. In Table 5.1, the forward-travelling power P_{f} and the power absorbed the load (assuming the lines and matching networks are lossless) P_{L} demonstrate the matching. Certain solution sets were repeated for various initial guesses and therefore omitted. In nearly all cases, the matching solutions nearer to $z = 0$ resulted in greater absorbed power, as the effect of the mode delays decreased with smaller coupling lengths.

Each matching network solution in the coupled-line system was checked on Agilent's Advanced Design System. All power values were verified with under 1% error; these resulted from termination value truncations and substrate approximations.

5.4 Calibration and Measurement Results

To demonstrate the validity of the matching strategies on coupled three-line systems, several microstrip structures were constructed from the synthesized results given in Table 5.1 and the dimensions given in the previous section. Focusing on the stub-corrected "short" mismatch (solution 1: $d = 7.3$ mm, $l = 10.5$ mm), the structure in Fig. 5.2 was first fabricated on Kepro FR-4 circuit boards.

Tight physical coupling between lines precluded adjacent connectors in Fig. 5.2. Thus, the coupled lines were accessed with fan-ins and fan-outs, as shown in Fig. 5.4. Lines 1 and 3 were angled 20° from the z-axis and continued 17.58 mm from the reference planes to the board edges. SMA flange mount connectors (female 3.5 mm coaxial cable to microstrip tab adapter) were then soldered directly to the lines at these edges. The bend discontinuity suffered a simulated mismatch of no greater than 52 Ω; in fact the worst discontinuity measured via time-domain reflectometry

(TDR) was 55 Ω for one case, which we believe can be attributed to a poor solder connection.

We sought to validate the matching networks by measuring the conductor and mode reflection coefficient matrices from measured S-parameters, performed on an HP 84510C automatic network analyzer (ANA). Furthermore, characterization of the coupled line sections in the multimode domain was essential. We therefore employed the multimode TRL (MMTRL) algorithm [45] and a renormalization algorithm [38]. Three necessary standards (thru, reflect, and line) with the same fan-in and fan-out sections were also constructed on identical board material using an identical chemical etching process. Identical SMA connectors and solder joints were also used.

For the conductor S-parameters, we used a hybrid "two-tier" calibration. First, a 3.5 mm short-open-load-termination (SOLT) calibration de-embedded the test cables. Then, to de-embed the microstrip-coax junction, the input line, and the angular discontinuity of each fan-in or fan-out line, we employed the common "thru-reflect-line" (TRL) [52]. Thus the calibration established reference planes at coupled-line system inputs labeled in Fig 5.4. The major source of error in this calibration procedure is obviously that it did not account for coupling in the fan-in and fan-out sections, where the lines undoubtedly couple, especially close to the reference planes. Furthermore, this calibration involved six distinct TRL calibrations and eight distinct standards (the MMTRL standards were not used, and each fan-in or fan-out line was isolated on a separate board) to measure the six sets of (2×2) S-parameters needed to extract the eight coefficients and fully characterize the structure in Fig. 5.2. Though some of these results were redundant, they provided an understanding of the symmetry limitations, which were tangible, but for our purposes, negligible. The TRL coefficients for each calibration configuration were calculated in software and graphically examined to save time in repeating measurements affected by bad connections, though connections were shown to be repeatable. More importantly, this process revealed resonance frequencies in certain thru and line calibration standard fixtures (one of which was the MMTRL thru) which affected results at certain frequencies.

Symmetry and reciprocity of the structure in Fig. 5.2 reduces the total independent S-parameters to 13. Furthermore, if $D = 2d$ in Fig. 5.2 (which applied to our measurements), symmetry reduces the required number of measurements to 8: S_{11},

S_{12}, S_{13}, S_{14}, S_{15}, S_{16}, S_{22}, and S_{25}.

Using the complete (6×6) conductor and mode S-parameter matrices, referenced as per Fig. 5.4, we computed both (3×3) conductor and mode input reflection coefficient matrices $\mathbf{\Gamma}^{\mathrm{c}}_{\mathrm{in}}$ and $\mathbf{\Gamma}^{\mathrm{m}}_{\mathrm{in}}$ seen by the source ($z = -D$) for prescribed load terminations $\mathbf{\Gamma}^{\mathrm{c}}_{\mathrm{L}}$ or $\mathbf{\Gamma}^{\mathrm{m}}_{\mathrm{L}}$ for the mismatched termination network corresponding to the "short." The general expression applicable to both conductor and mode quantities is

$$\mathbf{\Gamma}_{\mathrm{in}} = [\boldsymbol{S}]_{11} + [\boldsymbol{S}]_{12} \cdot \left([\mathbf{\Gamma}_{\mathrm{L}}]^{-1} - [\boldsymbol{S}]_{22}\right)^{-1} \cdot [\boldsymbol{S}]_{21}, \tag{5.18}$$

where $\boldsymbol{S}$ is the measured (6×6) S-parameter matrix and $[\boldsymbol{S}]_{ij}$ are its (3×3) submatrices. Matrix $\mathbf{\Gamma}_{\mathrm{L}}$ accounts for the load mismatch at port 2' (the load in Fig. 5.2) and is calculated from (5.5),

The mode and conductor characteristic admittances were the only quantities not directly measured. Instead we applied the numerical approximation to $\boldsymbol{Y}^{\mathrm{c}}_{\mathrm{ch}}$ (generated using RLGC and verified with other quasi-static methods), which was used in the simulations and synthesis. Results were negligibly sensitive to this approximation.

Good correlation between the simulated and measured $\mathbf{\Gamma}^{\mathrm{c}}_{\mathrm{in}}(z = -D)$ results is observed in Fig. 5.5. Reflection minimization at the design frequency 2.0 GHz demonstrates that reflected power can be almost eliminated for the simple mismatch cases. The disturbance at 3.8 GHz in Fig. 5.5 represents one of the resonant frequencies encountered for a particular fixture (a thru) with no available substitute. Measured phase followed the general trend, with deviation mainly confined to DC and high-frequency regions. The major assumptions concerned consistent solder connections, consistent substrate in each TRL standard, and matched terminations.

Finally, the MMTRL allowed mode reflection coefficient measurement as per (5.18). Results are shown in Fig. 5.6 and are in good agreement with the simulated values shown in Fig. 5.3. Only mode 3 appeared to suffer from large error; this results from its relatively low reflection in this stub structure. This arises due to the field configuration of mode 3, where more field energy between the center and outer lines negates the effects of the stubs. Thus, we find unsurprisingly that measurements are more sensitive for small reflection. Propagation constants were extracted and compared to our simulation quasi-TEM values (generated from RLGC). The phase constants are shown in Fig. 5.7, and clearly agree with the quasi-TEM values with acceptable error. The attenuation constants are shown in Fig. 5.8 and are somewhat higher than predicted by quasi-TEM simulations, but still acceptable

and increase with frequency, as expected.

Several structures incorporating the interline reactance matching networks for mutual mismatches were also fabricated. Measurments are currently being conducted and will be presented in future work. The quarter-wave transformer should be expected to yield similar, though less significant matching, as observed in simulations (see Table 5.1). For now, the main goal of validating one of the matching networks (tuning stubs) has been accomplished, and the stub strategy would clearly be applicable to transistor amplifiers or coupled-line bus systems with mismatched drivers on the outer lines.

5.5 Conclusions

This chapter has introduced several new matching techniques for a coupled-line microstrip structures. Practical applications will certainly include more complicated mismatches and greater coupling lengths for which the matching methods detailed in this paper may be individually less effective. However, the main goal was validation of the techniques, made possible through frequency-domain measurements. Certainly, more extensive measurements and more precise calibration procedures are under consideration. Some error factors remain to be corrected or improved, and the impact of several calibration and measurement assumptions will be further investigated.

Future work includes combination of these methods, hybridization with other methods, and development of better optimization procedures. Specifically, optimization of power functions given the excitations and boundary conditions will alleviate the dominant mode concern and the voltage-wave matching approach, thereby fully and unambiguously "matching" (maximizing the power delivered to the load). Bilateral matching to achieve maximum power transfer is obviously desired. Also, parallel stubs and other novel structures with possible matching capability should be investigated. Finally, full EM modeling will improve the discontinuity models and other significant effects arising with increasing application frequencies.

Table 5.1 Optimized parameters for stub and reactive element tuning cases.

Solution Set	$z = -d_{\text{guess}}$ (mm)	$z = d$ (mm)	l or X	$\boldsymbol{V}_{\text{S}}$ (V)	P_f P_L w/o match		P_f P_L with match	
Outer line "Open" mismatch with stub match								
1	14.2 ($\frac{3}{16}\lambda$)	13.9	25.6 mm	(1,1,1)	7.46	5.42	7.34	7.32
2	23.7 ($\frac{5}{16}\lambda$)	26.9	12.0 mm	(1,1,1)	7.46	5.42	7.45	7.15
Outer line "Short" mismatch with stub match								
1	4.7 ($\frac{1}{16}\lambda$)	7.3	10.5 mm	(1,1,1)	6.96	5.78	7.38	7.36
2	33.2 ($\frac{7}{16}\lambda$)	33.3	27.4 mm	(1,1,1)	6.96	5.78	7.56	7.45
Mutual mismatch "short" with interline reactance match								
1	4.0	8.14	0.90 pF	(0,1,0)	2.64	1.77	2.50	2.37
7	28.0	51.88	0.88 pF	(0,1,0)	2.65	1.84	2.49	2.33
8	32.0	35.60	0.15 nH	(0,1,0)	2.62	1.80	2.50	2.42
Mutual mismatch "short" with interline center-tune match								
1	2.0	6.1	1.19 pF	(0,1,0)	2.49	1.71	2.47	2.47
7	14.0	37.0	0.18 nH	(0,1,0)	2.53	1.75	2.48	2.48
9	18.0	49.2	1.21 pF	(0,1,0)	2.47	1.75	2.47	2.46
Realistic amplifier mismatch termination with interline reactance match								
1	8.0	48.0	0.14 pF	(0,1,0)	2.59	1.56	2.53	1.36
Realistic amplifier termination, interline center-tune match								
3	6.0	55.6	0.21 nH	(0,1,0)	2.23	1.55	2.62	2.16
5	10.0	26.5	1.45 pF	(0,1,0)	2.57	1.37	2.72	2.07
6	12.0	15.1	0.25 nH	(0,1,0)	2.41	1.30	2.66	2.09
Realistic termination with quarter-wave transformer match								
1	-	-	-	(0,1,0)	2.51	1.63	2.45	2.06

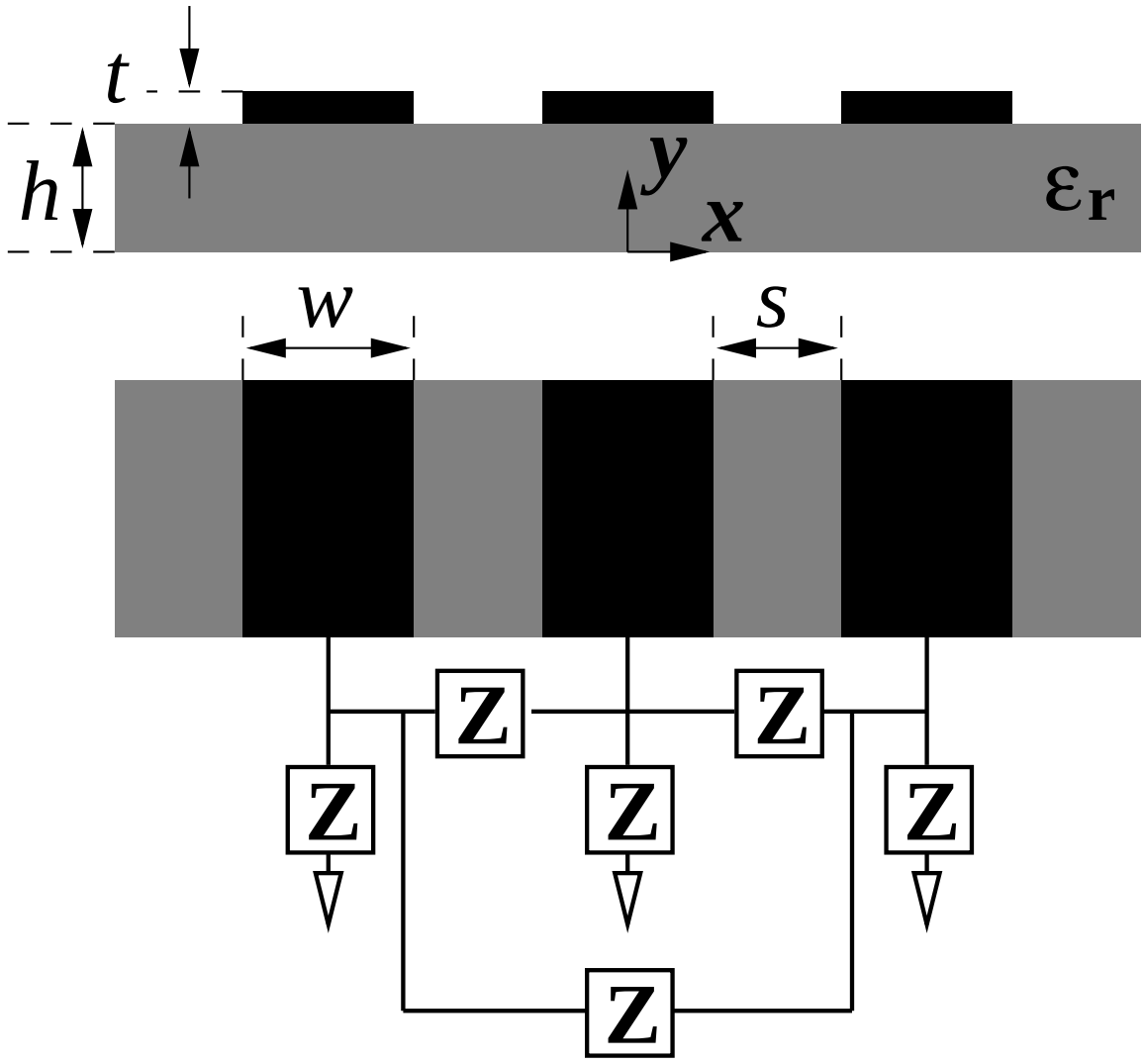

Figure 5.1 Cross-sectional and top view of microstrip structure showing dimensions and geometries. An arbitrary complex load is assumed with the Z network.

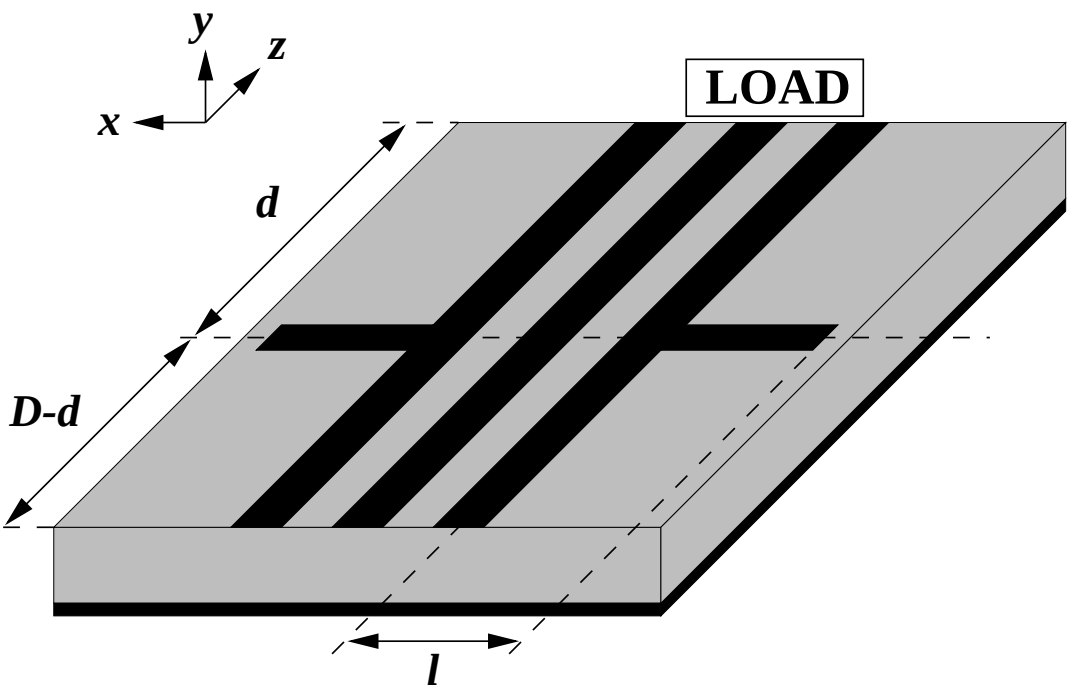

Figure 5.2 Three-coupled line system with load plane and tuning stubs.

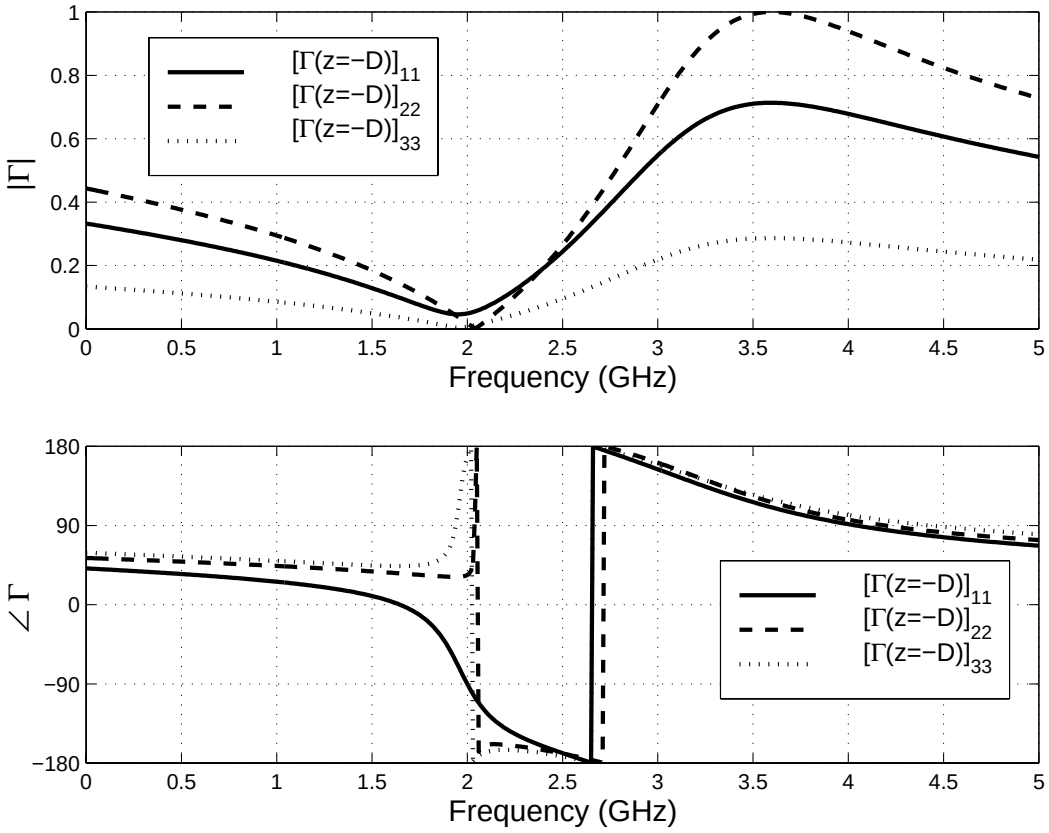

Figure 5.3 Modal reflection coefficient variation over frequency for mode self reflection terms $[\mathbf{\Gamma}_{\mathrm{L}}^{\mathrm{m}}(z=-D)]_{11}$, $[\mathbf{\Gamma}_{\mathrm{L}}^{\mathrm{m}}(z=-D)]_{22}$, $[\mathbf{\Gamma}_{\mathrm{m}}(z=-D)]_{33}$. Stubs optimized for 2.0 GHz with open on termination elements $[\boldsymbol{Z}_{\mathrm{L}}^{\mathrm{Y}}]_{11}$ and $[\boldsymbol{Z}_{\mathrm{L}}^{\mathrm{Y}}]_{33}$: $d = 7.32$ mm, $l = 10.58$ mm.

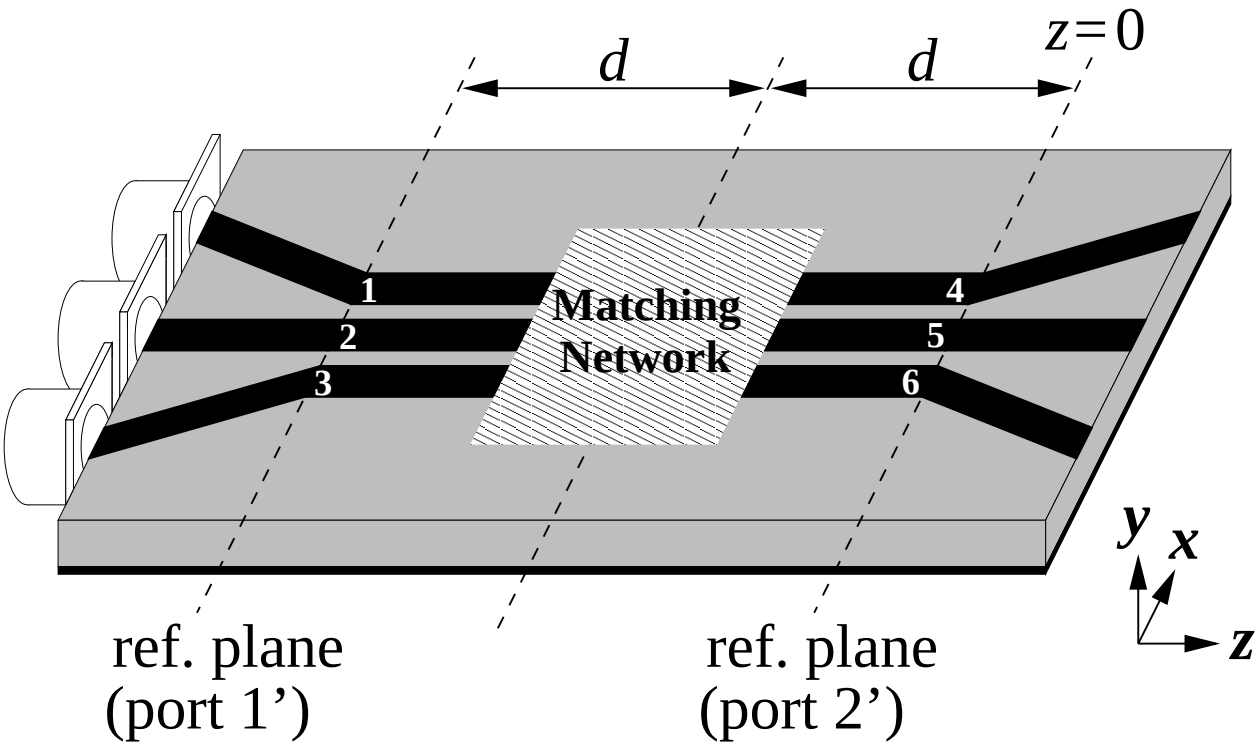

Figure 5.4 The device under test, with input and output sections, reference planes, and SMA connectors.

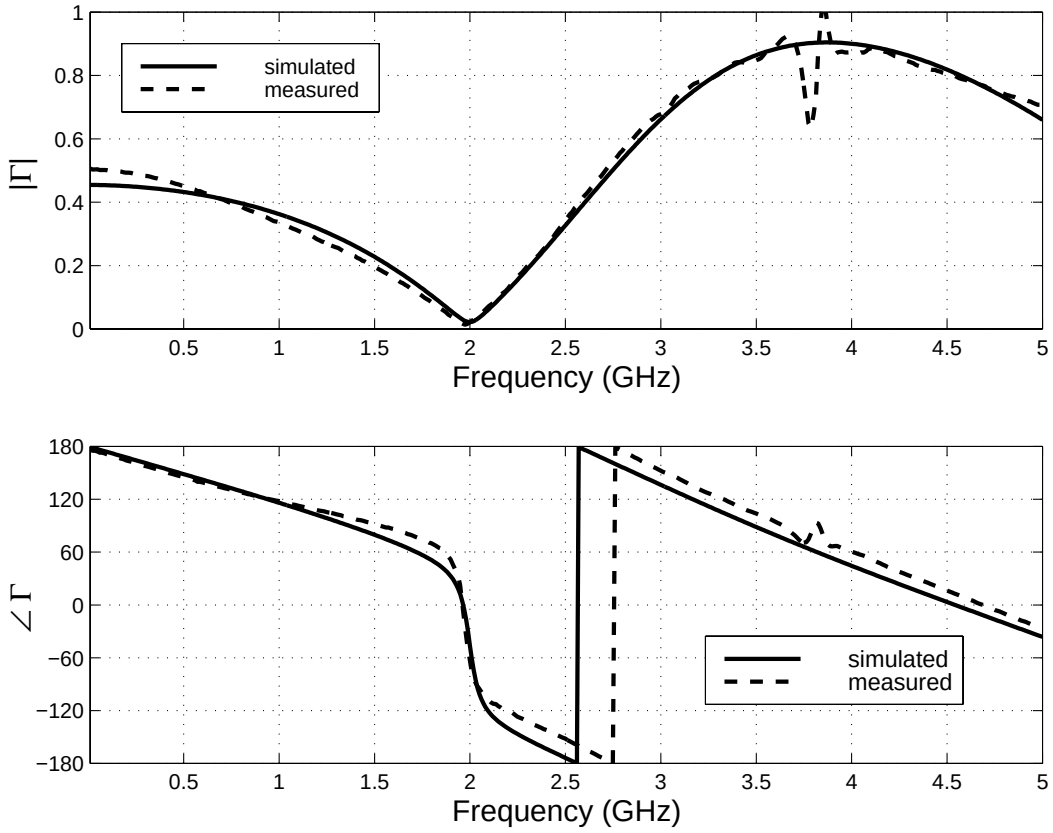

Figure 5.5 Comparison of measured and simulated frequency variation for conductor self-reflection terms $[\mathbf{\Gamma}_{\mathrm{L}}^{\mathrm{c}}]_{11,33}$ at $z = -21.1$ mm, with "short" mismatch corrected by stubs.

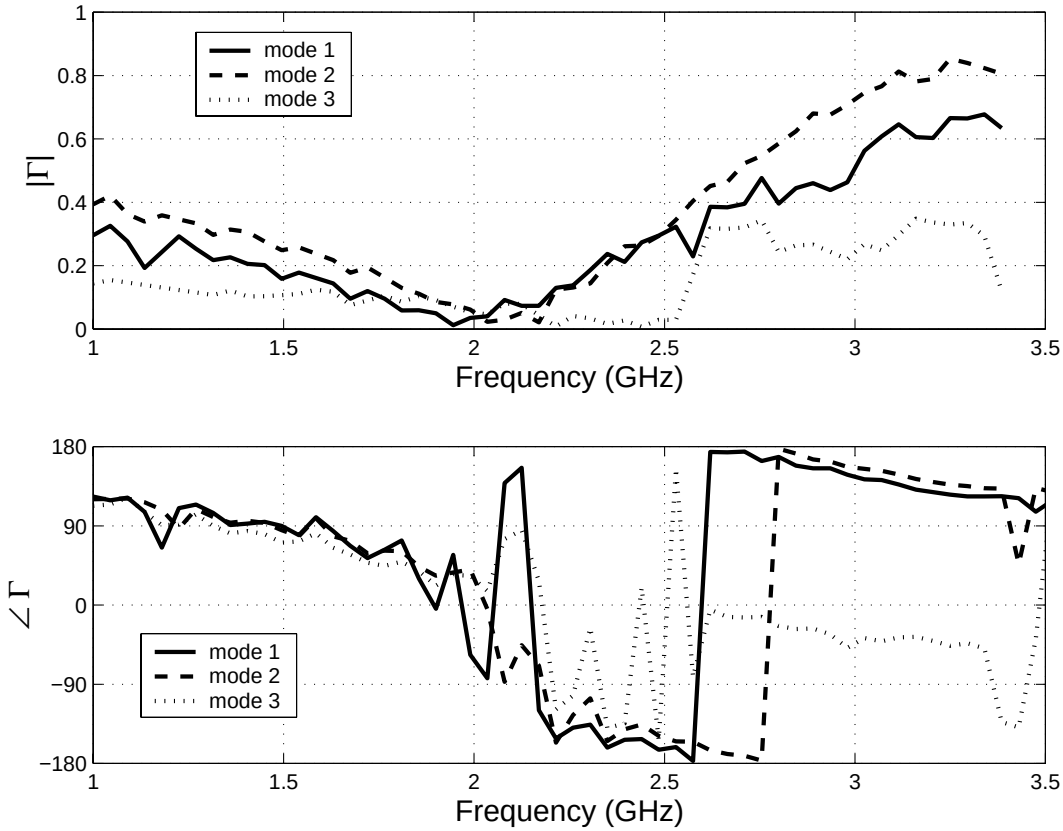

Figure 5.6 Measured mode reflection coefficient variation over frequency for mode self-reflection terms $[\mathbf{\Gamma}_{\mathrm{L}}^{\mathrm{m}}(z=-D)]_{11}$, $[\mathbf{\Gamma}_{\mathrm{L}}^{\mathrm{m}}(z=-D)]_{22}$, $[\mathbf{\Gamma}_{\mathrm{m}}(z=-D)]_{33}$. Stubs optimized for 2.0 GHz with open on termination elements $[\boldsymbol{Z}_{\mathrm{L}}^{\mathrm{Y}}]_{11}$ and $[\boldsymbol{Z}_{\mathrm{L}}^{\mathrm{Y}}]_{33}$: $d = 7.32$ mm, $l = 10.58$ mm.

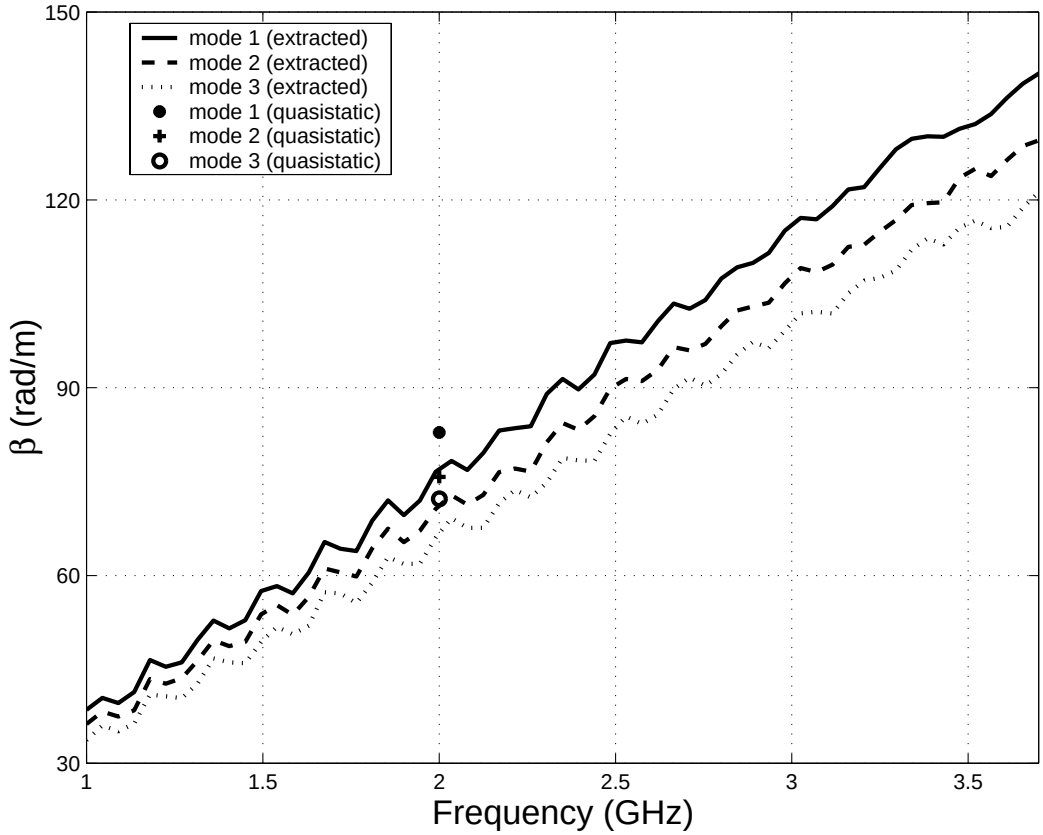

Figure 5.7 Measured phase constants from the MMTRL algorithm compared with RLGC-simulated values at 2.0 GHz.

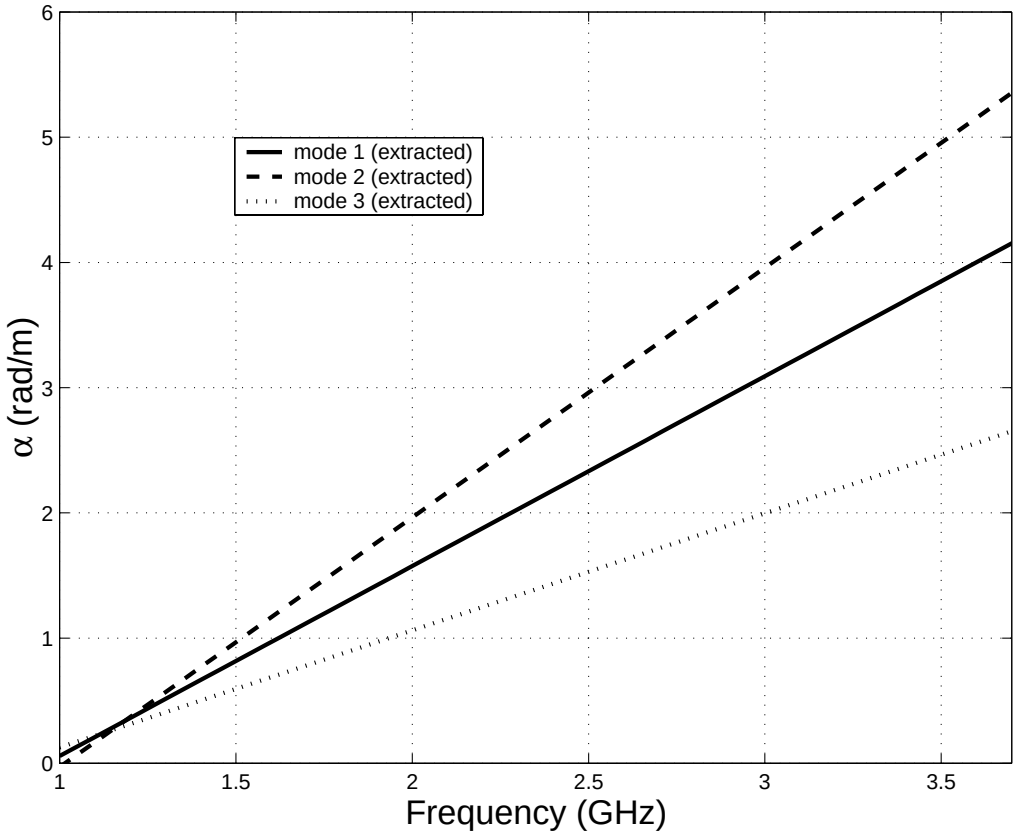

Figure 5.8 Extracted and linearly fitted attenuation constants for the three modes in the line standard.

CHAPTER 6

MTL AMPLIFIER SYNTHESIS

Synthesis procedures for microwave transistor amplifiers (MTAs) on two- and three-coupled microstrip line structures are presented. This novel design utilizes coupled microstrip with one or more of the lines grounded at the system input and output. Coupled-line matching network design techniques are applicable. The basic idea is to utilize the fabrication advantages of coplanar technology while saving conductor material. This alleviates the need for through-holes and vias necessary in ordinary MTAs.

6.1 Introduction

Narrowband low- and medium-power microwave transistor amplifier (MTA) design is necessary for a plethora of microwave devices and systems, including wireless communications, signal generation, and radar. One of the most common and fundamental MTA designs utilizes microstrip technology. Here, closed-form expressions are readily available to facilitate the design of the matching networks and biasing circuits necessary for the amplifier (e.g. [53], [54]).

Several recent works have addressed finite-ground coplanar waveguide (FG-CPW) lines [55], [15] and devices in FG-CPW lines [56]. In order to preserve the advantages of planarity inherent to CPW technologies, while eliminating their large swaths of conductor material, we explored the synthesis of amplifiers in coupled-microstrip technology, where one or more lines are connected to ground. However, this requires considerably more numerical analysis [29] and coupled-line matching networks [44] incorporated into well-known multiconductor transmission line (MTL) formulations. The result applies the coupled microstrip matching networks [29] to a transistor amplifier for improved gain, and whose design requires no vias, through-holes, or large substrate conductive planes at the signal level, which translates to fabrication savings.

Despite the topological similarities with FG-CPW (our three-line ground-signal-ground structure is identical), coupled microstrip designs utilize the ground plane so that propagating waves are confined mostly to the dielectric and may include parallel-plate modes. The ground plane is not optional because our designs consider the "ground lines" to be connected to ground at the input or output ports or both in the system with vias, wraps, or some chassis or structural connection. Or, where these connections are undesirable, FG-CPW-to-microstrip transitions may be employed [57]. However, to preserve fabrication simplicity between these transitions, ground equalization is not considered.

A comparative study between FG-CPW and three-coupled microstrip lines will be warranted to clarify these design issues. We will not examine them here, however, and we only emphasize that coupled microstrip devices and systems will be practical as an alternative to FG-CPW in hybrid applications where multiple waveguiding technologies are necessary.

We start the paper by overviewing the necessary theoretical formulations for microwave transistor amplifier design extended to the coupled-microstrip domain, including the transistor discontinuity characterization and the simulataneous conjugate match in MTL systems. After describing the functioning prototype amplifier, we present a generalized methodology for coupled-microstrip amplifiers. This will allow accurate synthesis of amplifiers and other devices in coupled-microstrip systems with arbitrary numbers of lines.

6.2 Multiconductor Transistor Amplifier Formulations

General synthesis of coupled-microstrip line amplifiers follows from well-known fundamentals for the single line case [54]. The amplifier contains excitations, terminations, matching networks, bias networks, and the transistor. Each section in the MTL-MTA, however, is described by a $(2n \times 2n)$ immittance parameter matrix, where n is the number of lines (see Fig. 6.1).

Practically, n will be limited in single-channel or single-signal analog applications. Our three-line amplifier could also be realized with two lines, though several engineering issues would differ.

6.2.1 The transistor discontinuity

The transistor and the coupled lines within its vicinity represent a discontinuity. Ideally, this section (between points $z = -t_S$ and $z = -t_L$ shown in Fig. 6.2) should be modeled or measured as a full $2n$-port (or "n-dimensional two-port") in the frequency domain, yielding a $(2n \times 2n)$ frequency-dependent S-parameter matrix $\boldsymbol{S}_T(\omega)$, shown in Fig. 6.1, and given by

$$\boldsymbol{S}_T = \begin{bmatrix} \boldsymbol{S}_{11} & \boldsymbol{S}_{12} \\ \boldsymbol{S}_{21} & \boldsymbol{S}_{22} \end{bmatrix}, \tag{6.1}$$

which is normalized to a 50-Ω uncoupled system with characteristic impedance matrix

$$\boldsymbol{Z}_0 = 50 \cdot [\mathbf{1}_{2n}]\ \Omega. \tag{6.2}$$

$\boldsymbol{S}_T(\omega)$ is usually obtained from ANA frequency-domain measurements. However, for multiline systems with tightly coupled lines, this measurement requires the MMTRL algorithm [45], or coupled line fan-ins and fan-outs [29], [33]. Furthermore, the trend toward smaller device and system size necessitates microprobe measurements and appropriate full-port characterization techniques [38].

For an initial prototype, our primary concern was to obtain a functioning amplifier, without necessarily designing according to a comprehensive methodology. Thus, given readily available apparatus for conducting two-port, single-line MTA measurements of a biased transistor in the common-emitter configuration, we consider a two-port approximation of the $2n$-port. In other words, the two-port S-parameter description of the transistor is obtained directly by measurement, and embedded into a coupled transmission line model, from which one obtains the $2n$-port S-parameter description of the transistor discontinuity. We will address the shortcomings of such an approximation in Section 6.3.

6.2.2 Simultaneous conjugate matching

The simultaneous conjugate match (SCM) conditions necessary to achieve maximum transducer power gain for the amplifier system in Fig. 6.1, where each each block is a $2n$-port, are

$$\boldsymbol{\Gamma}_S = \boldsymbol{\Gamma}_{in}^*, \tag{6.3a}$$

$$\boldsymbol{\Gamma}_L = \boldsymbol{\Gamma}_{out}^*, \tag{6.3b}$$

where $\boldsymbol{\Gamma}_L$ and $\boldsymbol{\Gamma}_S$ are the $(n \times n)$ line reflection coefficient matrices at the input and output sides of the transistor discontinuity (at $z = -t_S$ and $z = -t_L$) looking

toward the source and the load terminations of the system, or the input and output of the coupled-line amplifier, respectively. The input and output reflection coefficient matrices $\boldsymbol{\Gamma}_{\text{in}}$ and $\boldsymbol{\Gamma}_{\text{out}}$ looking into the transistor section are

$$\boldsymbol{\Gamma}_{\text{in}} = \boldsymbol{S}_{11} + \boldsymbol{S}_{12}(\boldsymbol{\Gamma}_{\text{L}}^{-1} - \boldsymbol{S}_{22})^{-1}\boldsymbol{S}_{21} \tag{6.4}$$

$$\boldsymbol{\Gamma}_{\text{out}} = \boldsymbol{S}_{22} + \boldsymbol{S}_{21}(\boldsymbol{\Gamma}_{\text{S}}^{-1} - \boldsymbol{S}_{11})^{-1}\boldsymbol{S}_{12}. \tag{6.5}$$

In the scalar case, the SCM solutions to Γ_{L} and Γ_{S} are found using the quadratic formula. For coupled lines, the nonlinear matrix system requires numerical optimization for $\boldsymbol{\Gamma}_{\text{L}}$ and $\boldsymbol{\Gamma}_{\text{S}}$. Several approaches to this optimization are possible, including genetic algorithms to minimize the Frobenius matrix norm of (6.3). However, one cannot optimize arbitrary reflection coefficients; these are constrained by passivity, reciprocity, and realizability conditions for general lossy passive matching networks. (Their stability, in fact, must be verified by positive definiteness of the equivalent impedance and admittance matrices $\boldsymbol{Z}_{\text{L}}$ and $\boldsymbol{Y}_{\text{L}}$.) Instead, one must maximize the power delivered to the load as functions of the terminations, transistor description, and matching network parameters. However, athough the transducer power gain in single-line systems is given by the relatively simple formula [54]

$$G_T = |S_{21}|^2 \frac{1 - |\Gamma_{\text{L}}|^2}{(1 - |\Gamma_{\text{S}}|^2)|1 - S_{22}\Gamma_{\text{L}}|^2}, \tag{6.6}$$

the equivalent gain in MTA systems is a complicated matrix function that can be derived using multiline signal flow graph analysis:

$$G_T = \frac{2P_{\text{L}}}{2P_{\text{AVS}}} = \frac{\boldsymbol{b}_{\text{S}}^* \cdot \boldsymbol{A}^* \cdot [\mathbf{1}_n - \boldsymbol{\Gamma}_{\text{L}}^* \boldsymbol{\Gamma}_{\text{L}}] \cdot \boldsymbol{A} \cdot \boldsymbol{b}_{\text{S}}}{\boldsymbol{b}_{\text{S}}^* \cdot ([\mathbf{1}_n - \boldsymbol{\Gamma}_{\text{S}} \boldsymbol{\Gamma}_{\text{S}}^*]^{-1})^* \cdot \boldsymbol{b}_{\text{S}}}, \tag{6.7}$$

where P_{L} denotes the power delivered to the load, P_{AVS} denotes the available source power, and the matrix $\boldsymbol{A}$ is given by

$$\boldsymbol{A} = [\mathbf{1}_n - \boldsymbol{S}_{22}\boldsymbol{\Gamma}_{\text{L}}]^{-1}\boldsymbol{S}_{21}\ (\mathbf{1}_n - \boldsymbol{\Gamma}_{\text{S}}\boldsymbol{\Gamma}_{\text{in}})^{-1}. \tag{6.8}$$

An important observation regarding (6.7) is its dependence on the source excitation $\boldsymbol{b}_{\text{S}}$, which differs from the single-line scalar case (6.6).

6.3 Results

For our design, we used a Motorola MRF-901 bipolar junction transistor (BJT) in common-emitter configuration. As explained in the previous section, we approximated the transistor as a two-port that was measured using a separate fixture which fastened the package to the board and signal lines for measurement. This fixture

did not include ground lines adjacent to the signal lines, as would be the case in the three-coupled line amplifier. Instead, the emitters where grounded to a separate block of conductor raised through the substrate from the ground plane. Therefore, the fixture introduces error for high frequencies since the two-port representation fails to accurately model the true coupled-line environment of the amplifier. Thus the $(2n \times 2n)$ S-parameter simulation of the measured transistor 2-port embedded in three coupled lines will significantly differ from the actual $(2n \times 2n)$ S-parameter description of the transistor discontinuity in three lines.

Synthesis of coupled-line matching networks in a standard MTL-MTA requires formulations for longitudinal MTL functions [29]. Traditional matching network techniques may be extended to coupled lines, and for this problem each matching network consists of two chip capacitors of equal value, each interconnecting lines 2 and 1 and lines 2 and 3 at locations $z = -m_{\mathrm{S}}$ and $z = -m_{\mathrm{L}}$ as in Fig. 6.2 (equal capacitances maintain symmetry and suppress the odd mode). The chip capacitors used are made by Dielectric Laboratories and have a width of 110 mils. Biasing voltages for this transistor were supplied to the base and collector through ports 1 and 2 of the network analyzer for both the transistor measurement and the final amplifier measurement.

We must emphasize that for MTL matching, one network may not necessarily be adequate. Given three lines, one of the aforementioned network of interline capacitors does not generally provide a complete match. Consider an arbitrary number n of coupled lines with strong enough coupling such that their $(n \times n)$ characteristic admittance matrix is dense. A general, full, lossless match at some longitudinal distance requires reactive elements interconnecting each of the $n+1$ nodes (the lines and the ground plane). Tuning stubs are usually impractical for inside lines (the signal line in our three-line amplifier). Furthermore, for three or more lines, mismatches of admittance between nonadjacent lines may not be practically matched unless bridges are used. Therefore, perfect matching is generally not possible for $n \geq 3$.

For the transistor two-port to $2n$-port model and the matching network opimization, we used ADS. Gain, S_{21} was maximized while the reflections S_{11} and S_{22} were minimized by optimizing the capacitances $\mathrm{C_S}$ and $\mathrm{C_L}$ (limited to the discrete values of 0.4, 0.8 and 1.2 pF) and the distances $z = -m_{\mathrm{S}}$ and $z = -m_{\mathrm{L}}$ (bounded only by the the input/ouput connectors and transistor junction). The optimization and final simulations included conductor thickness, substrate loss, end-effect capacitance,

and T-junctions. The SMA connectors were accounted for in simulation via 70 mil transmission lines. Their actual length was approximately 200 mils.

Figure 6.3 shows the final amplifier with connectors, the transistor, and the matching chip capacitors. Final matching network results ($C_S = 0.4$ pF, $m_S - t_S = 1040$ mil, $C_L = 0.4$ pF, $t_L - m_L = 1550$ mil) are compared to the unmatched amplifier in Fig. 6.4 to validate the design. Matching reduced S_{11} and S_{22} and increased gain by 3.4 dB (from 1.8 dB to 5.2 dB) at the design frequency, 3.1 GHz.

Figure 6.5 shows a small discrepancy between the simulated matching network optimum and the actual measured optimum (1.5 dB). This was likely the result of the $2n$-port discontinuity approximation from the two-port transistor measurement. This is close to the maximum attainable transducer gain which we approximated as 8.7 dB, but as predicted, our optimization cannot achieve this figure because a full match is unattainable with only one interline capacitance network for each side.

6.3.1 Filtering, feedback, and mode delay effects

Coupled-microstrip configurations, while ideal for planarity and fabrication, are susceptible to adverse filtering effects. In particular, the nulls in the frequency responses of gain (e.g., 2.5 GHz, see Fig. 6.4) are the result of filtering behavior where the signal essentially bypasses the transistor. When the total board length (for our case, 3800 mils) from input to output is an integer multiple of one-half wavelength, there are essentially two quarter wave filters on each side of the transistor, and a signal launched at the input (line 2) couples to lines 1 and 3 (little appears at the base of the transistor for amplification) and then couples on the output side back to line 2 to the output. To verify this filtering, we removed the transistor package and measured the passive three-line board. Results are shown in Fig. 6.6; clearly, the amplifier gain is compromised when the filter transmission is maximum (at 2.5 GHz), while the feedback, S_{21} for the filter in Fig. 6.6, is very large around this frequency.

Obviously, the total structure could be reduced in size to mitigate the filtering. Again, this device is essentially conceptual, and would be realized in practice on a much smaller scale. But provided that the device dimensions are electrically large, such transmission line filtering behavior occurs. Cascaded amplifiers are one solution which will increase bandwidth and gain, though at higher material cost.

Note that the matching networks may also increase feedback (> -15 dB) and still result in relatively poor reflection, particularly for the input. The obvious trade-

off seems to be bypassing for matching. For both sides, better matching sacrifices the signal magnitude incident upon the transistor gate and collector. For the input, this causes signal bypass and gain degradation; for the output, the result is signal feedback.

In this symmetric case where the transistor is removed, the nulls and peaks in the filter responses have neither consistent shape nor magnitude. While increasing loss plays a role, the "mode delays" due to unequal propagation velocities are also significant. Of the three even quasi-TEM modes that propagate in this system, the input signals excite two of these modes, the so-called even-even and even-odd modes, whose relative delays result in a phase difference of 32° upon reaching the junction at the design frequency of 3.1 GHz.

6.3.2 Matching network sensitivity

Matching network optimization should employ a method. Genetic algorithms should be limited to problems with many parameters, such as double matching. Otherwise, traditional gradient methods may suffice. Consider the placement of the chip capacitors after their optimized distances are determined.

For improved bandwidth, it is usually desirable to restrict the matching network location to within a half-wavelength of the mismatch. Figure 6.7 shows a power contour taken for the matching network that we presented in a previous work [29] for a lossline interline capacitor matching case. Capacitance value and longitudinal distance from the load are the horizontal and vertical parameters, while the white-shaded areas correspond to higher power absorption in the load and better match. The horizontal periodicity of the maxima correspond to the effective half-wavelengths (where the effective propagating mode consists of some combination of the distinct propagating modes whose delays are negligible). Note that load power absorption falls off for large matching capacitor value, since large capacitors increasingly appear to short the lines.

Clearly, this power contour is smooth, and lends itself to traditional gradient methods. Furthermore, this property incurs flexibility in the value and the placement of the capacitor. Figure 6.8 shows the measured amplifier gain (S_{21}) for the input-side capacitor at four different longitudinal locations, and verifies that deviation of the capacitor from the optimized location does not significantly degrade the gain within 260 mils, although the alteration incurs some frequency shift in the maximum. A

maximum increase of 6.5 dB for 3.22 GHz was observed for $m_S - t_S = 1180$ mil.

6.4 General Methodology

The aforementioned results have validated the synthesis of power amplifiers in MTL systems. With current trends toward smaller and faster interconnects at the board, package, and chip levels, a general methodology for amplifiers in these increasingly coupled-line systems must be developed. While this will account for an arbitrary number of lines, there will usually be only one input and one output. The remaining ports will be terminated appropriately (usually to ground via wrap-arounds or to other grounded fixturing).

Extending upon this work, a general methodology for an n-coupled line transistor amplifier proceeds as follows:

- Characterize the coupled microstrip system in terms of its normal mode parameters or distributed circuit parameters [58].
- Measure the $(2n \times 2n)$ scattering parameters of the transistor discontinuity (should include any biasing circuitry to be present in the actual amplifier) using appropriate calibration techniques and algorithms.
- Numerically optimize passive, lossless matching network parameters for maximum power transfer. These must be constrained by passivity, reciprocity, and realizability conditions. Two approaches are possible: a power function quantifying power delivered to the load could be maximized, or the SCM conditions could be minimized.
- Realize the matching networks.
- Simulate the final design, and measure a fabricated amplifier using appropriate calibration techniques and algorithms.

This methodology assumes that the lines are sufficiently short that filtering effects and transistor bypassing are negligible. It is even valid for devices with interline coupling but electrically short longitudinal distances that do not exhibit transmission line behavior.

6.5 Conclusions

A novel coupled micostrip amplifier in three lines has been synthesized, built, and measured. We reiterate that this device's primary value is conceptual; a more practical approach involves a smaller device fabricated on chip, for future work.

Measurements from a small MTL-MTA in three-coupled microstrip validate the synthesis and lead to the formulation of a general methodology. This full coupled-line amplifier methodology involves a multimode TRL calibration of the transistor discontuinuty (including biasing networks), a simultaneous conjugate match in the MTL domain, and the synthesis of the matching networks. Unlike its single-line counterpart, the coupled-line amplifier concept requires no drill holes or vias resulting in fabrication savings. Furthermore, if designed properly, it could be a viable alternative to similar coplanar devices for technologies which include ground planes.

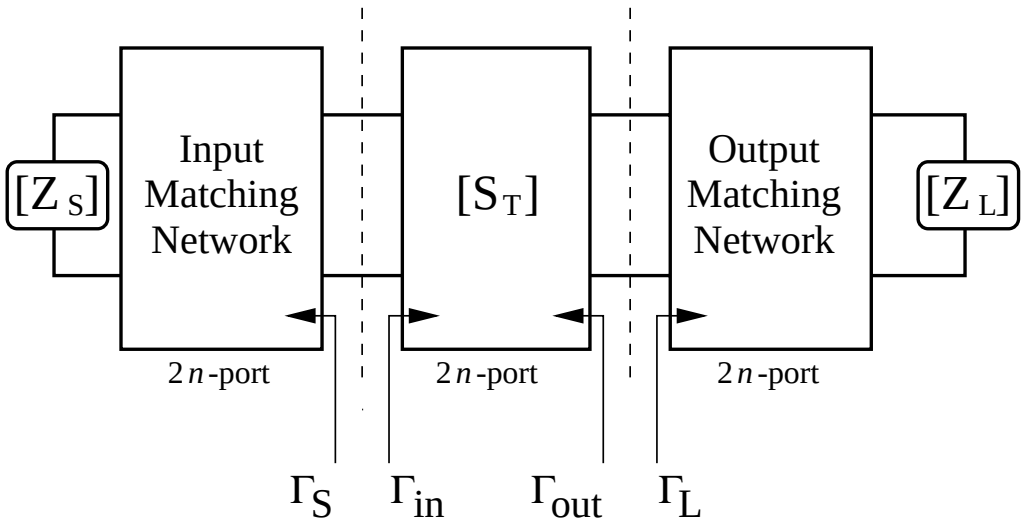

Figure 6.1 Major components of the general MTL-MTA. Note that each block is represented with a $(2n \times 2n)$ immittance parameter matrix (usually S- or T-parameters).

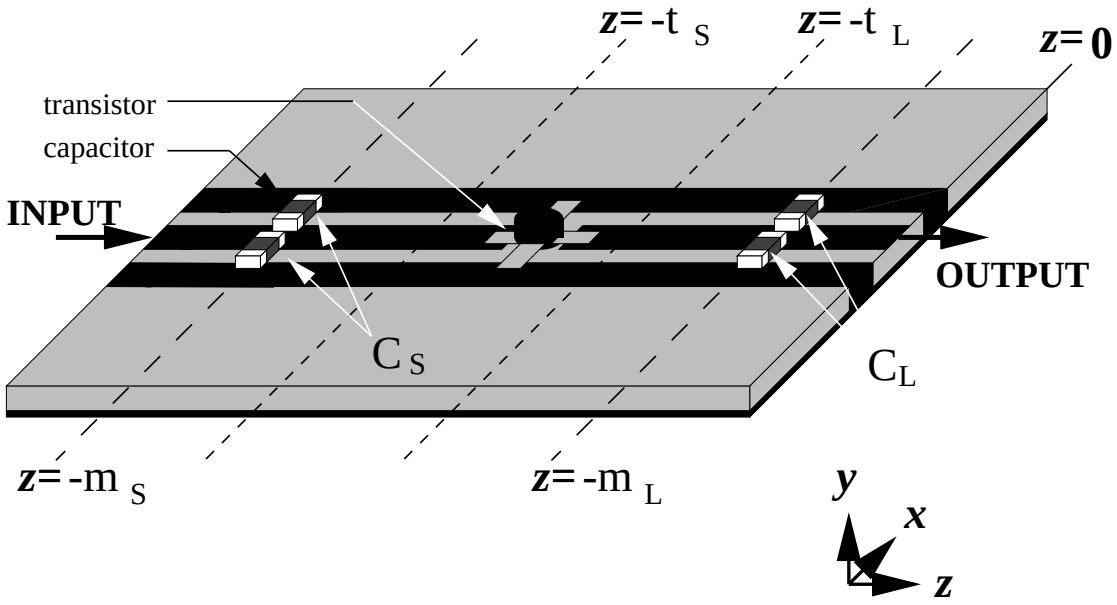

Figure 6.2 Three-coupled microstrip line transistor amplifier with interline capacitance matching networks, the transistor package, and relevant feature locations.

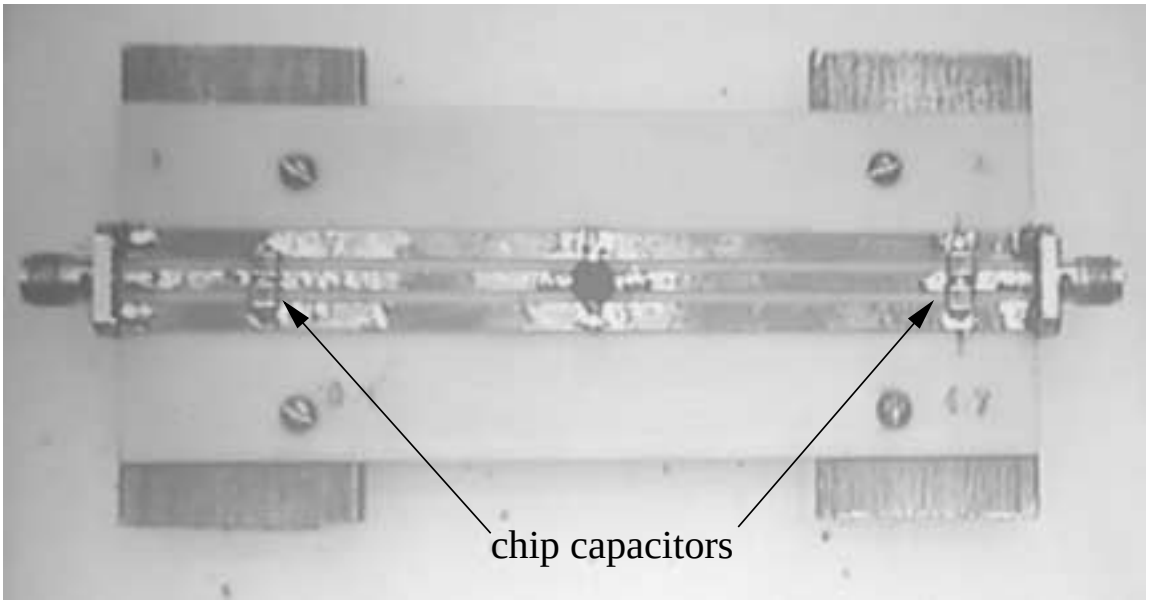

Figure 6.3 Photograph of the matched three-coupled microstrip line transistor amplifier.

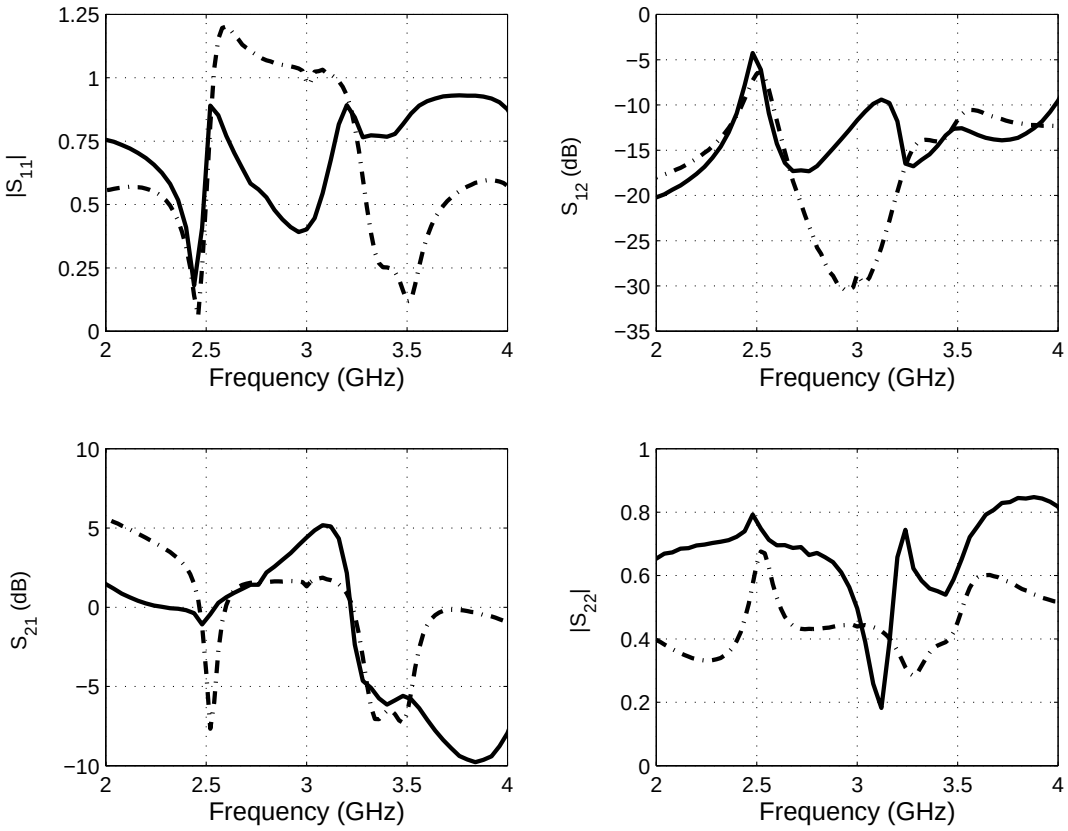

Figure 6.4 Measured S-parameters for the unmatched (dotted line) and the final matched (solid line) amplifier.

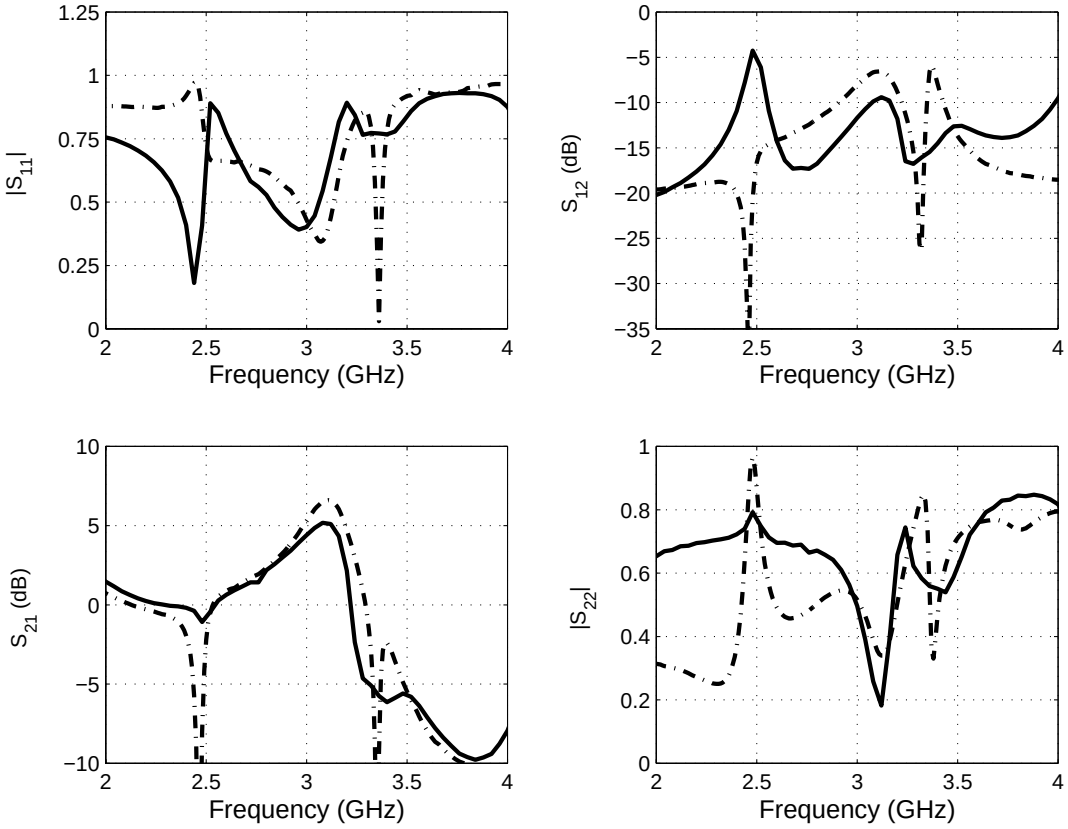

Figure 6.5 Comparison between the measured and simulated amplifier with matching networks. The optimum for S_{21} at 3.1 GHz was clearly attained.

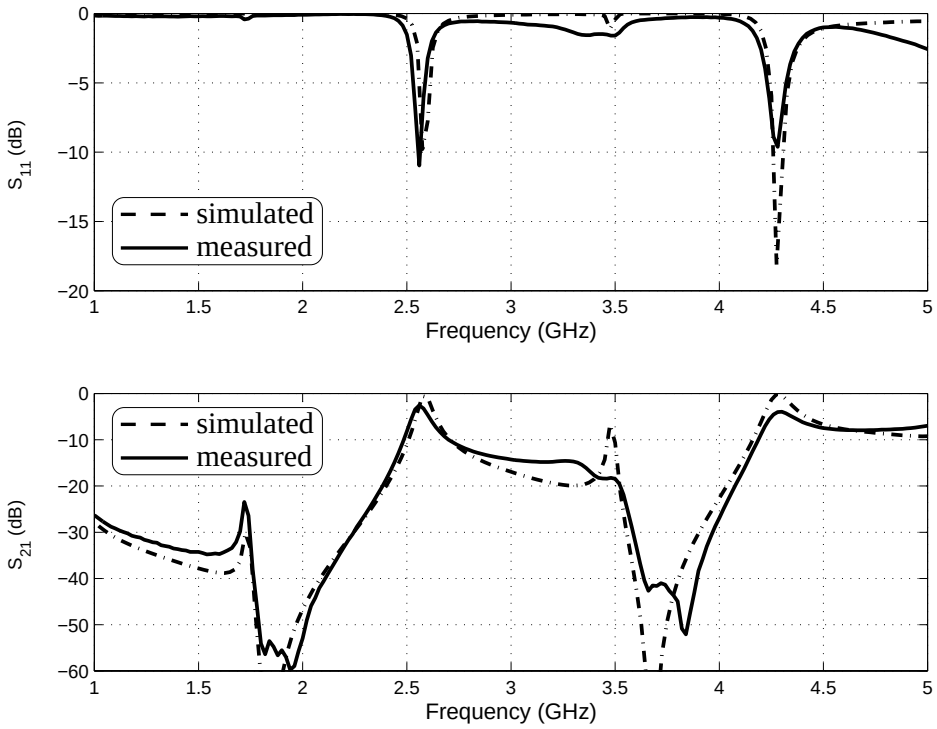

Figure 6.6 Comparison between the reflection and transmission parameters of the coupled microstrip filter resulting from the removal of the transistor package from the unmatched amplifier.

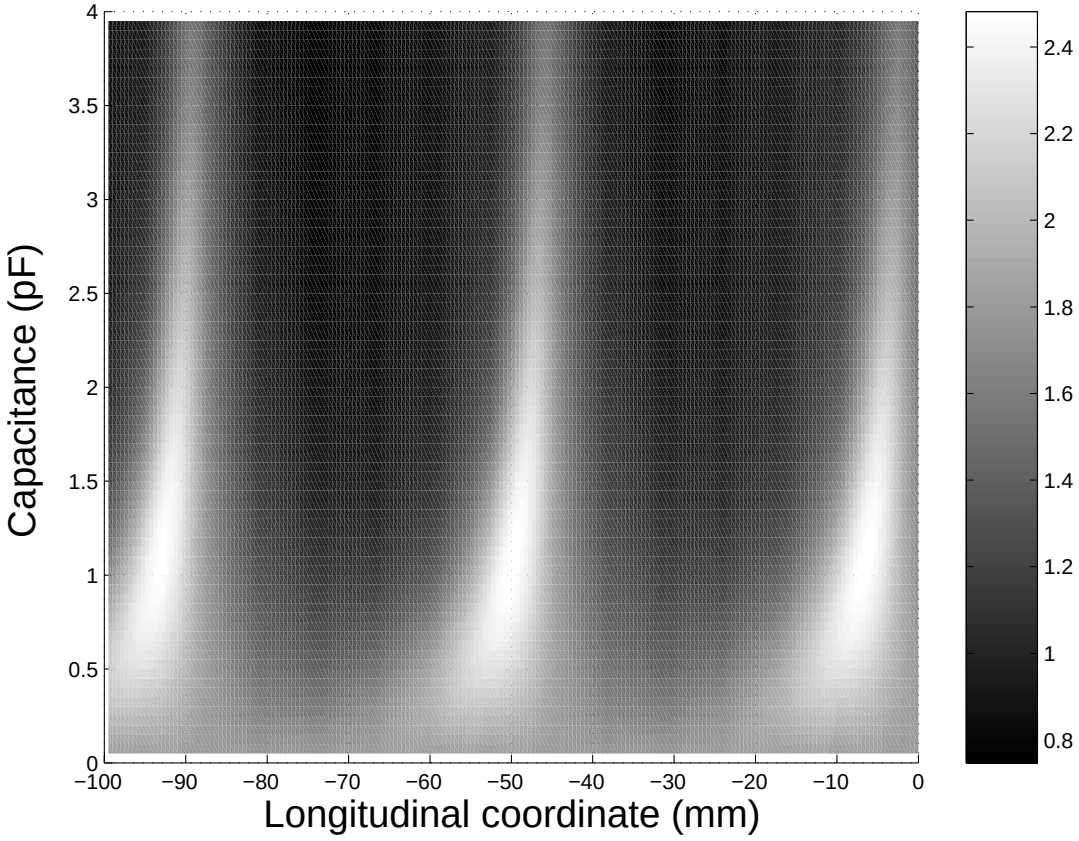

Figure 6.7 Contour plot showing the power absorbed in the load as a function of the matching network parameters. White regions indicate the best matching parameters.

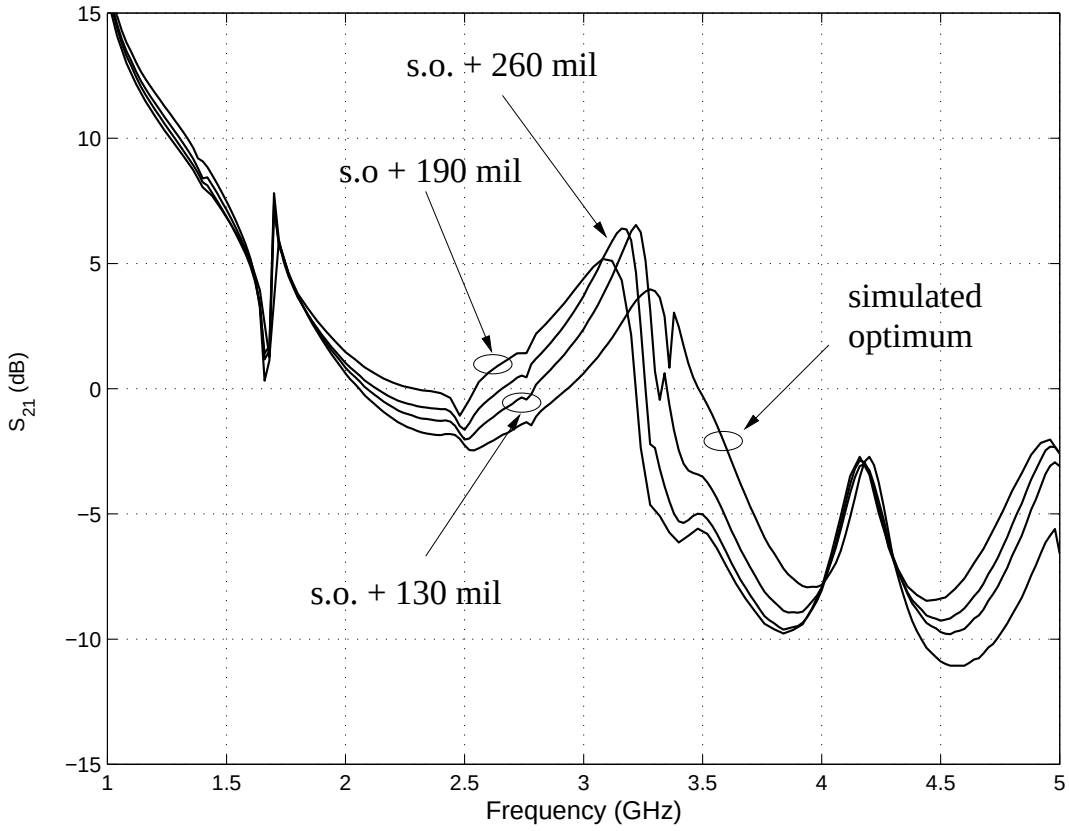

Figure 6.8 Parametrized S_{21} curves matching networks location deviation.

CHAPTER 7
SUMMARY AND FUTURE WORK

7.1 Summary

This thesis concerned the synthesis of microwave systems in MTLs, focusing on coupled microstrip technology. In Chapter 1 the circuit theory utilized in coupled tranmission line systems was presented. Then, the full MTL theory was explained, and relevant quantities were derived. All major circuit variables and quantities were introduced, in both modal and state domains. Physical interpretation and explanation accompanied these relations. All results were generalized to n-lines where possible.

In particular, focus on longitudinal behavior of the MTL functions allowed necessary understanding of the dynamics of terminated, source-driven MTL systems. The effects of quasi-TEM mode delay on these longitudinal functions was fully detailed. Comprehensive mathematical formulations coupled with physical interpretations showed passivity, reciprocity, and losslessness were preserved despite superficially problematic bahavior, especially in the LIMFs. Though n-coupled line analysis is far more complex than single lines, some of the basic tools and procedures of single transmission line microwave theory apply.

Then, a normal mode parameter extraction method (or transformation) was developed for coupled tranmission line S-parameter representations. This method provides a mechanism to "extract" the $RLGC$ parameters from the S-parameters or transform the S-parameters to normal mode parameters under quasi-TEM conditions. While theoretically important, this method has a significant practical advantage: it allows the characterization of a uniform MTL structure on which an amplifier or matching network was being fabricated. Thus, in the course of design, only one additional measurement of the uniform coupled-line section would provide a validation of the characteristics of the coupled-line dimensions, which would instill confidence in the software tools used in the synthesis.

The above analyses and developments were necessary for the synthesis of active devices in MTL coupled micostrip topologies. Naturally, these involved consideration of matching networks in MTL systems; these were hence explored in depth. This problem is fundamentally an extension of traditional trans mission line matching network theory, and may employ reactive elements, stubs, and transformers. Synthesis rules intially considered the unilateral case, where the matching strategies required few numerical iterations and practical solutions were determined quickly and accurately. They are easily visualized via Smith chart theory, which clarifies the wavelengths and dominance of a propagating mode. Several matching strategies for coupled-line systems in this case were synthesized and provided successfully matching of several simple types of terminations.

However, unilateral approximations presented are useful when the source impedance is relatively matched to the characteristic impedance of the lines; this places an obviously specific constraint on the problem. Therefore, in practical systems the bilateral matching criteria should be used to account for both input and output terminations. Furthermore, design of amplifiers in MTL topology requires consideration of the transistor discontinuity, from which input and output matching networks are synthesized.

Finally, the fully object-oriented software tool XMatch was developed and introduced. The purpose of this tool is to optimize matching networks for MTL systems using direct searches, quasi-Newton methods, and genetic algorithms. It parses a user input page and is capable of inputting frequency-dependent RLGC or normal mode parameters for the transmission characterization. Results validate the tool's effectiveness, and comparisions with synthesis approximations and independent software tools validate its accuracy.

7.2 Future Work

Since the longitudinal MTL functions and governing parameters of coupled microstrip were thoroughly examined, scant theoretical work is further warranted. Much of the background work including the LIMF and MTL investigation was motivated by the desire to synthesize matching networks in coupled microstrip topologies with mismatched terminations. Preliminary matching network measurements for moderately coupled lines functioned as expected.

Thus, while much was pioneered in this thesis, many interesting avenues for re-

search remain. First, experimental validation of the mode delay effects upon LIMFs is necessary. Furthermore, measurements of uniform coupled line systems, using the multimode TRL algorithm and accounting imperfect reflection in standards, are necessary to validate the normal mode parameter extraction method presented. On that note, full multiline, multimode calibration schemes and more refined measurement techniques will increase accuracy of the frequency-domain S-parameter measurements, and more thoroughly account for the fields in the input sections and connectors. Determination of the propagation constants and mode coefficients, whether by TDR or Fourier analysis of swept frequency measurements, will allow for a full experimental characterization.

These measurements will likely be conducted in the frequency domain. Additional types of matching networks should also be considered and tested in simulation, and also measured for practicality. These include microstrip gap capacitances, low-Q inductors, and broadband stubs.

In regards to simulation, the transmission line computer codes employed common microwave engineering approximations where possible, particularly in modeling the various discontinuities, and of course assumed quasi-TEM propagation. Certainly, full EM simulation and experimental characterization is warranted, not only to account for frequency dependence of circuit parameters, but to estimate errors due to modeling and assumptions.

XMatch must be expanded and streamlined for efficiency. Currently, it can solve problems using direct search and quasi-Newton methods, but it is time-consuming. The genetic algorithm optimization is also extremely slow, and optimization typically entails a number of parameters equal to twice the number of matching networks, so this must be improved. Finally, multiobjective numerical optimization should be considered for advanced amplifier and oscillator design.

Finally, the methodology for a full MTL-topology amplifier has been developed. This will allow a considerably more accurate MTL amplifier design than that presented in this thesis. The design will proceed in the detailed steps, including the bias networks, from which the XMatch software tool will optimize the matching networks. The initial transistor discontinuity and final amplifier will be measured using the multimode TRL algorithm.

APPENDIX A

PROOF OF S-PARAMETER SYMMETRY

Proof of the generalized S-parameter matrix symmetry in reciprocal systems is given as follows.

The generalized S-parameter matrix given by (3.22) is repeated here for convenience:

$$\boldsymbol{S} = (\boldsymbol{Z}^{\mathrm{c}}_{\mathrm{ch}})^{1/2}\,[\boldsymbol{Z}^{\mathrm{c}}_{\mathrm{ch}} + \boldsymbol{Z}^{\mathrm{c}}_{\mathrm{L}}]^{-1}\,[\boldsymbol{Z}^{\mathrm{c}}_{\mathrm{L}} - \boldsymbol{Z}^{\mathrm{c}}_{\mathrm{ch}}]\,(\boldsymbol{Z}^{\mathrm{c}}_{\mathrm{ch}})^{-1/2}\,. \tag{A.1}$$

This matrix describes a reciprocal system; its symmetry is proved as follows. Taking the transpose of (A.1) results in

$$\boldsymbol{S}^t = (\boldsymbol{Z}^{\mathrm{c}}_{\mathrm{ch}})^{-1/2}\,[\boldsymbol{Z}^{\mathrm{c}}_{\mathrm{L}} - \boldsymbol{Z}^{\mathrm{c}}_{\mathrm{ch}}]\,[\boldsymbol{Z}^{\mathrm{c}}_{\mathrm{ch}} + \boldsymbol{Z}^{\mathrm{c}}_{\mathrm{L}}]^{-1}\,(\boldsymbol{Z}^{\mathrm{c}}_{\mathrm{ch}})^{1/2}\,, \tag{A.2}$$

where each factor is symmetric by reciprocity. Now, if $\boldsymbol{Z}^{\mathrm{c}}_{\mathrm{ch}}$ is nonsingular,

$$\boldsymbol{S}^t = (\boldsymbol{Z}^{\mathrm{c}}_{\mathrm{ch}})^{-1/2}\,\boldsymbol{Z}^{\mathrm{c}}_{\mathrm{ch}}(\boldsymbol{Z}^{\mathrm{c}}_{\mathrm{ch}})^{-1}\,[\boldsymbol{Z}^{\mathrm{c}}_{\mathrm{L}} - \boldsymbol{Z}^{\mathrm{c}}_{\mathrm{ch}}]\,[\boldsymbol{Z}^{\mathrm{c}}_{\mathrm{ch}} + \boldsymbol{Z}^{\mathrm{c}}_{\mathrm{L}}]^{-1}\,\boldsymbol{Z}^{\mathrm{c}}_{\mathrm{ch}}(\boldsymbol{Z}^{\mathrm{c}}_{\mathrm{ch}})^{-1}\,(\boldsymbol{Z}^{\mathrm{c}}_{\mathrm{ch}})^{1/2}\,. \tag{A.3}$$

To simplify the algebra, we let

$$\boldsymbol{A} = (\boldsymbol{Z}^{\mathrm{c}}_{\mathrm{ch}})^{-1}\,[\boldsymbol{Z}^{\mathrm{c}}_{\mathrm{L}} - \boldsymbol{Z}^{\mathrm{c}}_{\mathrm{ch}}]\,[\boldsymbol{Z}^{\mathrm{c}}_{\mathrm{ch}} + \boldsymbol{Z}^{\mathrm{c}}_{\mathrm{L}}]^{-1}\,\boldsymbol{Z}^{\mathrm{c}}_{\mathrm{ch}}. \tag{A.4}$$

Note that $\boldsymbol{A}$ is similar to a reflection coefficient. Now,

$$\begin{aligned}
\boldsymbol{A} &= (\boldsymbol{Z}^{\mathrm{c}}_{\mathrm{ch}})^{-1}\boldsymbol{Z}^{\mathrm{c}}_{\mathrm{L}}\,[\boldsymbol{Z}^{\mathrm{c}}_{\mathrm{ch}} + \boldsymbol{Z}^{\mathrm{c}}_{\mathrm{L}}]^{-1}\,\boldsymbol{Z}^{\mathrm{c}}_{\mathrm{ch}} - [\boldsymbol{Z}^{\mathrm{c}}_{\mathrm{ch}} + \boldsymbol{Z}^{\mathrm{c}}_{\mathrm{L}}]^{-1}\,\boldsymbol{Z}^{\mathrm{c}}_{\mathrm{ch}} \\
&= \{\boldsymbol{Z}^{\mathrm{c}}_{\mathrm{ch}})^{-1}\,[\boldsymbol{Z}^{\mathrm{c}}_{\mathrm{ch}} + \boldsymbol{Z}^{\mathrm{c}}_{\mathrm{L}}]\,(\boldsymbol{Z}^{\mathrm{c}}_{\mathrm{L}})^{-1}\boldsymbol{Z}^{\mathrm{c}}_{\mathrm{ch}}\}^{-1} - [\boldsymbol{Z}^{\mathrm{c}}_{\mathrm{ch}} + \boldsymbol{Z}^{\mathrm{c}}_{\mathrm{L}}]^{-1}\,\boldsymbol{Z}^{\mathrm{c}}_{\mathrm{ch}} \\
&= \{\mathbf{1}_n + (\boldsymbol{Z}^{\mathrm{c}}_{\mathrm{L}})^{-1}\boldsymbol{Z}^{\mathrm{c}}_{\mathrm{ch}}\}^{-1} - [\boldsymbol{Z}^{\mathrm{c}}_{\mathrm{ch}} + \boldsymbol{Z}^{\mathrm{c}}_{\mathrm{L}}]^{-1}\,\boldsymbol{Z}^{\mathrm{c}}_{\mathrm{ch}} \\
&= \{(\boldsymbol{Z}^{\mathrm{c}}_{\mathrm{L}})^{-1}\,[\boldsymbol{Z}^{\mathrm{c}}_{\mathrm{ch}} + \boldsymbol{Z}^{\mathrm{c}}_{\mathrm{L}}]\}^{-1} - [\boldsymbol{Z}^{\mathrm{c}}_{\mathrm{ch}} + \boldsymbol{Z}^{\mathrm{c}}_{\mathrm{L}}]^{-1}\,\boldsymbol{Z}^{\mathrm{c}}_{\mathrm{ch}} \\
&= [\boldsymbol{Z}^{\mathrm{c}}_{\mathrm{ch}} + \boldsymbol{Z}^{\mathrm{c}}_{\mathrm{L}}]^{-1}\,\boldsymbol{Z}^{\mathrm{c}}_{\mathrm{L}} - [\boldsymbol{Z}^{\mathrm{c}}_{\mathrm{ch}} + \boldsymbol{Z}^{\mathrm{c}}_{\mathrm{L}}]^{-1}\,\boldsymbol{Z}^{\mathrm{c}}_{\mathrm{ch}} \\
&= [\boldsymbol{Z}^{\mathrm{c}}_{\mathrm{L}} + \boldsymbol{Z}^{\mathrm{c}}_{\mathrm{ch}}]^{-1}\,[\boldsymbol{Z}^{\mathrm{c}}_{\mathrm{L}} - \boldsymbol{Z}^{\mathrm{c}}_{\mathrm{ch}}]\,.
\end{aligned} \tag{A.5}$$

The derivation for $\boldsymbol{A}$ is obviously applicable to (3.8) and (3.9).

Using (A.5) with (A.4) and (A.3), we arrive at

$$\begin{aligned}
\boldsymbol{S}^t &= (\boldsymbol{Z}^{\mathrm{c}}_{\mathrm{ch}})^{1/2}\,\boldsymbol{A}\,(\boldsymbol{Z}^{\mathrm{c}}_{\mathrm{ch}})^{-1/2} \\
&= (\boldsymbol{Z}^{\mathrm{c}}_{\mathrm{ch}})^{1/2}\,[\boldsymbol{Z}^{\mathrm{c}}_{\mathrm{L}} + \boldsymbol{Z}^{\mathrm{c}}_{\mathrm{ch}}]^{-1}\,[\boldsymbol{Z}^{\mathrm{c}}_{\mathrm{L}} - \boldsymbol{Z}^{\mathrm{c}}_{\mathrm{ch}}]\,(\boldsymbol{Z}^{\mathrm{c}}_{\mathrm{ch}})^{-1/2}\,.
\end{aligned} \tag{A.6}$$

Finally, we have that

$$\boldsymbol{S} = \boldsymbol{S}^t, \tag{A.7}$$

which agrees with [59], who defines $\boldsymbol{S}$ according to (A.2).

REFERENCES

[1] K. D. Marx, "Propagation modes, equivalent circuits, and characteristic terminations for multiconductor transmission lines with inhomogeneous dielectrics," *IEEE Trans. Microwave Theory Tech.*, vol. 21, pp. 450–457, July 1973.

[2] C. R. Paul, "On uniform multimode transmission lines," *IEEE Trans. Microwave Theory Tech.*, vol. MTT-21, pp. 556–558, Aug. 1973.

[3] C. R. Paul, "Decoupling the multiconductor transmission line equations," *IEEE Trans. Microwave Theory Tech.*, vol. 44, pp. 1429–1440, Aug. 1996.

[4] D. F. Williams, L. A. Hayden, and R. B. Marks, "A complete multimode equivalent-circuit theory for electrical design," *J. Res. Natl. Stand. Technol.*, pp. 405–423, Aug. 1997.

[5] J. T. Kuo and C. H. Tzuang, "A termination scheme for high-speed pulse propagation on a system of tightly coupled coplanar strips," *IEEE Trans. Microwave Theory Tech.*, vol. 42, pp. 1008–1015, June 1994.

[6] S. Amari and J. Bornemann, "Optimum termination networks for tightly coupled microstrip lines under random and deterministic excitations," *IEEE Trans. Microwave Theory Tech.*, vol. 45, pp. 1785–1789, Oct. 1997.

[7] D. A. Hill, K. H. Cavcey, and R. T. Johnk, "Crosstalk between microstrip transmission lines," *IEEE Trans. Electromagn. Compat.*, vol. 36, pp. 314–321, Nov. 1994.

[8] J. E. Schutt-Aine and R. Mittra, "Analysis of pulse propagation in coupled transmission lines," *IEEE Trans. Circuits Syst. I: Fundam. Theory Appl.*, vol. CAS-32, pp. 1214–1219, Dec. 1985.

[9] J. E. Schutt-Aine and R. Mittra, "Nonlinear transient analysis of coupled transmission lines," *IEEE Trans. Circuits Syst. I: Fundam. Theory Appl.*, vol. 36, pp. 959–966, July 1989.

[10] G. T. Lei, G. W. Pan, and B. K. Gilbert, "Examination, clarification, and simplification of modal decoupling method for multiconductor transmission lines," *IEEE Trans. Microwave Theory Tech.*, vol. 43, pp. 2090–2100, Sep. 1995.

[11] K. Reiss and O. A. Palusinski, "Procedure for direct calculation of characteristic admittance matrix of coupled transmission lines," *IEEE Trans. Microwave Theory Tech.*, vol. 44, pp. 152–154, Jan. 1996.

[12] G. C. Gentili and M. Salazar-Palma, "The definition and computation of modal characteristic in quasi-TEM coupled transmission lines," *IEEE Trans. Microwave Theory Tech.*, vol. 43, pp. 338–343, Feb. 1995.

[13] Y.-Y. Sun, "Matrix theorems of multiconductor transmission lines," *J. Chin. Inst. Eng.*, vol. 1, pp. 37–41, Sep. 1978.

[14] V. K. Tripathi, "On the analysis of symmetrical three-line microstrip circuits," *IEEE Trans. Microwave Theory Tech.*, pp. 726–729, Sep. 1977.

[15] G. E. Ponchak and L. P. B. Katehi, "Open- and short-circuit terminated series stubs in finite-width coplanar waveguide on silicon," *IEEE Trans. Microwave Theory Tech.*, vol. 45, pp. 970–976, June 1997.

[16] Y.-Y. Sun, "On multiconductor quarter-wave matching section," *J. Chin. Inst. Eng.*, vol. 3, pp. 147–152, 1980.

[17] T.-M. Winkel, L. S. Dutta, H. Grabinski, and E. Groteluschen, "Determination of the propagation constant of coupled lines on chips based on high frequency measurements," in *IEEE Multi-Chip Module Conference*, 1996, pp. 99-104.

[18] A. K. Agrawal, K.-M. Lee, L. D. Scott, and H. M. Fowles, "Experimental characterization of multiconductor transmission lines in the frequency domain," *IEEE Trans. Electromagn. Compat.*, pp. 20–27, Feb. 1979.

[19] J. van der Merwe, H. C. Reader, and J. H. Cloete, "S-parameter measurements yielding the characteristic matrices of multiconductor transmission lines," *IEEE Trans. Electromagn. Compat.*, vol. 40, pp. 249–256, Aug. 1998.

[20] A. Tripathi and V. K. Tripathi, "Characterization of multiconductor coupled lines from multiport TDR measurements," in *IEEE MTT-S Int. Microw. Symp. Dig.*, 1997, pp. 1777-1780.

[21] A. Tripathi and V. K. Tripathi, "Characterization of multiconductor inhomogeneous uniformly coupled lines from TDR data," in *Electr. Perform. Electr. Packaging*, 1997, pp. 167-170.

[22] D. K. Chang, *Field and Wave Electromagnetics.* New York: Addison-Wessley, 1992.

[23] K. S. Oh and J. E. Schutt-Aine, "Efficient modeling of interconnects and capacitive discontinuities in high-speed digital circuits." Electromagnetic Communication Laboratory, University of Illinois, Urbana-Champaign, Tech. Rep. 95-1, June 1995.

[24] V. K. Tripathi and H. Lee, "Spectral-domain computation of characteristic impedances and multiport parameters of multiple coupled microstrip lines," *IEEE Trans. Microwave Theory Tech.*, vol. 37, pp. 215–221, Dec. 1985.

[25] H. Anton, *Elementary Linear Algebra.* New York: Wiley & Sons, 1973.

[26] L. Weinberg, *Network Analysis and Synthesis.* New York: McGraw-Hill, 1962.

[27] D. F. Williams, L. A. Hayden, and R. B. Marks, "A complete multimode equivalent-circuit theory for electrical design," *J. Res. Natl. Stand. Technol.*, vol. 102, pp. 405–423, Jul.-Aug. 1997.

[28] T. R. Arabi, T. K. Sarkar, and A. R. Djordjevic, "Time and frequency domain characterization of multiconductor transmission lines," *Electromagn.*, vol. 9, pp. 85–112, 1989.

[29] J. G. Nickel and J. E. Schutt-Aine, "Narrowband matching networks for quasi-TEM coupled microstrip lines," *IEEE Trans. Microwave Theory Tech.*, submitted for publication.

[30] Y.-Y. Sun, "Immittance matrices of multiconductor transmission lines," *J. Franklin Inst.*, vol. 307, pp. 59–67, Jan. 1979.

[31] T. Cholewicki, "Some properties of immittance matrices of a nonuniform n-wire transmission line," *Bull. L'Acad. Pol. Sci., Ser. Sci. Tech.*, vol. 30, pp. 101–107, 1982.

[32] L. Carin and K. J. Webb, "Characterisitic impedance of multilevel, multiconductor hybrid mode microstrip," *IEEE Trans. Magn.*, vol. 24, pp. 2947–2949, 1989.

[33] J. G. Nickel, "Synthesis of several narrow-band matching networks for quasi-TEM coupled microstrip lines with passive terminations," M.S. thesis, University of Illinois, Urbana-Champaign, 1999.

[34] R. Carson, *High-Frequency Amplifiers*. New York: Wiley & Sons, 1982.

[35] R. M. Fano, L. J. Chu, and R. B. Adler, *Electromagnetic Fields, Energy, and Forces*. New York: Wiley, 1960.

[36] F.-Y. Chang, "Transient analysis of lossless coupled transmission lines in a nonhomogeneous medium," *IEEE Trans. Microwave Theory Tech.*, vol. 18, pp. 616–626, Sep. 1970.

[37] J. G. Nickel and J. E. Schutt-Aine, "The effects of quasi-TEM modal dispersion on longitudinal immittance matrix functions of lossless, symmetric, coupled-microstrip systems," Feb. 2000.

[38] S. Sercu and L. Martens, "Characterizing n-port packages and interconnections with a 2-port network analyzer," in *Electr. Perform. Electr. Packaging*, 1997, pp. 163-166.

[39] J. C. Tippet and R. A. Speciale, "A rigorous technique for measuring the scattering matrix of a multiport device with a 2-port network analyzer," *IEEE Trans. Microwave Theory Tech.*, pp. 661–666, May 1982.

[40] D. F. Williams, "Multiconductor transmission line characterization," *IEEE Trans. Compon. Packag. Manuf. Technol. Pt. B*, vol. 20, pp. 129–132, May 1997.

[41] Y. Wang and H. Ling, "Multimode parameter extraction for multiconductor transmission lines via single-pass FDTD and signal-processing techniques," *IEEE Trans. Microwave Theory Tech.*, vol. 46, pp. 89–96, 1998.

[42] V. K. Tripathi and J. B. Rettig, "A SPICE model for multiple coupled microstrips and other transmission lines," *IEEE Trans. Microwave Theory Tech.*, vol. 33, pp. 1513–1518, Dec. 1985.

[43] D. E. Bockelman and W. R. Eisenstadt, "Combined differential and common-mode scattering parameters: Theory and simulation," *IEEE Trans. Microwave Theory Tech.*, vol. 45, pp. 1530–1539, Jul. 1995.

[44] J. G. Nickel and J. E. Schutt-Aine, "Investigation of the longitudinal multiconductor transmission line functions for symmetric coupled-microstrip systems," *IEEE Trans. Microwave Theory Tech.*, to be published.

[45] C. Seguinot, P. Kennis, J.-F. Legier, F. Huret, E. Paleczny, and L. Hayden, "Multimode TRL - a new concept in microwave measurements: theory and experimental verification," *IEEE Trans. Microwave Theory Tech.*, vol. 46, pp. 536–542, May 1998.

[46] J. J. Choma, *Electrical Networks : Theory and Analysis.* New York: Wiley, 1985.

[47] J. E. Schutt-Aine, "Transient analysis of coupled transmission lines," Ph.D. dissertation, University of Illinois at Urbana-Champaign, May 1988.

[48] *EM-Sonnet Software User's Manual,* Version 6.0, Sonnet Software Inc.

[49] K. S. Oh, D. B. Kuznetsov, and J. E. Schutt-Aine, "Capacitance computations in multilayered dielectric medium using the closed-form spatial green's functions," *IEEE Trans. Microwave Theory Tech.*, vol. 42, pp. 1443–1453, Aug. 1994.

[50] K. C. Gupta, R. Garg, and R. Ghadha, *Computer-Aided Design of Microwave Circuits.* Dedham, MA: Artech House, 1981.

[51] Wolfram Research, Inc., "Mathematica" [program]. Champaign, Illinois: Wolfram Research, Inc., 1991.

[52] G. F. Engen and C. A. Hoer, "Thru-reflect-line: An improved technique for calibrating the dual six-port automatic network analyzer," *IEEE Trans. Microwave Theory Tech.*, pp. 987–993, Dec. 1979.

[53] D. M. Pozar, *Microwave Engineering*. New York: Addison-Wesley, 1990.

[54] G. Gonzalez, *Microwave Transistor Amplifiers*. Englewood Cliffs, NJ: Prentice-Hall, 1984.

[55] J. Papapolymerou, J. East, and L. P. B. Katehi, "GaAs versus FGC lines for MMIC applications," *IEEE Trans. Microwave Theory Tech.*, vol. 46, pp. 1790–1793, Nov. 1998.

[56] J. Papapolymerou, F. Brauchler, J. East, and L. P. B. Katehi, "W-band finite ground coplanar monolithic multipliers," *IEEE Trans. Microwave Theory Tech.*, vol. 47, pp. 614–619, May 1999.

[57] G. P. Gauthier, L. P. B. Katehi, and G. M. Rebeiz, "W-band finite ground coplanar waveguide (FGCPW) to microstrip transition," in *IEEE MTT Int. Symp. Dig.*, 1998, pp. 107-109.

[58] J. G. Nickel and J. E. Schutt-Aine, "Frequency-domain multiconductor transmission line normal mode parameter extraction," Aug. 2000.

[59] Y. K. Chin, "Analysis and applications of multiple coupled line structures in an inhomogeneous medium," Ph.D. dissertation, Oregon State University, May 1982.

VITA

Joshua George Nickel was born on November 27, 1974, in Lancaster, Pennsylvania. From August 1993 to May 1997 he attended the Pennsylvania State University at University Park and received the Bachelor of Science in Electrical Engineering with honors.

During his undergraduate work, Mr. Nickel held several summer internships in electrical and mechanical engineering. In the summer of 1997, he worked for the MITRE Corporation in Reston, Virginia, working on telecommunications documentation for the Defense Information Systems Agency.

In August 1997, Mr. Nickel began his graduate studies at the University of Illinois at Urbana-Champaign. He has held a research assistantship with the Center for Computational Electromagnetics under the supervision of Professor Jose Schutt-Aine. He has participated in several research projects, including the construction of a 16-processor parallel Linux cluster, or "Beowulf" supercomputer, and some measurement and modeling of novel microelectromechanical switch (MEMS) devices. His main research thrust has been the simulation and analysis of coupled microstrip and coplanar lines and the synthesis, design, and measurement of matching networks and transistor amplifiers in these topologies.

He also held a teaching assistantship for six semesters, starting in 1998, involving an automated microwave measurements course. In the summer of 1998, Mr. Nickel worked at the IBM corporation in Poughkeepsie, New York, in the high-performance electrical design team. He was responsible for the measurement and simulation of coupled noise in the multichip module for the S-390 Parallel Enterprise Server.

In the summer of 1999, he worked at SAIC/Demaco in Champaign, Illinois as a software engineer. In October 1999, he received the Master of Science in Electrical Engineering. He continued part-time work at SAIC/Demaco in 2000 until March 2001, when he began part-time work at Silicon Bandwidth, Inc. in Fremont, California.